8-2017

Mitigation and Evaluation of Alkali-Silica Reaction (ASR) and Freezing and Thawing in Concrete Transportation Structures

Richard Albert Deschenes Jr.
University of Arkansas, Fayetteville

Mitigation and Evaluation of Alkali-Silica Reaction (ASR) and Freezing and Thawing in Concrete Transportation Structures

A dissertation submitted in partial fulfillment
of the requirements for the degree of
Doctor of Philosophy in Engineering
with a Concentration in Civil Engineering

by

Richard A. Deschenes Jr.
University of Arkansas
Bachelor of Science in Civil Engineering, 2012
University of Arkansas
Masters of Science in Civil Engineering, 2014

August 2017
University of Arkansas

This dissertation is approved for recommendation to the Graduate Council.

Dr. W. Micah Hale Dissertation Chair	Dr. Gary Prinz Committee Member
Dr. Mark Arnold Committee Member	Dr. Thano Drimalas Ex-Officio Member
Dr. Benoit Fournier Ex-Officio Member	Dr. Eric Giannini Ex-Officio Member

ABSTRACT

An evaluation of alkali-silica reaction (ASR) and freezing and thawing (F/T) in concrete transportation structures is presented along with mitigation methods for slowing the rate of deterioration in concrete. A combination of field and laboratory testing confirms ASR deterioration is exacerbated by exposure to F/T. Laboratory testing indicates an aggregate previously deemed inert to ASR, caused ASR deterioration in several concrete pavement and transportation structures. Existing standard test methods deem this aggregate safe for use in concrete. A modified test method shows the concrete can deteriorate rapidly when subjected to cycles of conditions promoting ASR and F/T. Several structures containing this aggregate deteriorated rapidly and severely during exposure to F/T. The interstate pavement underwent less deterioration as the incorporation of some Class C fly ash limited the development of ASR, and improved the durability to F/T. A three-year field test of various treatments applied to concrete barriers indicates silane reduces the moisture state of the concrete and slows the development of F/T and ASR deterioration as compared to untreated sections. A corresponding three-year evaluation of silane applied to concrete pavements, indicates silane slows F/T deterioration over time by reducing the moisture state of the concrete.

Measuring the moisture state of concrete in the field proved difficult. Results of field and laboratory testing indicate measuring vapor pressure may prove more useful for evaluating the efficacy of treatments in reducing the moisture within concrete. The moisture state of the concrete is critical to the development of both ASR and F/T, as concretes protected from external moisture did not develop deleterious deterioration while specimens exposed to additional moisture deteriorated. This indicates limiting the ingress of external moisture is a viable method for slowing both ASR and F/T deterioration in concrete.

ACKNOWLEDGMENTS

I would like to thank my Lord and savior Jesus Christ for strengthening, encouraging, and guiding me throughout my life, and especially these past three years. Without his provision and grace none of this would have been possible.

I also appreciate the encouragement and advice of Dr. W. Micah Hale who helped me to achieve my dreams of becoming a professor of civil engineering. Over the last five years he has guided me to complete my research and dissertation. I also thank my committee members, Dr. Eric Giannini, Dr. Thano Drimalas, Dr. Benoit Fournier, Dr. Gary Prinz, and Dr. Mark Arnold for their advice and expertise which led to the completion of this dissertation.

My wife Ester encouraged me to work hard and apply myself to finish my research and dissertation. She is so patient and understanding as I put in the hours required to finish this dissertation. My family also pushed me to continue my education and complete my PhD, and I am grateful for their loving encouragement.

I also want to thank my friends and colleagues Cameron Murray, Casey Jones, Cahn Dang, Alberto Ramirez, William Philips, Doddridge Davis, Joseph Daniels, Ryan Hagedorn, and Ali Al-Salman for all their help in completing my research. I also appreciate the help of and support of the personnel at AHTD who went out of their way to facilitate the work done in this dissertation.

DEDICATION

I dedicate this dissertation to my wife Ester and my family, who encouraged me to pursue and complete my PhD.

TABLE OF CONTENTS

TITLE PAGE **1**

ABSTRACT **2**

ACKNOWLEDGMENTS **3**

DEDICATION **4**

TABLE OF CONTENTS **5**

LIST OF TABLES **10**

LIST OF FIGURES **12**

NOTATIONS **17**

LIST OF PUBLISHED AND SUBMITTED PAPERS **18**

1. INTRODUCTION AND RESEARCH OBJECTIVES **1**

1.1. INTRODUCTION 1

1.2. RESEARCH OBJECTIVES 4

1.3. LITERATURE REVIEW 6

1.3.1. Alkali-Silica Reaction (ASR) *6*

1.3.2. Freezing and Thawing (F/T) *39*

1.4. RELATIVE HUMIDITY IN CONCRETE (RH) 50

1.4.1. Relative Humidity and ASR *56*

1.4.2. Relative Humidity and F/T *60*

1.5. DISSERTATION ORGANIZATION 61

1.6. REFERENCES 62

2. PAPER 1: ALKALI-SILICA REACTION IN CONCRETE WITH PREVIOUSLY INERT AGGREGATES 69

2.1. INTRODUCTION 70

2.2. EXPERIMENTAL INVESTIGATION 72

2.2.1. Concrete Materials 73

2.2.2. Laboratory Testing 75

2.2.3. Field Testing 78

2.3. EXPERIMENTAL RESULTS AND DISCUSSION 82

2.3.1. Laboratory Testing 82

2.3.2. Field Monitoring 89

2.4. CONCLUSIONS AND RECOMMENDATIONS 91

2.5. FUTURE RESEARCH 92

2.6. ACKNOWLEDGMENTS 93

2.7. REFERENCES 93

3. PAPER 2: MITIGATION OF ALKALI-SILICA REACTION AND FREEZING AND THAWING THROUGH SURFACE TREATMENT 96

3.1. INTRODUCTION 97

3.2. RESEARCH SIGNIFICANCE 99

3.3. EXPERIMENTAL PROCEDURE 99

3.3.1. Materials 100

3.3.2. Specimens 102

3.3.3. Items of investigation 104

3.4. ANALYTICAL PROCEDURE 104

3.5. Experimental Results and Discussion 105
3.5.1. Temperature-normalized vertical strain 105
3.5.2. Internal relative humidity and temperature 114
3.6. Further Research 117
3.7. Conclusions 117
3.8. Acknowledgments 119
3.9. References 119

4. PAPER 3: MITIGATION OF ASR AND FREEZE THAW IN CONCRETE PAVEMENT THROUGH SILANE SURFACE TREATMENTS 121

4.1. Introduction 123
4.2. Research Significance 128
4.3. Experimental Procedure 128
4.3.1. Materials 129
4.3.2. Specimens 131
4.3.3. Items of Investigation 135
4.4. Analytical Procedure 136
4.5. Experimental Results and Discussion 138
4.6. Conclusions 148
4.7. Acknowledgements 150
4.8. References 151

5. PAPER 4: ANOTHER LOOK AT THE EFFECTS OF RELATIVE HUMIDITY, TEMPERATURE, AND FREEZING AND THAWING ON ASR 155

5.1. Introduction 157

5.2. Research Significance 164
5.3. Experimental Investigation 165
5.3.1. Relative Humidity (RH) *165*
5.3.2. ASR, W/D, and F/T *167*
5.4. Experimental Results and Discussion 170
5.4.1. Relative Humidity (RH) and Vapor Pressure (VP) *170*
5.4.2. ASR, W/D, F/T *177*
5.5. Conclusions and Recommendations 181
5.5.1. Relative Humidity (RH) and Vapor Pressure (VP) *181*
5.5.2. ASR, W/D, F/T *182*
5.6. Acknowledgements 183
5.7. References 183
6. CONCLUSIONS AND CONTRIBUTIONS 186
6.1. Synthesis of Results 186
6.2. Conclusions 188
6.2.1. Paper 1 ..... *188*
6.2.2. Paper 2 ..... *189*
6.2.3. Paper 3 ..... *190*
6.2.4. Paper 4 ..... *191*
6.3. Contributions 193
7. REFERENCES 195
8. APPENDIX 204

8.1. APPENDIX A: INTERSTATE 49 BARRIER DATA 204

8.2. APPENDIX B: INTERSTATE 49 PAVEMENT DATA 238

LIST OF TABLES

Table 1.3-1. DRI petrographic features and weighing factors (Villeneuve et al., 2012)..... 35

Table 2.3-1. Strain Rate Date for Barrier Wall Control Sections. 90

Table 3.3-1–Application rate and cost analysis of surface treatments..... 101

Table 3.5-1–Strain rate for sections and per season 106

Table 4.3-1. Job-approved concrete mixture design. 130

Table 4.3-2. Silane treatments and application rates 131

Table 4.3-3. DRI petrographic features and weighting factors [23, 27]. 136

Table 4.5-1. Statistical analysis of results. 141

Table 4.5-2. Summary of internal-RH (%) data with yearly-averages and overall change. 143

Table 4.5-3. Summary of results for silane treatments. 147

Table 5.3-1. Materials used for CPT prisms. 166

Table 5.3-2. RH (%) and VP (kPa) salt solutions for highly-reactive prisms [25, 26, 27]. 167

Table 5.3-3. RH (%) and VP (kPa), salt solutions for moderately-reactive prisms [25, 26, 27].

..... 167

Table 5.3-4. Concrete mixture for prisms subjected to ASR, W/D, and F/T..... 168

Table 5.3-5. Storage cycles for ASR, W/D, and F/T (prisms exposed to 21 repeated cycles). . 169

Table 8.1-1. Interstate 49 barrier wall data for sections with minimal deterioration..... 205

Table 8.1-2. Interstate 49 barrier wall data for sections with moderate deterioration 216

Table 8.1-3 Interstate 49 barrier wall data for sections with severe deterioration..... 227

Table 8.2-1. Interstate 49 control panels raw data 239

Table 8.2-2. Interstate 49 Silane 40A panels raw data 243

Table 8.2-3. Interstate 49 Silane 100 panels raw data 247

Table 8.2-4. Interstate 49 Silane 40B panels raw data.. 251

LIST OF FIGURES

Fig. 1.1-1–Typical deterioration in concrete barriers due to F/T and ASR (by Richard Deschenes Jr.). 3

Fig. 1.1-2–Typical deterioration in concrete pavements due to F/T and ASR (by Richard Deschenes Jr.). 3

Fig. 1.3-1–Typical DEMEC gauge measurement and grid (by Richard Deschenes Jr.). 29

Fig. 2.2-1–Typical CPT containers (by Richard Deschenes Jr.)..... 78

Fig. 2.2-2–A. Interstate wall map view. B. Minimal damage. C. Moderate damage. D. Severe damage (by Richard Deschenes Jr)..... 80

Fig. 2.3-1–ASTM C1260 (AMBT) results. 83

Fig. 2.3-2–ASTM C1567 (AMBT) results. 84

Fig. 2.3-3–ASTM C1293 (CPT) results..... 85

Fig. 2.3-4–Comparison of 14-day AMBT and one-year CPT results..... 86

Fig. 2.3-5–Portland cement alkali content with respect to time. 87

Fig. 2.3-6–Concrete barrier wall alkali content for wall sections of minimal, moderate, and severe deterioration..... 88

Fig. 2.3-7–Barrier wall normalized vertical strain..... 91

Fig. 3.3-1–Typical barrier section with severe damage (by Richard Deschenes Jr.)..... 99

Fig. 3.3-2–Barrier sections treated with elastomeric paint (left) and silane (right) (by Richard Deschenes Jr.). 101

Fig. 3.3-3–Typical strain measurement grid on barrier section after treatment with silane (by Richard Deschenes Jr.)..... 103

Fig. 3.5-1–Temperature-normalized vertical strain (%) with respect to: (a) time (date); and (b) differential strain for sections of minimal damage. 108
Fig. 3.5-2–Temperature-normalized vertical strain (%) with respect to: (a) time (date); and (b) differential strain for sections of moderate damage. 110
Fig. 3.5-3–Temperature-normalized vertical strain (%) with respect to: (a) time (date); and (b) differential strain for sections of severe damage. 112
Fig. 3.5-4–Silane-treated section (left) as compared to untreated section (right) (by Richard Deschenes Jr.). 113
Fig. 3.5-5–Temperature-normalized vertical strain (%) with respect to: (a) time (date) for control sections with seasons highlighted; and (b) internal relative humidity (%) with respect to time (date) for sections of minimal damage. 116
Fig. 4.3-1 –Diagram of Interstate 49 test sections. Three commercially available silanes were applied to the indicated test panels, and three sections remained untreated as control samples. 132
Fig. 4.3-2–Panel with pins for strain measurements (by Richard Deschenes Jr.). 132
Fig. 4.3-3–Typical DRI sample with reference grid (by Richard Deschenes Jr.). 135
Fig. 4.5-1—Temperature-corrected strain (%) measured in the travel direction for control and silane-treated pavement panels. Error bars represent the 90% confidence of the mean. 138
Fig. 4.5-2–Temperature-corrected strain (%) measured in the transverse direction for control and silane-treated pavement panels. Error bars represent the 90% confidence of the mean. 139
Fig. 4.5-3–Joint spalling (left) and discoloration (right) (by Richard A. Deschenes). 140
Fig. 4.5-4–Temperature (°C) with respect to date, error bars indicate 90% confidence of the mean, Interstate 49. 142

Fig. 4.5-5– Internal-RH (%) with respect to time, error bars indicate 90% confidence of the mean, Interstate 49. 143
Fig. 4.5-6–DRI for core samples taken from pavement panels, error bars represent standard deviation, Interstate 49. 146
Fig. 4.5-7–Photomicrograph of coarese-aggregate particle with microcracking (A) and corroded aggregate particles, indicated by red arrow (B). Field of view is 10.0 mm x 10.0 mm (15X magnification) (by Richard Deschenes Jr.). 147
Fig. 5.1-1-D-Cracking in concrete pavement, Interstate 49 (by Richard Deschenes Jr.). 160
Fig. 5.4-1–Strain (%) with respect to time (days), highly-reactive fine aggregates (A, B, C) and moderately-reactive aggregates (D, E, F). 173
Fig. 5.4-2–Strain (%) with respect to VP (kPa), highly-reactive aggregate (A) and moderately-reactive aggregate (B). 176
Fig. 5.4-3– Strain (%) (A) and mass change (B) with respect to time (days), concrete prisms exposed to conditions which promote ASR, F/T, or ASR and F/T. 179
Fig. 5.4-4– Strain (%) (A) and mass change (B) with respect to time (days), concrete prisms exposed to conditions which promote a combination of ASR and F/T. 180
Fig. 8.1-1–Horizontal (A) and vertical (B) strain (%) with respect to date, Interstate 49 barrier wall exhibiting minimal deterioration, control section (C-1). 211
Fig. 8.1-2–Horizontal (A) and vertical (B) strain (%) with respect to date, Interstate 49 barrier wall exhibiting minimal deterioration, silane section (S-1). 212
Fig. 8.1-3–Horizontal (A) and vertical (B) strain (%) with respect to date, Interstate 49 barrier wall exhibiting minimal deterioration, linseed section (L-1). 213

Fig. 8.1-4–Horizontal (A) and vertical (B) strain (%) with respect to date, Interstate 49 barrier wall exhibiting minimal deterioration, elastomeric paint section (EP-1). 214
Fig. 8.1-5–Horizontal (A) and vertical (B) strain (%) with respect to date, Interstate 49 barrier wall exhibiting minimal deterioration, silane 2 section (S2-1)..... 215
Fig. 8.1-6–Horizontal (A) and vertical (B) strain (%) with respect to date, Interstate 49 barrier wall exhibiting moderate deterioration, control section (C-2)..... 222
Fig. 8.1-7–Horizontal (A) and vertical (B) strain (%) with respect to date, Interstate 49 barrier wall exhibiting moderate deterioration, silane section (S-2). 223
Fig. 8.1-8–Horizontal (A) and vertical (B) strain (%) with respect to date, Interstate 49 barrier wall exhibiting moderate deterioration, linseed section (L-2)..... 224
Fig. 8.1-9–Horizontal (A) and vertical (B) strain (%) with respect to date, Interstate 49 barrier wall exhibiting moderate deterioration, elastomeric paint section (EP-2)..... 225
Fig. 8.1-10–Horizontal (A) and vertical (B) strain (%) with respect to date, Interstate 49 barrier wall exhibiting moderate deterioration, silane 2 section (S2-2). 226
Fig. 8.1-11–Horizontal (A) and vertical (B) strain (%) with respect to date, Interstate 49 barrier wall exhibiting severe deterioration, control section (C-3). 233
Fig. 8.1-12–Horizontal (A) and vertical (B) strain (%) with respect to date, Interstate 49 barrier wall exhibiting severe deterioration, silane section (S-3)..... 234
Fig. 8.1-13–Horizontal (A) and vertical (B) strain (%) with respect to date, Interstate 49 barrier wall exhibiting severe deterioration, linseed section (L-3)..... 235
Fig. 8.1-14–Horizontal (A) and vertical (B) strain (%) with respect to date, Interstate 49 barrier wall exhibiting severe deterioration, elastomeric paint (EP-3)..... 236

Fig. 8.1-15–Horizontal (A) and vertical (B) strain (%) with respect to date, Interstate 49 barrier wall exhibiting severe deterioration, silane 2 section (S2-3). 237
Fig. 8.2-1–Strain (%) with respect to time for Interstate 49 control panels, travel (A) and transverse (B). 242
Fig. 8.2-2–Strain (%) with respect to time for Interstate 49 Silane 40A panels, travel (A) and transverse (B). 246
Fig. 8.2-3– Strain (%) with respect to time for Interstate 49 Silane 100 panels, travel (A) and transverse (B). 250
Fig. 8.2-4–Strain (%) with respect to time for Interstate 49 Silane 40B panels, travel (A) and transverse (B). 254

NOTATIONS

AAR:	Alkali-Aggregate Reaction
ASR:	Alkali-Silica Reaction
F/T:	Freezing and Thawing
RH:	Relative Humidity
DEMEC:	Detachable Mechanical Strain Gauge
DRI:	Damage Rating Index
SDT:	Stiffness Damage Test
PFE:	Potential for Further Expansion
FWD:	Falling Weight Deflectometer
W/D:	Wetting and Drying
CCA:	Closed Cracks in the Aggregate Particles
OCA:	Opened Cracks in the Aggregate Particles
OCAG:	Opened Cracks in the Aggregate with Gel Product
CAD:	Debonded Coarse Aggregates
DAP:	Dissaggregated Aggregate Particles
CCP:	Cracks in the Cement Paste
CCPG:	Cracks in the Cement Paste with Gel Product

LIST OF PUBLISHED AND SUBMITTED PAPERS

Chapter 2: Deschenes, R. Jr., and Hale, W. M. (2016). "Alkali-silica reaction in concrete with previously inert aggregates." *Journal of Performance of Constructed Facilities*, ASCE, 31(2), 8 pp. DOI: 10.1061/(ASCE)CF.1943-5509.0000946. (Published).

Chapter 3: Deschenes Jr. R., Murray C.D., and Hale W. M. (2017). "Mitigation of ASR and freezing and thawing through surface treatment." *ACI Materials Journal*, 114(2), 307-314. DOI: 10.14359/51689493. (Published).

Chapter 4: Deschenes Jr., R. A., Giannini, E., Drimilas, T., Fournier, B., and Hale, W. M. (2017). "Mitigation of ASR and freeze thaw in concrete pavement through silane surface treatments." (Submitted for review).

Chapter 5: Deschenes Jr., R. A., Giannini, E., Drimilas, T., Fournier, B., and Hale, W. M. (2017). "Another look at the effects of relative humidity, temperature, and freezing and thawing on the development of alkali-silica reaction." (Submitted for review).

1. INTRODUCTION AND RESEARCH OBJECTIVES

1.1. INTRODUCTION

Concrete durability is an important consideration when developing structures with design lives from twenty to over one-hundred years. Alkali-silica reaction (ASR) and freezing and thawing (F/T) durability issues develop over extended periods of time in concrete and reduce the useful service life. Deterioration of concrete structures may occur when constituents within the concrete are not durable under the exposure conditions. ASR occurs when certain siliceous phases within the aggregates react deleteriously with hydroxyl ions in the cement pore solution. As a result, expansive alkali-silica gel forms and imbibes pore solution resulting in swelling, cracking, and possibly failure of the concrete element. The dissolution of silica increases with temperature and the formation of alkali-silica gel is accelerated at higher temperatures. Once alkali-silica gel forms, swelling occurs as pore solution is drawn into the gel product by osmotic pressure. This process requires sufficient moisture within the pore solution. When sufficient moisture is not available, the alkali-silica gel does not swell and deterioration does not occur. ASR deterioration occurs first as microcracks within the aggregate particles and cement paste. As deterioration proceeds, the microcracks propagate and interconnect to form a network of microcracks within the concrete. If deterioration continues visible macrocracks may form at exposed surfaces of the concrete. As ASR expansion causes radial stresses, cracks typically appear randomly in unrestrained concrete. The pattern of cracking is sometimes described as map cracking. When the concrete is restrained along one axis, oriented cracks may form parallel to the restraint, as can be seen in **Fig. 1.1-1**. Severe expansion may lead to crushing at the joints and when sufficient alkali-silica gel forms, the gel may be exuded from the concrete causing discoloration. Deleterious ASR is typically prevented during construction by minimizing the

risk of alkali-silica gel formation. This can be accomplished by: (1) reducing the alkalinity of the cement pore solution; (2) replacing the reactive aggregate; or (3) incorporating an admixture which changes the pore solution chemistry, or alters the cement paste or alkali-silica gel composition. Supplementary cementitious materials (SCMs) such as fly ash, slag cement, or silica fume reduce porosity and bind alkalis and calcium within hydration products reducing the risk of ASR. Alternatively, lithium salts can be added to the concrete mixture to prevent the formation of expansive alkali-silica gels by altering the chemistry of the pore solution and gel.

F/T deterioration occurs in concrete when the cement paste or aggregate deteriorate due to water freezing within the cement paste or aggregates. Water within the cement paste or aggregate expands and moves as it cools, causing pressure on the cement paste which leads to cracking and deterioration. Water moves through the tortuous pore spaces within the cement paste, resulting in viscous resistance to flow and pressure. When water moves too far, the resulting pressure may cause deterioration of the cement paste. This is typically averted by entraining air voids into the concrete, which are spaced closely enough to prevent deleterious pressure from developing. Deterioration can also occur if D-cracking susceptible coarse aggregate particles become critically saturated, and water is expelled on cooling. The water may be expelled too quickly to dissipate safely into the surrounding cement paste and air-voids. Therefore, the cement paste in the interfacial transition zone (ITZ) deteriorates. Deterioration occurs first as microcracks within the ITZ, on repeated cycles of F/T, the cracks propagate and interconnect forming a network. The cracks often appear at the exposed surfaces of concrete adjacent to joints. In air-entrained concrete pavements, the cracks curve along the joints at corners forming a typical D pattern known as D-cracking. An example of D-cracking is shown in **Fig. 1.1-2**.

Fig. 1.1-1–Typical deterioration in concrete barriers due to F/T and ASR (by Richard Deschenes Jr.).

Fig. 1.1-2–Typical deterioration in concrete pavements due to F/T and ASR (by Richard Deschenes Jr.).

Both ASR and F/T require moisture within the concrete for deterioration to occur, and both are exacerbated by the ingress of moisture. Therefore, symptoms are often worsened near joints, where the concrete more readily absorbs water. As deterioration progresses and cracks form along the surface, the concrete becomes more permeable and deterioration accelerates. The formation of ASR related deterioration can exacerbate F/T deterioration as additional water is absorbed into the concrete over time. Alkali-silica gel draws water towards the reaction site maintaining the concrete at a higher moisture state and increasing the risk of F/T. The alkali-silica gel product also fills microscopic air voids reducing the space for water to occupy on freezing, thereby reducing the F/T durability of concrete.

Although ASR and F/T can be prevented in concrete following best-practices and specifications, cases arise due to inadequate material testing. When ASR or F/T deterioration are diagnosed in a transportation structure, originally designed to last twenty to one-hundred years, mitigation measures are required to extend the remaining useful life of the structure. When practical, reducing the availability of moisture within concrete has been most effective for extending the service life. Materials such as silane are applied externally to concrete structures, blocking liquid water from entering the concrete while allowing water-vapor-transmission over time. As a result, the concrete dries towards ambient conditions. A review of the relevant literature is presented in **Section 1.2**. The literature indicates silane treatment are effective in mitigating cases of ASR in concrete barriers and columns with large surface-area-to-volume ratios and drying from multiple sides. Currently, results are promising for concrete elements within bridge structures and barrier walls. However, results are not available to decide on the efficacy of silane applied to concrete pavements. Additionally, research indicated silane may be a viable measure for slowing deterioration due to a combination of ASR and F/T in concrete elements and pavements. These limitations in the current literature lead to the study presented within this dissertation.

1.2. RESEARCH OBJECTIVES

The primary scientific objective of this research was to investigate the combined effects of ASR and F/T deterioration in concrete structures. This objective was furthered by investigation methods for mitigating the effects of ASR and F/T in concrete barrier walls and pavements.

The objective was achieved through an investigation involving the following phases:

1. Determine the cause of premature deterioration observed in several concrete transportation structures in Arkansas, which were constructed using an aggregate previously thought to be inert.
2. Determine the combined effect of F/T and ASR deterioration in concrete containing moderately-reactive fine aggregates through field-monitoring and validate the results through laboratory testing.
3. Conduct a field investigation of ASR and F/T deterioration in concrete transportation structures following current FHWA guidelines. Observe limitations of current practices and provide recommendations for refining future research programs.
4. Develop mitigation measures for concrete barriers exhibiting moderate to severe deterioration due to a combination of ASR and F/T. Measure the efficacy of surface treatments over a three-year period through expansion and RH monitoring.
5. Develop practical methods to extend the service life of concrete pavements deteriorating due to ASR and F/T. Monitor the efficacy of treatment for three-years through expansion, RH, and petrographic methods.
6. Evaluate the relationship between temperature, RH, and time on the development of ASR in concretes containing moderately and highly reactive fine aggregates. Determine a threshold-RH required for the development of deleterious ASR expansion in concrete at various temperatures.
7. Develop a modified test method which accelerates deterioration due to a combination of ASR and F/T and simulates the conditions observed in the field. Investigate the effects of F/T and wetting and drying on the development of ASR in concrete containing a borderline reactive aggregate which passes current standardized ASR test methods.

1.3. LITERATURE REVIEW

1.3.1. Alkali-Silica Reaction (ASR)

Stanton (1940) documented the first case of alkali-silica reaction (ASR) diagnosed in the United States, while investigating the premature deterioration of several concrete structures in California. The deterioration appeared to result from internal expansive stresses that could not be explained by any known process. Stanton (1940) began a laboratory assessment of the aggregates and cement used in the concrete. Using various curing conditions, including wetting, drying and elevated temperatures, no excessive expansion was noted (Stanton, 1940). However, similar samples containing high alkali cement and stored under high humidity developed excessive expansion after one year. Stanton (1940) observed that when low alkali cements were used, no excessive expansion occurred. Stanton (1940) concluded certain minerals present within the aggregates develop excessive expansion when used in combination with high alkali cement. A limit of 0.6% cement alkalis was proposed to prevent expansion in concrete containing these aggregates (Stanton, 1940).

Powers and Steinour (1955) provided a comprehensive look at the mechanism of ASR. Silica phases range in structure from dense structured minerals such as quartz to highly disordered amorphous forms such as opal and volcanic glass. In the presence of alkali hydroxides, the silica structure can be attacked, replacing hydroxyl ions along the surface with sodium or potassium. The process continues with the breakdown of silica-oxygen bonds and the dissolution of the silica structure (Powers and Steinour, 1955). Calcium hydroxide has a role in the development of swelling alkali-silica gels, and at higher concentrations tends to produce water-insoluble calcium-alkali-silica products. To explain the presence of alkali-silica gel in concrete containing excess calcium, Powers and Steinour (1955) postulated the diffusion rate of calcium, and much

lower solubility relative to alkalis, accounts for limited transportation of calcium to the reaction site allowing swelling alkali-silica gels to develop. The process was described as a layer of lime (calcium) alkali-silica which develops at the periphery of the reaction site and the surrounding cement paste, and inhibits the transport of additional calcium to the reaction site thereby preventing an excess of calcium. Swelling of the alkali-silica gel occurs as water moves from the cement paste toward the reaction site, due to a gradient in energy states between the pore solution and alkali-silica gel (Powers and Steinour, 1955). The pore solution is drawn into the alkali-silica gel by osmotic pressure and reacts with the silica structure displacing alkalis and attaching to the exposed oxygen, resulting in an expanded structure. Swelling results in an increase in volume and has sufficient energy to produce a net pressure on the surrounding concrete matrix (Powers and Steinour, 1955).

Chatterji (1989) proposed an alternate hypothesis to explain the formation of alkali-silica gel and the swelling mechanism. The high pH of concrete results in a high concentration of hydroxyl ions (OH^-) in the pore solution. The hydroxyl ions attack and penetrate the siliceous mineral phases, followed by the absorption of cations. The absorption rate of cations into silica depends on the concentration of cations present in solution (e.g. K^+, Na^+, Li^+, Ca^{++}). Smaller cations, such as Na^+, will penetrate faster than larger cations like Ca^{++} (Chatterji, 1989). The hydrolyses of siloxane bonds weakens the silica structure allowing the reaction to proceed further into the silica phase. As the reaction proceeds, silica diffuses out of the mineral at a rate governed by the Ca^{++} concentration of the pore solution (Chatterji, 1989). Expansion occurs when more solution (Na^+, Ca^{++}, OH^-, or water) enters the reactive silica phase than diffuses out into solution. The mechanism hypothesized by Chatterji (1989) also explains the relationship between alkali-silica reaction rates and increasing concentrations of alkali salts (NaOH, KOH). The ionic strength of

these salts solutions, at increasing concentrations, increases absorption of solution into the reaction site and increases swelling. The hypothesis also resolves some of the limitations in the Powers and Steinour (1955) explanations. Swelling alkali-silica gels may still occurs when calcium rich pore solution is present, because calcium is absorbed into the reaction site although at a slower rate than other cations. The role of pozzolans in reducing the occurrence of expansive alkali-silica gels is explained by the additional transformation of $Ca(OH)_2$ into C-S-H in the pozzolanic reaction, which decreases the concentration of OH^-, K^+, Na^+, and Ca^{++} in pore solutions.

Diamond (1989) provided another look at the mechanism of ASR, starting with the important distinction between the development of alkali-silica gel and the process of swelling. When sufficient Ca^{++} is not available, alkali-silica gel can develop without leading to deleterious swelling (Diamond, 1989). Diamond (1989) offers a similar explanation for ASR expansion as Powers (1955), in that osmotic pressure causes swelling. The difference in energy states between the pore solution and alkali-silica gel results in an absorption of pore solution into the gel. The absorption causes swelling, which results in pressure on the surrounding matrix. Due to the insolubility of alkali-silica gel in pore solution, the gel itself acts as a semi-permeable membrane separating the pore solution from the solution within the alkali-silica gel. This permits the development of a concentration gradient and osmotic pressure (Diamond, 1989). The process of ASR expansion is similar to that proposed by Powers (1955) and Chatterji (1989): first, a high concentration of alkali hydroxides is present in the pore solution; these release hydroxyl ions into solution which break down the silica phase in the aggregate to produce alkali-silica gel. The alkali-silica gel is insoluble in pore solution and retains a portion of alkalis absorbed from the pore solution.

Diamond (1989) recognized a linear relationship between the hydroxyl ion concentration of the pore solution and the alkali content of the cement (in equivalent alkalis Na_2O_{eq}). This relationship indicates that higher alkali cements directly increase the concentration of hydroxyl ions in the cement pore solution, which results in increased dissolution of silica in the aggregate and the development of ASR gel. Again, calcium is proven as a required component in the development of swelling alkali-silica gels. Diamond (1989) found that silica which dissolved in the presence of alkalis, without any Ca^{++}, does not form swelling alkali-silica gel (Diamond, 1989). Diamond (1989) notes the presence of calcium hydroxide typically found at the interfacial zone between aggregates and cement paste, which would be necessary for the development of expansive alkali-silica gels.

Wang (1991) provided an extension of the hypothesis presented by Chatterji (1989). The reaction begins at the interface between the silica phases and pore solution. The pore solution contains cations (Na^+, K^+, and Ca^{++}) and an equilibrium concentration of hydroxyl ions (OH^-). The silica surface is composed of silanol (Si-O-H) groups; the hydrogen proton (H^+) is first replaced by an alkali ion, releasing the proton into solution. Sodium or potassium may be released from the surface in exchange for calcium, and proceed to attack internal siloxane bonds within the silica mineral. As a result, additional silanol bonds are exposed to the pore solution allowing the process to continue (Wang, 1991). The alkali ions, which have formed bonds with exposed silanol groups, are then replaced with available calcium ions freeing up alkalis to further the reaction process. The alkali-silica groups formed along the surface tend to produce a colloidal alkali-silica structure with a strong affinity for water and result in swelling at the reaction site. The rate at which ions diffuse to the reaction site is higher for alkalis (Na^+, K^+) as compared to calcium hydroxide ($Ca(OH)_2$). Wang (1991) attributes this to the higher solubility

and concentration of potassium and sodium in the pore solution. As the reaction proceeds, calcium diffuses into the silica recycling alkalis to continue the process. The exchange of alkalis for calcium occurs due to the much higher energy state of calcium as compared to alkalis.

Based on the hypothesized reaction mechanism, Wang (1991) postulates that a gradation in alkali concentrations will be present along the reaction rim of the silica particle. Due to the exchange of alkalis for calcium, the concentration of a band of alkalis should be present along the leading edge of the reaction rim, while a band with higher calcium concentration should follow (Wang 1991). This theory has been supported by electron probe microanalysis and X-ray spectrometry.

In a study of ASR in concretes containing fly ash, Bleszynski (1998) provided evidence to support the ASR mechanism proposed by Wang (1991). Using backscatter electron imaging to map the concentration of alkali-silica gel within reactive aggregate particles, Bleszynski (1998) found a band of high calcium along the outer edge of the reactive particle. The leading edge of the reaction rim, however, contained less calcium and more silica. The analysis also revealed a layer of sodium-rich silica at the aggregate interface and a layer of potassium-rich silica between this layer and the calcium-rich later. The study reinforces the alkali recycling and the need for Ca^{++} in the development of swelling alkali-silica gels (Bleszynski, 1998).

Helmuth (1993) provided a comprehensive look at ASR reaction and expansion mechanisms. An important factor in the occurrence and rate of ASR is the type of silica phases present within the concrete. Silica ranges from highly ordered forms, such as quartz, to amorphous, disordered silica such as opal. Quartz minerals contain primarily three-dimensional silica, with all four oxygen atoms linked to adjacent silicon atoms in a siloxane bond (Helmuth, 1993). Opal, however, contains broken siloxane bonds that have linked with protons (H^+) to form silanol (Si-O-H) groups.

Helmuth (1993) provides a similar reaction process to that proposed by Wang (1991) and Chatterji (1989), which is supported by NMR testing. The reaction begins with the breakdown of silanol groups along the surface, due to hydroxyl ions present in the pore solution. Alkalis (K^+, Na^+) then replace protons (H^+) in the silanol groups (Helmuth 1993). This process is followed by hydroxyl ions attacking the siloxane bonds, and provide additional silanol sites for alkalis to bond with. This process continues, and exposed silanol groups draw additional pore solution into the alkali-silica gel formed within the reactive aggregate, resulting in expansion (Helmuth, 1993). Calcium is again important in the development of ASR; the solubility of calcium hydroxide is lower than that of alkalis (Helmuth, 1993). The pore solution is saturated with calcium hydroxide; however, the concentration of calcium is lower in solutions containing alkalis. This is due to calcium-silicate-hydrates which form within the reactive silica, thereby releasing alkalis to continue the reaction (Helmuth, 1993). Alkali-silica gels that are transported from the reaction site also contain additional calcium products, which form because of exposure to calcium rich pore solution during transport (Helmuth, 1993).

The understanding of the ASR mechanism has improved along with the technology used to characterize the components (aggregate, cement, pore solution) and reaction products (alkali-silica gel). Rajabipour et al. (2015) provided an update on the current understanding of the reaction mechanisms of ASR. The reaction occurs first when metastable silica phases dissolve in the presence of pore solution, followed by formation of a nano-colloidal silica sol. The nano-colloidal silica sol later transforms into gel and begins to swell (Rajabipour et al. 2015). Highly-degraded silica phases were found to transform directly into alkali-silica gel when sufficient structure remained within the silica.

Rajabipour et al. (2015) noted the dissolution of silica is often the slowest phase of the reaction and controls the rate of ASR formation in concrete. The rate of dissolution depends on silica phases present and the alkalinity and temperature of the concrete. The rate and amount of swelling depends on the availability and transport rate of water within the concrete. The silica phases found in aggregates differ and include macro-crystalline, micro or nano crystalline, and amorphous (Rajabipour et al. 2015). Similar to the process described by Helmuth (1993), the dissolution of silica in pore solution occurs when hydroxyl ions attack the silanol groups exposed to the solution. The formation of alkali-silica gel should lead to a decrease in alkalinity within the cement pore solution as alkalis are incorporated into the gel (Rajabipour et al. 2015). However, Rajabipour et al. (2015) noted, in agreement with previous studies, that some alkalis may be replaced by calcium and recycled into the pore solution. As this process continues, and the concentration of calcium within the cement pore solution decreases, calcium hydroxide dissolves into solution replenishing calcium and increasing the pH (Rajabipour et al., 2015).

Rajabipour et al. (2015) improved on the understanding of the reaction mechanism and showed that silica phases may dissolve into solution until the cement pore solution is saturated with Si. When Ca^{2+} (and smaller concentration of Fe^{2+} and Al^{3+}). are present within the cement pore solution, nucleation and condensation of nano-colloidal silica sol occurs. This continues until larger metal silicate structures lead to the formation of either silicate gel or macro-scale precipitates (Rajabipour et al., 2015).

The mechanism by which gel adsorbs water and swells is still not fully understood. (Rajabipour et al., 2015). One possible mechanism similar to that presented by Diamond (1989) notes that alkali-silica gel is water-insoluble and porous with a large hydrophilic surface area which acts as a semi-permeable membrane. The gel allows water to pass while preventing the diffusion of

silica ions out of the gel (Rajabipour et al., 2015). The difference in Gibbs free energy between the cement pore solution and gel results in an osmotic pressure gradient which transports water into the gel followed by swelling. Prezzi et al. (1997) and Rodrigues, et al. (1999) provide an alternative explanation after observing that swelling may occur due to the electrical double-layer repulsive forces at the surface of solid particles within the gel (Rajabipour et al., 2015).

Rajabipour et al. (2015) also discussed the important role of internal alkali sources in the development of ASR. Alkalis are introduced into the cement pore solution primarily from the cement, but partially from aggregates and SCMs. Certain phases within some aggregates have been found to release alkalis into solution. Synthetic glass and volcanic aggregates may release significant alkalis. Feldspar minerals can release alkalis in exchange for calcium increasing the pore solution alkalinity (Rajabipour et al., 2015).

Bérubé (2002a) measured the contribution of alkalis from certain aggregates indirectly by measuring the cement pore solution alkali concentration of concrete samples. The pore solution alkalinity was measured using the hot water extraction method, which only measures the water-soluble alkali concentration. The samples were pulverized and then boiled in water to dissolve alkalis. The concentration of alkalis was measured using absorption spectroscopy, and the cement alkalis estimated and corrected by comparison with control samples of known alkali concentrations. The same test method was then repeated for samples with various aggregates, and notable differences in alkali concentrations were attributed to the available alkalis introduced by the aggregates. Depending on the aggregate type, large quantities of alkalis can be introduced into the pore solution over time. The highest level observed by Bérubé (2002a) was 12.7 kg/m^3, which is more than sufficient to sustain ASR if a reactive aggregate is present. Aggregates rich in feldspar are more likely to leach alkalis than other mineral types.

1.3.1.1. Symptoms of ASR

SHRP published the *Handbook for The Identification of Alkali Silica Reactivity in Highway Structures* in 1991. The handbook discusses the development of macroscopic symptoms of ASR. The first visible symptom of ASR is often randomly oriented cracks at the surface, which are sometimes described as map cracking due to the random nature. As cracking progresses, the cracks interconnect and widen. In restrained concrete, cracks parallel to the direction of restraint widen more than those in the perpendicular direction. Surface cracking often occurs due to an alkali and strain gradient between the exposed surface of the concrete and the interior concrete (Stark, 1991). The exposed surfaces of the concrete expand less due to alkali leaching and drying, while the internal concrete expand faster. This causes macrocracking near the surface, which is not present throughout the depth of the concrete.

The Federal Highway Administration released the *Alkali-Silica Reactivity Field Identification Handbook* in 2011 (Thomas, 2011). The handbook covers the visible symptoms of ASR as related to different concrete structures. The first visible symptom is often cracking, which appears at first as random pattern cracks. If expansion is restrained in one direction, greater expansion occurs perpendicular to the direction of restrain, and therefore cracking will occur parallel to the direction of restraint. As expansion continues, deformation and relative displacement of the concrete element may occur. After the concrete has expanded and the joints have closed, the concrete will experience local crushing at the joints (Thomas, 2011). In unreinforced pavements, wider and more defined cracks will form in the travel direction, because there is less transverse restraint and the concrete more readily expands in this direction. In jointed pavements, the panels are restrained by adjacent pavement, and deformation may lead to crushing in severe cases. In cases where the pavement panels can displace, adjacent panels may

move panels causing relative displacement at the joints. Another symptom of ASR is popouts of aggregates near the surface of the concrete, which is similar to popouts caused by F/T. The concrete surface may also be discolored near cracks, as alkali-silica gel may be exuded.

Some symptoms of ASR are similar to some other deterioration mechanisms and petrographic examination is required to confirm ASR. Additionally, ASR may occur in combination with other deterioration mechanisms such as F/T (Thomas, 2011). The formation of alkali-silica gel and cracking can decrease the F/T resistance of concrete, even when proper air entrainment is used (Thomas, 2011).

1.3.1.2. Diagnosis of ASR

Microscopic investigation of concrete deterioration is necessary to diagnose the mechanism of deterioration within the concrete. The macroscopic features of ASR may be similar to other deterioration mechanisms such as F/T or D-cracking. An investigation of microscopic features can be used to determine the original deterioration mechanism and to test for the presence of alkali-silica gel. Some readily observed petrographic features of ASR include reaction rims within reactive aggregate particles, microcracking originating at reacted aggregates and propagating into the cement paste and aggregates, and ASR reaction products (Stark, 1991).

Petrography is required to diagnose the presence and extent of ASR in concrete (Walker, 2006; Fournier et al., 2010). If ASR is suspected, then a petrographic assessment can identify the cause of deterioration within the concrete. The petrographic features of interest are cracks within the coarse aggregate, alkali-silica gel filled cracks in the coarse aggregate particles, de-bonded coarse aggregate particles, reaction rims on aggregate particles, corroded aggregate particles, cracks in the cement paste, alkali-silica gel deposits in cracks, and air voids lined/filled with alkali-silica gel (Fournier et al., 2010). Some of these features are not exclusive to ASR and

therefore should be weighted to account for the likelihood of the deterioration being caused by ASR. Alkali-silica gel deposits can be analyzed by SEM or microprobe analysis of thin sections.

Samples are prepared before analysis by cutting and polishing the exposed face. After the sample is prepared, cracks are analyzed under stereomicroscopic magnification (Walker, 2006). Symptoms of ASR are distinguished by considering the presence of reaction products and cracks in the cement paste and aggregates. Cracks which originate in reacted aggregate particles and progress into the surrounding cement paste and aggregates are typical of ASR. The progression of cracks in to the concrete is observed to determine if cracks proceed around aggregate particles or through them as expansion continues (Walker, 2006). The aggregate should be studied to determine whether reaction rims have occurred due to ASR.

An important step in diagnosing ASR is characterizing the reaction products. In cases where ASR has progressed significantly the alkali-silica gel is visible and identifiable. However, without further testing the alkali-silica gel cannot be verified as alkali-silica gel. Therefore, SEM/EDS testing is required to identify the presence of alkali-silica gel and the chemical compositions within the sample. Stark, (1991) and Walker (2006) discusses the uranyl acetate method which can be used to reveal deposits of alkali-silica gel and reaction rims on aggregate particles that are not apparent under visible light. This method is however difficult to conduct due to the risks of working with uranyl acetate. Therefore, SEM/EDS and microprobe methods are more common today.

1.3.1.3. Prevention of ASR

Preventing the development of ASR in concrete can be achieved through a range of measures, which provide increasing likelihood that ASR will not occur over the life of the concrete. A simple yet often extreme method is to replace the susceptible aggregate with an alternative

source that is inert. However, in many cases this is not an economic alternative and the reactive aggregate must be used. Therefore, preventative measures must be followed to ensure ASR does not occur. The first method for reducing the occurrence of ASR was identified by Thomas Stanton (1940) and simply requires limiting the alkalis within the concrete. Stanton (1940) suggested a limit of 0.60% Na_2O_{eq} to prevent ASR when using the reactive aggregates and cements used in his investigation. However, it is now recommended to limit the total alkali content in concrete rather than limiting the alkalinity of the cement (ASTM C1778)

Alkalis: Diamond (1989) observed the linear relation between cement alkali content and the hydroxyl ion concentration of the pore solution, which is a function of cement alkalis, cement content, and water content. Therefore, limiting cement alkalis leads to a direct reduction in pore solution alkalinity. The ACI *State of the Art Report on Alkali-Aggregate Reactivity* (1998) warns that some reactive aggregates may react with cement alkalis as low as 0.40%. Limiting alkali loading better accounts for the range of cement contents used in concrete and reflects the available alkalis within the mixture that may be introduced by aggregates, SCMs, or other sources. Some reactive aggregates may develop ASR with alkali loadings as low as 2.3 kg/m^3 (ACI, 1998). Therefore, the recently published ASTM C1778 specification recommends a maximum alkali loading between 1.8 and 3 kg/m^3 depending on aggregate reactivity and the level of prevention required.

SCMs: Another method of preventing ASR is using supplementary cementitious materials (SCMs), which alter the hydration products and pore solution of concrete. Some examples of SCMs used to prevent ASR include fly ash, slag cement, and silica fume. The primary mechanism by which SCMS mitigate ASR is through the pozzolanic reaction, which converts

calcium hydroxide ($Ca(OH)_2$) into C-S-H and binds alkalis and calcium lowering the pore solution alkalinity (Chatterji, 1989).

The presence of SCMs changes the pore solution to inhibit the development of ASR. SCMs appear to improve the pore solution in two ways: first, they dilute the cement content and therefore the alkalis provided by the cement; second, they form additional C-S-H which adsorbs alkalis and reduces the alkalinity and pH of the pore solution (Helmuth, 1993). Duchesne (1994) conducted an analysis of the SCMs mechanisms which inhibit ASR. Concrete samples containing Class C fly ash or Class F fly ash showed a reduction in pore solution alkalinity over time, which occurred due to alkalis bound within pozzolanic hydration products.

Thomas (1995) wrote a review on the mechanisms by which fly ash and slag cements prevent ASR. There were many conflicting studies that proposed various mechanisms. This was in part due to the alkalis contributed by the SCMs and the variation in chemical, physical, and mineralogical properties of the SCMs (Thomas, 1995). The total alkali content of fly ash was found to range between 1 and 8% Na_2O_{eq}, but tended to be less than 5%. The alkali content of slag ranged from 0.3 to 2.6% Na_2O_{eq}, and tended to be less than 1. % (Thomas, 1995). Much of the alkalis are bound within non-water-soluble phases, with the water-soluble alkali content less than 0.1 percent. The insoluble alkalis, however, may be soluble when exposed to pore solution (Thomas, 1995). The available alkali content, as measured by leaching into saturated $Ca(OH)_2$ solution, was found to be 30 to 40% of the total alkalis for Class F ash, 50 to 75% for Class C ash, and 40 to 60% for slag (Thomas, 1995).

Considerable variability in the efficacy of SCMs as determined through laboratory testing is present due to several factors. The type of aggregate used affects the reactivity of the sample, and therefore the amount of SCM required to inhibit the reaction. The characteristics of the

SCM also impact the ability of the SCM to inhibit ASR. Other factors include cement properties, mix proportioning, sample size, storage conditions, and duration (Thomas, 1995). Thomas (1995) considered the mechanism by which SCMs mitigate ASR in concrete and points out that most laboratory studies do not allow the mechanism to be determined. No consideration is taken for cement alkalis removed from the mixture when replacing a portion of cement with an SCM. Therefore, the effect of dilution alone could be responsible for the changes in expansion measured (Thomas, 1995). Thomas (1995) proposed a few test methods which could be used to determine the mechanism of SCMs beyond simply diluting cement content. These methods including comparing expansion of concrete that contains fly ash to a concrete containing an inert replacement of cement. Alternatively, a portion of the aggregate could be removed and the Portland cement content maintained, or alkalis could be added to compensate for the Portland cement replacement. A method for indirectly measuring the contribution of alkalis from the SCM was proposed (Thomas, 1995). The method involves determining the relationship between expansion in concrete containing an SCM and additional alkalis, to account for alkalis diluted by replacing cement, to the expansion of a control sample without an SCM (Thomas, 1995). The effective alkali contribution of the SCM is then the difference between the expansion for the control and that of the sample with an SCM replacement.

Bleszynski and Thomas (1998) found concrete without fly ash exhibits a high calcium band within the silica particle which acts as a membrane and prevents the diffusion of alkalis from the alkali-silica gel. This is followed by swelling as pore solution is absorbed into the alkali-silica gel. Concrete containing fly ash developes an entirely different alkali-silica gel (Bleszynski and Thomas, 1998). The reactive aggregate particles do not exhibit a high calcium band, and silica simply dissolves in the presence of the high alkali pore solution and diffuses into the pore

solution. More $Ca(OH)_2$ is bound within hydration products by the addition of fly ash, which prevents the formation of insoluble and swelling alkali-silica gels (Bleszynski and Thomas, 1998).

Shehata et al. (1999) evaluated the influence of fly ash composition on the pore solution of hydrated cement. Concrete samples with various combinations of cement and fly ash were prepared and the pore solution extracted for analysis. Several Class C ash and Class F fly ashes were evaluated, which contained different alkali contents. The Class C fly ashes with higher CaO content had a higher available alkali content than ashes with less CaO. Fly ashes with low CaO reduced further the pore solution alkalinity than would be expected due to dilution alone. In general, the higher the alkali concentration of the fly ash the less a reduction provided to the pore solution alkalinity. The greater portion of alkalis releases by higher CaO ashes was explained by a lower proportion of alkali binding by the hydration products or more of the alkalis being soluble and therefore being released into the pore solution (Shehata et al., 1999).

Thomas et al. (2013a) noted the ability of an SCM to mitigate ASR depends primarily on the silica content of the SCM, but also the chemical and physical composition of the SCM. As the silica content of the SCM decreases, or the alkali and calcium content increases, the efficacy of an SCM decreases and a higher replacement of cement is required. He observed that as aggregate reactivity and alkali availability (from the cement, SCM, aggregate, or external sources) increases, the amount of SCM required to mitigate ASR increases. Thomas et al. (2013a) and Rajabipour et al. (2015) both stated that the primary mechanism by which SCMs mitigate ASR is through the formation of insoluble reaction products (C-S-H) which bind alkalis from the cement pore solution. Rajabipour et al. (2015) noted that the pozzolanic reaction converts calcium hydroxide to C-S-H which binds alkalis and reduces the concentration of Ca^{2+}

within the cement pore solution. Although alkali-silica gel may continue to form, the gel is less viscous, and therefore less hygroscopic and expansive (Rajabipour et al., 2015).

Some SCMs (and aggregates) contain soluble alkalis which increase the pore solution alkalinity of concrete over time (Shehata, 1999; Bérubé et al., 2002a; Rajabipour et al., 2016). Bérubé (2002a) and Duchesne (1994) found that fly ash and slag cements release available alkalis over time into the pore solution. The test revealed that 100% of cement alkalis and 40% of SCM alkalis are initially soluble within the pore solution. However, the remaining alkalis within the SCM are released over time and 100% become soluble within one year. A portion of cement and SCM alkalis become trapped within pozzolanic hydrates (C-S-H) and do not enter solution (Duchesne, 1994). The SCMs (which did not contain excess alkalis) incorporated more alkalis into hydration products than released into the pore solution. A conservative estimate of available, or soluble, alkalis contributed by silica fume, fly ash, and slag cement, are 100%, 17%, and 50%, respectively (Duchesne, 1994).

Thomas et al. (2013a) provided an extensive review on the alkali-binding capacity of SCMs. Generally, SCMs lower the cement pore solution alkalinity of concrete. However, high calcium and high alkali SCMs are less effective at binding alkalis. The ratio of calcium to silica (Ca/Si) has been used to estimate the ability of pozzolanic hydrates (C-S-H) to bind alkalis. More recently, an improved relationship, or chemical index, was developed which accounts for both the ratio of Ca/Si and alkalis. This chemical index predicts the ability of SCMs to decrease pore solution alkalinity and was developed based on results from various authors. The chemical index provides a relationship between the chemical constituents of SCMs and the concrete pore solution alkalinity. The index was developed from pore solution data from two-year CPT prisms (Thomas et al. 2013a). A chemical index of $(Na_2O_{eq} \times CaO)/(SiO_2)^2$ had the best correlation

with pore solution alkalinity data. This model, however, is based on the oxide and alkali content of the SCMs, and does not consider the physical or mineralogical properties, which may also affect the efficacy.

1.3.1.4. Mitigation of ASR

Moisture is one of the key ingredients necessary for ASR to occur and proceed within concrete. Without sufficient moisture, alkali-silica gel becomes dormant, and swelling does not occur within the concrete. Stark (1990) and Bérubé et al. (2002b) conducted research to measure the moisture level required for ASR to occur within concrete. Both researchers determined that when moisture, measured as internal-RH, decreases below 80% (21 to 24 °C), the swelling mechanism becomes dormant. Therefore, reducing the available moisture within concrete is a viable remediation method. Subsequent research conducted by Bérubé et al. (2002b), Folliard et al. (2012), Drimalas et al. (2012), Thomas et al. (2012), and others demonstrates the efficacy of such remediation methods.

Surface treatments produce a vapor-transmissive hydrophobic layer, which penetrates and bonds to the surface of the concrete. This layer inhibits liquid water from entering the concrete, while allowing water vapor to pass (Rust, 2009). If the concrete element is sufficiently thin, with a large surface area (surface-are-to-volume ratio), and the concrete is protected from rain-water and runoff, the RH within the concrete will tend toward equilibrium with the average ambient-RH (Stark, 1990). In many environments, the average ambient-RH is less than 80%, and ASR related expansion will cease when the internal-RH of the concrete drops below 80%.

Several vapor-transmissive surface treatments are available, including alkylalkoxysilane, oligosiloxane, and elastomeric paint. Bérubé et al. (2002b), Folliard et al. (2012), Drimalas et al. (2012), Thomas et al. (2012), and others have evaluated the efficacy of surface treatments

applied to concrete transportation structures including median barriers and bridge elements. Limited research, however, considers surface treatments applied to concrete pavements.

Silanes consist of silicone molecules, which have several functional groups. The functional groups react with cement alkalis to bond to the surface of the concrete and develop a silicone resin network. The silicone also contains hydrocarbons attached to the silicone network, which provide a hydrophobic network along the exposed surface of the concrete. The advantage of penetrating sealers, such as silane, is they remain breathable thereby allowing water vapor to escape from the concrete while preventing liquid water from entering (Rust, 2009).

Several workers have evaluated surface treatments in an effort to mitigate ASR, and silanes have exhibited the most promising results when applied to median barriers, bridge elements, and columns. Stark et al. (1993) provides short-term results of silane treatments applied to concrete pavement. The following sections discuss the beneficial conclusions from research into silane surface treatments, followed by limitations of the research.

Early work published by Kobayashi et al. (1989) first investigated silane as an ASR mitigation method in the laboratory. The silanes used in the study included poly-siloxane and alkyl-alkoxyl-silane, referred to as modified silane or simply as silane. The results demonstrate silane beneficially reduces expansion related to ASR. Unfortunately, the results from a 1991 field trial deemed silane an ineffective treatment method for concrete pavements with ASR (Stark et al., 1993). The test setup relied on internal-RH measurements to determine the efficacy of silane in reducing moisture within concrete bridge decks and a concrete pavement. Within the bridge deck, internal-RH remained below 81% (21 °C) even in the untreated sections. Therefore, the results of treatment were inconclusive. However, in the pavement, internal-RH ranged from below 80% (21 °C) within the top 25 mm (1 in.) of the pavement, to 95% (21 °C) in the middle

of the slab. Less than two years of monitoring were conducted, whereas a minimum of three years is recommended to determine the efficacy of a sealer (Fournier et al, 2010; Thomas et al., 2013b). More than three years of monitoring may be required for concrete pavements as drying only occurs through one exposed face.

An additional research program, conducted by the Nevada DOT, evaluated silane sealers applied to ASR-affected interstate pavements (Stark et al., 1993). The research method involved *falling weight deflectometer* (FWD) measurements before treatment, and again one year after treatment. The FWD test method measures the deflection in a pavement panel after impact with a falling weight. The test method is correlated to elastic modulus of the concrete and repeated measurements can be used to quantify deterioration. The silane treated section showed a small decrease in deflection over the same period, indicating no additional deterioration occurred. However, the change in FWD was not statistically significant during the one-year monitoring period. No additional results from FWD monitoring have been published and it remains unclear if this method is effective in monitoring the progress of ASR in concrete pavements. The author concluded silane did not slow the rate of deterioration relative to the untreated control sections. Without additional monitoring of concrete pavements, no conclusion should be made on the efficacy of silane.

A ten-year study of silane and siloxane sealers applied to median barriers, conducted by Bérubé et al. (2002b), indicated silane as an effective method for reducing moisture (RH) and expansion within concrete. The treatments evaluated included silane, oligosiloxane, and polysiloxane. No information is available on the types of silanes used in the study. After ten years of monitoring, the concrete median barriers treated with silane or siloxane exhibited average internal-RH below 80% (21 °C). In addition, expansion within the treated sections continued to decrease relative to

the control section six years after treatment. Both silane and siloxane sealers proved effective; while, the siloxane was less effective than silane and began showing reduced effectiveness after six years. Bérubé et al. (2002b) suggests reapplication of sealers after six years of exposure.

The FHWA *ASR development and deployment program* included several field trial programs, where surface treatments applied to concrete transportation structures were evaluated. Thomas et al. (2012) and Drimalas et al. (2012) provide preliminary results from several of these trials. The field trials included surface treatment with silanes, including alkylalkoxysilane and alkyltrialkoxysilane. Updated results on this project were published in a final report, and are discussed later in this section (Thomas et al., 2013b). The evaluation program consisted of expansion, internal-RH, and cracking index measurements, in addition to non-destructive test methods. Core samples were also extracted for Damage Rating Index (DRI) and Stiffness Damage Test (SDT) before treatment.

Drimalas et al. (2012) discussed several field trials from the FHWA *ASR development and deployment program*. The field trials included concrete transportation structures such as bridge columns, and median barriers. The selected treatments included lithium nitrate, elastomeric paint, and three different silanes. The silanes consisted of either 20% or 40% water-based alkylalkoxysilane. Monitoring included expansion, internal-RH, and cracking index measurements. The preliminary results, from six years of monitoring, show silane provides the greatest reduction in expansion as compared to the control sections.

Folliard et al. (2012) reported results of surface treatments applied to ASR-reactive concrete blocks, slabs, and columns, were evaluated at an outdoor exposure site at The University of Texas at Austin. The surface treatments included several lithium nitrate application rates and both 40% and 100% silanes. Preliminary results from three years of expansion and internal-RH

monitoring show lithium was ineffective and both silanes reduced expansion in the treated specimens as compared to the control.

Thomas et al. (2013b) provided an updated report to the Federal Highway Administration (FHWA) on the outcomes of the research programs initiated by Thomas et al. (2012), Drimalas et al. (2012), and Folliard et al. (2012). The report covered a range of treatment methods and monitoring techniques applied to transportation structures throughout the United States. Results from treatment and monitoring of an arch bridge in Alabama reveal that even three years after treatment the humidity in the concrete had not significantly decreased and expansion had continued. The concrete arch elements were close to 1 m (39 in.) thick and exposed to very warm and humid conditions. The elements were likely too thick for the silane treatment to be effective.

In November 2011, a section of concrete pavement near Pine Bluff, Arkansas was diagnosed with ASR (Thomas et al. 2013b). The pavement was 28 cm (11 in.) thick and spanned 19 km (12 mi). Core samples were extracted for petrographic examination including DRI. Pavement sections were instrumented for expansion and internal-RH monitoring and then treated with silane. However, only one year of results were reported in Thomas et al. (2013b). And no monitoring has been conducted since, therefore the long-term efficacy of the silane treatment remains unknown.

A barrier wall in Leominster, Massachusetts was diagnosed with ASR in 2005. Several sections of the wall were treated with silane in 2005 and then with elastomeric paint in 2010. After five years of monitoring, the silane treated sections appear to be expanding slower than untreated control sections and the visual appearance of the concrete was noticeably improved (Thomas et al., 2013b). An interesting note from the project was the issues with measuring RH. The sleeves

and plugs used for measuring internal-RH were often damaged from plowing, and the undamaged sleeves were often found to have water condensation between measurements, which affects the measured RH (Thomas et al., 2013b).

Bridge columns with ASR in Houston, Texas were treated with a range of surface treatments. Expansion of the concrete and internal-RH were monitored over the test duration. Silane was observed to mitigate expansion over the seven-year monitoring program. Expansion was measured at the surface of the column, but it is unclear if this strain represents the expansion of the cover or bulk concrete. The columns had a large cross section of 2 m by 2 m (6.6 ft.) which may have been partially hollow. Given the thickness, it was surprising that silane was effective for such a massive concrete element. The column was internally reinforced, which limits expansion of the internal concrete, and alkali leaching slows expansion in the unrestrained cover. Silane was, however, observed to mitigate expansion in the column, although some expansion continued to occur.

In 2010, a section of median barrier in Montpelier, Vermont was diagnosed with ASR and treated with silane. Sections of the barrier were instrumented for expansion and internal-RH monitoring. At the time of the report only two years of monitoring data was available, which was not sufficient to determine the efficacy of silane (Thomas et al., 2013b).

1.3.1.5. Field Investigations

After diagnosing ASR in concrete, field monitoring is necessary to determine the rate of deterioration. Several field-monitoring techniques are available to assess the progress of damage within concrete elements. When assessing concrete transportation elements, field-monitoring practices include periodic expansion, internal-RH, crack mapping, or non-destructive test (NDT) measurements. Fournier et al. (2010), Thomas et al. (2013a), and Thomas et al. (2013b) have

summarized field monitoring techniques in detail, and the three standard methods are discussed below.

Expansion: The expansion of concrete is a quantifiable symptom of ASR deterioration. Several methods for measuring expansion are available and the most practical method depends on the concrete element. Surface strain gauges are a practical for periodically monitoring expansion in concrete transportation structures. Fournier et al. (2010) recommended measuring expansion in transportation structures by instrumenting the concrete element with a 0.5 m (20 in.) grid (Thomas et al., 2013). Gauge pins are a is embedded into the concrete at each corner of the grid with epoxy. Each pin has a pre-drilled indentation on the exposed face which is matched up with the points on the *detachable mechanical strain gauge (*DEMEC). The DEMEC gauge has a fixed end and a pivoting arm on the free end. The points on both ends are inserted into the indented pins on the concrete, and length-change is reported on the digital gauge. Strain is then determined from the length-change and the initial gauge length. Alternatively, gauge studs and a DEMEC gauge can also be used to monitor expansion or relative displacement across joints.

The advantage of a square grid is two strain measurements from each perpendicular axis. Multiple measurements along each axis provides reduced error and redundancy if a pin is damaged. Typical DEMEC gauges provide an accuracy of ±0.001 mm, or ±0.0002% strain. A typical grid for measuring expansion and CI is shown in **Fig. 1.3-1** along with a 500-mm DEMEC gauge.

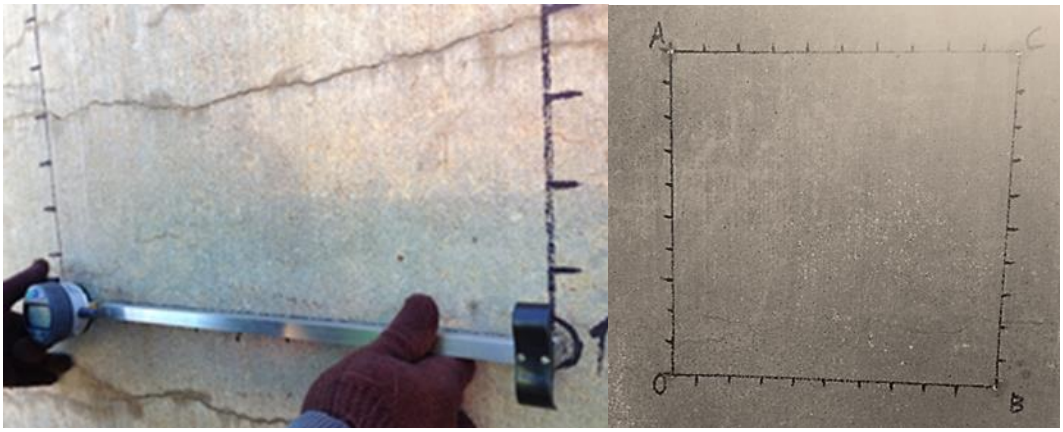

Fig. 1.3-1–Typical DEMEC gauge measurement and grid (by Richard Deschenes Jr.).

Relative Humidity (RH): Moisture is required to the formation of alkali-silica gel and the expansive reaction. Moisture within the concrete can be indexed to internal-RH. Internal-RH is therefore an index of the potential for ASR related expansion to occur within concrete. Stark (1990) and Bérubé et al. (2002b) determined that expansion ceases when the internal-RH of concrete decreases below 80% (21 to 24 °C).

The methods used by Stark (1990) and Bérubé et al. (2002b) to measure internal-RH had advantages and limitations. Stark (1990) pulverized concrete samples by drilled a 28-mm diameter hole into the concrete and collecting samples at various depths within the concrete elements. The samples were collected from 15 mm of concrete, and were stored in hermetically sealed containers. The containers were stored at 21 °C until the sample was in equilibrium. An electric-resistivity hygrometer was used to measure the RH within the container (Stark, 1990). This method provided internal-RH measurements at a controlled temperature of 21 °C and several depths within the concrete element. This method potentially lead to loss of moisture and an artificially low RH due to heating of the concrete sample and destruction of the microstructure during drilling.

Bérubé et al. (2002b) discussed a new for measuring internal-RH in the field method, which was developed by Bérubé et al. (1996). A 150-mm deep hole was drilled into the concrete element and a humidity probe inserted. The probe remained in the concrete until reaching equilibrium with the surrounding concrete. This test method provides a direct measure of internal-RH in the field, but is subject to several limitations. First, the concrete temperature fluctuates with ambient conditions during measurements, which prevents equilibration between the concrete and probe (Thomas et al., 2013b). Second, moisture condenses within the port due to temperature fluctuates causing artificially high RH measurements. Finally, each hole can only be used to measure internal-RH single depth.

Deschenes (2014) used a modified method to reduce the time required for equilibration between the concrete and RH probe. Holes were drilled to the selected depth and cleaned with compressed air. A 50 mm PVC sleeve and tight-fitting cap were inserted into the hole and epoxied in place. On each site visit, the air in the hole was already in temperature and RH equilibrium with the surrounding concrete. The cap was removed and a capacitive probe inserted. The probe remained in place until reaching temperature equilibrium with the air in the port and RH and temperature were recorded. Unfortunately, the hole contained a volume of trapped air and water-vapor. The water-vapor within the hole condensed on cooling and the measured RH was artificially high. The system should be improved by inserted a plug into the hole, which occupies more of the volume and reduce the amount of water-vapor trapped in the system. The system also provides internal-RH measurement at single depth.

Thomas et al. (2013b) reported on various field investigation of ASR in concrete transportation structures. Internal-RH was measured using capacitive type probes, installed into the concrete at three depths. This was done to measure the RH gradient between the exposed surface of the

concrete and the bulk concrete. Holes (16 mm diameter) were drilled to depths of 25, 50, and 75 mm and then fitted with a plastic sleeve and rubber stopper. The stopper was removed and a RH probe inserted. After equilibrium between the RH sensor and the concrete, RH was recorded. Measuring RH at various depths provides insight into the depth of drying occurring in the concrete. The results can be used to determine the efficacy of treatments in reducing RH throughout the depth of a concrete member. Thomas et al. (2013b) also noted the difficulty in measuring RH in the field as water condensation within the plastic sleeves prevented RH repeatable measurements. This method was employed for monitoring internal-RH in the Interstate 530 pavement in Pine Bluff, Arkansas. However, the sleeves were often damaged by traffic or plowing and sometimes filled with water due to inadequate sealing (Thomas et al., 2013b).

Cracking: Researchers have developed several methods for monitoring surface cracking to assess the deterioration of concrete (Thomas et al., 2013b; Fournier et al., 2004; ISE, 1992). The method involvef drawing a grid (or set of lines) on the surface of the concrete and then measuring the width of cracks crossing the lines. The cracking index (CI) involves drawing a square grid on concrete surface, and then measuring the crack widths crossing the grid (LCPC, 1997; Fournier et al., 2010). A one-meter square grid is drawn, with lines on all four sides and both diagonals (Smaoui et al., 2004). Alternatively, a 500-mm square grid is used, along with gauge pins installed at each corner (Thomas et al., 2013b). This provides a grid for measuring both expansion and CI in the same location. Each side of the grid (or line) is divided into 100-mm segments, to assist in locating crack widths. The cracking index (CI) is then determined as the width of cracks passing the grid, normalized to one meter. The cracking index method is useful for tracking the progression of deterioration in concrete in the field. However, the method

has limitations when examining rough or tined surfaces with very fine random cracking (Fournier et al., 2004; Fournier et al., 2010).

1.3.1.6. Laboratory Investigation

There are several laboratory test methods available for assessing the deterioration of concrete elements. These test methods include the damage rating index (DRI), stiffness damage test (SDT), hot-water extraction method for alkali extraction, expressed pore solution analysis, and the potential for further expansion (PFE). Each of these test methods quantifies (or indexes) the damage attained to date in concrete, or provides an estimate of the future deterioration potential of the concrete.

The test methods listed above require core samples extracted from the concrete element under investigation. Concrete condition can be highly variable in the field and each of these test methods should be conducted on samples collected from several locations within the concrete element (Fournier et al., 2004; Fournier et al, 2010). When applicable, according to Fournier et al. (2010), core samples should be extracted from locations with different exposure conditions, deterioration levels, and depths within the element. Assessing the efficacy of a remediation technique requires quantification of the deterioration throughout the concrete elements. These test methods provide additional information on the deterioration mechanisms and the ability of remediation methods to mitigate deterioration.

Mechanical Properties: The mechanical properties of concrete are related to the level of deterioration and cracking within the concrete. Mechanical properties of interest include compressive strength, tensile strength, elastic modulus, and flexural strength. The development of interconnected microcracks leads to expansion and the deterioration of mechanical properties (ACI, 1998). The mechanical property most directly affected by cracking is tensile capacity

(Fournier et al., 2010). Tensile capacity and elastic modulus decrease as expansion and cracking proceeds (ACI, 1998; Fournier et al., 2010). Compressive strength decreases, to a lesser extent, when compared to other mechanical properties (Fournier et al., 2010). Although mechanical properties are important to assess the residual strength of a concrete structure, they are not always a useful method for evaluating the progression of deterioration.

Stiffness Damage Test (SDT): The SDT is a mechanical test method used for quantifying the deterioration of concrete due to ASR. The method is less subjective to operator experience, and readily automated. However, the method may be influenced by aggregate type within the concrete specimen, making comparison between multiple concrete mixtures difficult (Sanchez et al., 2016b; Sanchez et al., 2017). The SDT was first developed and proposed by Crisp et al. (1989), and involves cyclic compressive loading of concrete core specimens. Core samples are loaded to 5.5 MPa and then unloaded, through 5 cycles. The hysteresis area, plastic deformation, and modulus of elasticity can then be correlated to concrete deterioration (Sanchez, 2014; Sanchez, 2015). Plastic deformation within the concrete depends on the extent of deterioration and cracking at the time of loading. The energy dissipated during each loading cycle relates to the hysteresis area of the stress-strain curve, determined through loading and unloading. Plastic deformation and hysteresis area provide a quantification of the deterioration present in the concrete (Smaoui et al., 2004; Sanchez et al., 2014; Sanchez et al., 2015). Smaoui et al. (2004) recommend using a load of 10 MPa to completely close cracks within the concrete during loading, while preventing additional deterioration from occurring. Recent work by Sanchez et al. (2016b) and Sanchez et al. (2017) has shown that loading the core to 40% of the design compressive strength of the undamaged concrete provides more reliable results.

Although values obtained by the SDT vary depending on the specific concrete mixture and aggregates in use, it is an effective method for comparing and quantifying the degree of deterioration between concrete of the same original mixture and strength (deterioration occurring over time). The method provides a quantitative index of concrete deterioration which provides more insight into the deterioration mechanism than other mechanical tests.

Petrographic Analysis: The most important test method required for diagnosing the presence of ASR in concrete is the standard petrographic examination. This method is used for evaluating durability and deterioration within concrete and is readily conducted by several laboratories and experts. Petrography involves describing the state of concrete and aggregates on a macroscopic and microscopic level. The analysis results are used to diagnose deterioration and durability issues such as ASR and F/T. The petrographic analysis is conducted according to ASTM C856 *Standard Practice for Petrographic Examination of Hardened Concrete*. The analysis also provides details on the concrete mixture design, condition, quality, and any apparent durability issues. The method requires a trained operator, remains subjective to operator experience, and does not provide a quantification of deterioration.

Damage Rating Index (DRI): Dunbar and Grattan-Bellew (1995) originally developed the DRI method for quantifying deterioration in concrete. Samples are first extracted from the concrete structure. Each sample is cut and polished to provide a surface for analysis. A grid of 1 cm^2 cells is drawn on the polished surface, and each cell is analyzed under stereoscopic magnification (15 to 16X). The petrographic deterioration features are counted and multiplied by a weighting factor (Shrimer, 2000). The various deterioration features are counted and weighted separately, and the weighted total is normalized to 100 cm^2 and reported as the DRI. The DRI is typically reported as a bar graph, disaggregates into individual features present within the sample

(Sanchez, 2014). This system provides insight into the specific deterioration mechanisms present within the concrete (Rivard et al., 2002; Shrimer, 2000). Sanchez et al. (2016) and Sanchez et al. (2017) developed a correlation between expansion and DRI, and established values to distinguish the deterioration states between multiple concrete mixtures (Sanchez, 2014). The DRI therefore provides a semi-quantifiable index of the deterioration and mechanisms present within the concrete. The DRI method, however, remains subjective to operator experience (Rivard et al., 2002; Grattan-Bellew and Mitchell, 2006; Sanchez et al., 2016; and Sanchez et al., 2017).

Several authors have proposed and refined the lists of petrographic features and weighting factors. Dunbar and Grattan-Bellew (1995) initially included seven features and weighting factors, which over-emphasized alkali-silica gel deposits and reaction rims. The list of features and weighting factors have since been modified to reduce multi-operator variability and to emphasize deterioration caused by cracks in the cement paste (Villeneuve et al., 2012; Sanchez, 2014). The current features and weighing factors, recommended by (Villeneuve et al. 2012), are provided in **Table 1.3-1**.

Table 1.3-1. DRI petrographic features and weighing factors (Villeneuve et al., 2012)

Petrographic Feature	Weighting factor
Closed crack in the coarse aggregate (CCA)	0.25
Open crack in the coarse aggregate (OCA)	2
Open crack in the coarse aggregate with reaction product (OCAG)	2
Coarse aggregate debonded (CAD)	3
Corroded aggregate particle (DAP)	2
Crack in the cement paste (CCP)	3
Crack in the cement paste with reaction product (CCPG)	3

Non-Destructive Tests (NDT): Several non-destructive test (NDT) methods have been developed for identifying deteriorated regions within concrete elements. Many of these methods measure the response of an input acoustic wave traveling through the concrete. Methods like

Ultrasonic Echo, Impact Echo, Spectral Analysis of Surface Waves (SASW), or Impulse Response use an active source and a receiver to measure the response of waveforms traveling through the concrete (ACI, 228). Ultrasonic Echo methods are useful for detecting defects within a concrete element (ACI, 228). Surface wave methods, such as the SASW method are used to measure the stiffness profile of pavements and deterioration within concrete elements. The Sonic Echo and Impulse Response can be used to measure the depth of concrete elements and continuity of elements which are buried or difficult to access (ACI, 228). Other methods use electrical or radiation transmissivity to measure electrical properties or to locate reinforcement or defects within a concrete element (ACI, 228).

Giannini (2012) provided an extensive evaluation of NDT methods applied to concrete with ASR or Delayed Ettringite Formation (DEF) deterioration. The Ultrasonic Pulse Velocity (UPV), Impact-Echo, SASW, and Surface Wave Testing (SWT) methods were all used for field and laboratory specimen testing. When an undamaged baseline is available, the UPV method was generally more effective at assessing the level of deterioration up to expansions of 0.2%, but was ineffective at higher expansions. (Giannini, 2012). The UPV method can be readily used to assess large concrete members, where coring and other test methods only assess a small portion of the member. The SASW and SWT methods were ineffective for measuring ASR related deterioration. A more sensitive time-shift non-linear acoustic method was shown to be more sensitive than the UPV method when characterizing deterioration in samples with low expansion and deterioration (Giannini, 2012; Moradi-Marani, et al., 2014). The NDT methods are useful for assessing the progression of deterioration within concrete, but are not currently valid for diagnosing ASR as the cause of distress.

Potential for Further Expansion (PFE): Laboratory test methods are useful for assessing the state of deterioration within concrete structures. It is sometimes necessary to assess the residual properties of concrete and its potential for future deterioration, especially when developing remediation measures. The potential for future deterioration in concrete elements can be estimated using the Potential for Further Expansion (PFE) method developed by Bérubé et al. (2002c). A combination of field and laboratory results are compiled to estimate the Potential Rate of ASR Expansion in Service (PRE). The residual expansion of concrete is estimated by accelerating ASR deterioration in core samples stored at high humidity and temperature (38 °C). The absolute degree of reactivity is determined by accelerating deterioration in cores stored in alkali solution. The residual water-soluble alkali content of the concrete is also measured through hot-water extraction to determine the available alkalis remaining in concrete (Bérubé et al., 2002c). The ambient conditions, including humidity, temperature, and applied stresses are assessed and compiled to calibrate the prediction of future deterioration in the field. Multon et al. (2008) cautions that the reliability of the PFE method depends on several parameters: the direction(s) of coring; moisture conditions assessment in the field; residual expansion testing; and the storage condition of core samples prior to testing.

At least six cores are required for the PFE method (nine preferred). The first set of cores (two or three) are submerged in water, the second set stored in air, and the final set stored in NaOH solution. All the samples are stored at 38 °C to accelerate ASR, and expansion is measured periodically. The cores stored in water are necessary to correct for expansion caused during saturation of the concrete. The cores stored air are used to determine the potential rate of expansion, and the cores stored in NaOH solution are used to determine the absolute degree of reactivity of the aggregates with excess alkalis (Bérubé et al., 2002c).

Assessing ambient conditions is more difficult as conditions fluctuate over time. Humidity and temperature conditions can be measured in the field with commercial humidity probes, which are inserted into holes drilled into the concrete element. Expansion is monitored in the field to track the actual rate of expansion under the existing stress (restraint) conditions. Predicting the stress conditions in the field is difficult. The reinforcement ratio and direction, along with current levels of deterioration, are used to determine the level of restraint and stress. The results from field and laboratory testing are then compiled to estimate the potential for further expansion in the field (Bérubé et al., 2002c).

The accuracy of this prognosis method is limited by the accuracy of the individual tests. The method does not propose to allow accurate estimates of future expansion within the concrete, but does allow an estimate of the potential for further expansion to occur during the lifetime of the structure (Bérubé et al., 2002c). The results are useful for developing a monitoring and management program (Fournier et al., 2004). Combined field expansion monitoring and SDT results provide an improved estimate of deterioration attained to date. The results are useful for scheduling remediation procedures, and estimating the remaining service life of a structure (Fournier et al., 2004; Fournier et al., 2010).

Alkali-Extraction: The water-soluble alkali extraction method may be useful for estimating the potential for future ASR deterioration in concrete structures. First, a sample of concrete is crushed to pass the 160 µm sieve. A 10-gram sample of the crushed concrete is then submerged in boiling water for 10 minutes, and then cooled over 24 hours to 21 °C. The sample is then filtered and diluted for analysis. The alkali (Na^+ and K^+) concentration is then measured through atomic absorption, emission, or flame spectroscopy (Bérubé et al., 2002a). Multiple samples should be evaluated from each concrete element to improve the accuracy of results.

The hot-water alkali extraction results are highly variable, but provide an estimate of available alkalis within the pore solution (Bérubé et al., 2002a). Alkalis which are not typically available in pore solution (from aggregates) may be released from the concrete due to crushing of the entire concrete sample (Bérubé and Fournier, 2004). However, this method does not measure the water-insoluble alkalis absorbed by reaction products, which would not be available in the pore solution. Pore solution expression and analysis is a more reliable method for measuring the alkali concentrations within the pore solution. The pore solution of hardened concrete can be expressed by compressing a sample of concrete until the pore solution is forced out of the concrete (Plusquellec et al., 2017). The solution can then be analyzed by spectroscopy to determine the alkali content. This method provides a better measure of pore solutions alkalinity and insoluble alkalis and alkalis from the aggregate are not incorporated into the samples.

1.3.2. Freezing and Thawing (F/T)

Powers (1945) provided one of the first working hypotheses of the mechanism of F/T deterioration in concrete. Hydrated cement was thought to have the properties of a colloidal gel, which is comprised of hydrated grains of cement bonded together by hydration products. As cement hydrates, cement grains are dissolved and hydration products form. The volume of hydration products is smaller than that of the cement grains, however the surface area is higher. The hydrated cement paste is comprised of a network containing interstitial spaces between hydrated cement grains. As hydration products form, water is adsorbed during the reaction resulting in desiccation of capillary spaces not occupied by cement grains. Additionally, air voids trapped within the cement paste empty as water is adsorbed by the cement paste and hydration products. The hydrated cement contains a network of capillary spaces and air voids interconnected by a tortuous network of interstitial spaces. The interstitial spaces are

approximately the size of eight water molecules (Powers, 1945). The water held in this space interacts strongly with the hydration products and never freezes. Capillary spaces develop because of pockets of water trapped within the concrete that are not occupied by cement grains. The capillary spaces empty during hydration and remain empty unless an external pressure forces water from the interstitial spaces into the cement pores (Powers, 1945).

Powers (1945) noted cement paste containing unsaturated pores is more durable to cycles of F/T than saturated cement paste. The pore solution within cement paste is not pure water but contains dissolved ions, which suppress the freezing point relative to pure water. Pore solution freezes progressively in cement paste primarily due to the microscopic size distribution of pores, but partly due to dissolved ions. The formation of ice occurs within the capillary network, rather than interstitial spaces, where water is relatively free from interactive forces with the cement paste. Ice cannot form within the interstitial spaces due to the pressure imparted on the water by the cement paste. Water expands as it cools until nucleation can occur and ice forms. Based on these rudimentary understandings of cement paste, Powers (1945) postulated the mechanism of F/T deterioration. Water expands, or imparts a pressure, during cooling which increases with each degree decrease in temperature. Hydrated cement paste is relatively brittle, and cannot expand sufficiently as pressure increases. If the cement paste is critically saturated, the expansion of water during cooling will cause deterioration of the paste. Cement paste is typically not saturated after hydration occurs, and enough unsaturated capillary spaces and air voids are available for water to occupy during expansion.

Powers (1945) explains the deterioration of unsaturated cement paste by considering a sequence of events. The exposed surface of a concrete element in contact with external water will contain more water than the bulk concrete. This surface will cool faster and freeze first as the cement

pores are more saturated, and freeze at a higher temperature than the drier bulk concrete. As freezing occurs, and water can no longer move through the frozen region, continued freezing accompanied by expansion, forces water away from the freezing front into the concrete. The water moves through the tortuous capillary network within the cement paste, inhibited by viscous resistance. The result is pressure which exceeds the tensile strength of the cement causing deterioration and microcracking. This hypothesis also explains why F/T deterioration in concrete often occurs as cracks parallel to the exposed surface. The exposed surface and region near joints are exposed to external sources of water, and therefore contain cement pores closer to critical saturation. A gradient occurs between the surface and bulk concrete. The exposed surface cools faster as it is directly exposed to the atmosphere. As freezing occurs at the surface and proceeds towards the bulk concrete, water is forced to migrate through the concrete. A critical plane occurs in the concrete when the migration of water induced pressures greater than the strength of the cement, resulting in a crack along the plane.

In addition to capillary spaces in the hydrated cement paste, concrete contains numerous larger pores (Powers, 1945). The cement pores range in size from micro to macroscopic. Due to desiccation, which occurs during hydration, the cement pores are rarely saturated. As a result, the concrete contains enough space to accommodate pressures which may develop during freezing. Under normal conditions, water does not flow from the capillary spaces into the pore space, as pressure is required to force water from the capillary spaces into the cement pores. On cooling, pressure forces water through the interstitial spaces into the capillary spaces. Deterioration can occur if destructive pressures develop as water migrates from the interstitial spaces into the capillary space. Powers (1945) noted a well dispersed network of small air voids,

reduces the distance over which water migrates and inhibits the development of destructive pressures.

The durability of cement paste during F/T depends on the degree of saturation at the time of freezing and the rate of sorption. The rate of thawing also determines the degree of deterioration in concrete, as it induces a drying effect on the paste. As water contracts on thawing, a negative pressure can be induced which draws water towards the thawing site, inducing viscous resistance in the interstitial spaces as water migrates. In fact, the water pushed out of the capillary space by freezing is fully restored by drying if water is not displaced from the concrete.

Powers and Helmuth (1953) further refined the earlier hypothesis considering a refined knowledge of cement paste. Hydrated cement grains range in size from 5 to 20 nm, with a porosity (or interstitial space) of 25% by volume (Powers and Helmuth, 1953). The hydrated cement paste (or gel) also contains unfilled capillary space and macroscopic air voids. The capillary spaces are small enough to prevent water from freezing at the normal freezing point, requiring a lower temperature before nucleation and the formation of ice crystals. The smaller the size of the capillary spaces, the lower temperature and higher pressure required for ice formation. During cooling, ice crystals form first in the largest cement pores, followed by smaller pores on further cooling. The freezing temperature is further suppressed by the degree of saturation within the cement paste. As saturation increases, the concentration of cations in solution decreases by dilution and surface tension (capillary forces) decreases. The free energy of water in the C-S-H gel is similar to that of free water in bulk, although depressed slightly by cations in solution. When ice forms in capillary space, the increase in free energy as temperature decreases slows, while the free energy of the solution in the cement paste continues to increase. This causes water from the paste to flow towards the ice crystals in the capillary space to

maintain thermodynamic equilibrium (Powers and Helmuth, 1953). As water diffuses into the capillary spaces, the ice crystal grows and the surrounding cement paste contracts. If cooling continues, the capillary space is filled and deleterious pressure is exerted on the surrounding cement paste. Interestingly, the ice crystals interact with the film of adsorbed water molecules at the boundary between the cement paste and ice. Surface diffusion occurs along the boundary and the cement paste shrinks as water is removed.

Water also diffuses from the cement paste into air voids. Air voids are rarely saturated after hydration, and the ice is not under external stresses. The free energy of ice in air voids is lower than that of ice in capillary spaces (Powers and Helmuth, 1953). As cooling occurs, and the water moves from the cement paste into the capillary spaces, a free energy balance occurs between the cement paste and capillary ice. Then water in the cement paste diffuses towards air voids due to the pressure exerted on the gel by the ice crystals in the capillary spaces. Again, the stress imparted on the cement paste is a function of the distance over which water must travel through the cement paste towards the nearest air void.

The boundary between cement paste and aggregates complicates the flow of water within concrete. The aggregate permeability can be lower or higher depending on porosity. The saturation state of the aggregate is also important, as water may be expressed from the aggregate particle and diffused into the cement paste. If the aggregate porosity is higher than that of the cement paste, the water expelled on freezing can damage the paste, leading to D-cracking or pop-outs in the concrete. If the aggregate porosity is lower, the aggregate forms a boundary through which water cannot flow on freezing. Therefore, water must move further to escape to an air void.

Vuorinen (1970) further investigated the relationship between the degree of saturation and F/T durability of concrete. Noting the presence of cement pores (1.5 to 2 nm), capillary spaces (1.25 μm), and air voids (10 um to 2 mm), Vuorinen (1970) observed not all the water in concrete is free or evaporable. Due to the size of pores in the cement paste, water is held in place by surface forces, while the free water in capillary spaces can evaporate as the internal-RH drops below 40%. A thin film of water within the capillary spaces interacts with the cement paste and does not evaporate. By comparison, air voids are a factor of magnitude larger and water within them is free to evaporate. The durability of concrete to F/T is related to the spacing factor of air voids, which should be less than 0.2 mm (0.008 in.) to limit the distance over which water must travel on freezing. Vuorinen (1970) noted the amount of hydraulic pressure on freezing is related to the degree of saturation. Water also moves towards capillary spaces during freezing as discovered by Powers (1953). Deterioration occurs when the distance over which water moves exceeds the threshold distance and viscous pressure is induced on the cement paste. Deterioration also occurs when dilation from formation of ice crystals in capillary spaces exceeds the contraction of cement paste due to water moving towards ice formation (Vuorinen 1970). The dilation of capillary spaces is balanced by the contraction of cement paste until the capillary space is filled and exerts pressure on the cement paste. After which water is pushed away from the capillary space into the cement paste and towards available space within larger capillary spaces or air voids. Depending on the degree of saturation, the process continues during cooling until the pressure is balanced when water moves into available voids, or deterioration of the concrete occurs (Vuorinen 1970).

Vuorinen (1970) developed a test method for measuring the saturation of cement pores within a concrete sample and the impact on durability. The volume of water filled (P_w) and air filled (P_a)

cement pores were determined by saturating the sample under atmospheric and high water-pressure, respectively. The weight of each sample was determined before and after saturation, and again after drying at 105 °C. The saturation degree (S_w) and pore ratio (P_r) are then given by Equation 1 and 2.

$$S_w = P_w/(P_w + P_a) \quad (1)$$

$$P_r = P_a/(P_w + P_a) \quad (2)$$

Vuorinen (1970) reported that concrete with P_r greater than 16% exhibit acceptable durability on F/T. The freezable water content in concrete was also measured as a function of the water-to-cement ratio and the hydration age of concrete. A saturation factor (S_f) was determined as the ratio of the volume of freezable water (W_f) to the volume of air voids as shown in Equation 3. The air void fraction (A), shown in Equation 4, is the ratio of the volume of air-filled voids to the cement content (C).

$$S_f = W_f/(W_f + A) \quad (3)$$

$$A= P_a/C \quad (4)$$

A critical saturation factor (S_f) of 70% is required for deterioration to occur in concrete specimens. The influence of drying on concrete was significant as the freezable water content decreases on curing and drying due to water adsorbed by hydration products and evaporated on drying. Vuorinen (1970) provided a relationship between water-to-cement ratio, curing and drying, and freezable water content. The relationship is reasonable for the cement used in the test, but cannot be broadly applied to all concretes. Therefore, the freezable water content needs to be measured in determining the S_f of concrete. The apparatus used in his testing is described as relatively simple but has not been adopted into common practice. Although saturation is

important to determining the durability of concrete, the standard F/T test (ASTM C666) is still commonly used in practice, which does not account for saturation state (Vuorinen 1970).

Powers (1975) revisited the mechanisms of deterioration during F/T. Advances in concrete technology indicated freezing in concrete is further suppressed by alkalis in solution and the microscopic size of cement pores (Powers, 1975). The earlier hydraulic-pressure hypothesis did not explain shrinkage which occurs in concrete on initial cooling as freezing is initiated. The hypothesis was revised to account for water moving from the cement pores towards the formation of ice in capillary spaces. The movement of water through the cement paste results in viscous resistance which imparts stresses on the cement paste. Water is drawn towards the formation of ice due to the concentration of alkalis remaining in the unfrozen solution and by thermodynamic equilibrium. As ice forms, the concentration of alkalis in solution increases, resulting in a thermodynamic gradient between the solution in cement paste and that remaining in the capillary spaces, the result is osmotic pressure which draws water towards the ice crystals. This pressure is sufficient to cause deterioration in the cement paste (Powers, 1975). The degree of expansion depends on the saturation of capillary spaces. When ice begins to form in the capillary spaces, water flows towards the solution in the capillary space until the air-filled space is occupied by water. During this phase, the cement paste shrinks as water diffuses into the capillary spaces. Once the capillary space is filled, further expansion of the ice causes a net dilation which induces pressure on the surrounding cement paste.

Entrained air bubbles of sufficiently close spacing prevent the development of osmotic pressure (Powers, 1975). Air voids contain a comparatively large volume of air due to desiccation that occurs during hydration. Water in the air voids freezes at a higher temperature than that in capillary spaces, and water in the cement paste is drawn towards the ice formation. However,

the air voids are not saturated and contain enough air-filled volume to hold the water moving out of the cement paste. As a result, no pressure is induced on the cement when ice forms (Powers, 1975). As water moves from the cement paste into the air voids, the paste contracts in what Powers (1975) describes as a freeze-drying effect. When the air-voids are closely spaced (0.2 mm) deleterious osmotic pressures are alleviated. Sufficient air-entrainment therefore protects cement paste from F/T deterioration.

However, concrete is a multiphase material, containing aggregates in addition to cement paste. Certain susceptible aggregates can be cause F/T deterioration in concrete (Powers, 1975). Aggregates contain a network of interconnected capillaries and can absorb and desorb water. When the porosity and interconnectivity of an aggregate is greater than that of cement paste, and the aggregate becomes saturated, water is expelled on freezing at a rate which the cement paste cannot sustain. The cement paste can therefore be damaged by freezing of water in the aggregates. Although some aggregates are durable to F/T, certain D-cracking susceptible dolomitic limestones contain porosity and sorption characteristics which tend towards saturation when the concrete is exposed to an external supply of water (Powers, 1975). Larger aggregates tend to be more destructive due to the decreased interfacial surface area between the aggregate and cement paste, through which a greater amount of water is forced on freezing. Air entrainment is not sufficient to mitigate the stresses induced when D-cracking susceptible aggregates are present within the concrete and become saturated. Therefore, preventing the aggregates from becoming saturated is the only means of preventing deterioration on F/T, even when the concrete is air-entrained.

Janssen (1994) also discussed the occurrence of deterioration due to saturated aggregates. Specifically evaluating pavements, the primary symptom of deterioration occurs as D-cracking

adjacent to pavement joints. This occurs when water penetrates the concrete through joints and saturates the concrete and aggregates. On F/T, the concrete deteriorates as water is expelled from the aggregate, resulting in cracks parallel to the joints. The susceptibility of concrete to D-cracking is related to the quantity and size of susceptible aggregates (Janssen, 1994). These susceptible aggregates tend to have a fine, interconnected pore structure (Walker, 2006). The aggregates may become saturated when the concrete is exposed to an external source of water. Cycles of F/T lead to microcracks, which interconnect on further F/T until macro cracks are apparent at the surface. Janssen (1994) reiterates D-cracking can occur in sufficiently air-entrained concrete.

1.3.2.1. Diagnosis and Symptoms of F/T

F/T can be diagnosed in concrete through petrographic analysis. The symptoms of interest include scaling, laminar cracking, and D-cracking (Walker, 2006). The symptoms of F/T distress depend on whether the deterioration occurs within the cement paste or aggregate phase. Typically, in air-entrained concrete, deterioration occurs due to saturation of D-cracking susceptible aggregates. For plain concrete, deterioration occurs as scaling along the exposed surface. The surface of concrete scales when the surface layer is exposed to F/T cycles. As water freezes, a layer of the surface flakes off due to stresses occurring perpendicular to the exposed surface along a plane parallel to the surface. The depth of scaling can range from 5 to more than 20 mm (Walker, 2006). Laminar cracking can occur in critically saturated concrete, which occurs as progressive scaling from the exterior inward.

Walker (2006) noted D-cracking occurs in concrete with unsound aggregates or without proper air entrainment. D-cracking occurs as cracks adjacent to joints, which become visible at the

surface. The name D-cracking comes from the appearance of the deterioration which parallels joints in the pavement, curving at the corners forming a curved D shape.

1.3.2.2. Prevention of F/T

Powers (1975) reiterated cement paste can be made completely durable to F/T by entraining air into the concrete. If the spacing factor (0.2 mm) and volume of entrained air (4 to 6%) is sufficient, the cement paste will be indefinitely durable to cycles of F/T (Powers, 1975; Janssen, 1994; Walker, 2006). However, the concrete can deteriorate if completely saturated or when the aggregates are susceptible to F/T. Janssen (1994) showed blending D-cracking susceptible aggregates with sound aggregates along with using smaller gradations of aggregates improves the durability of concrete to F/T. As with most durability issues in concrete, decreasing the permeability of concrete prevents moisture from entering which prevents saturation. Modern concrete mixtures with sufficiently low water-to-cement ratios, proper consolidation and compaction, and admixtures (SCMs) are less likely to become saturated.

1.3.2.3. Mitigation of F/T in Hardened Concrete

Typically repairing F/T deterioration requires removal and replacement of the affected portion of concrete. Janssen (1994) demonstrated laboratory samples treated with silane are less prone to saturation and deterioration, and silane treatment may extend the service life of structures deteriorating from F/T. The durability factor of laboratory concrete specimens was higher for silane treated samples as compared to untreated control samples. However, additional testing is required to validate this technique in larger concrete elements where drying occurs only through one exposed surface.

1.4. RELATIVE HUMIDITY IN CONCRETE (RH)

Methods for measuring *relative humidity* (RH) in concrete were developed in the 1930 and 40's (Gause, 1940). Prior to these efforts, the most practical method for measuring moisture in concrete was gravimetric measurements. This required destructive testing of concrete samples, which were weighed before and after oven drying to determine the moisture content. However, there was no practical way for conducting this method in the field. Gause (1940) developed a test method for measuring internal-RH in laboratory concrete samples. This test required a palladium wire hygrometer and a resistivity meter. The hygrometer was calibrated using saturated salt solutions, and then placed in holes within the hardened concrete. The hygrometer was sealed into the concrete using a rubber stopper and remained in the concrete until the concrete, air, and hygrometer were in temperature and humidity equilibrium. Hygrometers were placed at depths of 38, 76, and 152 mm (1.5, 3, and 6 in.) to determine the gradient of internal-RH (Gause, 1940).

Gause (1940) also measured the internal-RH of concrete samples stored in a hermetically sealed system. The humidity was measured at various temperatures to determine the relationship between RH and temperature. In a sealed container of air and water vapor, RH increases as temperature decreases until the air-water mixture is saturated. At this point, equilibrium occurs between water evaporating into the air and water vapor condensing into liquid water. However, hardened cement paste contains numerous pore spaces ranging in size from a few millimeters, down to nanometers. The cement paste acts as a gel or colloid, which absorbs water as RH increases, and desorbs water as RH decreases (Menzel, 1955). Additional water vapor is released from the colloidal cement paste as temperature increases, resulting in an increased

internal-RH (Gause, 1940). Gause (1940) found the internal-RH in hermetically sealed concrete samples in fact increased with temperature.

Menzel (1955) discusses the shrinkage and swelling characteristics of concrete as related to water exchange within the concrete. Water within concrete is in one of three forms (1) pore water, (2) free capillary water, and (3) chemically-combined water (Menzel, 1955). Free capillary water can evaporate and diffuse from the concrete freely as the concrete dries from a saturated to air-dried state. As RH increases, cement pore water is absorbed into the colloidal C-S-H gel and on drying the water is desorbed through evaporation. However, due to the small size of the pore space, the curvature of the water is higher than would be present in a larger volume. Due to surface tension, the water requires additional energy to desorb and, as such, requires higher temperature (Menzel, 1955). Chemically-combined water is chemically bound within hydration products and requires much higher temperatures before desorption. After free pore and capillary water evaporates, the internal-RH drops below 100%. Therefore, changes in internal-RH occur after most free water evaporates, and water vapor is present within the pore space (Menzel, 1955). The internal-RH humidity will continue to decrease toward equilibrium with the ambient-RH (Menzel, 1955).

Nilsson (1980) summarized several sources to develop a method for calculating moisture loss in hydrating concrete. The desorption and absorption isotherms for concretes of various age and compositions had to be determined to develop a relationship between moisture content and internal-RH in concrete (Nilsson, 1980). Internal-RH in concrete is related to the state of moisture within the concrete. Moisture within concrete can be described, at an early age, using the rate of hydration, sorption isotherm, and moisture flow (Nilsson, 1980). However, the hydration rate of concrete is much less important at later ages. Therefore, the factors of

importance for hardened concrete are the sorption isotherm and moisture flow rate. These factors are influenced by many variables and are unique for each concrete. Moisture flow within concrete is a function of water-cement ratio, pore interconnectivity, and hydration age. Concrete with a water-to-cement ratio less than 0.7 will generally have limited pore connectivity after sufficient hydration occurs (Nilsson, 1980).

Moisture within concrete is affixed in one of the three states described earlier. The moisture state within concrete will adjust to achieve equilibrium with the ambient conditions under which the concrete is stored (Nilsson, 1980). The sorption isotherm is the relationship between moisture content and internal-RH within the pore space (Nilsson, 1980). Chemically bound water is affixed to hydration products through hydrogen bonds and is only desorbed at temperature where these hydration products begin to dissolve. Physically bound water is entrapped by the cement paste structure (Nilsson, 1980). Additional pore water is affixed to the pore surface through van der Waal bonds, and the thickness of this water depends on humidity (Nilsson, 1980). At higher humidity, approaching saturation, water condenses within the capillary space and is suspended by surface tension forces. The small size of the pore space results in water surfaces in which the meniscus causes curvature (Nilsson, 1980). This curvature increases the energy required for water vapor to escape from the liquid water, meaning the saturation vapor pressure is lower than would be present over a surface with less curvature (Nilsson, 1980). The sorption of moisture within concrete therefore depends on the state of saturation, temperature, and porosity of the concrete. The sorption isotherm is unique to each concrete, and requires gravimetric and internal-RH measurements of concrete during drying at a range of temperatures. This makes it impractical to determine sorption isotherms for concrete structures. Therefore, internal-RH is often used as an index of moisture state within concrete,

with internal-RH less than 100% indicating the concrete is not saturated. Nilsson (1980) also discusses the importance of moisture and internal-RH in the development of ASR. For the concrete evaluated, a minimum internal-RH of 80% (21 °C) was required for alkali-silica gel to develop, and 85% was required for expansion to continue (Nilsson, 1980).

Quincot (2011) discusses the many methods available for measuring moisture and internal-RH in concrete. Water vapor sorption isotherms (WVSI) are again necessary to relate moisture content to internal-RH. These WVSI are measured gravimetrically at various controlled internal-RH points (Quincot, 2011). Concrete samples are stored in a controlled RH environment, produced using saturated salt solutions. The concrete is then allowed to equilibrate with the environment, either through desorption or adsorption (Quincot, 2011). After equilibrium, the concrete sample is weighed to determine the moisture loss or gain. The isotherm is a function of many material and physical properties of the concrete and is unique for each concrete mixture, as well as the ambient temperature (Quincot, 2011).

Moisture content in concrete is often measured as a method for determining the amount of free and absorbed water. The moisture content is determined through gravimetric measurements, which require the entire concrete sample to be weighed at several points during drying. The moisture within the concrete evaporates at different temperatures depending on fixation (Quincot, 2011). The concrete samples must be protected from moisture loss, or gain, during extraction and before the initial weight. Non-destructive test methods have also been developed for measuring moisture content. One such method relies on gamma radiation to measure variations of mass in concrete, which is then converted to moisture losses (Quincot, 2011).

Internal-RH is more convenient to measure than moisture content in concrete due to the availability of accurate electric (resistive or capacitive) hygrometers. Electric hygrometers based

on capacitive or resistive sensors are available with accuracies of ±1 to 2% RH for temperatures from 0 to 50 °C. Both sensors are composed of hygroscopic materials which have variable resistivity or capacitance, depending on the moisture state of the hygroscopic material within the sensor. As ambient humidity increases, the hygroscopic material absorbs additional moisture, changing the electric properties, which are then measures and converted to RH (Quincot, 2011). Internal-RH is an effective way of measuring the water content within concrete, as related to the saturation vapor pressure of an air-water mixture. The RH is an important factor in controlling and preventing durability issues within concrete, such as ASR, delayed ettringite formation (DEF), or F/T. Literature is available to show a threshold-RH required for these durability issues to persist in concrete. Nilsson (1980), Stark (1990), and Bérubé (1996) found that 80-85% internal-RH (21 °C) is required for ASR to develop and persist in concrete. Rust (2009) found that at least 90% internal-RH is required for DEF-related expansion in concrete. Janssen (1994) indicated an internal-RH greater than 85% is required for freezable water to exist within concrete. However, deterioration can occur below this point due to water moving on cooling.

Jensen (2003) and Quincot (2011) discussed an alternative hygrometer, which relies on a hygroscopic wooden stick to measure humidity. The wood (Gonystylus Macrophyllum) exhibits a wide range of conductivity depending on the moisture content of the wood (Quincot, 2011). The conductivity can therefore be accurately correlated to moisture content of the wood, and RH. The conductivity of the wood is measured by attaching a conductivity probe to the ends of the stick. Conductivity is correlated to RH by storing the wooden stick at various RH control points until equilibration occurs. The advantage of this method is the relatively small impact of temperature on the conductivity of the wood, resulting in stable RH measurements even as

temperature fluctuates. Each wooden stick must be calibrated over saturated salt solutions to produce a calibration curve over a range of RH (Quincot, 2011).

Another nondestructive, and indirect, method for measuring moisture content in concrete is by measuring the resistivity of the concrete. Concrete resistivity changes with moisture content, but is also a function of temperature and the material properties of the concrete (Qunicot, 2011). Due to the sensitivity of concrete resistivity to several rapidly changing variables, it is necessary to calibrate the results (Quincot, 2011). Gravimetric testing of a portion of the concrete, to determine the exact moisture content, is required for calibration. The test setup can alternatively be calibrated for RH measurements for indirect RH monitoring at selected depths within the concrete. The setup must be calibrated either using electric hygrometers placed within the concrete sample, or by testing sub samples of concrete at controlled RH points. The resistivity test setup requires at least two electrodes, through which a voltage is applied and the current passing through the concrete is measured (Quincot, 2011). Alternatively, four electrodes are placed at a selected depth within the concrete, and a voltage is applied across two electrodes and the current measured between the remaining two. The resistivity measurements are sensitive to temperature changes, with an inverse relationship between temperature and resistivity (Quincot, 2011). Therefore, calibration must consider concrete temperatures in addition to porosity, material properties, and moisture content (Quincot, 2011).

Several other nondestructive test methods indirectly measure RH or moisture content of concrete. Impedance and dielectric methods measure moisture content without contact points attached to the concrete. Microwave attenuation methods can measure moisture content in relatively thin cross sections (Quincot, 2011).

1.4.1. Relative Humidity and ASR

Stark (1990) performed an extensive investigation into the relationship between RH in concrete and the development of ASR and related expansion. Building on the work of Stanton (1940) and Vivian (1947), Stark (1990) conducted laboratory testing of ASR reactive mortar bars stored in a range of humid environments at a temperature of 38 °C. Non-reactive mortar bars were stored in the same humid environment to determine the strain caused by absorption and desorption of moisture due to humidity. The expansion results for the ASR reactive specimens were corrected by subtracting the strain due to sorption (Stark, 1990). Stark (1990) concluded from the test results that a threshold-RH of 80% (21 °C) is required for ASR to produce expansion in the mortar samples. Stark (1990) also noted mortar bars with ASR reactive aggregate shrank more during drying than companion samples with non-reactive aggregates. This was attributed to the shrinkage of cement paste and ASR gel during desorption.

Based on the results of Stark (1990), limiting moisture in concrete is a potential method of mitigating ASR in field concrete. Therefore, methods for quantifying internal-RH in concrete are necessary to develop and evaluate mitigation techniques which rely on reducing internal-RH in concrete. Stark (1990) developed and introduced the method for measuring internal-RH in concrete elements discussed in **Section 1.3.1.5**. This technique was demonstrated on several concrete structures, including pavement, bridge columns, and bridge decks. The results for concrete pavements showed, except for the top 2 in. (50 mm), the concrete pavement had an internal-RH greater than 80% even in warm, arid climates (Stark, 1990). The internal-RH was lowest at the surface and highest near the subgrade, due to drying occurring near the surface. For concrete columns not exposed directly to water, the internal-RH fluctuates with average ambient conditions. The interior of the column retains moisture as compared to the outer surface, but still

decreases below 80% (21 °C) internal-RH during the summer (Stark, 1990). During the winter, moisture is drawn out of the interior of the column by capillary forces near the drying front (Stark, 1990). Bridge deck pavements evaluated in various climates exhibited fluctuating internal-RH depending on ambient conditions. Drying occurred at the top and bottom of the slab and led to lower internal-RH as compared to pavement. Periods of elevated ambient humidity lead to increased internal-RH over 80% (21 °C), allowing ASR to occur. As ambient-RH decreases, the concrete dries and ASR stops when the RH drops below 80% (21 °C). Similar results for dam structures indicate the concrete remains saturated throughout the year, except for the outer 200 mm of concrete exposed to air (Stark, 1990).

Helmuth (1993) also reported on methods for measuring internal-RH in concrete. Data for pavements again show that internal-RH remains higher than 80% (21 °C) even in arid conditions. The internal-RH was observed to fluctuate with ambient conditions, with drying occurring at the exposed faces (to a depth of 50 mm) when the ambient-RH was lower than the internal-RH of the concrete. Drying produces capillary forces which transported moisture from the higher moisture regions of the concrete toward the drying front (Helmuth, 1993). Helmuth (1993) also reported that the internal-RH within a concrete column was greater than 80% (21 °C) during the winter and less than 80% (21 °C) during the summer. As a result, ASR may proceed during humid summer months, and then slow or stop during drier periods (Helmuth, 1993).

Bérubé (1996) conducted a laboratory and field experiment on the effects of wetting-and-drying on ASR. ASR reactive concrete cylinders were stored under cyclic moisture conditions to determine the effects of wetting-and-drying observed in the field. The two-week cycle consisted of 10 days at 100% ambient-RH (38 °C) followed by 4 days at 30 % ambient-RH (38 °C). As a result, the samples had 40% less expansion as compared to samples stored at 100% ambient-RH

(38 °C) over the same period. However, the samples had map-cracking at the surface due to the difference in expansion at the core of the concrete as compared to the surface (Bérubé, 1996).

The study also consisted of samples treated with silane or siloxane to increase drying. Treated samples had an internal-RH of 81% (21 °C) near the surface as compared to 96% (21 °C) for untreated samples. The treated samples developed less than 0.04% expansion at one year indicating humidity less than 80% (21 °C) is sufficient to prevent ASR related expansion (Bérubé, 1996). However, Bérubé (1996) notes that concrete containing highly-reactive aggregates may develop ASR when stored in an environment of 65% (21 °C) humidity, highlighting the difference between internal and ambient RH as related to ASR.

Bérubé (1996) also evaluated the internal-RH of field structures treated with silane. The internal-RH was measured using capacitive hygrometers, by first drilling to a depth of 150 mm and then inserting the probe into the hole and allowing equilibrium to occur between the concrete, air, and probe. The sections treated with silane or siloxane had an average internal-RH of 78 to 82% (21 °C) as compared to 90 to 93% (21 °C) in the untreated sections (Bérubé, 1996).

Rust (2009) discusses several methods for measuring internal-RH in concrete in-situ. The simplest method involves drilling a hole into the concrete to a selected depth. A plastic sleeve is inserted into the hole, followed by a rubber plug that fills the sleeve. After sufficient time passes for the remaining air in the sleeve to equilibrate with the concrete, the rubber plug is removed and a capacitive hygrometer is inserted. Again, time is allocated for equilibration between the concrete, air, and probe after which temperature and RH are recorded (Rust, 2009). Several commercial capacitive type hygrometers are available, which can measure RH with an accuracy of ±2% between 0 to 100% RH and 0 to 50 °C. These commercial probes include a capacitive sensor installed within a metal or plastic probe, with a proprietary port for connecting the probe

to a data logging system. Alternatively, capacitive type hygrometric sensors can be connected directly to a data acquisition system. These sensors are like commercial probes, but do not have proprietary communication port or hand-held data logger. The sensors are not calibrated and therefore must be calibrated over saturated salt solutions before use in concrete. The sensors must be protected from fresh concrete and are sometimes wrapped in Gor-Tex® to protect the sensor from water. The sensors can be embedded into the concrete in this fashion and provide a long-term monitoring system for internal-RH and temperature.

Small (12.5 mm diameter) self-contained RH sensors are also available. The sensors are stored in a durable casing which protects the sensor from the fresh and hardened concrete, and the sensor contains memory in which RH and temperature data is temporarily stored. The data is then transmitted wirelessly to a recording system for analysis (Rust, 2009).

Rust (2009) studied two methods for measuring internal-RH in concrete and compared the results for probe type hygrometers and sensor type hygrometers. Hygrometers were evaluated using two methods: installation into drilled holes, or embedded into the fresh concrete. The hygrometers were installed or embedded at depths of 13 mm, 25 mm, and, 38 mm at the surface of a 300-mm cube. For both the installed and embedded probes, plastic sleeves were inserted into the concrete, and the hygrometer was inserted into the tube. For the installed hygrometers, the sleeve was plugged with a rubber stopper until the hygrometer was installed. For the embedded hygrometers, the hygrometer was inserted into the sleeve and sealed with tape. The hygrometers remained in the concrete for four months, with periodic measurements. The internal-RH measured using embedded probes were within 4% of that measured using installed probes (Rust, 2009). This margin is within the expected accuracy of the different hygrometers used, meaning that no statistically meaningful difference in internal-RH was measured for

embedded as compared to installed hygrometers. However, a significant difference of up to 10% internal-RH was measured for the sensors placed within plastic sleeves that have excess air space between the sensor and the concrete. When the sensor does not occupy most of the air space within the plastic sleeve, excess moisture trapped within the space condenses on cooling, which causes an artificially high internal-RH measurement (Rust, 2009).

1.4.2. Relative Humidity and F/T

Janssen (1994) conducted testing relating the freezable water content with internal-RH. Concrete prisms were stored at a range of ambient-RH fixing points, and allowed to equilibrate until the mass change was less than 0.03% per week. The moisture content was determined from the change in mass. Powers (1947) found the internal-RH required for water to freeze at temperatures above -18 °C is equivalent to 85% (21 °C) (Janssen, 1994). Water can however, freeze at lower RH values for temperatures lower than -18 °C. For reasonable temperatures above -18 °C, there is no freezable water in concrete when the internal-RH falls below 85%. Therefore, a threshold-RH of 85% would be required for ice formation in concrete. This does not account for deterioration occurring due to saturated aggregates, in which case F/T deterioration can still occur. However, aggregates tend to dry towards equilibrium with the concrete over time. As observed by Stark (1990), concrete exposed to ambient conditions exhibits a drying gradient between the surface and bulk concrete. Results indicate drying occurs within the first 200 mm, while the bulk concrete remains close to 100% internal-RH after several years of exposure. Therefore, F/T deterioration is likely to occur in plain concrete, regardless of drying, if the concrete freezes to depths greater than 200 mm. Concrete directly exposed to external water by rain and runoff absorbs water, and desorbs water during periods of lower RH and no direct exposure to water. Joints provide an avenue for additional water to penetrate the

concrete, and the concrete adjacent to joints is more saturated than concrete further from joints. Therefore, concrete and aggregates are more likely to be saturated near the joints, which leads to cracks parallel and adjacent to joints.

1.5. DISSERTATION ORGANIZATION

Presented within is a compilation of four journal articles which support the primary objectives of this research. The dissertation is organized in eight chapters, containing an introduction, four papers, a summary of conclusions and recommendations, references, and an appendix. Chapter 1 describes the introduction, objectives, literature review, and motivation for the research presented herein. Chapter 2 discusses in detail the concrete materials examined within the following two papers. In addition, Chapter 2 covers the diagnosis of ASR in concrete containing an aggregate with a satisfactory field performance, which required additional analysis to determine the cause of deterioration. Chapter 3 summarizes an evaluation of treatment methods applied to a barrier wall exhibiting a range of deterioration states, caused by a combination of ASR and F/T. Chapter 4 covers an evaluation of silane treatments applied to a concrete pavement which deteriorated from ASR and F/T. Chapter 5 presents an evaluation of exposure conditions which promote the development of ASR and F/T and examines the effect of combinations of conditions promoting deterioration. A list of conclusions, recommendations, and scientific contributions is presented in Chapter 6. A complete list of references used within this dissertation is presented in Chapter 7. Chapter 8 contains Appendix A, which is a summary of data used for Paper 2; and Appendix B which is a summary of data used for Paper 4.

1.6. REFERENCES

ACI Committee 221, "Report on Alkali-Aggregate Reactivity (ACI 221.1R-98)," *American Concrete Institute*, Farmington Hills, MI, 1998, 31 pp.

ACI Committee 228. (2013). "Report on Nondestructive Test Methods for Evaluation of Concrete in Structures (Report No. ACI 228.2R-13)." *American Concrete Institute*, Farmington Hills, MI, 86 pp.

ASTM C1260-05. (2008a). "Standard test method for potential alkali reactivity of aggregates (mortar-bar method)." Annual Book of ASTM Standards 04.02, *American Society for Testing and Materials (ASTM)*, West Conshohocken, Pennsylvania, 676-680.

ASTM C1293-08b. (2012). "Standard test method for determination of length change of concrete due to alkali-silica reaction." Annual Book of ASTM Standards 04.02, *American Society for Testing and Materials (ASTM)*, West Conshohocken, Pennsylvania, 687-686.

ASTM C1778-14. (2016). "Standard Guide for Reducing the Risk of Deleterious Alkali-Aggregate Reaction in Concrete." West Conshohocken, PA: ASTM International, 11 pp. doi: https://doi.org/10.1520/C1778-16.

Bérubé, M. A., Chounard, D., Boisvert, L., Frenetter, J., and Pigeon, M. (1996). "Influence of wetting-drying and freezing-thawing cycles, and effectiveness of sealers on ASR." *Proceedings of the 10th Intonational Conference on Alkali-Aggregate Reaction (ICAAR),* ARRB Group, Australia, 1056–1063.

Bérubé, M.-A., Chouinard, D., Pigeon, M., Frenette, J., Boisvert, L., and Rivest, M. (2002). "Effectiveness of sealers in counteracting alkali silica reaction in plain and air-entrained laboratory concretes exposed to wetting and drying, freezing and thawing, and salt water." *Canadian Journal of Civil Engineering*, 29(2), 289–300.

Bérubé, M.A., Frenette, J., Rivest, M. and Vézina, D. (2002a). "Measurement of the Alkali Content of Concrete Using Hot Water Extraction." *Cement, Concrete, and Aggregates*, 24(1), 28-36.

Bérubé, M.-A., Chouinard, D., Pigeon, M., Frenette, J., Rivest, M., and Vézina, D. (2002b). "Effectiveness of sealers in counteracting alkali silica reaction in highway barrier walls exposed to wetting and drying, freezing and thawing, and deicing salt." *Canadian Journal of Civil Engineering*, 29(2), 329–337.

Bérubé, M.A., Frenette, J., Pedneault, A., Rivest, M. (2002c). "Laboratory Assessment of the Potential Rate of ASR Expansion of Field Concrete." *Cement, Concrete and Aggregates*, 24(1), 13-19.

Bérubé, M.A., Fournier, B. (2004). “Alkalis releasable by aggregates in concrete – significance and test methods. (invited Keynote paper).” *Proceedings of the 12th International conference on Alkali-Aggregate Reaction (AAR) in Concrete (ICAAR),* Beijing (China), Tang and Deng Editors, International Academic Publishers, Beijing World Publishing Corp., 1, 17-30.

Bleszynski, R. F., and Thomas, M. D. A. (1998). “Microstructural Studies of alkali-silica reaction in fly ash concrete immersed in alkaline solution.” *Advanced Cement Based Materials*, 7, 66-78.

Chatterji, S. (1989) “Mechanisms of Alkali-Silica Reaction and Expansion.” *Proceeding of the 8th International Conference on Alkali-Aggregate Reaction (ICAAR),* Kyoto, Japan, 101-105.

Crisp, T. M.; Waldron. P.; Wood. J. G. M. (1989) “Development of a non-destructive test to quantity damage in deteriorated concrete”. *Magazine of Concrete Research*, 45, 165 pp.

Deschenes, R.A. (2014). “Mitigation of Alkali-Silica Reaction (ASR) in an Interstate Median Barrier.” *Master’s Thesis*, University of Arkansas, Fayetteville Arkansas, 108 pp.

Diamond, S. (1989). “ASR—Another look at mechanisms.” *Proceeding of the 8th International Conference on Alkali-Aggregate Reaction (ICAAR),* Kyoto, Japan, 83–94.

Drimalas, T.; Folliard, K. J.; Thomas, M. D. A.; Fournier, B.; and Bentivegna, A., “Study of the Effectiveness of Lithium and Silane Treatments on Field Structures Affected by ASR,” *Proceedings of the 14th International Conference on Alkali-Aggregate Reaction (ICAAR),* Austin, TX, 2012, 10 pp.

Duchesne, J. and Bérubé, M. A. (1994). “The effectiveness of supplementary cementing materials in suppressing expansion due to ASR: Another look at the reaction mechanisms Part 2: pore solution chemistry.” *Cement and Concrete Research*, 24(2), 221-230.

Dunbar, P.A.; Grattan-Bellew, P.E. (1995). “Results of damage rating evaluation of condition of concrete from a number of structures affected by ASR”. *CANMET/ACI International Workshop on Alkali-Aggregate Reactions in Concrete*, Dartmouth, Canada.

Folliard, K. J.; Thomas, M. D. A.; Fournier, B.; Resendez, Y.; Drimalas, T.; and Bentivegna, A., “Evaluation of Mitigation Measures Applied to ASR-Affected Concrete Elements: Preliminary Findings from Austin, TX Exposure Site,” *Proceeding of the 14th International Conference on Alkali Aggregate Reaction (ICAAR),* Austin, TX, 2012, 10 pp.

Fournier, B., Bérubé, M.A., Thomas, M.D.A., Smaoui, N. & Folliard, K.J. (2004). Evaluation and Management of Concrete Structures Affected by Alkali-Silica Reaction - A Review (MTL 2004-11).” *Natural Resources*, Canada. Ottawa, 59 pp.

Fournier, B., Bérubé, M-A., Folliard, K.J., & Thomas, M.D.A. (2010). "Report on the Diagnosis, Prognosis, and Mitigation of Alkali- Silica Reaction (ASR) in Transportation Structures (Report No. FHWA-HIF-09-004)." *Federal Highway Administration*, U.S. Department of Transportation, Washington DC, 154 pp.

Gause, R. G. and Tucker, Jr. J. (1940). "Method for determining the moisture condition in hardened concrete." *Journal of Research of the National Bureau of Standards, 25, October, 14 pp.*

Giannini, R. (2012). "Evaluation of Concrete Structures Affected by Alkali-Silica Reaction and Delayed Ettringite Formation." *Doctoral Dissertation*, University of Texas, Austin Texas, 328 pp.

Grattan-Bellew, P.E., and Mitchell, L.D. (2006). "Quantitative petrographic analysis of concrete –The Damage Rating Index (DRI) method, a review". *Proceedings of the Marc-André Bérubé symposium on AAR in concrete*, CANMET/ACI Advances in concrete technology seminar, Montréal, Canada, 321-334.

Helmuth, R., Stark, D., Diamond, S., and Moranville-Regourd, M. (1993). "Alkali-silica reactivity: and overview of research (SHRP-C-342)." *Strategic Highway Research Program*, National Research Council, Washington, DC. 108 pp.

Institution of Structural Engineers (ISE). (1992). "Structural Effects of Alkali-Silica Reaction - Technical Guidance Appraisal of Existing Structures." *Institution of Structural Engineers*, 11 Upper Belgrave Street, London, 45 pp.

Janssen, D. J., and Snyder, M. B. (1994). "Resistance of concrete to freezing and thawing (No. SHRP-C-391)." *National Research Council*. Washington, DC. 217 pp.

Jensen, V. (2003). "Relative humidity measured by wooden stick method in concrete structures: long term measurements and reduction of humidity by surface treatment." *Norwegian Concrete and Aggregate Laboratory*. 13 pp.

Jensen, V. (2008). "Measurement of cracks, relative humidity and effects of surface treatment on concrete structures damaged by Alkali Silica Reaction." *Proceedings of the 13th Intonational Conference on Alkali-Aggregate Reaction (ICAAR),* Trondheim, Norway.

Kobayashi, A., Kirimura, K., Kuboyama, K., and Kojima, T. (1989). "Evaluation of surface treatment effect for preventing excessive expansion due to alkali-silica reaction." *Proceeding of the 8th International Conference on Alkali-Aggregate Reaction (ICAAR),* Kyoto, Japan, 821-826.

Laboratoire Central des Ponts et Chaussées (LCPC). (1997). “Détermination de l’indice de fissuration d’un parement de béton Méthode no. 47” *Ministère de l’équipement*, des transports et du logement, Paris.

Menzel, C. A. (1955) “A method for determining the moisture condition of hardened concrete in terms in of *relative* humidity.” *Proceedings of the American Society for Testing Materials*, 55, 1-26.

Moradi-Marani, F., Kodjo, S. A., Rivard, P., and Lamarche C-P. (2014). “Nonlinear Acoustic Technique of Time Shift for Evaluation of Alkali-Silica Reaction Damage in Concrete Structures.” *ACI Materials Journal*, 111(5), 581-591.

Multon, S. Barin, F.-X., Godart, B., Toutlemonde, F. (2008). “Estimation of the Residual Expansion of Concrete Affected by Alkali Silica Reaction).” *Journal of Materials in Civil Engineering*, ASCE, 20(1), 54-62.

Nilsson, L.-O. (1980). “Hygroscopic moisture in concrete—drying, measurements & related material properties,” *Division of Building Materials*, Lund University, Lund, Sweden, 162 pp.

Powers, T.C. (1945). “A working hypothesis for further studies of frost resistance of concrete.” *ACI Journal Proceedings*, 41(1), 245-272.

Powers, T. C. and Brownyard, T. L. (1947). “Studies of the Physical Properties of Hardened Cement Paste, Part 8.” *Journal of the American Concrete Institute*, 18(8), 933-969.

Powers, T. C. and R. A. Helmuth. (1953). “Theory of volume changes in hardened portland-cement paste during freezing.” *Highway Research Board Proceedings*, 32, 285-297.

Powers, T. C., and Steinour, H. H. (1955). “An interpretation of some published researches on the alkali-*aggregate* reaction. Part 1: The chemical reactions and mechanism of expansion.” J. *American Concrete Institute*, 51(2), 497–516.

Powers, T. C. (1975). “Freezing effects in concrete.” *American Concrete Institute Special Publication*, 47(1), 1-12.

Plusquellec, G., Geiker, M.R., Lindgård, J., Duchesne, J., Fournier, B., DeWeerdt, K. (2017). “Determination of the pH and the free alkali metal content in the pore solution of concrete: Review and experimental comparison.” *Cement and Concrete Research*, 96, 13-26.

Prezzi, M., Monteiro, P. J. M., and Sposito, G. (1997). “The alkali-silica reaction, part I: use of double layer theory to explain the behavior of reaction product gels.” *ACI Materials Journal*, 94(1), 10-16.

Quincot, G., Azenha, M., Barros, J., and Faria. R. (2011) "State of the art – methods to measure moisture in concrete." *Projetos De Investigação Científica E Desenvolvimento Tecnológico*, Portugal, 40 pp.

Rajabipour, F., Giannini, E., Dunant, C., Ideker, J. H., and Thomas, M. D. A. (2015). "Alkali-silica reaction: current understanding of the reaction mechanisms and the knowledge gaps." *Cement and Concrete Research*, 76, 130-146.

Rivard, P., Founrier, B., Ballivy, G. (2002). "The Damage Rating Index Method for ASR Affected Concrete—A Critical Review of Petrographic Features of Deterioration and Evaluation Criteria." *Cement, Concrete, and Aggregates*, 24(2), 1-11.

Rodrigues, F.A., Monteiro, P. J., and Sposito, G. (1999). "The alkali-silica reaction: the surface charge density of silica and its effect on expansive pressure." *Cement and Concrete Research*, 29(4), 527-530.

Rust, C. (2009). "Role of Relative Humidity in Concrete Expansion due to Alkali-Silica Reaction and Delayed Ettringite Formation: Relative Humidity Thresholds, Measurement Methods, and Coatings to Mitigate Expansion," *Master's Thesis*, University of Texas at Austin, Austin, TX, 120 pp.

Sanchez, L.F.M., Fournier, B., Jolin, M., and Bastien, J. (2014). "Evaluation of the Stiffness Damage Test (SDT) as a tool for assessing damage in concrete due to ASR: test loading and output responses for concretes incorporating fine or coarse reactive aggregates." *Cement and Concrete Research*, 56, 213-229.

Sanchez, L. (2014). "Contribution to the Assessment of Damage in Aging Concrete Infrastructures Affected by Alkali-Aggregate Reaction." *Doctoral Thesis*, Université Laval, Quebec, Canada, 401 pp.

Sanchez, L. F. M., Fournier, B., Jolin, M., and Bastien, J. (2015). "Evaluation of the Stiffness Damage Test (SDT) as a tool for assessing damage in concrete due to alkali-silica reaction (ASR): input parameters and variability of the test responses." *Construction and Building Materials*, 77, 20-32.

Sanchez, L. F. M., Fournier, B., Jolin, M., Duchesne, J. (2015). "Reliable quantification of AAR damage through assessment of the Damage Rating Index (DRI)." *Cement and Concrete Research*, 67, 74-92.

Sanchez, L. F. M., Fournier, B., Jolin, M., Bedoya, M. A. B., Bastien, J., & Duchesne, J. (2016). "Use of damage rating index to quantify alkali-silica reaction damage in concrete: fine versus coarse aggregate." *ACI Materials Journal*, 113(4), 395-407.

Sanchez, L.F.M., Fournier, B., Jolin, M., Bastien, J., Mitchell, D. (2016b). “Practical use of the Stiffness Damage Test (SDT) for assessing damage in concrete infrastructure affected by alkali-silica reaction.” Construction and Building Materials, 125, 1178-1188.

Sanchez, L.F.M., Fournier, B., Jolin, M., Mitchell, D., Bastien, J. (2017). “Overall assessment of Alkali-Aggregate Reaction (AAR) in concretes presenting different strengths and incorporating a wide range of reactive aggregate types and natures.” Cement and Concrete Research, 93, 17-31.

Shehata, M. H., Thomas, M. D. A., and Bleszynski, R. F. (1999). “The effect of fly ash composition on the chemistry of pore solution in hydrated cement pastes.” Cement and Concrete Research, 29, 1915-1920.

Shrimer, F. (2000). “Application and use of damage rating index in assessment of AAR-affected concrete-selected case studies.” Proceeding of the 11th International Conference on Alkali Aggregate Reaction *(ICAAR),* Quebec, Canada, 899-907.

Smaoui, N., Bérubé, M. A., Fournier, B., Bissonnette, B., & Durand, B. (2004). “Evaluation of the expansion attained to date by concrete affected by alkali-silica reaction. Part 1: Experimental study.” *Canadian Journal of Civil Engineering*, 31(5), 826-845.

Stanton, T. E. (1940). “Expansion of concrete through reaction between cement and aggregate.” *Proceedings of the American Society of Civil Engineering*, 66(10), 1781–1811.

Stark, D. (1990). “The Moisture Condition of Field Concrete Exhibiting Alkali-Silica Reactivity,” *CANMET/ACI International Workshop on Alkali-Aggregate Reaction in Concrete*, Halifax, NS, Canada, 19 pp.

Stark, D. (1991). “Handbook for the identification of alkali-silica reactivity in highway structures (SHRP-C/FR-91-101).” *Strategic Highway Research Program*, National Research Council, Washington, DC. 50 pp.

Stark, D. C., Morgan, B., Okamoto, P., & Diamond, S. (1993). Eliminating or minimizing alkali-silica reactivity (Report No. SHRP-C-343). *Strategic Highway Research Program (SHRP)*, National Research Council, Washington, DC, 266 pp.

Thomas, M. D. A. (1995). “The role of fly ash and slag alkalis in alkali silica reactions in concrete.” *CABNET/ACI Int. Workshop on Alkali-Aggregate Reactions in Concrete*, Natural Resources Canada, Canada, 181–204.

Thomas, M.D.A., Fournier, B., Folliard, K.J., Resendez, Y.A. (2011). “Alkali-Silica Reactivity Field Identification Handbook (FHWA-HIF-12-022).” *Federal Highway Administration,* U.S. Department of Transportation, Washington DC, 80 pp.

Thomas, M. D. A.; Folliard, K. J.; Fournier, B.; Drimalas, T.; and Rivard, P. (2012) "Study of Remedial Actions on Highway Structures Affected by ASR," *Proceedings of the 14th International Conference on Alkali-Aggregate Reaction (ICAAR),* Austin, TX, 10 pp.

Thomas, M.D.A., Folliard, K.J., Fournier, B., Rivard, P., Drimalas, T. (2013a). "Methods for evaluating and treating ASR-affected structures: results of field application and demonstration projects. Volume I: Summary of findings and recommendations (Report FHWA-HIF-14-002)." *Federal Highway Administration (FHWA),* U.S. Dept of Transportation, 70 pp.

Thomas, M.D.A., Folliard, K.J., Fournier, B., Rivard, P., Drimalas, T. (2013b). "Methods for evaluating and treating ASR-affected structures: results of field application and demonstration projects. Volume II: Details of field applications and analysis (Report FHWA-HIF-14-003)." *Federal Highway Administration (FHWA),* U.S. Dept of Transportation, 342 pp.

Villeneuve, V.; Fournier, B.; Duchesne, J. (2012). "Determination of the damage in concrete affected by ASR – The damage rating index (DRI)." *Proceedings of the 14th International conference on alkali-aggregate reaction (ICAAR).* Austin, Texas 10 pp.

Vivian, H. F. (1947). "Studies in Cement-Aggregate Reaction, VII-The Effect of Storage Condition on Expansion and tensile Strength Changes of Mortar*." Journal of the Council for Scientific and Industrial Research*, 20(4), 585-594.

Vuorinen, J. (1970). "On use of the dilation factor and degree of saturation in testing concrete for frost resistance." *Nordisk Berong*, 1, 37-64.

Walker, H. N., Lane, D. S., and Stutzman, P. E. (2006). "Petrographic Methods of Examining Hardened Concrete: A Petrographic Manual (No. FHWA-HRT-04-150)." *Federal Highway Administration,* U.S. Department of Transportation, Washington DC, 353 pp.

Wang, H., and Gillott, J. E. (1991) "Mechanism of alkali-silica reaction and the significance of calcium hydroxide." *Cement and Concrete Research,* 21, 647-654.

2. PAPER 1: ALKALI-SILICA REACTION IN CONCRETE WITH PREVIOUSLY INERT AGGREGATES

Richard A. Deschenes Jr.[1] and W. Micah Hale, Ph.D., P.E.[2]

[1]Graduate Assistant, Dept. of Civil Engineering, Univ. of Arkansas, Fayetteville, AR 72701 (corresponding author). E-mail: rdeschen@uark.edu

[2]Professor, Dept. of Civil Engineering, Univ. of Arkansas, Fayetteville, AR 72701.

Abstract: Alkali-silica reaction (ASR) is a persistent issue and has evaded eradication for nearly 80 years. The problem stems from a lack of standardized testing of aggregates. Cases occur when changes in material properties lead to potentially reactive aggregates reacting with higher alkali cements. A research program was established at the University of Arkansas to investigate cases of ASR, which occurred in combination with previously inert aggregates. In addition, locally available fly ashes were evaluated to determine replacement rates required to minimize the risk of ASR. A field monitoring program was established to evaluate deterioration mechanisms and mitigation measures. A concrete barrier wall located near the University of Arkansas was diagnosed with ASR that had considerable variation in the damage between sections of the wall. Deterioration ranges from minimal visible deterioration to severe damage or complete failure. The testing program reveals that certain aggregates that were previously deemed safe for use in concrete reacted deleteriously when other material properties changed.

DOI: 10.1061/(ASCE)CF.1943-5509.0000946.

Author keywords: Alkali-silica reaction (ASR); Median barrier; Freezing and thawing; Mitigation.

Note: This manuscript was submitted on February 5, 2016; approved on June 3, 2016; published online on July 18, 2016. Discussion period open until December 18, 2016; separate discussions must be submitted for individual papers. This paper is part of the Journal of Performance of Constructed Facilities, © ASCE, ISSN 0887-3828.

2.1. INTRODUCTION

Alkali-silica reaction (ASR) occurs when siliceous minerals dissolve in the presence of highly alkaline cement pore solution (Powers and Steinour, 1955). Ordered minerals, such as quartz, dissolve slower than amorphous minerals, such as opal. Chalcedony falls between the two extremes, reacting faster than crystalline quartz and slower than opal [ACI Committee 221 (ACI, 1998)]. Another factor in the reaction rate is the pore solution alkalinity; as the alkalinity increases, silica dissolves faster (Powers and Steinour, 1955). Once silica has dissolved and alkali-silica gel precipitated, the gel expands through the adsorption of fluid from the surrounding cement pore solution (Powers and Steinour, 1955; Diamond 1989). Expansion leads to cracking and deterioration of the concrete element.

Although ASR is a problem in several states, aggregate testing is not mandatory (Touma et al. 2001). Aggregates with a proven field performance record are considered safe for use in concrete without additional testing. However, material properties of aggregates and cements change over time, which may impact the alkali-silica reactivity of concrete.

Accelerated aggregate tests are available for evaluating potentially deleterious aggregates. These tests include ASTM C1260 (ASTM, 2008a) Standard Test Method for Potential Alkali Reactivity of Aggregates (Mortar-Bar Method), ASTM C1567 (ASTM, 2008b) Standard Test Method for Determining the Potential Alkali-Silica Reactivity of Combinations of Cementitious Materials and Aggregate (Accelerated Mortar-Bar Method), and ASTM C1293 (ASTM, 2012)

Standard Test Method for Determination of Length Change of Concrete Due to Alkali-Silica Reaction. These tests should be repeated yearly to account for variations in mineral and physical properties that may influence reactivity. All of the ASTM accelerated test methods refer to field performance history as the most reliable method for determining the potential deleterious reactivity of an aggregate (ASTM, C1293; ASTM, C1260). Under certain conditions, marginally reactive aggregates do not always show conclusive evidence of reactivity in accelerated testing. These aggregates may pass the test one year and fail the following year due to changes in properties. It is therefore necessary to address ASR through a combination of field performance and repeated accelerated testing.

Several cases of ASR were diagnosed in Arkansas after an increase in cement alkalis led to the development of ASR in combination with a previously inert aggregate. These cases were diagnosed through petrography only after deterioration was visible and mitigation measures were required. An interstate wall and two pavements have been monitored for several years to determine the rate of expansion and loss of physical properties. Field monitoring of existing structures is useful for evaluating concrete durability and assessing the field performance of concrete mixtures and aggregates. Monitoring the expansion rate and internal relative humidity (RH) of concrete is useful for prognosis of deterioration rate. The results can be used for developing mitigation and repair strategies. A study of remediation measures applied to the wall and pavements is ongoing and will be used to evaluate surface treatments as a means to control and slow the rate of ASR deterioration.

In the preliminary investigation to diagnose the deterioration mechanism present within the wall and pavements, core samples were sent for petrographic analysis, and conclusive evidence of ASR deterioration was noted. The diagnosis of ASR in these structures was surprising because

Arkansas River sand has been in use for decades without any previous cases of ASR. A laboratory investigation was required to determine the sources of reactive silica that lead to ASR, and accelerated test methods were used to evaluate the fine and coarse aggregate sources. Alkali extraction methods were also used to measure available alkalis within the concrete, because high alkalis are necessary for ASR to occur.

Preliminary conclusions indicate that sands from the Arkansas River in Arkansas have the potential to react deleteriously when high alkali cements are used. Based on historical records, the cement chemical composition varied for the locally produced cements used in construction of the wall and pavement. This may have led to higher cement alkalis in some sections of the wall. It is hypothesized that this variation in cement alkalis caused variability in the damage present within the wall. However, there was less variability observed in the deterioration within the pavement. Accelerated laboratory tests indicate that Arkansas River sand is deleteriously reactive, and that the local fly ash, used in the wall and pavements, was not effective in reducing the risk of ASR at replacement rates less than 30%. Field monitoring revealed that although ASR initiated deterioration within the concrete wall, the majority of expansion occurred during winter months, which infers that freezing and thawing deterioration exacerbated the expansion.

2.2. EXPERIMENTAL INVESTIGATION

The experimental investigation of the wall consisted of laboratory and field investigations. To confirm the presence of ASR in the wall, core samples were sent for petrographic examination. The examination results indicate that chalcedony minerals within the Arkansas River sand fine aggregate reacted to form alkali-silica gel and cracks radiating from the gel deposits. Laboratory tests were required to confirm the source of deleteriously reactive aggregates and to understand the change in concrete properties that led to deterioration from a previously inert aggregate. The

laboratory tests included ASTM C1260 [Accelerated Mortar Bar (AMBT)] and ASTM C1293 [Concrete Prism Tests (CPT)] to assess the reactivity of aggregates. These test methods are not sensitive to cement alkalinity and are used solely to confirm that the aggregate is potentially deleteriously reactive. Additional AMBT tests were conducted with samples of Class C fly ash from the same manufacturer and similar chemical composition as that used in the wall. This testing was done to determine the minimum replacement rate required to prevent ASR from occurring. To assess the effects of concrete alkalinity on the state of deterioration within the wall, core samples were evaluated through alkali extraction tests. In addition to the laboratory testing, the progression of deterioration in the wall was monitored to evaluate the mechanisms of deterioration.

2.2.1. Concrete Materials

The concrete mixture used in the wall contained 260 kg/m^3 (440 lb/yd^3) of cement and 46 kg/m^3 (78 lb/yd^3) of fly ash, or a replacement rate of 15%. The concrete mixture was not air-entrained and had a water to cementitious material (w/cm) ratio of 0.38. The aggregate content was approximately 1,216 kg/m^3 (2,050 lb/yd^3) for coarse, and 641 kg/m^3 (1,080 lb/yd^3) for fine. The concrete was placed continuously with a slip form system, and expansion joints were saw cut. The concrete contained fine aggregate from the Arkansas River sand and locally available crushed limestone as the coarse aggregate. The cement and fly ash were also produced locally. The cement contained between 0.46 and 1.01% Na_2O_{eq} (discussed later), and the fly ash contained approximately 24% CaO and 1.29% available alkalis.

Safe cement alkali limits suggested for preventing ASR date back to Stanton (1940), who suggested a limit of 0.60% Na_2O_{eq} (ACI 1998). In addition to limiting alkalis, a portion of the cement can be replaced with a supplemental cementing material (SCM) such as fly ash. Fly ash

dilutes the higher alkali cement and binds cement alkalis, which together reduces pore solution alkalinity (Thomas et al., 1999; 1995). The ability of fly ash to bind cement alkalis is a function of the CaO content of the fly ash (Thomas et al., 1999). Higher CaO fly ashes are less effective at reducing pore solution alkalinity than lower CaO fly ashes (Thomas et al., 1999). Therefore, higher replacement rates are required when using high CaO (Class C) fly ash compared to lower rates when using low CaO (Class F) fly ash. The concrete wall contained Class C fly ash at an estimated replacement rate of 10–15%, which was inadequate to prevent ASR.

2.2.1.1. Petrography

In 2012, core samples from the wall were extracted and sent to CTL Group for petrographic analysis (CTL Group, 2012). The petrographic report stated that the concrete was not air-entrained, with an estimated 3–4% air. Microcracking was common throughout the depth of the concrete and originated from alkali-silica gel deposits associated with chalcedony fine aggregate particles. The chalcedony particles also exhibited alteration rims. The coarse aggregate contained chert particles and microcracking. However, microcracks did not originate within the coarse aggregate particles and no reaction products originated from these particles.

2.2.1.2. Aggregates

Accelerated tests for potential ASR reactivity were conducted, using original aggregate sources. A stockpile of the original coarse aggregate was available for testing. However, a new sample of fine aggregate from the original source was substituted for evaluation, as the original aggregate stockpile was no longer available. Arkansas River sand for concrete is dredged in Van Buren (VB) and Pine Bluff (PB), Arkansas, and Muskogee (MK), Oklahoma. The sand contains chert and chalcedony minerals within the coarse fraction of the sand. Petrographic examinations of several ASR affected concretes, which contain Arkansas River sand from sources in Arkansas,

show evidence of ASR originating from chalcedony minerals. However, the sand from Oklahoma have not been associated with ASR. The coarse aggregate used in the wall consisted of a locally available, crushed limestone. Although this limestone contains trace amounts of chert, no conclusive evidence of ASR was found during petrographic examination. Samples of crushed, locally available granite and limestone coarse aggregates and Ottawa sand were evaluated as a possible nonreactive aggregate for use in concrete prism testing.

2.2.2. Laboratory Testing

2.2.2.1. AMBT

The aggregate sources used in the barrier wall concrete were evaluated in accordance with ASTM C1260. For each aggregate evaluated, the aggregate was sieved to the specified gradation and six mortar bars specimens were cast. The mortar bars were stored in 1.0 N NaOH solution at 80°C for 14 or 28 days. The expansion was determined from the average strain in six mortar bars.

The AMBT method subjects the mortar to a harsh storage environment to accelerate expansion and prevent alkali leaching. However, the environment also produces unreliable results in some aggregates (ASTM, C1260; Ideker et al., 2012). Aggregates that produce deleterious expansion in the AMBT should also be evaluated following the concrete prism test and considering field performance records to verify the results (ASTM, C1260).

2.2.2.2. ASTM C1567

A Class C fly ash containing 24% CaO was used at a replacement between 10 and 15% in the wall. The fly ash composition was less variable than the cement; however, there was concern that a low replacement of cement with a high CaO Class C fly ash was detrimental to the concrete performance. Therefore, ASTM C1567 was used to measure the effect of fly ash replacement.

Arkansas River sand and a Class C fly ash, from the same producer as the one used in the wall, were evaluated at various replacement rates to determine if any detrimental effect was observed at low replacement rates. Fly ash replacements between 10 and 40% were considered. For each fly ash replacement, six mortar bar specimens were evaluated for 28 days under AMBT conditions.

2.2.2.3. CPT

The aggregates that indicated potential deleterious reactivity in AMBT tests were reevaluated following ASTM C1293. The test outcomes from the CPT were compared to the field performance and AMBT outcomes. Each CPT consisted of six prisms cast with the selected aggregate sample and specified concrete mixture. A companion nonreactive fine aggregate was used in the concrete mixture when evaluating coarse aggregates, and vice versa, for evaluating fine aggregates. The coarse aggregate was sieved to match the ASTM C1293 specified gradation and the fine aggregate remained in the natural gradation. The concrete contained 420 kg/m^3 (708 lb/yd^3) of cement and a w/cm ratio of 0.45, as specified in ASTM C1293. A low alkali cement (0.53% Na_2O_{eq}) was used in the testing, and the alkalis were increased to 1.25% Na_2O_{eq}, to sustain the reaction throughout the one-year test duration. After curing for 24 h, the prisms were measured and then stored, over water, in containers at 38 °C. Periodic expansion measurements were conducted for one year. Before each measurement, the specimens were cooled to 23 °C. The storage containers were intended to develop a high humidity environment, which accelerates the development and progression of ASR.

The CPT is more reliable than other accelerated test methods and provides conclusive results (Ideker et al., 2012). However, the test method is subject to some difficulties. Alkali leaching can reduce the expansion attained during the test duration. Caution is required in using a storage

container that provides high humidity without developing a moisture gradient. The ASTM C1293 specification recommends the use of 19 L (5 gal.) buckets with lids, and a wicking material that prevents a humidity gradient from developing within the container.

The standard CPT container requires a large temperature controlled storage room when testing multiple samples simultaneously. To save laboratory space, smaller containers were used for all but one of the CPT tests conducted in this research. The containers were submerged in a water bath to achieve a temperature of 38°C. The smaller container allowed several samples to be stored in a single water bath, eliminating the need for a large environmental chamber. Before measurements, the containers were placed in an environmental chamber at 23°C to allow temperature equilibrium.

One of the limitation of the CPT method is alkalis leached from the sample during testing. The standard containers limit the amount of water precipitated onto the surface of the prisms, reducing the transport of alkalis from the concrete. During the cooling period, moisture within the containers condenses and precipitates onto the surface of the prisms. The water then provided an avenue for alkalis to be leached from the concrete and into the water at the bottom of the containers. The smaller containers led to higher alkali leaching than typical for ASTM C1293 recommended CPT container. This caused lower expansion than observed when using the recommended container. A typical container, as shown in **Fig. 2.2-1**, contains two prisms. Six prisms were cast for each aggregate evaluated, and although the prisms were stored in separate containers, the expansion results were consistent between containers.

Fig. 2.2-1–Typical CPT containers (by Richard Deschenes Jr.).

2.2.2.4. Soluble Alkalis

Due to the variability in the state of deterioration throughout the wall, soluble alkalis were measured via the hot water extraction method. The soluble alkali content for the concrete wall was measured using the method outlined by Bérubé et al. (2002a). Core samples were extracted from the control sections of the concrete wall in July 2014. Two 50-mm (2 in.) diameter, 150-mm (6 in.) long, core samples were removed from the control sections of minimal, moderate, and severe damage. The core samples were crushed to pass the 160-μm sieve. The samples were divided into 10-g subsamples, which were placed in boiling water for 10 min, and then allowed to cool for 24 h. The samples were then filtered using vacuum filtration and then diluted to 100 mL. The 100 mL samples were then evaluated using an ion chromatography (IC) analyzer to determine the dissolved Na and K concentration.

2.2.3. Field Testing

Bérubé et al. (2002b) conducted a 10-year investigation of ASR in concrete barrier walls. The investigation included surface expansion and internal-RH monitoring. The wall was instrumented with reference studs installed on the vertical face of the wall. A detachable strain gage was then used to measure the strain between the studs. In addition, 20-mm (0.79 in.)

diameter, 150-mm (6 in.) deep holes were drilled into the top of the wall for RH measurements. A commercial humidity probe was inserted into the hole and RH was measured after equilibrium occurred between the concrete and air surrounding the probe (Bérubé et al. 2002b). A similar program was implemented for the barrier wall in Arkansas to monitor deterioration and mitigation measures.

2.2.3.1. Field Monitoring

The wall is 7.1 km (4.4 mi) long, 1.1 m (3.5 ft) tall, and divided into 3.6–4.5 m (12–15 ft) sections at saw-cut joints. In an effort to catalog the level of deterioration along the full length of the wall, a visual survey of the wall was conducted in January 2013. Three damage classifications were selected based on the visual symptoms of distress. The damage classifications included minimal, moderate, and severe damage. Each section was assigned to one of the aforementioned three categories based on the visual distress symptoms. There was 3.7 km (2.3 mi) of wall that exhibited minimal damage (gray), 2.25 km (1.4 mi) with moderate damage (light grey), and 1.13 km (0.7 mi) with severe damage (dark gray) [**Fig. 2.2-2 (a)**]. A typical wall section with minimal damage is shown in **Fig. 2.2-2 (b)**. The concrete has minimal map cracking and no additional deterioration. The joints remain open enough to allow expansions without causing additional damage. The majority of the wall, 3.7 km (2.3 mi), remains in this condition. The state of deterioration along the wall varied between minimal [**Fig. 2.2-2 (b)**], in over half of the sections, to severe damage [**Fig. 2.2-2 (d)**] in a few sections. The sections with moderate damage have visible map cracking and a single longitudinal crack running the length of the section. The longitudinal crack has an opening width up to 2 mm. In addition, the joints between sections of moderate damage have closed. A typical section of moderate damage is provided in **Fig. 2.2-2 (c)**. The sections with severe damage range from map

cracking and multiple wide longitudinal cracks, to severe crushing and spalling. In addition, gel exudation and precipitation are present along the surface near larger cracks. The joints have completely closed, and in several places the crushing has caused large pieces of concrete to separate from the wall. The multiple longitudinal cracks are up to 6 mm wide at the surface [**Fig. 2.2-2 (d)**].

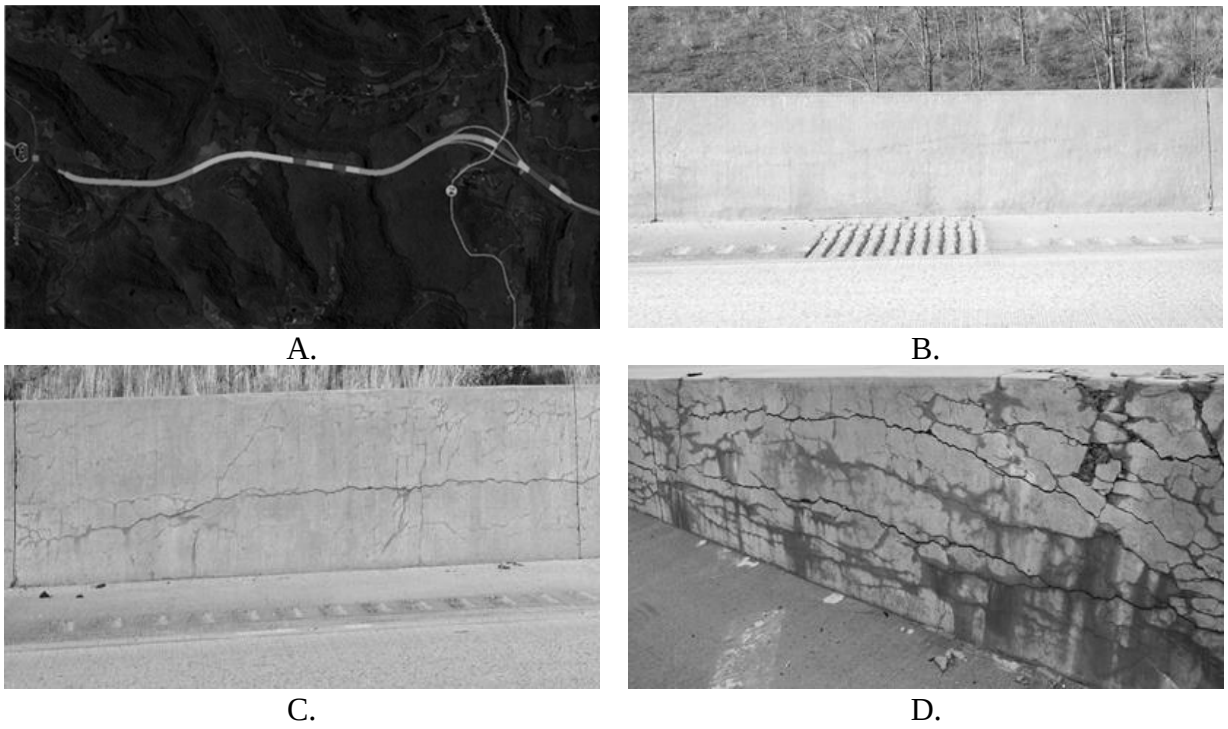

A. B. C. D.

Fig. 2.2-2–A. Interstate wall map view. B. Minimal damage. C. Moderate damage. D. Severe damage (by Richard Deschenes Jr).

The field-monitoring program included strain and internal-RH measurements. Fifteen sections of the wall were instrumented with reference studs for detachable mechanical (DEMEC) strain measurements. The reference studs were affixed at the corners of a 500 mm (20 in.) square grid on the vertical face of the wall. Periodic strain measurements were recorded for the longitudinal and vertical direction. Due to internal reinforcement and external restraint from the closure of contraction joints, longitudinal strain was prevented and the results were of little use. There was minimal vertical temperature reinforcement within the wall. The vertical strain data were

therefore normalized, ignoring internal restraint, to reduce fluctuation due to ambient temperature. The vertical strain data were normalized to a temperature of 24°C using a coefficient of thermal expansion (CTE) of 10×10^{-6} mm/mm/°C (5.6×10^{-6} in/in./°F) (FHWA 2011). The expansion rate for each damage level was calculated from the linear trend of the strain data. The wall sections were instrumented with ports for measuring internal-RH and temperature. A portable humidity probe was used to measure the internal-RH within the port. The internal-RH was measured when ambient conditions were approximately 21–24 °C.

In addition to monitoring the wall sections, several sections were treated with topical treatments in an effort to reduce the available moisture within the concrete and to slow the ASR-related deterioration in the concrete. At this time, 24 months of monitoring have been conducted; however, three or more years are required to evaluate the efficacy of mitigation measures. The results of mitigation measures will be summarized in a later publication.

The strain results provide insight into the different mechanisms of deterioration that occur during summer, when ASR damage occurs, and winter, when freezing and thawing distress predominates (Bérubé et al., 1996; 2002c). The ASR requires a warm, humid environment for gel to develop and expansion to occur (ACI, 1998). As temperature increases the rate of ASR also increases, and therefore the reaction accelerates, which will be discussed later in the paper (ACI 1998). Bérubé et al. (1996) reported on the influence of wetting and drying and freezing and thawing on expansion due to ASR. Bérubé et al. (1996) exposed cylinders to freezing and thawing cycles. Cylinders that had cracking initiated by ASR experienced accelerated expansion when exposed to freezing and thawing cycles. This increased expansion was caused by additional moisture entering the concrete through the cracked surface and due to the lower tensile capacity of the ASR deteriorated concrete (Bérubé et al. 1996). Bérubé et al. (1996) noted that

additional expansion did not occur in properly air-entrained concrete that had sustained ASR-related deterioration.

2.3. Experimental Results and Discussion

The results were evaluated to test the hypothesis that higher concentrations of alkalis were present in sections of the wall, which may have led to deterioration in combination with a potentially reactive aggregate. The aggregates were tested in accordance with two accelerated laboratory tests to determine the potential for the aggregate to develop ASR. The field monitoring results were summarized to determine the rate and prognosis of deterioration within the wall and to begin evaluating possible remediation measures.

2.3.1. Laboratory Testing

2.3.1.1. AMBT

The fine aggregate present within the wall consisted of Arkansas River sand from VB. The river sand contained chalcedony minerals, which are composed of a microcrystalline silica structure and are alkali-silica reactive. Two samples of Arkansas River sand from Arkansas were evaluated per ASTM C1260 (AMBT). As shown in **Fig. 2.3-1**, mortar bars containing VB sand developed a 14-day expansion of 0.17%. Mortar bars containing Arkansas River sand from PB also developed a 14-day expansion of 0.18%. Therefore, the VB and PB aggregates expanded more than the AMBT limit of 0.10% and were classified as potentially deleteriously reactive.

The coarse aggregate present within the wall was a crushed limestone from West Fork, Arkansas (WF). Mortar bars containing crushed WF developed a 14-day expansion of only 0.01%, and was classified as inert as shown in **Fig. 2.3-1**. The WF aggregate contained trace amounts of chalcedony minerals. However, the petrographic analysis revealed limited evidence of alkali-silica reaction originating from these minerals.

Additional fine aggregate from an Arkansas River source in MK was evaluated. However, this aggregate developed a 14-day expansion of 0.07%, and was classified as inert (**Fig. 2.3-1**). No instances of ASR have been reported in concrete containing aggregate from this aggregate source.

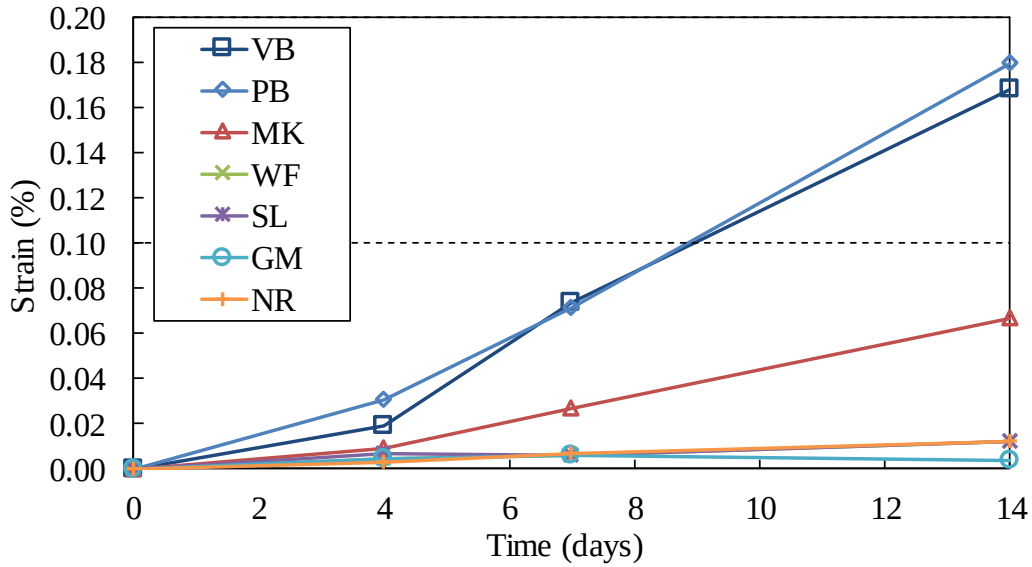

Fig. 2.3-1–ASTM C1260 (AMBT) results.

Three additional aggregates were tested to ensure the aggregates were inert, these aggregates were then used in the CPT as an inert companion aggregate when testing other aggregates for potential reactivity. These aggregates included crushed coarse limestone from the Sharps quarry (SL), crushed coarse granite from the Granite Mountain quarry (GM), and fine Ottawa sand (NR). All three of these aggregates had 0.01% or less expansion at 14 days.

2.3.1.2. ASTM C1567

The combination of fine aggregate and fly ash used in the wall were evaluated per ASTM C1567. River sand VB and Muskogee, Oklahoma Class C fly ash (FA 24% CaO content) were tested with fly ash replacement rates ranging from 10 to 40%. The test duration was extended to 28 days for samples containing fly ash as recommended in ASTM C1567. The 28-day average expansion was 0.17 and 0.05% for fly ash replacement rates of 15 and 30% fly ash, respectively

(**Fig. 2.3-2**). For the prevention of ASR, recommended replacement rates for Class C fly ash are between 40 and 50% (ACI, 1998; Shehata and Thomas, 2000). This range is often necessary for highly reactive aggregates. However, the rate of replacement is conservative for slowly reactive aggregates such as VB sand. As indicated in **Fig. 2.3-2**, a replacement rate of 30% is adequate, and the sample passes the ASTM C1567 test with a 28-day expansion of 0.05%.

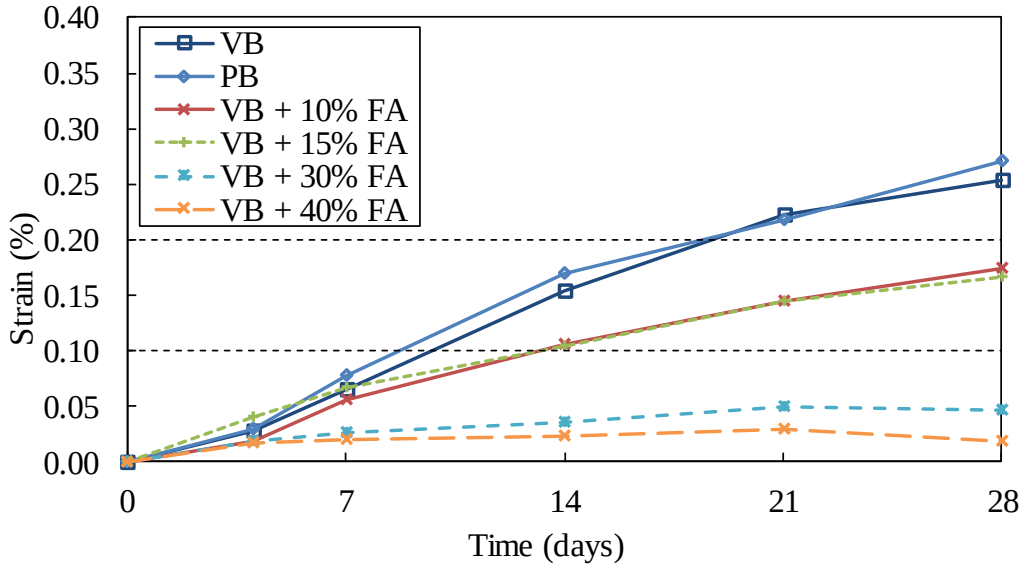

Fig. 2.3-2–ASTM C1567 (AMBT) results.

2.3.1.3. CPT

The VB aggregate was evaluated following ASTM C1293 (CPT). The prisms, containing VB fine aggregate and the nonreactive SL, developed a one-year average expansion of 0.03%. The CPT is used to evaluate either a potentially reactive fine or coarse aggregate, and a nonreactive companion aggregate is required to produce a concrete mixture. Prisms containing river sand from PB and SL had a one-year expansion of 0.02%. Both sands were classified as inert, per ASTM C1293 (**Fig. 2.3-3**). However, this classification is in contradiction with the petrographic analysis and AMBT results and is discussed in the synthesis of results.

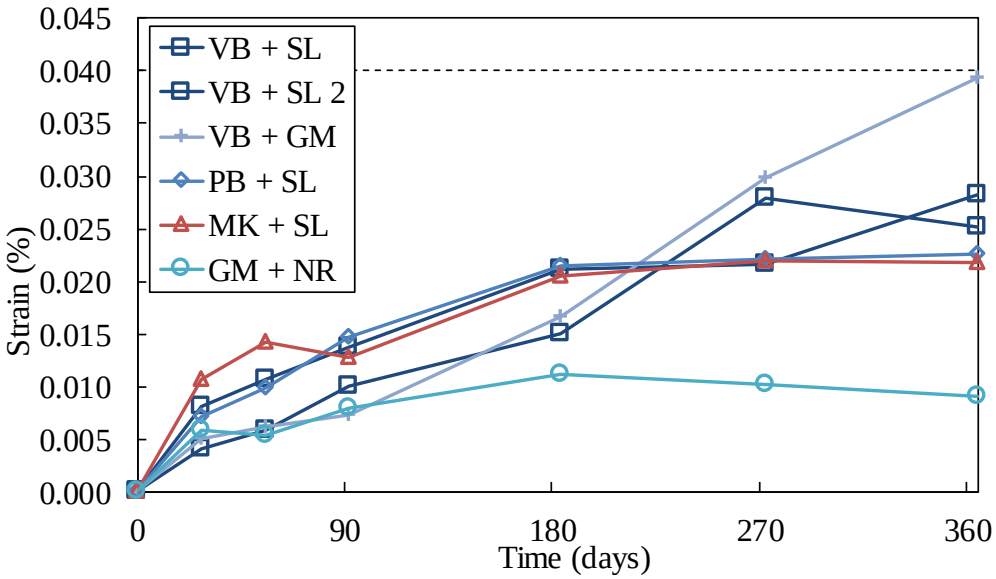

Fig. 2.3-3–ASTM C1293 (CPT) results.

An additional fine aggregate source from the region was evaluated per ASTM C1293, with SL coarse aggregate used as the companion nonreactive aggregate. River sand from MK produced similar expansion to that of VB and PB river sand. However, no cases of ASR have been reported in concrete that contained this aggregate. The GM coarse aggregate, tested in conjunction with a nonreactive (as indicated by ASTM C1260 test results) Ottawa sand, NR, developed only 0.01% expansion at one year, and was classified as inert.

As seen in the **Fig. 2.2-1**, water precipitated on the surface of the prisms during temperature equilibrium. The containers were used to determine if a smaller container could be substituted for the standard container. A smaller container would allow more CPT samples to be evaluated simultaneously without the need for a large environmental chamber set to a temperature of 38°C. Unfortunately, the smaller containers did not adequately prevent alkali leaching. Because of the concerns of alkali leaching, additional tests of VB fine aggregate in combination with GM or SL coarse aggregate were conducted using the ASTM C1293 recommended storage containers. After one year, the samples had an average expansion of 0.039 and 0.025%, respectively. The test with GM coarse aggregate indicates the aggregate as potentially deleteriously reactive,

whereas the test with SL indicates the aggregate is inert. The result with GM aggregate is in agreement with field performance records and ASTM C1260 results. The results for specimens stored in the alternative containers used in this research are called into question, because the containers led to alkali leaching, which for the VB aggregate resulted in a final expansion 29% less than measured when using the container recommended by ASTM C1293.

A comparison between the AMBT and CPT results is provided in **Fig. 2.3-4**, similarly to the manner presented in Fournier and Bérubé (2000). The six aggregates evaluated showed a majority of the local aggregates to be inert in both test methods. The VB and PB fine aggregates are potentially deleteriously reactive as indicated by ASTM C1260 results and petrographic analysis results for core samples from the wall containing the aggregate from the Arkansas River VB source. The VB and PB fine aggregates fall into the false negative category for the one-year CPT results, because they do not react deleteriously in CPT tests, while reacting deleteriously in AMBT tests.

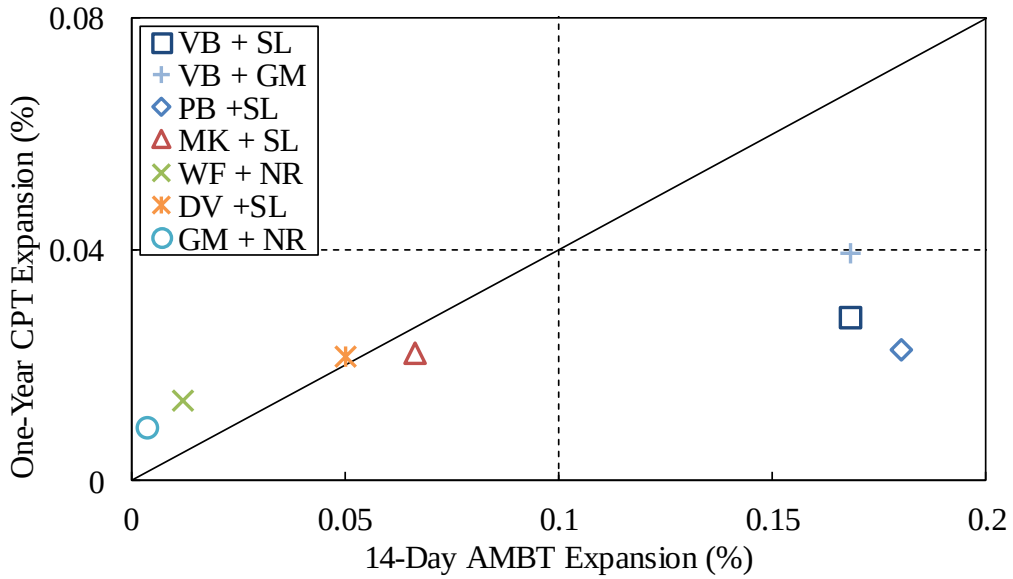

Fig. 2.3-4–Comparison of 14-day AMBT and one-year CPT results.

2.3.1.4. Cement Alkalis

The cement alkalis varied throughout the duration of construction of the wall. The cement was manufactured between 1997 and 1998. The average cement alkali content was 0.73% Na_2O_{eq}. However, the alkali content changed by as much as 0.19% from one day to the next. This variability was due to the manufacturing process and material properties of the limestone in use at the time. This variation partly explains the erratic damage level between sections of the wall. The high alkali content caused the development of ASR in concrete containing the slowly reactive Arkansas River sand. Conversely, when the alkali content dropped below a safe level, no alkali-silica reaction developed. Data from the cement manufacturer reveal the considerable variation in cement alkalis from day to day (**Fig. 2.3-5**).

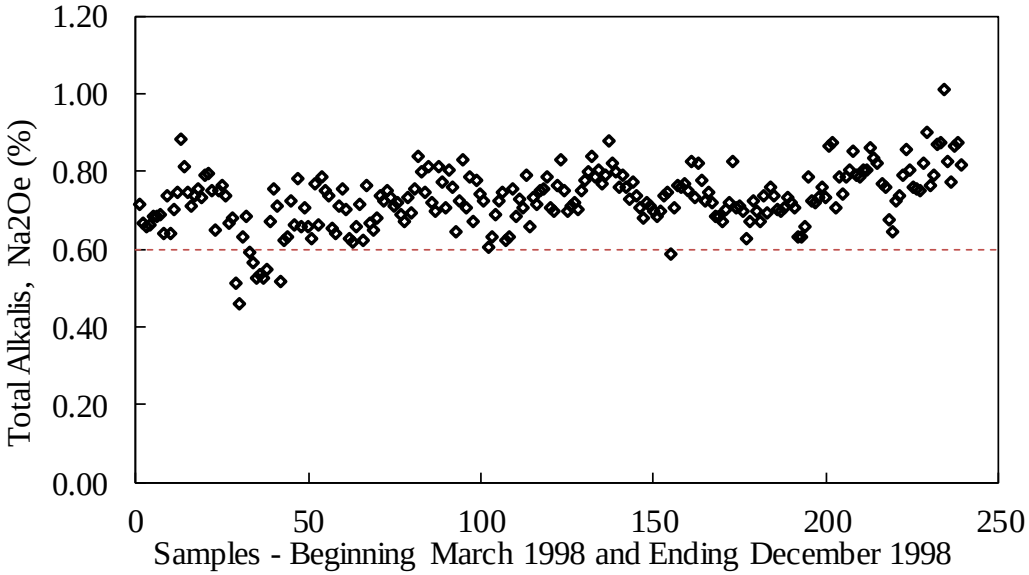

Fig. 2.3-5–Portland cement alkali content with respect to time.

2.3.1.5. Soluble Alkalis

The soluble alkali content for the hardened concrete was evaluated using the soluble alkali extraction method (Bérubé et al. 2002a). The concentrations for control sections of minimal, moderate, and severe damage are provided in **Fig. 2.3-6**. Two core samples were extracted from each wall section, and three hot water extraction tests were conducted for each core. Therefore,

six tests were used in determining the average soluble alkali content at each damage level. The bar graph shows the lowest result, the average, and the highest result, along with error bars indicating the standard deviation of the results. The average soluble alkali contents were 2.11, 1.46, and 1.10 kg/m^3 for the minimal, moderate, and severe damage sections, respectively. The soluble alkali content consisted only of alkalis that have not been leached out of the concrete or adsorbed into insoluble reaction products. Therefore, the alkali content at the time of construction was likely greater, for all damage classification, than measured using alkali extraction, and greater than the suggested limit of 3 kg/m^3 (ACI 1998; Fournier and Bérubé 2000). The concentration decreases as the damage level increases. It is hypothesized that this occurs due to alkalis adsorbed into insoluble reaction products, and additional alkalis leached from the severely damaged concrete. It is impossible to know the original alkali content in the severely and moderately damaged sections as compared to the minimally damaged sections. However, an increase in alkalinity increases the likelihood of siliceous minerals dissolving and forming ASR.

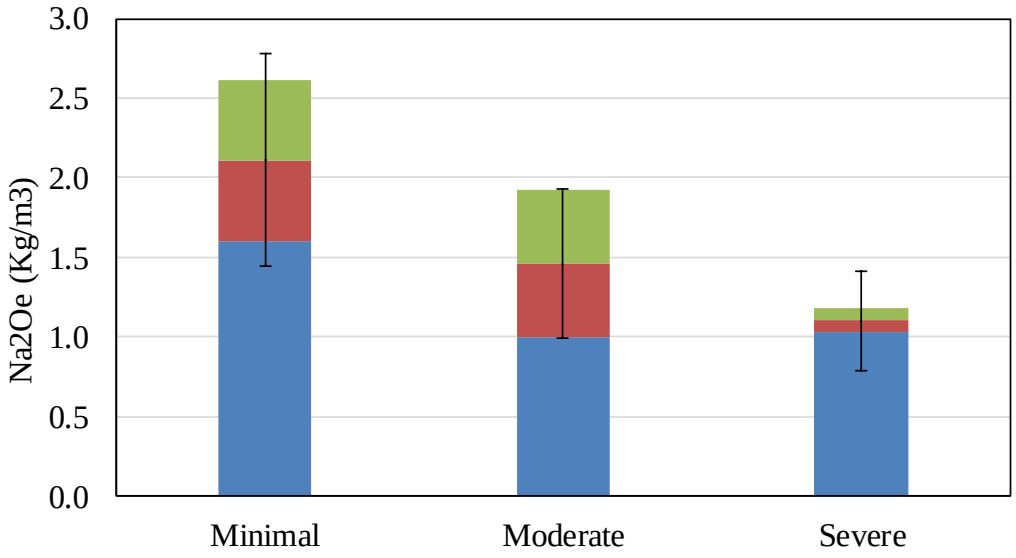

Fig. 2.3-6–Concrete barrier wall alkali content for wall sections of minimal, moderate, and severe deterioration.

2.3.1.6. Fly Ash

The local Class C fly ash had chemical properties that did not vary considerably over time. The CaO content varied between 24.7 and 28%, and the available alkali content varied between 0.96 and 1.69%. The fly ash is classified as Class C fly ash per ASTM C618, and low-alkali Type CH per Shehata and Thomas (2000). Based on Shehata and Thomas (2000) and ASTM C1567 test results, at least 30% fly ash is, therefore, recommended to prevent expansion. Unfortunately, due to design specification the fly ash replacement was limited to 20% and only 15% replacement was used in the wall, which was not sufficient to prevent ASR.

2.3.1.7. Synthesis of Results

The ASR in the concrete wall was not initially suspected because the aggregates had a proven field performance history. However, the increase in cement alkalis conceivably caused ASR to develop with an aggregate that is safe when used with low alkali cements (<0.6% Na_2O_{eq}). Although Class C fly ash did not contribute to the development of ASR, the replacement rate was too low to prevent ASR with the high alkali cement. Several other instances of ASR occurred in concrete pavements cast in the same period using the same fine aggregate sources. More cases likely exist that have not been discovered or reported. The Arkansas State Highway and Transportation Department (AHTD) has since implemented changes to their specification limiting cement alkalis in transportation structures to 0.6% Na_2O_{eq}.

2.3.2. Field Monitoring

The strain results from the wall show an increase in expansion in sections of moderate and severe damage as compared to the section of minimal damage. **Fig. 2.3-7** summarizes the temperature normalized vertical strain (%) that occurred in wall sections from each of the three damage

levels. The sections were untreated and included minimal damage (C-1), moderate damage (C-2), and severe damage (C-3).

From **Fig. 2.3-7**, it is apparent that the section with severe damage (C-3) had a higher strain rate between 40 and 90 days (0.016%) than between 90 and 260 days (0.001%). Again, the strain rate increases between 260 and 350 days (0.024). These periods coincide with the winter of 2013, the summer of 2013, and the winter of 2014, respectively (**Table 2.3-1**). The sharp increase in strain rate in the winter months is due to freezing and thawing deterioration. The same trend is apparent, although less so, in the sections of moderate damage. However, the sections of minimal damage do not show any increase in strain rate for the winter months. There is less cracking in the minimally damaged concrete, which limits moisture from entering the concrete. However, if cracking is initiated by ASR, freezing and thawing distress will accelerate the deterioration. **Table 2.3-1** provides a comparison of strain rates between the three damage levels.

Table 2.3-1. Strain Rate Date for Barrier Wall Control Sections.

Strain Rate		Section		
Time Period	Unite	Minimal	Moderate	Severe
Winter 2013	Percent/month	0.006	0.008	0.016
Sumer 2013	Percent/month	0.000	0.001	0.001
Winter 2014	Percent/month	0.000	0.005	0.024
Average	Percent/month	0.001	0.003	0.001
Average	Percent/year	0.008	0.037	0.114

The section with minimal damage has, on average, not expanded or contracted over two years, whereas the sections of moderate and severe damage are expanding 0.04 and 0.11% per year, respectively. Ideker et al. (2012) reported that unrestrained concrete would develop visible cracking when expansion exceeded 0.04%. Therefore, the sections of moderate and severe damage expand enough in a single year to produce visible cracks in the concrete.

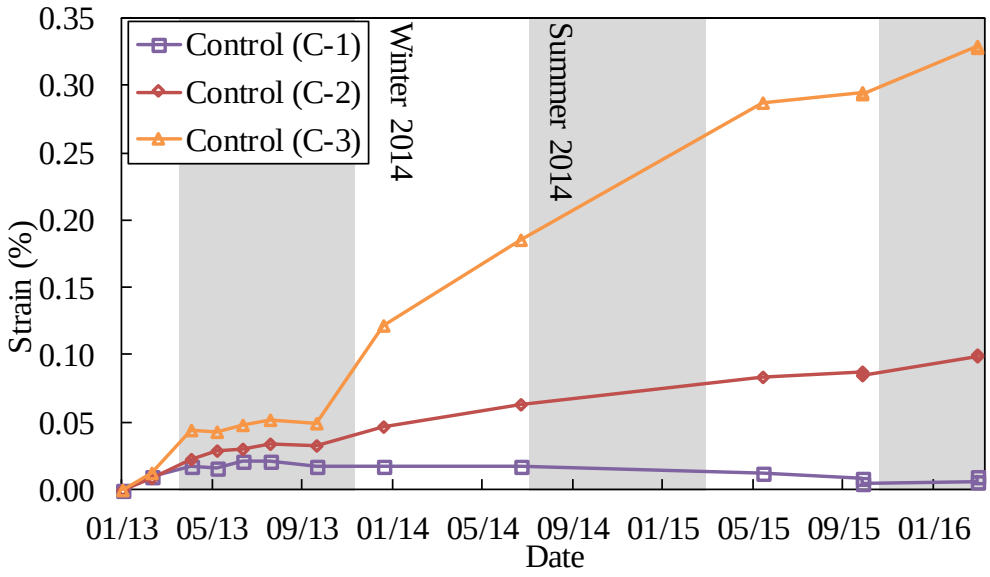

Fig. 2.3-7–Barrier wall normalized vertical strain.

Sections of the wall were treated with topical water barrier that will reduce the available moisture within the concrete. This will prevent additional microcracks and reduce the ingress of moisture and subsequent freezing and thawing distress. Long-term monitoring of the treated sections is required to evaluate the efficacy of treatments. In addition, sections of moderate to severe damage will require crack repair before a surface treatment is applied.

2.4. Conclusions and Recommendations

Arkansas River sand, which has a long-proven field performance record, developed ASR due to the use of higher-alkali cements. An increase in cement alkalis caused several instances of ASR in concrete containing a previously safe aggregate. This aggregate is the only economic source of fine aggregate in the region, to continue using the sand in concrete, the reactivity of the sand and alkalinity of the cement must be more closely monitored. Field performance records alone are not sufficient when considering concrete for use in essential structures. Limiting cement alkalis to less than 0.6% Na_2O_{eq} will reduce the occurrence of ASR but does not guarantee that ASR will not occur, and additional measures such as fly ash may be required. Tests with various

replacement rates of fly ash reveal that Arkansas River sand used in concrete with high-alkali cements require at least 30% Class C fly ash to prevent ASR.

- Laboratory testing of aggregates in concrete should be used in combination with field performance records when determining the potential reactivity of concrete mixtures. Variations in cement and aggregate compositions can lead to ASR in mixtures that have performed well in the past.
- The concrete wall had good freezing and thawing resistance despite not being air entrained. However, deterioration in the sections of wall with ASR-related cracking experienced freezing and thawing deterioration as a result of reduced durability. As ASR progressed and cracks formed at the surface of the concrete, additional moisture entered the concrete, which left the concrete saturated during freezing, and deterioration was exacerbated.
- Alkali extraction tests revealed that water-soluble alkalis within the concrete decreases as deterioration proceeds. This is likely due to alkalis becoming insoluble when adsorbed into reaction products, and due to alkalis leached from the concrete as cracking worsens.

2.5. FUTURE RESEARCH

The wall expansion and internal-RH will be monitored for a total of three years to determine the efficacy of remediation measures, including silane treatments, in reducing ASR-related expansion. The field test program will help in developing mitigation measures for concrete that exhibits moderate to severe deterioration at the time of treatment. An outdoor exposure site is under development and will help in determining minimum safe replacement rates for Class C fly ash in preventing ASR. In addition, the maximum safe alkali limit for use with Arkansas River sand will be determined. No other sources of fine aggregate are available in the northwest region

of Arkansas, and cement alkalis and aggregate reactivity must be monitored regularly to continue using the aggregate source without risk of new cases of ASR.

2.6. ACKNOWLEDGMENTS

The authors would like to thank the Arkansas State Highway Transportation Department (AHTD) for funding and supporting this project. AHTD personnel were instrumental in providing access to the concrete wall during site visits throughout the duration of the project. Mack Blackwell Rural Transportation Center (MBTC) also provided support for the research program. Headwaters Resources, Inc., and Ash Grove cement provided materials used in the laboratory portion of the study. Several students at the University of Arkansas, Department of Civil Engineering were invaluable in conducting the research program.

2.7. REFERENCES

ACI (American Concrete Institute). (1998). "State-of-the-art report on alkali-aggregate reactivity." ACI 221.1R-98, Farmington Hills, MI.

ASTM. (2008a). "Standard test method for determining the potential alkali-silica reactivity of combinations of cementitious materials and aggregate (accelerated mortar-bar method)." ASTM C1567-04, West Conshohocken, PA, 772–775.

ASTM. (2008b). "Standard test method for potential alkali reactivity of aggregates (mortar-bar method)." ASTM C1260-05, West Conshohocken, PA, 676–680.

ASTM. (2012). "Standard test method for determination of length change of concrete due to alkali-silica reaction." ASTM C1293-08b, West Conshohocken, PA, 687–686.

Bérubé, M. A., Chounard, D., Boisvert, L., Frenetter, J., and Pigeon, M. (1996). "Influence of wetting-drying and freezing-thawing cycles, and effectiveness of sealers on ASR." Proc., 10th Int. Conf. on Alkali-Aggregate Reaction (ICAAR), ARRB Group, Australia, 1056–1063.

Bérubé, M. A., Frenette, J., Rivest, M., and Vézina, D. (2002a). "Measurement of the alkali content of concrete using hot water extraction." Cem. Concr. Aggregates, 24(1), 28–36.

Bérubé, M.-A., Chouinard, D., Pigeon, M., Frenette, J., Boisvert, L., and Rivest, M. (2002b). "Effectiveness of sealers in counteracting alkali silica reaction in plain and air-entrained laboratory concretes exposed to wetting and drying, freezing and thawing, and salt water." Can. J. Civ. Eng., 29(2), 289–300.

Bérubé, M.-A., Chouinard, D., Pigeon, M., Frenette, J., Rivest, M., and Vézina, D. (2002c). "Effectiveness of sealers in counteracting alkali silica reaction in highway barrier walls exposed to wetting and drying, freezing and thawing, and deicing salt." Can. J. Civ. Eng., 29(2), 329–337.

CTL Group (Construction Technology Laboratories Group). (2012). "Petrographic examination of concrete specimens from I-540 roadway and barrier wall." CTL Group Project No. 157501, Skokie, IL.

Diamond, S. (1989). "ASR—Another look at mechanisms." Proc., 8th Int. Conf. on Alkali-Aggregate Reaction (ICAAR), Elsevier, Essex, England, 83–94.

FHWA (Federal Highway Administration). (2011). "Coefficient of thermal expansion in concrete pavement design." Rep. No. FHWA-HIF-09-015, U.S. Dept. of Transportation, Washington, DC.

Fourner, B., and Bérubé, M. A. (2000). "Alkali-aggregate reaction in concrete: A review of basic concepts and engineering implications." Can. J. Civ. Eng., 27(2), 167–191.

Ideker, J. H., Bentivegna, A. F., Folliard, K. J., and Juenger, M. C. G. (2012). "Do current laboratory test methods accurately predict alkali silica reactivity?" ACI Mater. J., 109(4), 395–402.

Powers, T. C., and Steinour, H. H. (1955). "An interpretation of some published researches on the alkali-aggregate reaction. Part 1: The chemical reactions and mechanism of expansion." J. Am. Concr. Inst., 51(2), 497–516.

Shehata, M. H., and Thomas, M. D. A. (2000). "The effect of fly ash composition on the expansion of concrete due to alkali-silica reaction." Cem. Concr. Res., 30(7), 1063–1072.

Stanton, T. E. (1940). "Expansion of concrete through reaction between cement and aggregate." Proc. Am. Soc. Civ. Eng., 66(10), 1781–1811.

Thomas, M. D. A. (1995). "The role of fly ash and slag alkalis in alkali silica reactions in concrete." CABNET/ACI Int. Workshop on Alkali- Aggregate Reactions in Concrete, Natural Resources Canada, Canada, 181–204.

Thomas, M. D. A., Shehata, M. H., and Shashiprakash, S. G. (1999). "The use of fly ash in concrete: Classification by composition." Cem. Concr. Aggregates, 21(2), 105–110.

Touma, W. E., Fowler, D. W., and Carrasquillo, R. L. (2001). “Alkali-silica reaction in portland cement concrete: Testing procedures and mitigation methods.” Research Rep. ICAR 301-1F, International Center for Aggregates Research, Austin, TX.

3. PAPER 2: MITIGATION OF ALKALI-SILICA REACTION AND FREEZING AND THAWING THROUGH SURFACE TREATMENT

Title No. 114-M29

by Richard A. Deschenes Jr., Cameron D. Murray, and W. Micah Hale

Biography: ACI member **Richard A. Deschenes Jr.** is a Graduate Assistant at the University of Arkansas, Fayetteville, AR, where he received his BS and MS in civil engineering in 2012 and 2014, respectively. He is currently a civil engineering PhD candidate at the University of Arkansas. He received the 2013 ACI Schwing American Scholarship and the 2015 ACI BASF Construction Chemicals Student Fellowship. His research interests include durability issues of concrete structures.

Cameron D. Murray is a Research Assistant in the Department of Civil Engineering and Environmental Science at the University of Oklahoma, Norman, OK, where he is pursuing his PhD. He received his BS and MS in civil engineering from the University of Arkansas. He was the 2012 recipient of the ACI Baker Student Fellowship. His research interests include shear in prestressed concrete girders and prestressing strand bond.

W. Micah Hale, FACI, is a Professor in the Department of Civil Engineering at the University of Arkansas. He is Chair of ACI Committee 363, High-Strength Concrete, and is a member of ACI Committees 233, Ground Slag in Concrete, and 239, Ultra-High-Performance Concrete; and Joint ACI-ASCE Committee 423, Prestressed Concrete. He received his BS, MS, and PhD in civil engineering from the University of Oklahoma. His research interests include concrete materials, mixture proportioning, and prestressed concrete.

Abstract: The research program included an investigation of mitigation methods applied to concrete barrier walls that exhibited damage due to alkali-silica reaction (ASR) and freezing and thawing. The damage within the barrier varies inconsistently between sections. Although most of the barrier exhibits minimal visible damage, large portions of the barrier show moderate damage, and several sections exhibit severe damage or complete failure. Several sections of the median barrier, with different initial damage, were instrumented to monitor strain and internal relative humidity. Sections were then treated with surface treatments and monitored for three years. Preliminary conclusions show that silane is effective in controlling ASR within the damaged sections of the barrier. The sections of moderate and severe damage expanded rapidly during winter months due to freezing and thawing distress. However, silane reduced the ASR and freezing and thawing-related distress in the moderate and severely damaged sections.

Keywords: alkali-silica reaction (ASR); breathable vapor barrier; elastomeric paint; freezing and thawing; linseed oil; mitigation; silane.

ACI Materials Journal, V. 114, No. 2, March-April 2017. MS No. M-2016-275, doi:10.14359/51689493, received July 22, 2016, and reviewed under Institute publication policies.

3.1. INTRODUCTION

Alkali-silica reaction (ASR) is a deleterious expansive reaction that occurs in concrete. Reactive noncrystalline amorphous siliceous minerals, present within some aggregates, may dissolve in the presence of alkaline concrete pore solutions. This is followed by the formation of alkali-silica

gel, which under the right conditions will adsorb water from the surrounding concrete pore solution and expand. The expansive pressure overcomes the tensile capacity of the concrete and leads to microcracks in the aggregates, followed by microcracking in the cement matrix. As microcracks continue to expand, macrocracks extend to the surface of the concrete element. The presence of ASR and cracking decreases the freezing and thawing resistance of the concrete and can lead to corrosion in reinforced members, exacerbating deterioration.

A concrete median barrier and interstate pavement in Northwest Arkansas were diagnosed with ASR and freezing and thawing deterioration in March 2012. The damage within the median barrier was not consistent, and varied from minimal visible damage to severe damage and complete failure. A research program was initiated to determine the cause of ASR and to evaluate methods for mitigation. Due to the variability in the damage, several mitigation methods were evaluated to determine the most effective and practical treatment for each damage level. Although ASR was the instigating factor leading to premature deterioration in the concrete barrier, the concrete was not air-entrained and freezing and thawing deterioration occurred because of the onset of cracking caused by ASR.

An investigation into the cause of ASR and variability of damage within the median barrier is documented in another publication by the authors **[**1]. This document discusses the preliminary findings of the mitigation methods that were implemented in March 2013. Three or more years of investigation were necessary to determine the most effective treatment regimen for each damage level. The findings and preliminary conclusions after three years of monitoring are presented herein.

3.2. Research Significance

Although literature on the efficacy of silane used for treating concrete affected by ASR is well established, the level of damage present at the time of treatment is often minimal to moderate. In addition, the current literature on long-term mitigation of the combination of ASR and freezing and thawing is limited. This research project provides information on the efficacy of several mitigation methods applied to concretes affected by a combination of ASR and freezing and thawing. The damage level within the concrete at the time of treatment ranges from minimal to severe.

3.3. Experimental Procedure

Premature deterioration was noted in several sections of interstate median barrier in Northwest Arkansas during a 2012 inspection. A sample of concrete was sent for petrographic analysis and the presence of ASR and freezing and thawing damage was noted. The degree of damage varied considerably throughout the 4.4 mile (7.1 km) length of median barrier. Approximately 2.3 miles (3.7 km) of the median barrier showed minimal visible damage, 1.4 miles (2.3 km) had moderate damage, and 0.7 miles (1.1 km) showed severe damage (**Fig. 3.3-1**). An experimental program was initiated in January 2013 to evaluate methods for mitigating the ASR. Several surface treatments were evaluated to slow the progress of ASR and freezing and thawing, for sections of minimal, moderate, or severe damage.

Fig. 3.3-1–Typical barrier section with severe damage (by Richard Deschenes Jr.).

The most promising method for mitigating ASR in concrete structures is through reducing the availability of moisture for expansion. Research by Stark [2] indicated that reducing the internal relative humidity (RH) of a concrete element below 80% (referenced to a temperature of 70 to 75°F [21 to 24°C]) will slow or stop ASR related expansion. Later results produced by Bérubé et al. [3] reinforced these findings. Several breathable vapor barriers were evaluated by Bérubé et al. [4] to reduce internal-RH for concrete median barriers. The median barriers were instrumented to monitor strain and internal-RH in a similar manner as in the current research project. Several silane and siloxane surface treatments were evaluated, and effectively reduced the internal-RH and strain within the treated sections for 5 or more years. Bérubé et al. [3, 4] measured the efficacy of silane treatments applied to concrete exposed to a combination of ASR and freezing and thawing. Freezing and thawing cycles exacerbated deterioration in concretes with existing ASR deterioration. Concrete with existing ASR deterioration was treated with silane, which reduced RH and prevented additional deterioration even when exposed to freezing and thawing cycles [3, 4]. In addition, sections of different initial deterioration reacted differently to treatment [3]. However, all the treated sections showed a beneficial reduction in RH and strain as compared to the untreated control sections.

3.3.1. Materials

The concrete materials and mixture information is outlined in an earlier publication by the authors, [1] results from aggregate and concrete testing were also provided. In the present study, three damage categories were selected based on visible symptoms and each median barrier section was assigned to one of the damage categories. Not all the surface treatments were practical for application along the entire median barrier. Therefore, three surface treatments were evaluated on sections from each damage category to determine the most effective and efficient

treatment. The surface treatments, costs, and application rates are provided in **Table 3.3-1**. The silane and linseed oil were applied with a hand-operated sprayer, and the application rate was controlled by volume. The elastomeric paint was applied with a paint roller and was again controlled by volume. After treatment, a silicon sealant was used to fill any cracks wider than 0.04 in. (1 mm) at the surface. A section treated with elastomeric paint adjacent to a section treated with silane is shown in **Fig. 3.3-2**.

Table 3.3-1–Application rate and cost analysis of surface treatments

Treatment	Silane	Elastomeric Paint	Linseed Oil
Cost, 5 gal (19L)	$217	$248	$174
Application Rate, ft^2/gal (m^2/L)	150 (3.7)	100 (2.5)	300 (7.4)
Cost, \$/ft^2 (\$/m^2)	\$0.29 (\$3.12)	\$0.50 (\$5.34)	\$0.12 (\$1.25)

Fig. 3.3-2–Barrier sections treated with elastomeric paint (left) and silane (right) (by Richard Deschenes Jr.).

Silane treatment is viscous and able to penetrate existing cracks on the surface of the concrete. Silane penetrates the concrete substrate and chemically bonds to the concrete. Silane is comprised of a silicon resin network which is hydrophobic and prevents liquid water from entering the concrete. The silicon network of silane is permeable to water vapor, which allows the concrete's internal-RH to equilibrate with the ambient-RH [5]. Thus, the concrete dries over time, reducing ASR-related expansion and freezing and thawing- related stresses. Due to the variability in damage in the sections of median barrier, and the extent of damage in several

sections, there was concern that silane alone would not provide a beneficial reduction in RH and strain for sections of moderate or severe damage. Therefore, an elastomeric paint was also selected for evaluation. Elastomeric paint can bridge small cracks, and is viscoelastic allowing it to stretch as cracks expand. Research published by Drimalas et al. [6] and others provided preliminary findings on the efficacy of elastomeric paint applied to columns that exhibited moderate ASR damage [7, 8]. In the current study, boiled linseed oil was evaluated as an economic alternative method for treating the large surface area of the concrete median barrier. Boiled linseed oil has been used for years to protect bridge decks from external moisture. Due to the low viscosity of boiled linseed oil, it may be applied with a sprayer and will enter larger cracks and prevent moisture from entering. However, linseed oil is not a breathable membrane, and any moisture within the concrete at the time of treatment is trapped.

Each surface treatment was applied to one 12 to 15 ft. (3.7 to 4.6 m) section of each damage level. At each damage level, the first section was left untreated as a control, the second section was sprayed with silane, the third section was sprayed with linseed oil, the fourth section was painted with elastomeric paint, and the final section was sprayed with two applications of silane (the second application was applied 6 months after the initial treatment). The day after treatments were applied, larger cracks (opening wider than 1/16 in. [1.5 mm]) in the moderate and severely damaged sections were sealed with a commercial silicon crack sealant to prevent water from collecting in the cracks.

3.3.2. Specimens

The typical median barrier sections were 12 to 15 ft (3.66 to 4.57 m) in length, 3.5 ft (1.07 m) tall, with a trapezoidal cross section that tapers from 24 in. (61 cm) at the base to 8 in. (20 cm) at the top. A total of 15 sections were selected for treatment and monitoring. Of the 15 sections,

five each were of minimal, moderate, and severe damage. The sections were differentiated based on visible symptoms of distress.

The vertical face of each section was instrumented with stainless steel gauge studs for measuring strain. The gauge studs were 3 in. (75 mm) long and 3/8 in. (9.5 mm) diameter, with a small indentation drilled into the end of the gauge stud. The indentation is made to mate with the points on the detachable mechanical (DEMEC) strain gauge used for measurements. Four gauge studs were affixed to the vertical face of each median barrier section. The gauge studs were placed at the corners of a 20 in. (500 mm) square grid (**Fig. 3.3-3**). The grid allowed for two vertical and two horizontal strain measurements, providing a better understanding of the strain in each direction.

A port was drilled alongside the strain measurement grid (**Fig. 3.3-3**) for inserting a portable humidity probe. The port was drilled to a depth of 6 in. (150 mm) with an inside diameter of 33/64 in. (13.1 mm). A 2 in. (50 mm) long, 1/2 in. (12.7 mm) nominal-diameter polyvinyl chloride (PVC) pipe was epoxied into this hole to allow the humidity probe to fit securely. The port was closed off between measurements using an airtight cap. Portable humidity probes were used for internal-RH and temperature measurements.

Fig. 3.3-3–Typical strain measurement grid on barrier section after treatment with silane (by Richard Deschenes Jr.).

3.3.3. Items of investigation

Strain and internal-RH were measured monthly for the first 6 months and then every 3 months until 1 year. After 1 year, the measurements were conducted every 6 months. Strain was determined using a DEMEC gauge with an accuracy of $\pm 2.5 \times 10^{-4}$% strain. Length change was measured along the four sides of each strain grid by the first operator and then again by a second operator. The results were then averaged to minimize operator error.

When using the Vaisala probes, internal-RH was measured by inserting the portable probe into the pre-drilled port. The probe measures RH within ±1.5% for temperatures between 32 and 10 0°F (0 and 38 °C). The probe could equilibrate with the air temperature in the port for a minimum of 30 minutes. Because the air in the port was already in equilibrium with the concrete, relatively little time was required for humidity equilibrium. Therefore, after the probe reached temperature equilibrium, RH measurements could be made without waiting for humidity equilibrium to occur. When possible, additional time could ensure that the air in the port was in equilibrium with the concrete. However, an improvement in accuracy was not observed. The LabJack probes were inserted into 3 in. (75 mm) holes that were drilled at the time of measurements. The probe remained in the hole for 4 to 5 hours for equilibration.

3.4. ANALYTICAL PROCEDURE

The raw strain data from the median barriers was subject to variability due to the ambient temperature at the time of measurements. The strain data for all sections was normalized to a temperature of 70°F (21°C). The internal concrete temperature was measured using the RH probes, which include a temperature sensor. The coefficient of thermal expansion (CTE) of the concrete was assumed at 3.9×10^{-6} in./in./°F (7.0×10^{-6} mm/mm/°C). This value was selected based on typical values for CTE of concrete and calibrated to minimize the difference in strains

measured on the same day at different temperatures. The internal-RH was measured when the air temperature was between 70 and 75 °F (21 and 24 °C) and no temperature normalization was applied.

Strain was measured on each side and then the results of the two sides were averaged to produce a single strain value. Due to the restraint provided by the adjacent median barrier sections, strain in the horizontal direction was limited. Therefore, only the vertical strain is reported and discussed herein. The treated sections are hereafter referred to by an alphanumeric sequence, which includes the treatment (indicated by letters) and damage level of the treated concrete on a 1-to-3 scale (for example, the section of minimal damage and treated with silane will be referred to as S-1, whereas the section with severe damage and treated with elastomeric paint is referred to as EP-3).

In addition to the strain data for each section, the differential strain as compared to the untreated control section was determined. The differential strain was computed from the difference between the strain in each treated section and the strain in the corresponding control. The differential strain is plotted with strain (%) on the ordinate and time (date) on the abscissa.

3.5. Experimental Results and Discussion

3.5.1. Temperature-normalized vertical strain

The temperature normalized strain data for each treated section, in addition to the untreated control, were plotted in a separate figure for each damage classification. The scale of the strain data is different for sections of moderate and severe damage as compared to sections of minimal damage. The vertical strain results for sections of minimal damage are provided in **Fig. 3.5-1 (a)**; the initial measurement was made on January 31, 2013. For comparison, the strain rate data for all sections broken down by season is provided in **Table 3.5-1**. This table provides the linear rate

of strain for the sections disaggregated into summer and winter seasons over the monitoring period. The results indicate the strain rate during winter months is higher than that during the summer months.

Table 3.5-1–Strain rate for sections and per season

Section	Strain Rate (%/Mo.)				
	Winter 2013	Summer 2013	Winter 2014	Average	Yearly
Control (C-1)	0.006	0.000	0.000	0.000	0.004
Silane (S-1)	0.007	0.000	0.000	0.000	0.002
Linseed (L-1)	0.004	-0.001	0.000	0.000	-0.004
Elastomeric Paint (EP-1)	0.004	0.000	0.000	0.000	-0.001
Silane 2 (S2-1)	0.006	-0.001	0.000	0.000	-0.003
Control (C-2)	0.007	0.002	0.005	0.003	0.034
Silane (S-2)	0.006	0.001	0.005	0.002	0.030
Linseed (L-2)	0.008	0.001	0.011	0.005	0.057
Elastomeric Paint (EP-2)	0.005	0.000	0.012	0.003	0.042
Silane 2 (S2-2)	0.010	0.001	0.005	0.002	0.022
Control (C-3)	0.015	0.001	0.025	0.009	0.108
Silane (S-3)	0.017	-0.002	0.014	0.005	0.063
Linseed (L-3)	0.013	-0.001	0.011	0.005	0.056
Elastomeric Paint (EP-3)	0.016	0.000	0.029	0.010	0.120
Silane 2 (S2-3)	0.008	0.000	0.008	0.004	0.043

Minimal damage—The control section (C-1) achieved a maximum of 0.018% strain at 1 year, and no additional visible cracking was observed. The control section contracted between 1 and 3 years and had a final strain of 0.01%. The section treated with silane (S-1) had higher strain than section C-1 throughout the first year, and the greatest expansion for sections of minimal damage. The other treated sections had less expansion throughout the monitoring period, and showed an overall contraction. The section treated with boiled linseed oil (L-1) had a maximum expansion of only 0.012% and a final contraction of 0.015%. The section treated with elastomeric paint (EP-1) had a maximum expansion of 0.016% and a final contraction of 0.008%. The second

section treated with silane (S2-1) had a higher maximum expansion of 0.027%, but ended with a final contraction of 0.006%.

The differential strain for sections of minimal damage is provided in **Fig. 3.5-1 (b)**, which again has strain (%) on the ordinate and time (date) on the abscissa. The sections treated with boiled linseed oil, elastomeric paint, and the second section treated with silane fared better than the untreated control. The section treated with linseed oil (L-1) had a final strain 0.021% lower than the control section, which suggests that there was a beneficial reduction in expansion as compared to the control. The section treated with elastomeric paint (EP-1) and the second section treated with silane (S2-1) had 0.012 and 0.021% less strain than the control, respectively. In the second year after treatment, the section treated with silane (S-1) began to contract faster than the control section and had 0.012% less expansion than the untreated control section at the end of monitoring. The single application of silane took longer to slow the rate of expansion than the section treated with two applications; however, silane provided a beneficial reduction in expansion in both silane treated sections.

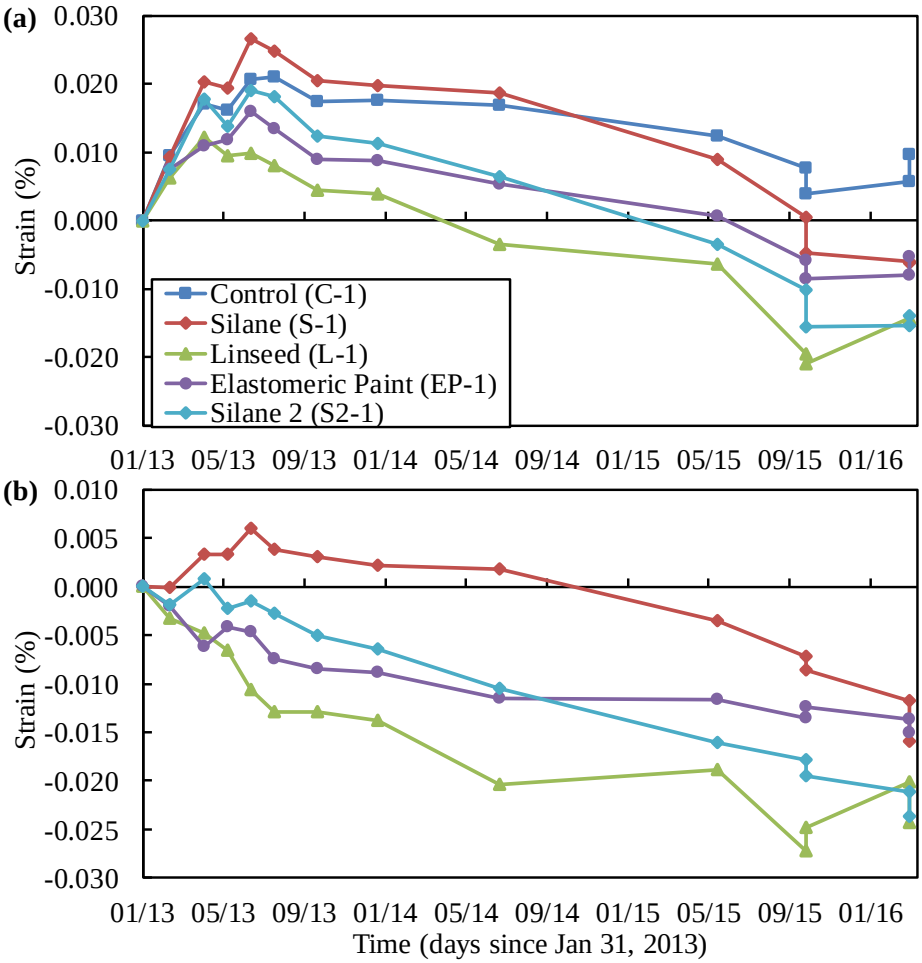

Fig. 3.5-1–Temperature-normalized vertical strain (%) with respect to: (a) time (date); and (b) differential strain for sections of minimal damage.

Moderate damage—The sections of moderate damage exhibited final strains that were up to 10 times greater than that of the sections with minimal damage. This result suggests that the classification based on visible damage was successful in distinguishing between sections of minimal and moderate expansion. The final expansion for the control section (C-2) was 0.10%, which is greater than the 0.04% expansion generally required to produce visible cracking in unrestrained concrete [9]. This rapid expansion did not occur throughout the year, and varied with the season and ambient conditions. ASR expansion is accelerated at higher temperatures and therefore occurs most rapidly during the summer months, and then slows during the winter. As evident in the strain data for sections of moderate damage, shown in **Fig. 3.5-2 (a)**, the strain

rate is higher during the winter (between January and March 2013 and then between October and December 2013), and then slows during the summer (between April and September 2013, and then between March and September 2014). This trend suggests that most expansion occurring in these sections is in fact due to freezing and thawing and not ASR. However, as evident in the petrographic examination, the freezing and thawing damage was onset by the occurrence of ASR. Also, ASR damage continues to provide additional microcracking and gel, which is followed by freezing and thawing damage.

The section treated with elastomeric paint (EP-2) had a reduced rate of expansion during the first summer with expansion below that of the control (C-2). However, the expansion rate rapidly increased during the winter and was greater than the control section. The sections treated with silane (S-2 and S2-2) exhibited a reduction in expansion, which continued throughout the monitoring period. The silane-treated sections S-2 and S2-2 had final expansions of 0.087% and 0.056%, respectively. The sections had expansion 0.011% and 0.043% less than that of the control section, respectively (**Fig. 3.5-2(b)**). However, the sections treated with boiled linseed oil (L-2) or elastomeric paint (EP-2) did not exhibit any reduction in expansion, and fared worse than the control during the winter months. Both sections had a final expansion greater than that of the control section. This result is counterintuitive and may be due to the reduced mobility of moisture both into and out of the concrete caused by the surface treatment. Water could not escape from the concrete during freezing, leading to increased damage during freezing and thawing.

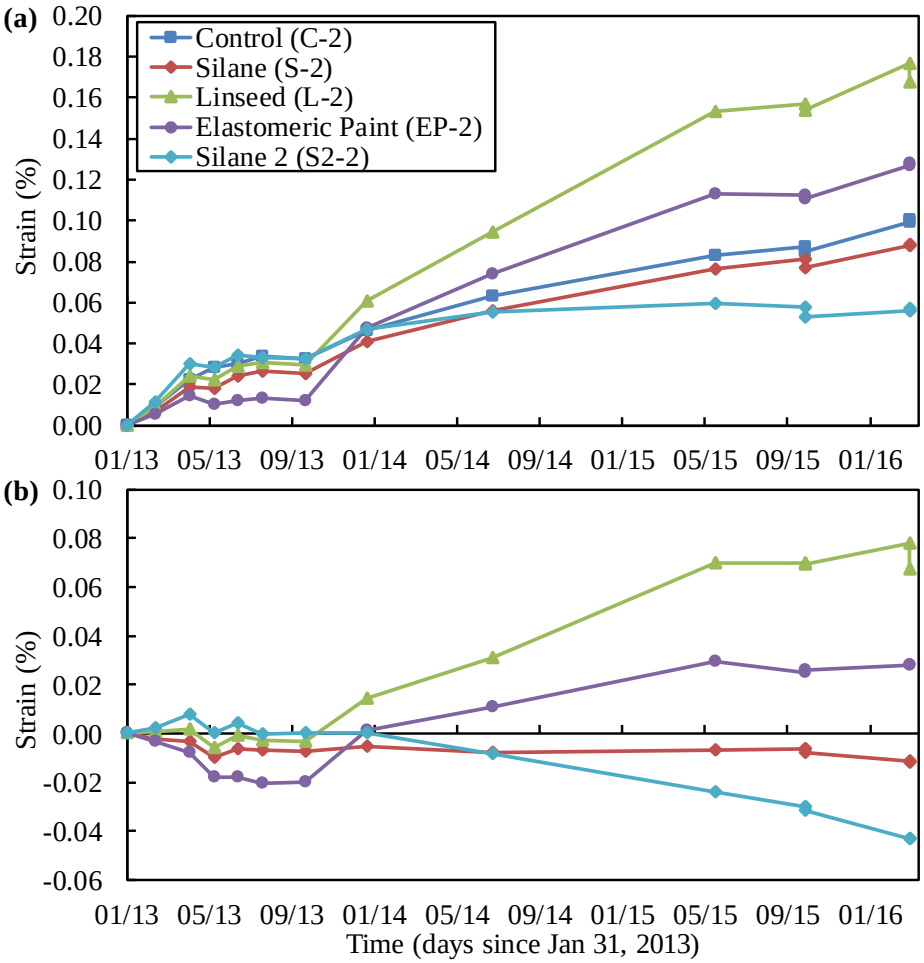

Fig. 3.5-2–Temperature-normalized vertical strain (%) with respect to: (a) time (date); and (b) differential strain for sections of moderate damage.

Severe damage—The 3-year strain in sections of severe damage was three times greater than that of sections of moderate damage, and 33 times greater than that of minimal damage. Again, the rate of expansion was directly related to the level of damage that had already occurred in the concrete. The strain data for sections of severe damage are summarized in **Fig. 3.5-3 (a)**. The final strain in the control section (C-3) was 0.33%, most which occurred during the winter months. Both boiled linseed oil and silane reduced expansion for sections of severe damage. The final strain in the section treated with silane (S-3) was 0.19%, and the final strain in the section treated with two applications of silane (S2-3) was 0.13%. A second application of silane provided better coverage of the concrete surface and newly exposed concrete within large cracks.

Thus, the section treated with two applications of silane expanded less than the section treated with only one application. Similarly, the section treated with boiled linseed oil (L-3) had a final strain of 0.17%. Although the strain in these sections was lower than that of the untreated control section (C-3), the strain was still greater than that of the sections of moderate damage and sufficient to cause additional visible deterioration. The elastomeric paint was not sufficient to protect the section (EP-3) from additional damage, and the final strain was 0.37%. The elastomeric paint could not bridge the wide cracks within the section at the time of treatment, even with the larger cracks being sealed with silicon sealant. The lower-viscosity surface treatments such as silane could reduce expansion as compared to the untreated control section (**Fig. 3.5-3 (b)**).

Except for the section treated with two applications of silane (S2-3), all the sections of severe damage had similar expansion throughout the first 9 months. However, during the winter months, the control section (C-3) and elastomeric paint treated section (EP-3) experienced a severe increase in expansion. Meanwhile, the sections treated with silane (S-3 and S2-3) and linseed oil (L-3) exhibited less expansion. The differential strains at 3 years for the silane-treated sections (S2-3) and (S-3) were 0.20% and 0.14%, respectively, and 0.16% in the section treated with linseed oil (L-3). Although these strains are considerably lower than that of the control section, the rate of expansion is still sufficient to cause failure in only a few years.

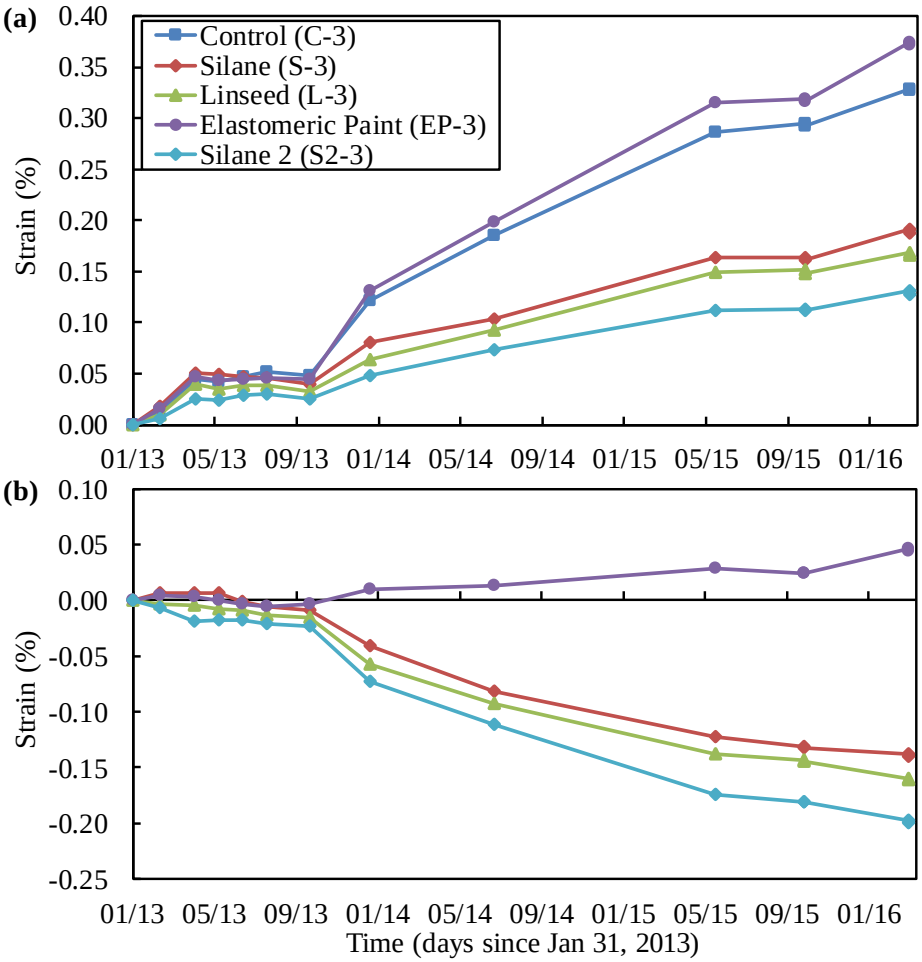

Fig. 3.5-3–Temperature-normalized vertical strain (%) with respect to: (a) time (date); and (b) differential strain for sections of severe damage.

A measurable reduction in expansion was developed in sections treated with lower-viscosity treatments applied with a hand sprayer. This may be explained by the ability of these treatments to enter the larger cracks that were present at the time of treatment and to seal the additional surface area. This prevented excess water from entering microcracks and causing additional freezing and thawing damage during the winter months. In addition, the treatments protect the concrete from external moisture and limit expansion due to ASR and the formation of new microcracks. If the surface treatments continue to slow the rate of expansion, the service life of the structure will be increased. Silane provided the most consistent reduction in expansion for sections of all damage levels. As shown in **Fig. 3.5-4**, the section treated with silane (left)

exhibits markedly less cracking 3 years after treatment. The silane treatment limited the ingress of water, which improved the ASR and freezing and thawing durability of the concrete. Similarly, boiled linseed oil reduced expansion in sections of minimal and severe damage. However, linseed oil was ineffective for the section with moderate damage. Linseed oil was better able to penetrate the large cracks in the severely damaged concrete and therefore had a greater effect than in the moderately damaged concrete.

Fig. 3.5-4–Silane-treated section (left) as compared to untreated section (right) (by Richard Deschenes Jr.).

As noted in the results for the sections of different deterioration levels, the strain rate in all the sections of moderate and severe damage exhibited an increased strain rate in the winter months as compared to the summer. This is counter intuitive because ASR generally accelerates at warmer temperatures. However, it was concluded that freezing and thawing was in fact the cause of deterioration during these months. As summarized in **Fig. 3.5-5 (b)**, the strain rate in the control sections is much higher during the highlighted winter seasons as compared to the summer months. This confirms that more expansion occurs during the winter, as compared to the summer months. The expansion occurring in the winter is due to freezing and thawing, as ASR formation is dormant or slowed at lower temperatures [9]. The formation of ASR gel and cracking within the concrete leaves the concrete susceptible to accelerated freezing and thawing deterioration as noted by Bérubé et al. [3]. The strain rate results for all the sections are summarized in **Table**

3.5-1, and confirms that the strain rate for the moderate and severely damaged sections increases during the winter and slows in the summer.

3.5.2. Internal relative humidity and temperature

The primary mitigation mechanism of surface treatments in concrete is the reduced availability of moisture for the expansive alkali-silica gel. Studies have revealed that reducing the internal relative humidity below 80% slows or stops ASR related expansion [2, 4, 10]. Several methods have been used for measuring the relative humidity within a concrete element [2, 4, 6]. The method employed by Stark [2] allowed the humidity at various depths to be monitored and the humidity gradient to be analyzed. However, for treatment to be effective, the humidity throughout the full depth of the concrete element needs to fall below 80%, especially during warmer weather when most ASR expansion occurs. Therefore, the humidity measurements for the current research project were measured at a depth of 6 in. (150 mm), which is half the thickness of the median barrier at the height of the port. The internal relative humidity at this depth is less susceptible to fluctuations due to ambient conditions and will generally be higher than the humidity near the surface [2]. However, there were several issues with measuring RH using this method. Moisture often condensed and precipitated within the ports, resulting in measuring a RH of close to 100%.

A second method was employed to improve the accuracy of measurements. This method involved drilling fresh holes to a depth of 3 in. (75 mm) at each site visit, and inserting a LabJack probe into the hole. The probe was secured with silicon sealant to prevent ambient air from passing over the RH sensor. The probe remained in the hole for 4 to 5 hours to allow equilibrium between the concrete and the air in the probe. This method was further evaluated in the laboratory, where 24 to 72 hours were allowed for equilibrium. However, an increase in accuracy

was not observed when allowing additional time for equilibration. The limitation of this method is the air space within the LabJack probes. Temperature often fluctuates several degrees during the monitoring period, and moisture condenses on the sensor resulting in artificially high RH, approaching 100% as time increased.

The internal-RH and internal temperature were measured at each visit, the internal temperature at the time of measurements was not always between 70 and 75°F (21 and 24°C), as recommended by Stark [2]. Internal-RH values in concrete cannot readily be normalized to a set temperature [11]. Therefore, the results cannot be compared to the proposed threshold-RH of 80% at 70°F (21°C) proposed by Stark [2]. However, the temperature in the treated sections and control section were the same at the time of each measurement, and the results can be used to indicate if the treatments reduced the RH of treated sections as compared to the control section. The internal concrete temperature from each measurement visit is summarized in **Fig. 3.5-5 (b)**. During the 3 years of monitoring, only sections of minimal damage developed a measurable reduction in internal-RH.

The internal-RH data for sections of minimal damage are provided, along with ambient-RH, in **Fig. 3.5-5 (b)**, with RH (%) on the ordinate and time (date) on the abscissa. The sections treated with silane (S-1 and S2-1) exhibited a lower RH than the untreated control section (C-1). The internal-RH in the section treated with silane (S-1) decreased throughout the first year of monitoring and was below 80%. The internal-RH for the section treated with two applications of silane (S2-1) decreased similarly to the section treated with silane (S-1); however, it had increased to 86% by 2 years and over 95% by 3 years. Both sections treated with silane (S-1 and S2-1) had an internal relative humidity of only 82% 6 months after treatment. It is expected that the internal-RH will fluctuate throughout the year as the ambient conditions change [4].

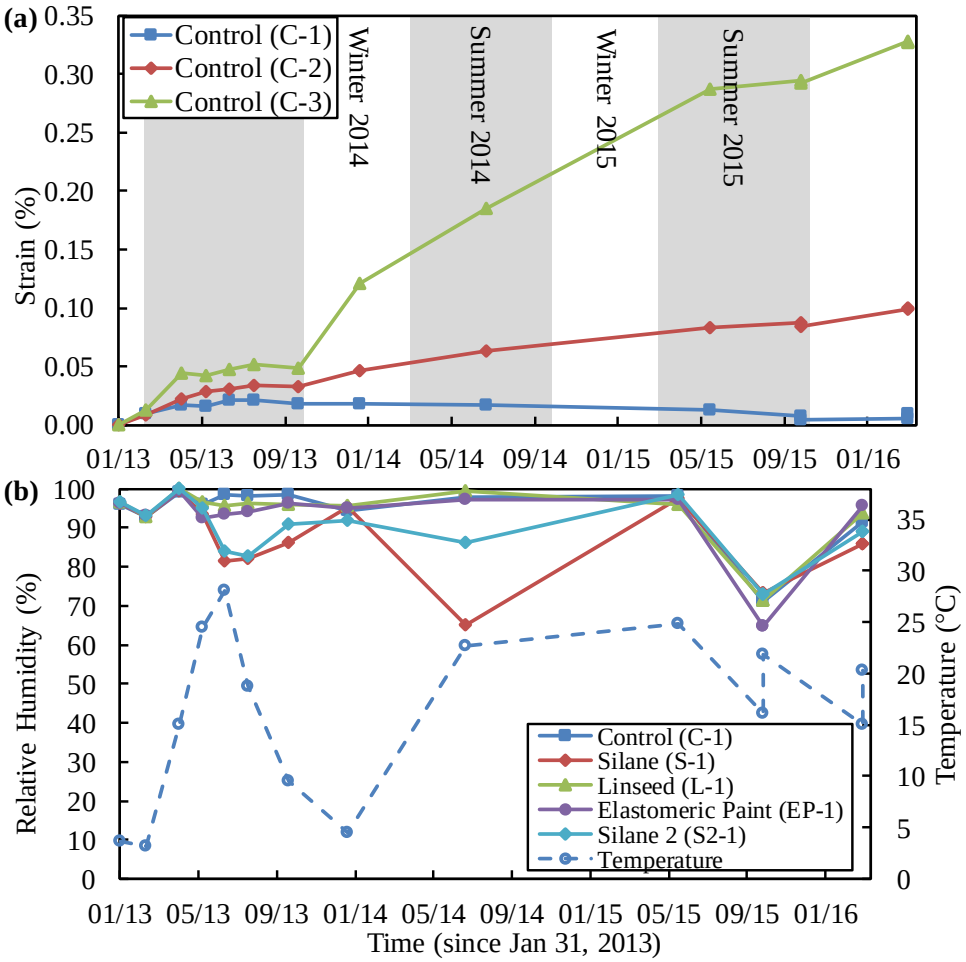

Fig. 3.5-5–Temperature-normalized vertical strain (%) with respect to: (a) time (date) for control sections with seasons highlighted; and (b) internal relative humidity (%) with respect to time (date) for sections of minimal damage.

Unfortunately, the sections of moderate and severe damage did not exhibit any meaningful reduction in internal-RH. The internal-RH remained within 2% of the untreated control sections for both damage levels. It is the authors' opinion that the sections benefitted from treatment by reducing the availability of external moisture, and therefore reducing freezing and thawing deterioration. However, the cracking in the moderately and severely damaged sections allowed moisture to enter the concrete faster than water vapor could escape. Consequently, no reduction in internal-RH was measured. To improve the effectiveness of the surface treatments, the concrete could first be impregnated with a low-viscosity epoxy or resin that fills larger cracks and allows a breathable vapor barrier to form when the silane or elastomeric paint is applied.

3.6. FURTHER RESEARCH

Currently, 3 years of results are available and provide preliminary conclusions on the efficacy of mitigation methods for concrete affected by a combination of ASR and freezing and thawing. In addition to the median barrier, several miles (km) of interstate pavement have developed ASR. Sections of the pavement were instrumented similarly to the method employed for the median barrier. Several commercial silanes were applied to the pavement for evaluation. The strain and relative humidity will be monitored for 3 years to determine the efficacy of silane at reducing the internal relative humidity within concrete pavements. The study will include a laboratory investigation of silane treated concrete exposed to ASR, freezing and thawing, and a combination of both.

3.7. CONCLUSIONS

Mitigation of ASR and freezing and thawing using surface treatments requires laboratory and field investigation. Each case is subject to a different set of environmental and initial conditions. The current research program provides preliminary conclusions on the efficacy of several different surface treatment methods applied to concrete of various initial damage. Silane has proven the most effective treatment option across all three damage levels. The silane treatment reduced expansion as compared to the untreated control sections for moderately and severely damaged concrete.

- Silane-treated sections exhibited a reduction in expansion as compared to the untreated control sections for all damage levels. Silane also produced a measurable reduction in internal-RH for sections of minimal damage. It is recommended that the median barrier be treated with silane to prevent most of the concrete, which has minimal damage, from cracking and providing an avenue for freezing and thawing.

- As noted in the sections of moderate and severe damage, expansion occurs primarily during the winter months due to freezing and thawing. This is not present in the sections of minimal damage because significant cracking has not reached the surface and provided an avenue for water to enter and be trapped within the concrete. It is hypothesized that as ASR progresses, void space is occupied by ASR reaction products, which reduces space for moisture during freezing [4]. The gel entraps water which cannot readily move during freezing, increasing stresses.
- Although silicon crack sealant was not sufficient to prevent moisture from entering large cracks, impregnation with a low-viscosity crack sealant before treatment with silane or linseed oil may provide better protection from freezing and thawing for sections of moderate and severe damage. Alternatively, the concrete could be impregnated with a high-strength epoxy resin that would seal cracks and increase the tensile strength of the mass concrete.
- The results of treatment and monitoring indicate that silane treatment reduced freezing and thawing-related deterioration for sections of moderate to severe damage. The silane treatment provided a breathable barrier on the surface of the concrete, which over time reduces the internal-RH of the concrete. The concrete becomes less saturated over time, falling below the critical saturation state required for freezing and thawing stress to develop. The result is improved freezing and thawing performance for non-air-entrained concrete with existing cracking. This hypothesis needs to be confirmed through laboratory evaluation, but the results indicate that silane may be an effective treatment for slowing freezing and thawing-related deterioration in concrete elements.

- The barrier sections with moderate and severe damage, treated with a second application of silane 6 months after the initial application, performed better in ASR and freezing and thawing than the sections with only a single application.

3.8. ACKNOWLEDGMENTS

The authors would like to acknowledge the Arkansas State Highway and Transportation Department (AHTD); Headwaters Resources, Inc.; and Mack Blackwell Rural Transportation Center for providing financial support. Thanks also to Ash Grove Cement Co. for the donation of materials used in the research program. The authors would also like to thank W. Phillips, C. Dang, and D. Davis of the University of Arkansas Department of Civil Engineering for the help in conducting instrumentation and monitoring in the field.

3.9. REFERENCES

1. Deschenes, R. Jr., and Hale, W. M., "Alkali-Silica Reaction in Concrete with Previously Inert Aggregates," Journal of Performance of Constructed Facilities, ASCE, 2016, p. 04016084. doi: 10.1061/(ASCE) CF.1943-5509.0000946.

2. Stark, D., "The Moisture Condition of Field Concrete Exhibiting Alkali-Silica Reactivity," CANMET/ACI International Workshop on Alkali-Aggregate Reaction in Concrete, Halifax, NS, Canada, 1990, 19 pp.

3. Bérubé, M.-A.; Chouinard, D.; Pigeon, M.; Frenette, J.; Rivest, M.; and Vézina, D., "Effectiveness of Sealers in Counteracting Alkali-Silica Reaction in Highway Median Barriers Exposed to Wetting and Drying, Freezing and Thawing, and Deicing Salt," Canadian Journal of Civil Engineering, V. 29, No. 2, 2002, 329-337. doi: 10.1139/l02-010

4. Bérubé, M.-A.; Chouinard, D.; Pigeon, M.; Frenette, J.; Boisvert, L.; and Rivest, M., "Effectiveness of Sealers in Counteracting Alkali-Silica Reaction in Plain and Air-Entrained Laboratory Concretes Exposed to Wetting and Drying, Freezing and Thawing, and Salt Water," Canadian Journal of Civil Engineering, V. 29, No. 2, 2002, 289-300. doi: 10.1139/ l02-011

5. Rust, C., "Role of Relative Humidity in Concrete Expansion due to Alkali-Silica Reaction and Delayed Ettringite Formation: Relative Humidity Thresholds, Measurement Methods, and Coatings to Mitigate Expansion," master's thesis, University of Texas at Austin, Austin, TX, 2009, 120 pp.

6. Drimalas, T.; Folliard, K. J.; Thomas, M. D. A.; Fournier, B.; and Bentivegna, A., "Study of the Effectiveness of Lithium and Silane Treatments on Field Structures Affected by ASR," Proceedings of the 14th Inter- national Conference on Alkali-Aggregate Reaction (ICAAR), Austin, TX, 2012, 10 pp.

7. Thomas, M. D. A.; Folliard, K. J.; Fournier, B.; Drimalas, T.; and Rivard, P., "Study of Remedial Actions on Highway Structures Affected by ASR," Proceedings of the 14th International Conference on Alkali-Aggregate Reaction (ICAAR), Austin, TX, 2012, 10 pp.

8. Folliard, K. J.; Thomas, M. D. A.; Fournier, B.; Resendez, Y.; Drimalas, T.; and Bentivegna, A., "Evaluation of Mitigation Measures Applied to ASR-Affected Concrete Elements: Preliminary Findings from Austin, TX Exposure Site," Proceeding of the 14th International Conference on Alkali Aggregate Reaction (ICAAR), Austin, TX, 2012, 10 pp.

9. Ideker, J. H.; Bentivegna, A. F.; Folliard, K. J.; and Juenger, M. C. G., "Do Current Laboratory Test Methods Accurately Predict Alkali-Silica Reactivity?" ACI Materials Journal, V. 109, No. 4, July-Aug. 2012, 395-402.

10. ACI Committee 221, "Report on Alkali-Aggregate Reactivity (ACI 221.1R-98)," American Concrete Institute, Farmington Hills, MI, 1998, 31 pp.

11. Nilsson, L.-O., "Hygroscopic Moisture in Concrete-Drying, Measurements & Related Material Properties," Division of Building Materials, Lund University, Lund, Sweden, 1980, 162 pp.

4. PAPER 3: MITIGATION OF ASR AND FREEZE THAW IN CONCRETE PAVEMENT THROUGH SILANE SURFACE TREATMENTS

Richard Deschenes Jr., Eric Giannini, Thano Drimalas, Benoit Fournier, and W. Micah Hale

Biography: ACI member **Richard A. Deschenes Jr.** is a Graduate Assistant at the University of Arkansas, Fayetteville, where he received his BS and MS in civil engineering in 2012 and 2014, respectively. He is currently a PhD candidate in civil engineering at the University of Arkansas. He received the 2013 ACI Schwing American Scholarship and the 2015 ACI BASF Construction Chemicals Fellowship. His research interests include the durability of concrete.

ACI member **Eric R. Giannini** is an Assistant Professor at The University of Alabama. He is a member of several ACI committees including 123, Research and Current Developments; 201, Durability of Concrete; and 228, Nondestructive Testing of Concrete. He also chaired subcommittee 228-B. His research interests include alkali-silica reaction and nondestructive testing. He received his PhD in civil engineering from The University of Texas at Austin in 2012.

ACI member **Thanos Drimalas** is a Research Associate in the Department of Civil, Architectural, and Environmental Engineering at the University of Texas at Austin. He received a PhD in civil and environmental engineering from the University of Texas at Austin in 2007. He is a member of ACI Committees 201, Durability of Concrete; and 350, Environmental Engineering Concrete Structures. His research interests include durability of concrete materials and alkali-aggregate reaction.

Benoit Fournier is a professor in the Department of Geology and Geological Engineering at Université Laval. He is a member of the ACI Durability Committee 201 and chair of CSA AAR

TSC in Canada. His research interests include aggregate technology, durability of concrete, alkali-aggregate reactions, and incorporating SCMs.

ACI Fellow **W. Micah Hale** is Professor and Head of the Department of Civil Engineering at the University of Arkansas. He is Chair of ACI Committee 363, High Strength Concrete, and is a member of ACI Committees 239, Ultra-High-Performance Concrete, 233, Slag Cement, and 423 Prestressed Concrete. His research interests include concrete materials, mixture proportioning, and prestressed concrete. He holds a B.S., M.S., and Ph.D. in Civil Engineering from the University of Oklahoma.

Abstract: Alkali-silica reaction (ASR) and freezing and thawing (F/T) issues cause premature deterioration of concrete structures. These reduce the useful service life of structures and are difficult to mitigate in existing concrete pavements once deterioration occurs. However, slowing the rate of deterioration may increase the remaining useful life of the pavement. This research program evaluates the efficacy of silane surface treatments used to reduce the internal relative humidity (RH) of concrete pavements, thereby reducing further deterioration from ASR and F/T. The pavement test section evaluated contained a moderately-reactive fine aggregate and marginal air entrainment. The efficacy of silane was evaluated by instrumenting a pavement test section with devices for monitoring strain and internal-RH. In addition, core samples were extracted before and after silane application. The core samples were evaluated using the damage rating index (DRI). Results indicate silane treatments reduced the rate of expansion and deterioration in the concrete pavement, as compared to the untreated control section.

Keywords: Alkali-silica reaction (ASR); freezing and thawing (F/T); mitigation; concrete pavements; silane.

4.1. INTRODUCTION

Alkali-silica reaction (ASR) and freezing and thawing (F/T) are deterioration mechanisms which affect concrete infrastructures, reducing their useful service life. Both reactions mechanisms are dependent on the exposure conditions of the concrete element. The mechanisms of deterioration are also related to the availability of moisture within the concrete. The rate of deterioration can potentially be slowed by reducing the available moisture within the concrete. Surface treatment with silane has been efficacious for slowing deterioration in concrete elements with high surface-area-to-volume ratios, which dry towards ambient conditions over time.

Alkali-silica reaction (ASR): ASR causes premature deterioration of concrete structures, and has affected structures in many regions of North America and throughout the world. The reaction occurs when reactive siliceous phases, within some aggregates, dissolve in the presence of hydroxyl ions within the cement pore solution. Dissolved silica forms a gel product, which adsorbs pore solution from the surrounding cement paste, and expands. The expansive reaction leads to microcracks, which develop over time forming a network of microcracks that extends from one reactive aggregate particle to another through the cement paste. The cracking can lead to visible symptoms of deteriorating including map/oriented cracking (depending on the extent of restraint and reinforcement detailing), deterioration at joints, and discoloration. The reaction stops when the available siliceous minerals, alkalis, or water are no longer sufficiently available. Concrete with a large exposed surface area relative to the volume, and protected from rain or runoff, may dry over time until ASR related expansion ceases.

Freezing and thawing (F/T): F/T deterioration is another deterioration mechanism which reduces the service life of concrete. Pressure leading to deterioration occurs when water in the cement or aggregate pores freezes, causing spalling or cracking in the cement phase [1, 2]. As

discussed by Powers [3] and others [2], when the concrete is critically saturated, excess pressure develops in the concrete leading to deterioration. This is prevented by properly entraining the concrete with sufficiently small and dispersed air voids [2]. F/T deterioration can also occur when water within D-cracking-susceptible aggregates freezes repeatedly due to cycles of F/T. When such aggregates are near the joints of concrete pavements and become saturated, water may be expelled from the aggregates during frozen and cause microcracking in the cement paste. On repeated F/T, D-cracking forms adjacent to the joints. This form of F/T deterioration can be prevented by reducing the quantity or particle size of unsound aggregates, and by limiting the ingress of moisture into the concrete, especially near joints. Bérubé et al. [4] demonstrated that F/T cycles exacerbate deterioration of concrete containing microcracking initiated by ASR. Additionally, cracks at the exposed surface of the concrete provide an avenue for additional water to enter the concrete, increasing the saturation state and leading to deterioration.

Relative Humidity (**RH):** Reducing the moisture state of the concrete, measured as internal-RH, is a viable method for mitigating ASR related deterioration [5, 6, 7, 8, 9, 10]. When the RH within concrete is reduced below a threshold, the alkali-silica gel within the concrete no longer expands. Internal-RH fluctuates depending on the surface area, thickness, and exposure conditions of a concrete element. Thin elements (less than 12 in. (300 mm)) with large surface areas relative to the volume tend to dry towards the average ambient-RH over time [11]. The water lost on drying may be replenished by an external source of water such as rain or runoff. Expansion from ASR slows or ceases in concrete protected from external sources of water while drying continues.

Silane Sealers: Silanes are penetrating sealers, consisting of silicon molecules which penetrate the surface of concrete and form a silicone resin network [12]. This network contains

hydrocarbon chains which produce a hydrophobic network along the exposed concrete surface, inhibiting liquid water from entering the concrete while allowing water vapor to pass [13]. Typical modern silane products consist of water-based alkylalkoxysilane, solvent-based alkyltrialkoxysilane, or non-solvent based isobutylalkoxysilane silane compounds [12, 13, 14]. In general, alkoxysilanes have long, alkali-resistant, carbon side chains which provide the hydrophobic characteristics [12]. Silane treated concrete has a hydrophobic layer which allows vapor transmission while preventing liquid water absorption. The concrete expands as water is absorbed through the surface into cracks and alkali-silica gel. If the silane treatment is sufficiently hydrophobic, sorption of liquid water is reduced and the concrete tends to dry. Therefore, less deterioration occurs during F/T and alkali-silica gel expands less. Silane is a useful tool in mitigating ASR in concrete elements such as columns and barrier walls [6, 8, 9]. Research indicates that silanes can reduce ASR-related expansion over time, potentially extending the service life of concrete structures [6, 9].

Mitigation: ASR and F/T are more difficult to mitigate in pavements than other concrete elements. Pavements have a large surface-area-to-volume ratio, which increases the rate of water absorption or desorption. However, only the exposed surface of the pavement can be treated with silane, while the subgrade may be a source of external moisture. Pavements with sufficient subgrade drainage should dry towards ambient conditions over time. Based on the results of two field trials, Stark et al. [5] found silane ineffective for pavements based on one-year of monitoring internal-RH. However, strain was not monitored and one year of monitoring was not sufficient for a measurable reduction in RH to develop within the pavement [5]. Silane was again evaluated in 2011 as part of the FHWA *ASR development and deployment program* [10]. Silane was applied to a test section of the Interstate 530 pavement in Pine Bluff, Arkansas,

USA. Strain and internal-RH were monitored periodically for one year before the research program ended [10]. Deterioration in the pavement increased rapidly and rehabilitation was required before sufficient results could be gathered. The project results were inconclusive and the long-term efficacy of silane applied to concrete pavements remains unknown.

Field-Monitoring: Measuring the efficacy of silane treatments requires a system of monitoring strain, internal-RH, and rate of deterioration of the concrete. Strain (expansion) is a quantifiable symptom of ASR, and other expansive deterioration mechanisms. Strain is typically measured in transportation structures using a *Demountable Mechanical* (DEMEC) strain gauge, which measures the change in length between pins installed into the concrete [14, 15].

Internal-RH is a quantifiable measure of the potential for ASR and F/T deterioration to continue within a concrete element. Stark [16] suggested that when internal-RH of concrete decreases below 80% (70 to 75 °F [21 to 24 °C]), expansion ceases. These findings were substantiated through laboratory and field-testing reported by Bérubé et al. [4]. The relationship between internal-RH and saturation state of concrete is complex and dependent on the microscopic properties and hydration state of the concrete [13]. Therefore, it is difficult to quantify the critical saturation necessary for F/T to occur by measuring internal-RH [2, 3, 4]. However, the internal-RH of concrete decreases as the concrete dries, and RH is an index of moisture within the concrete [16]. Drying produces a RH gradient between the exposed surface and internal concrete, drying faster at the surface. Moisture enters the concrete through capillary action and diffusion when exposed to external moisture. Bérubé et al. [7] and others [6, 10, 17, 18] measured internal-RH in concrete using commercial RH probes inserted into holes drilled into the concrete surface. However, measuring RH at a single depth does not provide information on

the RH throughout the pavement depth. Measuring internal-RH accurately also proved difficult when concrete temperatures fluctuated during measurements [10, 18].

Damage Rating Index (DRI): Petrographic methods are used to diagnose and monitor deterioration mechanisms in concrete. The Damage Rating Index (DRI) is a semi-quantitative index of deterioration present within concrete. The method accounts for deterioration which occurred throughout the life of the concrete. In addition, the DRI method accounts for expansion occurring out-of-plane, which is less restrained and likely to increase faster. The DRI samples provide a small portion of the pavement cross-section, allowing a measure of internal deterioration which cannot be measured using surface strain or cracking index methods. The DRI results provide greater insight into the cause and extent of deterioration within the concrete.

The DRI method is used to evaluate and compare the deterioration state of concrete, although the method is subjective to operator experience and judgement [19, 20, 21, 22, 23, 24]. Sanchez et al. [23] demonstrated a correlation between ASR expansion and DRI values, and established ranges to distinguish between concretes of different deterioration states [25, 26]. Several authors have provided lists of features and weighting factors for the DRI method. Dunbar and Grattan-Bellew [22] included seven features and weighting factors which emphasized gel deposits and reaction rims. However, these weighting factors have been revised to reduce operator subjectivity and to emphasize deterioration caused by cracks in the cement paste [19, 27]. The method has also been applied to differentiate between deterioration caused by ASR and F/T [23].

Objective: Previous research programs investigated topical treatments of lithium or silane to mitigate ASR in concrete pavements [5, 10, 11]. These programs were short-term (one-year) monitoring of pavement performance [5, 10]. Lithium treatments largely proved ineffective due to limited penetration into the concrete substrate. Sufficient monitoring was however not

available to determine the efficacy of silanes [10, 11]. The objective of this research is to establish the long-term efficacy of silane treatments applied to concrete pavements deteriorating from a combination of ASR and F/T. The Interstate 49 pavement in Northwest Arkansas was instrumented for monitoring strain and internal-RH in January 2014, treated in March 2014, and monitored until October 2016. Core samples were collected before treatment as an initial assessment of deterioration in the test section. Samples were collected two years after treatment to assess changes in the pavement condition and any differences in deterioration between treated and untreated sections of the pavement.

4.2. RESEARCH SIGNIFICANCE

Mitigating ASR and F/T deterioration in concrete pavement is necessary to extend their service life and slow deterioration. This paper presents the longest-running study on the efficacy of silanes applied to pavements, and includes three-years of strain and internal-RH monitoring. This work also evaluates silane as a possible means of slowing F/T related deterioration in pavements. The research program follows the guidelines of the *Report on the Diagnosis, Prognosis, and Mitigation of Alkali-Silica Reaction (ASR) in Transportation Structures* to assess and mitigate ASR [14]. This paper will be of interest to those responsible for pavement management and selecting treatments to extend service life.

4.3. EXPERIMENTAL PROCEDURE

A portion of Interstate 49 in Arkansas, USA was selected as a test section in 2012. The pavement is jointed plain concrete, with transverse and center joints. Several pavements in the region deteriorated prematurely due to ASR, and were replaced before testing could occur. The Interstate 49 pavement showed early signs of deterioration including map cracking, D-cracking, and discoloration at the joints, first noted in 2011. The concrete aggregates passed all state

required soundness and durability tests at the time of placement. Other cases of D-cracking related to the limestone coarse aggregate have not been documented, and the quarry is no longer in use. No limit was placed on alkali content, and previous research found the alkali content of the cement to range from 0.4 to 1.1% Na_2O_{eq} [28]. Petrographic analysis of core samples found definitive symptoms of ASR and F/T [29]. Deterioration included microcracking throughout the depth of the pavement, tending to be parallel to the surface; reaction rims; microcracks within fine aggregate particles and cement paste; and deposits of alkali-silica gel [29]. Topical treatment with silane was selected to try slowing down the rate of deterioration and extending the service life of the pavement. Therefore, the pavement was instrumented for measuring strain and internal-RH. Sections were treated with a range of commercially-available silane products, to evaluate their efficacy as a long-term mitigation measure. Core samples were extracted before and after treatment to evaluate the extent of deterioration, and changes imparted by the treatment regimen.

4.3.1. Materials

The Interstate 49 pavement was constructed in 1998 and opened to traffic in 1999. The concrete mixture design is summarized in **Table 4.3-1**. The pavement test section is 18 mi. (29 km) in length, with two traffic lanes in both directions. Each lane is 12 ft. (3.66 m) wide, with saw cut joints at 15 ft. (4.57 m) intervals, and the thickness is 12 in. (30 cm). The pavement was constructed on an open-graded asphalt base layer.

A 2011 petrographic examination of the concrete confirmed the presence of alkali-silica gel and F/T deterioration [29]. The air content in the pavement was estimated by the petrographer to be between 2.8 and 3.8% (individual air contents and spacing factors were not measured for the pavement), which is lower than the specified air content in the mixture design [2, 29]. The

aggregates were tested following ASTM C1260 and C1293 (in combination with inert control coarse and fine aggregates, respectively) [28, 30, 31]. The river sand fine aggregate tested moderately reactive per ASTM C1293 and C1778, with a one-year expansion of 0.040%. The 14-day ASTM C1260 expansion for the river sand was 0.17% [28]. The 14-day expansion for the coarse aggregate was 0.01%, indicating the aggregate to be innocuous. The river sand has the potential to cause deleterious expansion if sufficient alkalis are available. The sand contains chert and chalcedony in the coarse fraction 0.25 in. (6.35 mm). The aggregate has a checkered field performance history, with several cases of ASR resulting in premature failure of pavement and median barrier structures.

Table 4.3-1. Job-approved concrete mixture design.

Material	**lb./yd^3**	**kg/m^3**	**Information**
Cement	451	224	Type I
Fly Ash	113	56	Class C, 20% Replacement Rate
Air			6±2% specified
Water	214	106	
Coarse Aggregate	2051	1217	Limestone, 1.5 in. (38 mm)
Fine Aggregate	1082	537	River Sand
w/cm	0.47		Slump < 2 in. (51 mm)

The silanes evaluated herein are readily-available in the United States. Each silane was applied by spraying, using a hand-operated pressure canister. The manufacturer-recommended application rate was followed, which was regulated by applying a predetermined volume of silane to each panel, based on the surface area of the panel. The silane was applied consistently over the surface area until a thin film of excess material covered the pavement. The type, application rate, and composition of each silane is summarized in **Table 4.3-2**.

Table 4.3-2. Silane treatments and application rates

Treatment	Silane 40A	Silane 40B	Silane 100
Application Rate, ft^2/gal (m^2/L)	150 (3.7)	150 (3.7)	(250) 6.1
Chemical Composition	alkylalkoxysilane	alkylalkoxysilane	alkyltrialkoxysilane
Concentration	40% water-based emulsion	40% water-based emulsion	Methanol-based

4.3.2. Specimens

Pavement panels: The pavement was instrumented for strain and internal-RH measurements in January 2014. Twelve panels, over a 282 ft. (86 m) long section of pavement, were instrumented. The test panels were all in a straight, flat region with adequate drainage and similar visible surface deterioration. At the time of treatment, the panels exhibited consistent moderate D-cracking, minor map cracking, and discoloration adjacent to joints. Twelve core samples were extracted from the beginning, middle, and end of the test section. The DRI was used to assess the initial condition of the pavement and the remaining cores were used to measure the potential for further expansion (PFE). Silane treatments were applied to the selected panels in March 2014. A diagram of the treatment locations is shown below in **Fig. 4.3-1**. Between each of the three instrumented panels, six panels were left untreated and without instrumentation.

The pavement panels were instrumented with a grid for measuring strain, following the method documented by Fournier et. al. [15]. Stainless-steel pins were installed at the corners of a 20 in. (0.5 m) square grid for measuring strain. The pins were embedded into the concrete with the indented surface 0.08 in. (2 mm) below the pavement surface to ensure the pins were not damaged during maintenance, plowing, or grinding of the pavement surface. The grid was placed in the middle of the pavement panel, between the tire paths to avoid wearing. The grid was aligned to provide two strain measurements in the travel direction and two in the transverse

direction. An example pavement panel with pins installed is shown in **Fig. 4.3-2**. The advantage of multiple measurements along each axis is reduced error, and redundancy if a pin is damaged. Strain measurements were conducted using a DEMEC gauge with points that align with the indentations on the pre-installed pins. Typical DEMEC gauges provide a resolution of ±0.00005 in. (0.001 mm), or ±0.0002% strain.

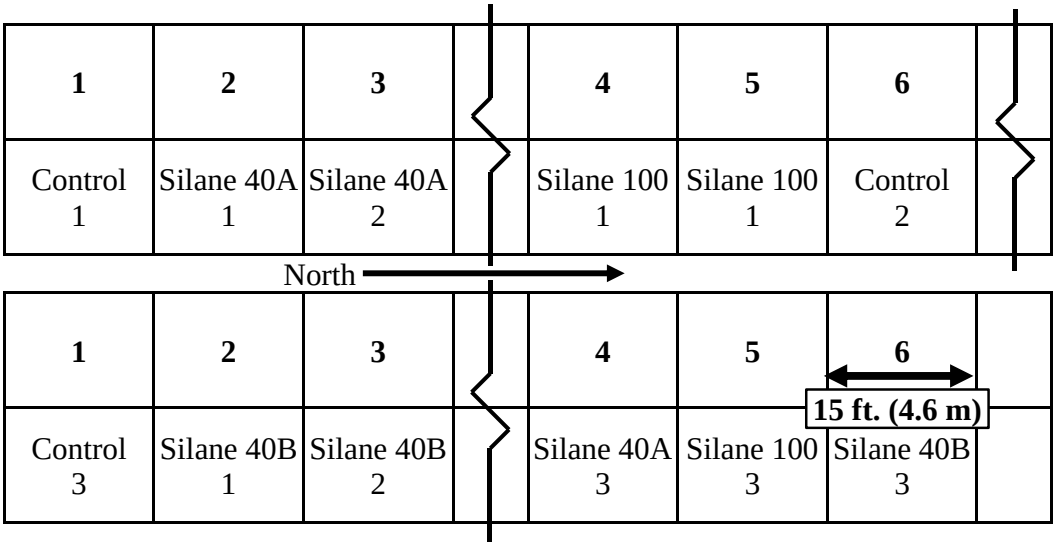

Fig. 4.3-1 –Diagram of Interstate 49 test sections. Three commercially available silanes were applied to the indicated test panels, and three sections remained untreated as control samples.

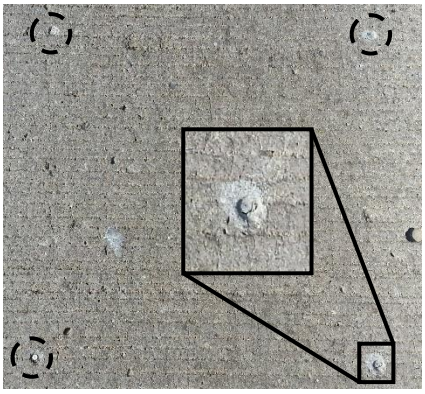

Fig. 4.3-2–Panel with pins for strain measurements (by Richard Deschenes Jr.).

internal-RH was measured within each pavement panel. Two methods of measuring internal-RH were used over the course of monitoring. The first involved drilling 0.625 in. (15.8 mm) diameter holes to a depth of 3 in. (7.5 cm) near the shoulder of the pavement. The holes were capped with a 2 in. (5 cm) section of PVC pipe and a plastic cap between measurements. Three

Vaisala HMP40S probes were initially selected. The probes are accurate throughout the full 100% RH range, with an accuracy of ±2.5% RH between 90 and 100% RH (0 to 40 °C). The probes were inserted into the holes during measurements and equilibrated for one hour (due to the limited number of probes available). This method caused several issues which limited the accuracy of measurements. The plastic caps did not fill the empty volume within the PVC pipe and hole, which allowed water vapor to condense within the hole. When the cap was removed and a humidity probe inserted, the liquid water caused an artificially high internal-RH.

After one year, fifteen LabJack EI-1050 probes were selected as an alternative. The LabJack probes have an accuracy of ±3.0% over a range of 0 to 100% RH (0 to 40 °C). At each site visit fresh holes were drilled, near the pavement shoulder, to a depth of 3 in. (7.5 cm). The hole was dry-drilled and cleaned with compressed air. A humidity probe was immediately inserted and temporarily sealed with silicon. The probes remained in place for four hours, allowing time for equilibration, which improved the accuracy of internal-RH measurements.

To validate this method, the probes were installed into concrete slab specimens at the University of Arkansas Field Exposure Site. The probes were monitored for 72 hours after installation. Results indicate that within four hours after installation, the probe had reached equilibrium with the surrounding concrete [33]. A limitation of the LabJack probe is the 0.5 in. (12 mm) diameter by 3 in. (75 mm) long plastic sleeve, which contains the RH sensor and a large volume of air. A temperature gradient develops between the end of the probe embedded in the concrete and the end exposed to ambient conditions. When the probe remains embedded in concrete for more than 24 hours, water vapor condenses on the inside of the sleeve and caused the RH to increase towards 100% over a few days. Measuring internal-RH for more than four hours was therefore difficult due to temperature changes [33]. Some researchers recommended only measuring

internal-RH when the ambient temperature is approximately 70 °F (21 °C) and the weather is overcast [15], this can be challenging when scheduling site visits requiring lane closure and advanced warning. Site visits for this research were scheduled in spring and fall, when ambient conditions were favorable.

Cores specimens: Full depth, 12 in. (300 mm), by 4 in. (100 mm) diameter core samples were extracted from the test section in 2011 and sent to CTLGroup for petrographic evaluation. Additional cores were extracted in March 2013 for DRI and PFE testing, and a final set were extracted from the test panels in June 2016 for DRI testing. The cores were extracted using a wet drilling process, after which the cores were surface dried and wrapped with cellophane and stored at 21 °C until testing.

DRI: In 2013, the DRI was measured for three core samples extracted from the beginning, middle, and end of the test section. The DRI results were averaged as a pre-treatment baseline. An additional nine cores, extracted in 2013 for PFE testing, were stored at 100 °F (38 °C) for one year and examined for ASR related deterioration. In 2016, two cores were extracted from each treated and control panel. All cores were removed from the middle portion of test panels, adjacent to the length-change grid.

The DRI method was performed following the procedure detailed by Villeneuve et al. [27]. The sample preparation involved cutting the samples axially into two equal halves. This process provided an exposed face of dimensions 100 mm (4 in.) by 300 mm (12 in.). The exposed face was then polished using a pneumatic, hand-held-polisher and diamond impregnated polishing pads. The samples were prepared using polishing pads of 50 to 3000 grit. After polishing, a grid of 0.4 in. (1.0) cm squares was drawn onto the face of each sample. The first 0.2 in (5 mm) at

each edge were not included in the grid, leaving a 90 by 290 mm (3.54 x 11.42 in.) area for examination. An example of a prepared sample is provided in **Fig. 4.3-3**.

Fig. 4.3-3–Typical DRI sample with reference grid (by Richard Deschenes Jr.).

4.3.3. Items of Investigation

Strain and RH: Strain and internal-RH were periodically measured. Visits to the test section were scheduled on overcast days when the expected temperatures were between 62 and 82 °F (16.5 and 28 °C). At the beginning of each visit, the humidity probes were embedded in the concrete and sealed in place. Strain was measured for the test panels, and the concrete temperature recorded. After three hours, strain was measured a second time, and temperature of the concrete recorded. Internal-RH was measured and recorded along with internal temperature.

DRI: After preparing the samples, the procedure involves placing each grid square within the view finder of the stereo-microscope. A magnification of 15X provides a viewable area roughly the same size as a 0.4 in. (1.0 cm) square. The square was inspected for petrographic features, and the features recorded on a spreadsheet. As the concrete contains a reactive fine aggregate, petrographic features were counted in aggregates 0.04 in (1 mm) and larger. Petrographic features of interest were counted and multiplied by the weighting factors summarized in **Table**

4.3-3. The total features present within the sample were normalized to a surface area of 15.50 in.^{2} (100 cm^2), and reported as the DRI.

Table 4.3-3. DRI petrographic features and weighting factors [23, 27**]**.

Petrographic Feature	Deterioration Mechanism	Weighting factor
Closed crack in coarse aggregate (CCA)	ASR, F/T	0.25
Opened crack in coarse aggregate (OCA)	ASR, F/T	2
Opened crack in coarse aggregate w/ reaction product (OCAG)	ASR	2
Coarse aggregate de-bond (CAD)	ASR	3
Corroded aggregate particle (DAP)	ASR	2
Crack in the cement paste (CCP)	ASR, F/T	3
Crack in the cement paste with reaction product (CCPG)	ASR	3

Sanchez [23] used the DRI method to evaluate concrete specimens with a combination of ASR and F/T deterioration and reported increased CCP and OCA deterioration features due to F/T. The CCA and OCA features are ambiguous features which may be caused by aggregate processing, F/T, and/or ASR. However, CCP features can also be caused by F/T, ASR, or fatigue. The remaining features (OCAG, CAD, DAP, and CCPG) occur primarily due to ASR, and indicate the presence of deterioration caused by ASR.

4.4. Analytical Procedure

Strain and Internal-RH: Although visible deterioration was more prevalent adjacent to joints, strain was measured near the center of the test panels. Several of the joints were scheduled for full-depth replacement in 2016, and the expansion grids were placed to avoid removal during maintenance. Of note is potential vertical or out-of-plane strain which has relatively less restraint, but could not be measured. The DRI method was used to provide some insight into deterioration occurring within the pavement and is discussed later. Each test panel had two strain measurements along each axis (travel and transverse direction). Each individual length-change measurement was conducted in duplicate, by separate operators, to ensure accuracy and reduce error. These measurements were averaged, producing a single value for each side of the

measurement grid. The average and standard error of the strain data were also determined, from three panels for each treatment and the control. Length-change for all twelve panels was measured within 20 to 30 minutes from start to finish, thus minimizing the impact of temperature fluctuations. On each site visit, length-change was measured a second time three hours after the initial measurement, after which the concrete temperature had typically changed between 1 and 5 °F (2 and 9 °C). These data were used to estimate the coefficient of thermal expansion (CTE) of the restrained concrete. An average CTE was calculated from the initial and final strain results from each site visit, along with the measured internal concrete temperature. Using the calculated CTE, the strain data was indexed to an internal temperature of 75.2 °F (24 °C). The CTE was calculated independently for the transverse and travel directions as restraint differed in the two directions. The average CTE for the travel direction was 0.6×10^{-6} 1/°C (1.0×10^{-6} 1/°C), while that of the transverse direction was 2.0×10^{-6} 1/°F (3.6×10^{-6} 1/°C). Any differences in strain between panels measured at the same time are attributed to deterioration. The calculated CTE values were lower than the typical value of CTE of 5.6×10^{-6} 1/°F (10×10^{-6} 1/°C) used for unrestrained concrete. The low CTE in the travel direction indicates significant restraint from the adjacent panels. Despite restraint, the temperature-corrected strains in the control sections were similar in the travel and transverse direction. This indicates internal stresses were sufficient to overcome restraint during the monitoring period.

To summarize, at each site visit, twelve strain measurements were collected in each direction for each treatment and the control panels (3 panels per treatment x 2 per panel x 2 per site visit). Internal-RH data was collected once per site visit and represents the average of only three samples. The results were plotted with the average and standard deviation for comparison with the untreated control samples. The temperature of the control sections was also plotted.

4.5. Experimental Results and Discussion

Strain: Strain monitoring began in January 2014 and continued until October 2016. As summarized in **Fig. 4.5-1**, the final average strain in the control panels was 0.0091±0.0028%. The final average strain for the treated panels were 0.0048±0.0015%, 0.0036±0.0014%, and 0.0034±0.0010%, for the Silane 40A, Silane 100, and Silane 40B panels respectively. The ranges provided are 90% confidence envelopes of the standard error of the mean (also shown as error bars in the figure). The average rate of strain was calculated from the slope of the strain data with respect to date. In the travel direction, the rate of strain for panels treated with Silane 40A, was 0.0008%/yr. as compared to 0.0022%/yr. for untreated control sections. The average rate of travel-direction strain for the Silane 100 and Silane 40B panels was 0.0001%/yr. and 0.0004%/yr., respectively. Despite external restraint in the travel direction, the control panels expanded 2.4 times faster than the treated sections.

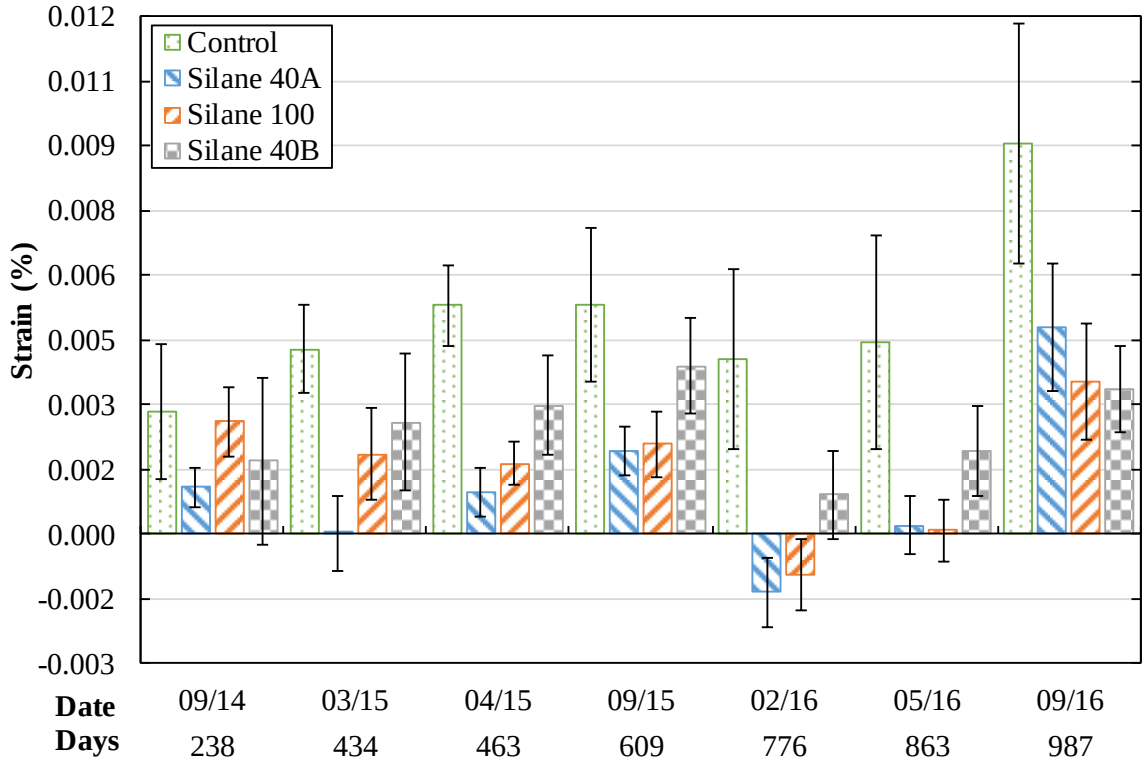

Fig. 4.5-1—Temperature-corrected strain (%) measured in the travel direction for control and silane-treated pavement panels. Error bars represent the 90% confidence of the mean.

The pavement was less restrained in the transverse direction as the partial depth asphalt shoulder is flexible and provides relief for stresses in the pavement. As summarized in **Fig. 4.5-2**, the final average transverse-direction strain for the control sections was 0.0081±0.0023%. The final average strain for Silane 40A and Silane 40B sections were 0.0080±0.0023% and 0.0084±0.0032%, respectively. In comparison, the average final strain for the Silane 100 treated sections was 0.0042±0.0017%. The average rate of strain for the control sections was 0.0026%/yr. in the transverse direction. Whereas the average rates of strain for the Silane 40A and Silane 40B treated panels were 0.0027%/yr. and 0.0024%/yr., respectively. The average rate of strain for the Silane 100 treated panels was only 0.0009%/yr.

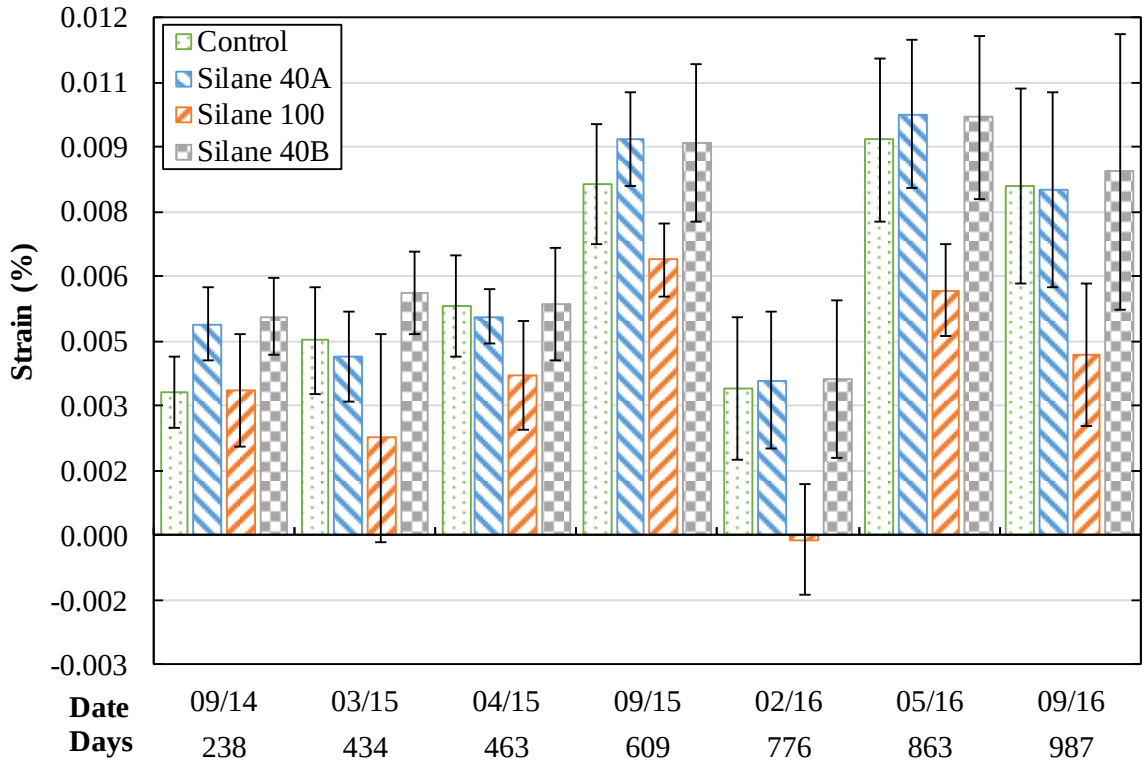

Fig. 4.5-2–Temperature-corrected strain (%) measured in the transverse direction for control and silane-treated pavement panels. Error bars represent the 90% confidence of the mean.

Panels treated with Silane 100 exhibited the best performance, as the average strain in both the directions was lower than that of the control panels. Noting the strain results from September 2014 and September 2015 the strain within the Silane 100 treated panels was similar to that of

the untreated control panels. However, by September 2016 the strain in the Silane 100 treated panels was half that of the control panels. This difference in strain cannot be attributed to temperature, as the strain was measured at the same time and temperature. Therefore, some other factor caused the control panels to expand faster than the panels treated with Silane 100. Drying potentially explains the lesser expansion measured in the Silane 100-treated panels. However, it is unclear if this explains the lesser travel-direction expansion measured in the Silane 40-treated panels, as the panels continued to expand similarly to the control panels in the transverse-direction. Drying may cause a measurable reduction in travel-direction strain first, as stresses induced by adjacent panels are relieved. This is initially apparent in the travel direction, and only apparent in the transverse direction on further drying, as observed in the Silane 100-treated panels. Wehrle [11] did note that 100% (solvent-based) silane compounds perform better than 40% (water-based) silane products for concrete with higher permeability (w/c).

After three years, the test panels exhibited visible symptoms of deterioration: including map-cracking, D-cracking, and discoloration near the joints. Deterioration in some of the untreated panels worsened over the monitoring period as shown in **Fig. 4.5-3**, and spalling at the joints required remediation measures.

Fig. 4.5-3–Joint spalling (left) and discoloration (right) (by Richard A. Deschenes).

Statistical Analysis: Given the error introduced by the DEMEC gauge (±0.0001% average from 1200 data points), temperature (±0.00023%/°C), and the large standard deviation (0.002%), it is

difficult to confirm the efficacy of silane treatments applied to pavements based on strain alone. Therefore, a statistical analysis of the results was performed. The average strain for each treatment was determined from three panels, with two measurements per panel. The average standard deviation for the twelve test panels was 0.002% strain. As the data were reasonably symmetric about the mean, hypothesis testing was a valid means of determining the statistical significance in measured strain. The results were examined using a one-tailed-t-test, assuming unequal-variances with an alpha of 0.05. Therefore, a probability less than 0.05 indicates the mean of the treated section is statistically lower than that of the control. The results for the statistical analysis are summarized in **Table 4.5-1**, along with the standard deviation and final strains for the treated sections.

Table 4.5-1. Statistical analysis of results.

	Direction	**σ (90%)**	**final strain ± σ (%)**		**Rate (%/yr.)**	**t-test* (α = 0.05)**	
Control	Travel	±0.00279	0.00607	0.01165	0.0022	--	
	Transverse	±0.00226	0.00584	0.01037	0.0026		
Silane 40A	Travel	±0.00147	0.00313	0.00607	0.0008	0.028	< 0.05
	Transverse	±0.00225	0.00576	0.01027	0.0026	0.482	> 0.05
Silane 100	Travel	±0.00134	0.00200	0.00469	0.0001	0.008	< 0.05
	Transverse	±0.00242	0.00178	0.00661	0.0010	0.021	< 0.05
Silane 40B	Travel	±0.00194	0.00123	0.00510	0.0004	0.006	> 0.05
	Transverse	±0.00320	0.00523	0.01164	0.0024	0.449	> 0.05

* t-test based on the 1000-day mean of the control and treated panels ($\alpha < 0.05$ indicates the results are statistically significant).

The average strain was statistically lower in both directions for the Silane 100 treated panels. Therefore, the 100% alkyltrialkoxysilane (Silane 100) imparted a statistically significant change in strain over the monitoring period. However, the average travel-direction strain in the Silane 40A and Silane 40B treated panels were less than that of the control by a statistically significant margin, whereas the transverse-direction strains were not.

Temperature and Internal-RH: Internal concrete temperature is summarized in **Fig. 4.5-4**. The error bars indicate the difference in temperature between the tested panels, which was within ±3.0 °C.

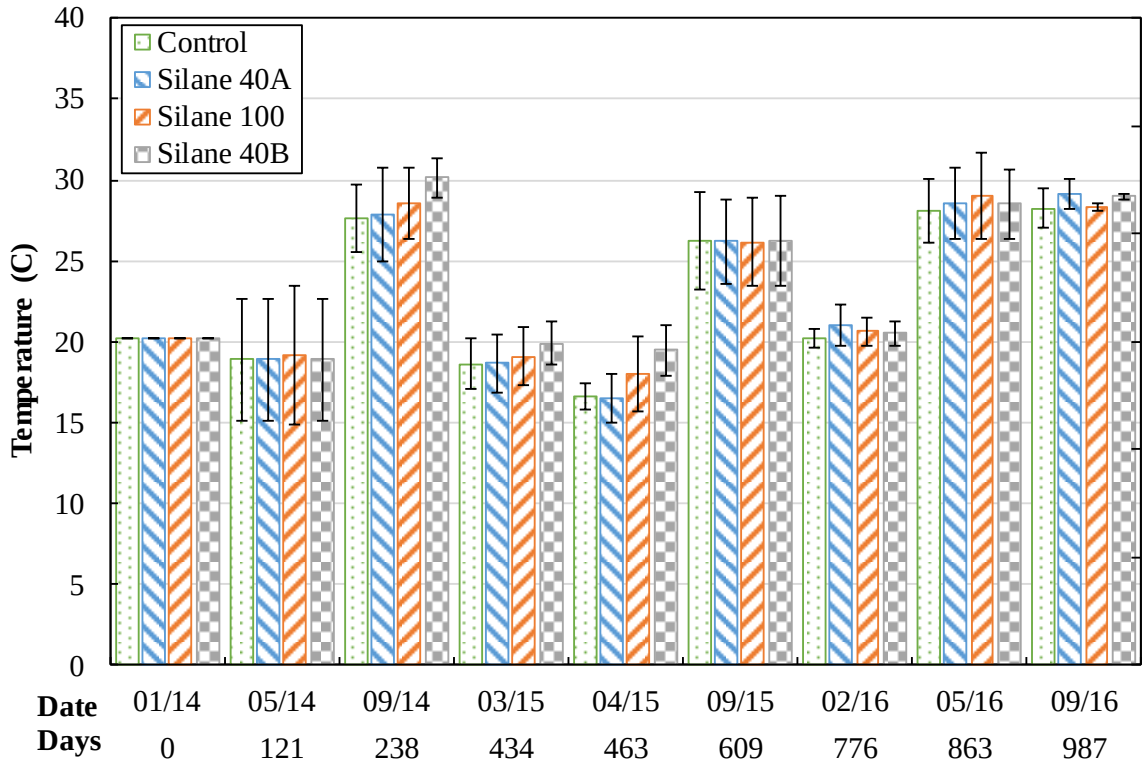

Fig. 4.5-4–Temperature (°C) with respect to date, error bars indicate 90% confidence of the mean, Interstate 49.

The average internal-RH data are summarized in **Fig. 4.5-5**. The yearly-average internal-RH for 2014 through 2016 are summarized in **Table 4.5-2**. The yearly-average internal-RH provides more insight into the change in internal-RH produced by the treatments. The largest change occurred in the Silane 100-treated panels, which decreased from 96.3±3.5 to 88.5±4.0% over three years. Average internal-RH for the Silane 100-treated panels was initially higher than that of the other panels, indicating the panels were more saturated. The panels were within the same test section and had similar drainage conditions. The higher internal-RH may be due to sensor variations as the accuracy of the probes is ±3.0%. Fluctuations in internal-RH were small given the difference in temperatures at the various site visits. However, the change in internal-RH over

three years was too small to make conclusions on the efficacy of treatment. In addition, internal-RH was only measured at a single depth, whereas drying produces an internal-RH gradient between the exposed surface and the concrete. Measuring internal-RH at several depths may prove more useful in determining the magnitude of drying imparted by silane treatment.

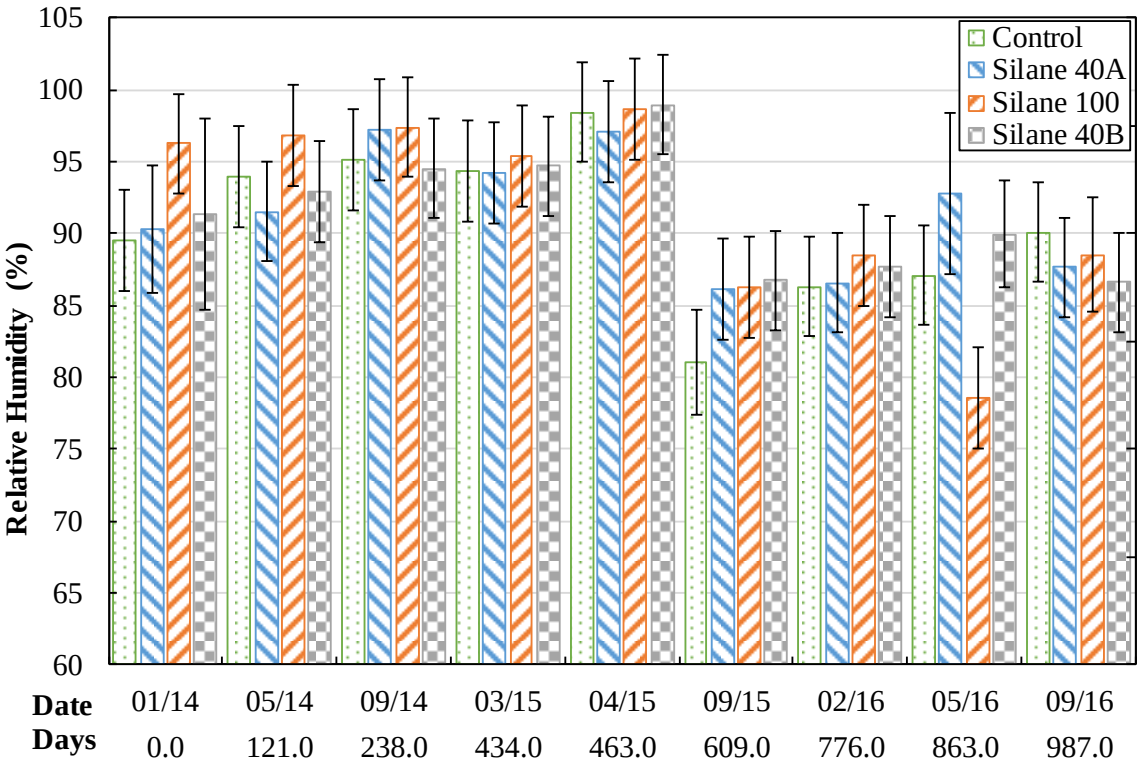

Fig. 4.5-5– Internal-RH (%) with respect to time, error bars indicate 90% confidence of the mean, Interstate 49.

Table 4.5-2. Summary of internal-RH (%) data with yearly-averages and overall change.

	Control (%)	**Silane 40A (%)**	**Silane 100 (%)**	**Silane 40B (%)**
January 2014	89.5±3.5	90.3±4.4	96.3±3.5	91.4±6.6
Average 2014	92.9±3.5	93.0±3.8	96.8±3.5	93.0±4.5
March 2015	94.3±3.5	94.3±3.5	95.4±3.5	94.7±3.5
Average 2015	91.3±3.6	92.5±3.5	93.5±3.5	93.5±3.5
September 2016	90.1±3.5	87.7±3.5	88.5±4.0	86.6±3.5
Average 2016	87.8±3.5	89.0±4.2	85.2±3.7	88.1±3.6
Change 2014-2016	-5.0±3.5	-4.0±3.8	-11.6±3.5	-4.9±4.5

Accurately measuring internal-RH in the field is difficult, and a large change is required for statistical significance. Bérubé et al. [6] monitored internal-RH for more than six years in a

highway median barrier, and reported a statistically meaningful decrease in RH after three years of monitoring. Other researchers have measured internal-RH at several depths within the concrete ranging from 1.5 to 3 in. (3.8 to 7.6 cm) depth, and found greater accuracy when the sensors were given sufficient time to equilibrate [13].

DRI: Strain was only measured over three years for the eighteen-year old pavement. Deterioration which occurred before monitoring began are not detected by these methods. The DRI method provides insight into deterioration which occurred prior to monitoring, along with quantifying deterioration occurring within the concrete cross-section.

A summary of DRI results is provided in **Fig. 4.5-6**. The baseline samples collected in 2013 (Control 13) had an average DRI of 331±80 (3 samples). Nine core samples from 2013 were also stored for one-years in conditions which accelerate the development of ASR. The samples stored in air (over water) at 100 °F (38 °C) and 100% RH, had an average expansion of 0.018% [34]. The average DRI of the samples (PFE 13 **Fig. 4.5-6**) was measured to be 400±80 (2 samples) after one year [34]. Based on the large standard deviation of the Control 13 and PFE 13 results, the increase in deterioration observed is not statistically significant. The amount of CCA and OCA features observed in the PFE 13 samples increased marginally relative to the Control 13 samples after one-year of accelerating conditions. This indicates a minimal potential for additional ASR deterioration to occur in the field. However, the storage conditions may leach alkalis from core samples, thereby reducing availability of alkalis as compared to pavement. Additional samples stored in NaOH solution at 38 °C expanded 0.104%, which indicates ASR deterioration can occur in the pavement when sufficient alkalis are available [34]. The samples stored in NaOH were not prepared for DRI testing as they crumbled during sawing

operation. The PFE 13 results indicate storing samples in conditions promoting ASR did not simulate the conditions occurring in the field.

The core samples extracted in 2016 exhibited increased deterioration as compared to the specimens from 2013. The control samples from 2016 (Control 16) had an average DRI of 536±76 (2 samples). The DRI was primarily composed of CCA, with a minor presence of OCA, CCP, OCAG, and CAD features. This indicates continued deterioration is occurring in the concrete and the deterioration is primarily due to other mechanisms and a minimal contribution of ASR. Considering the findings of the petrographic analysis, marginal air content, presence of D-cracking in the pavement, and the presence of OCA and CCP features without a comparable increase in OCAG and CCPG, the suspected deterioration mechanism is F/T. F/T deterioration typically leads to an increase in CCP features, which was not observed in this case. The Control 16-samples exhibited an increase in CCA features, which developed primarily within coarse aggregates. As such, it appears the deterioration is local to the coarse aggregate due to water freezing within the pores.

An example of this deterioration is shown in **Fig. 4.5-7 A**. Several coarse aggregate particles contain severe random microcracking, indicating the aggregate expanded from within. This deterioration may be due to F/T susceptibility of some coarse aggregate particles, and was found in all the samples. Additionally, samples contained corroded/disaggregated aggregate particles (DAP), which were comprised of chalcedony and found in the coarse fraction of the fine aggregate (1/4 in. (6 mm)). The presence of DAP particles appears to increase between 2013 and 2016 in the control and Silane 40B samples. The DAP particles exhibited reaction rims and were much softer than non-corroded particles, as shown in **Fig. 4.5-7 B**. Therefore, some ASR related deterioration is occurring in the pavement.

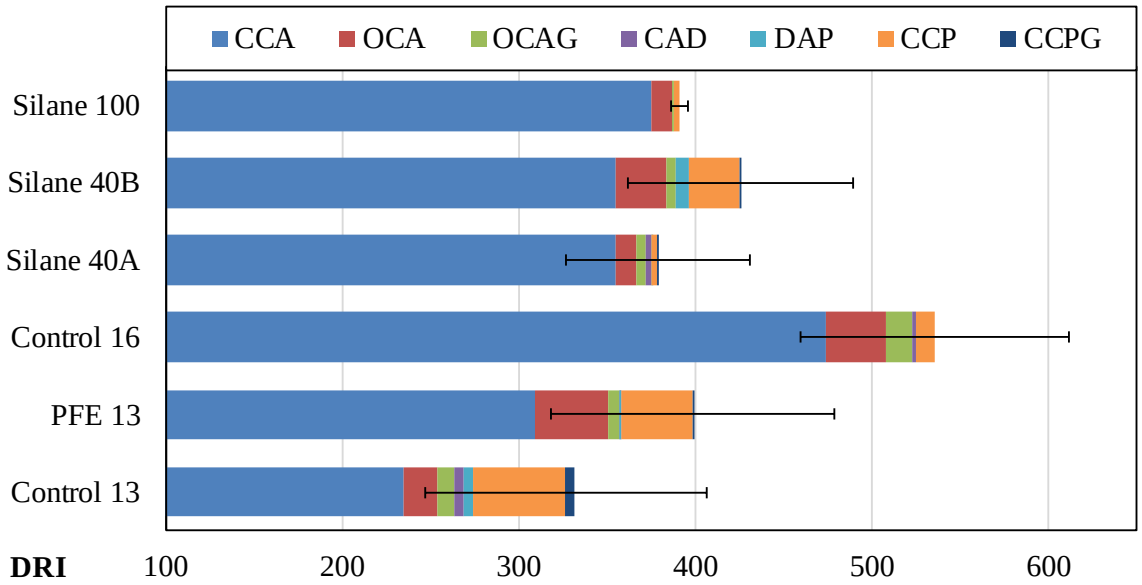

Fig. 4.5-6–DRI for core samples taken from pavement panels, error bars represent standard deviation, Interstate 49.

The samples, extracted in 2016, from pavement panels treated with Silane 40A, Silane 100, and Silane 40B had an average DRI of 380±52 (2 samples), 391±5 (2 samples), and 427±64 (2 samples), respectively. The samples contained minimal signs of ASR, including some OCAG, CAD, and DAP features. Deterioration primarily occurred as CCA features with a marginal quantity of OCA, and CCP features measured. The increase in CCA features relative to the Control 13 samples is evidence that deterioration may be occurring over time, which explains the increasing strain over the monitoring period. The deterioration in the treated section appears to be occurring at a slower rate than the untreated control sections. However, given the standard deviation of the results, the sensitivity of the DRI method is not sufficient to definitively attribute changes in deterioration to the treatment regimen.

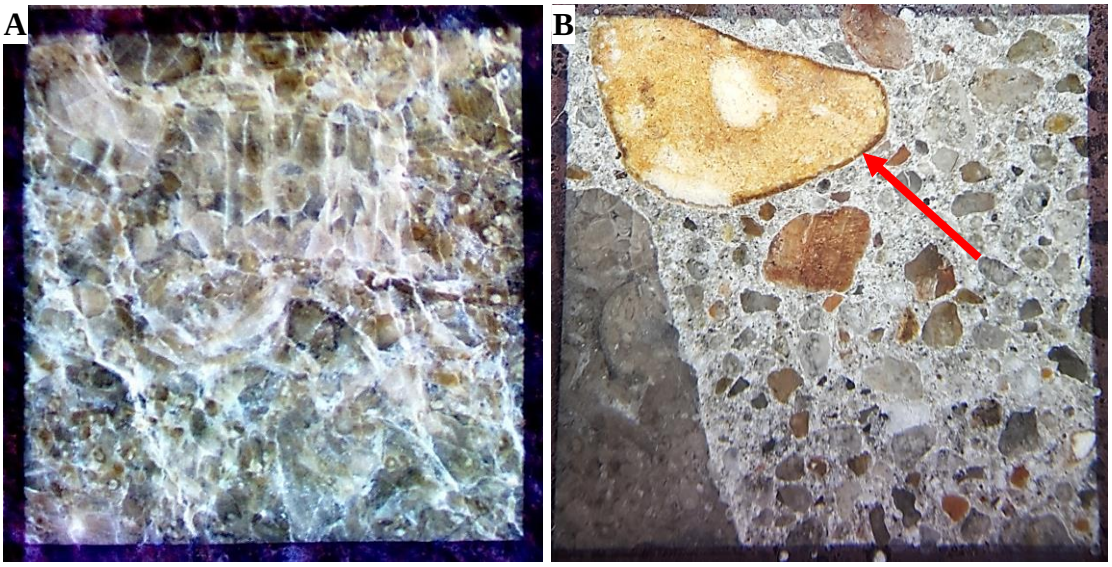

Fig. 4.5-7–Photomicrograph of coarese-aggregate particle with microcracking (A) and corroded aggregate particles, indicated by red arrow (B). Field of view is 10.0 mm x 10.0 mm (15X magnification) (by Richard Deschenes Jr.).

Synthesis of Results: The rate of deterioration in the test section is minimal and measuring a statistically meaningful effect of treatment is difficult given the three-year monitoring period. This is one of the difficulties with monitoring concrete deterioration over time, as more than three years is often necessary to measure any result. The pavement panels treated with silane exhibited a small, but measurable, change in strain, internal-RH, and DRI three years after treatment. The results are summarized in **Table 4.5-3**. Based on the field-testing results and petrography results, F/T deterioration appears to be the primary deterioration mechanism with a minor contribution from ASR. Deterioration is occurring more rapidly near the joints, and was not assessed well by strain measurements conducted near the center of the pavement panels.

Table 4.5-3. Summary of results for silane treatments.

Measurement	Control	Silane 40A	Silane 100	Silane 40B
Travel-strain	0.0090±0.0028	0.0048±0.0015[S]	0.0036±0.0014 [S]	0.0034±0.0010 [S]
Transverse-strain	0.0081±0.0023	0.0080±0.0023	0.0042±0.0017 [S]	0.0084±0.0032
Initial RH (%)	92.9±3.5%	93.0±3.8%	96.8±3.5%	93.0±4.5%
Final RH (%)	87.8±3.5%	89.1±4.2%	85.2±3.7%	88.1±3.6%
DRI	536±76	380±52	391±5	427±64
Performance	Control	Limited	Slowed expansion	Limited

[S] Denotes the average strain is statistically lower than that of the control.

Silane, which has been demonstrated to slow ASR in concrete elements such as barrier walls and bridge elements, appears to influence the rate of deterioration in pavements. Interestingly, the solvent-based 100% silane appears to limit further deterioration likely due to F/T, relative to the control. The difference in efficacy of the 40% water-based silane compounds as compared to the 100% solvent-based silane was unexpected. The concentration and base of silane products typically do not affect the efficacy, although 40% water-based silanes are typically more effective [11, 13]. However, Wehrle [11] reported higher concentration silane products appear to be more effective when applied to concretes of higher permeability (higher w/c).

The hypothesized mechanism, by which silane mitigates F/T distress, occurs when the moisture state of the concrete decreases over time. Janssen [32] noted that silane may be effective at reducing the moisture state of concrete near joints, thereby slowing F/T deterioration. The presence of microcracks allows more water into the concrete, maintaining the pavement closer to saturation. When treated with silane, the moisture state decreases from saturation, thereby inhibiting stresses from developing in the capillary spaces during F/T and inhibiting the ASR gel product from adsorbing moisture. Silane treatment effectively slowed F/T and ASR deterioration in median barriers for three to six years, as described by Berube et al. [6] and Deschenes et al. [18].

4.6. CONCLUSIONS

The concrete pavement test section used in this study exhibited symptoms of premature deterioration due to ASR and F/T. The concrete pavement contained a moderately-reactive fine aggregate, which led to the formation of a limited amount of ASR and microcracking in the concrete. The air entrainment used in the concrete was not sufficient to fully protect the concrete from F/T deterioration. Microcracks within the pavement allow additional water to enter the

concrete over time thereby increasing the moisture state of the concrete. Additionally, alkali-silica gel deposits reduce the available pore space for water during freezing.

- The Silane 100 treatment resulted in a statistically significant reduction in strain and a measurable reduction in internal-RH for the concrete pavement panels over a three-year monitoring period. The 100% alkyltrialkoxysilane was most effective in limiting strain in the concrete pavement, while the 40% alkylalkoxysilane water-based Silane 40A and Silane 40B products proved inconsistent. As observed by Wehrle [11], the solvent-based silane products are more effective when higher permeable concrete allows greater penetration of the silane.
- Three-years of strain and internal-RH monitoring was not sufficient to definitively confirm the efficacy of silane treatments in slowing the rate of ASR and F/T deterioration in concrete pavement.
- DRI results suggest silane treatments slow F/T deterioration in the treated sections relative to the untreated control sections. The presence of ASR deterioration was minimal in the control and treated samples. The treated sections underwent a minimal increase in CCA and OCA as compared to the control samples from 2013. The CCA and OCA features increased more in the control sections of the pavement than in the samples stored in conditions which accelerate ASR. This led to the conclusion that F/T, rather than ASR, produced the increased deterioration measured in the control panels
- The DRI method is an effective semi-quantitative measure of concrete deterioration. The DRI numbers measured in this study indicate fair to moderate deterioration per Sanchez et. al [35]. The results indicate a marginal difference in deterioration between control sections and treated sections within three years. However, the difference between control

and treated sections may be due to variations in the concrete rather than an effect of the treatment. Determining the statistical relevance of the results is difficult as only two samples were evaluated per test panel. All samples were evaluated by a single operator, reducing errors introduced by multiple operators.

- The DRI method requires experience and judgment, and remains subject to operator bias. The test method required between 6 and 8 hours per sample, limiting the number of samples which can be evaluated. However, the method provides a small cross-sectional analysis of the concrete, which is very useful for diagnostic purposes.
- Internal-RH is difficult to measure accurately in the field, and an improved method is required. The accuracy of internal-RH measured in the field depends on ambient conditions and the stability of the concrete temperature during measurements. The method employed in this research program proved more accurate when fresh holes were drilled at each site visit, and the probes were epoxied in place.
- Based on the findings of this research program, the 18-mile (29 km) section of Interstate 49, along with the test section, was diamond ground and treated with silane in October 2016. A 100% solvent-free, isobutylalkoxysilane (similar to the Silane 100 used in this research) was applied at a cost (materials and application) of \$0.27/ft.^{2} or \$16,900 per lane mile (\$10,500 per lane km). Monitoring of the test site will be continued to evaluate the efficacy of the applied silane treatment.

4.7. ACKNOWLEDGEMENTS

The authors would like to thank the Arkansas State Highway and Transportation Department (AHTD) and the Mack Blackwell Rural Transportation Center (MBTC) for providing financial support for this research program. AHTD also provided invaluable support and access to the

pavement test section throughout the three-year duration of the project. The authors greatly appreciate the help provided by W. Philips, C. Dang, C. Murray, M. Waidner, and R. Reed in conducting instrumentation and monitoring.

4.8. REFERENCES

1. Powers, T. C. (1975). "Freezing effects in concrete." *American Concrete Institute Special Publication*, 47(1), 1-12.

2. Tanesi, J., & Meininger, R. (2006). "Freeze-thaw resistance of concrete with marginal air content." *Federal Highway Administration* Report No. HRT-06-117, 1-96.

3. Powers, T.C. (1945). "A working hypothesis for further studies of frost resistance of concrete." *ACI Journal Proceedings*, 41(1), 245-272.

4. Bérubé, M-A., Chouinard, D., Pigeon, M., Frenette, J., Boisvert, L., & Rivest, M. (2002b). "Effectiveness of sealers in counteracting alkali–silica reaction in plain and air-entrained laboratory concretes exposed to wetting and drying, freezing and thawing, and salt water." *Canadian Journal of Civil Engineering*, 29, 289-300.

5. Stark, D. C., Morgan, B., Okamoto, P., & Diamond, S. (1993). "Eliminating or minimizing alkali-silica reactivity (Report No. SHRP-C-343)." *Strategic Highway Research Program (SHRP)*, National Research Council, Washington, DC, 266 pp.

6. Bérubé, M.-A., Chouinard, D., Pigeon, M., Frenette, J., Rivest, M., & Vézina D. (2002a). "Effectiveness of sealers in counteracting alkali–silica reaction in highway median barriers exposed to wetting and drying, freezing and thawing, and deicing salt." *Canadian Journal of Civil Engineering*, 29, 329-337.

7. Thomas, M.D.A., Folliard, K.J., Fournier, B., Drimalas, T., & Rivard, P. (2012). "Study of remedial actions on highway structures affected by ASR." *Proceedings of the 14th International Conference on Alkali-Aggregate Reaction (ICAAR)*, Austin, Texas, 10 pp.

8. Folliard, K.J., Thomas, M.D.A., Fournier, B., Resendez, Y., Drimalas, T., & Bentivegna, A. (2012). "Evaluation of mitigation measures applied to ASR-affected concrete elements: preliminary findings from Austin, TX Exposure Site." *Proceeding of the 14th International Conference on Alkali Aggregate Reaction (ICAAR)*, Austin, Texas, 10 pp.

9. Drimalas, T., Folliard, K.J., Thomas, M.D.A., Fournier, B., & Bentivegna, A. (2012). "Study of the effectiveness of lithium and silane treatments on field structures affected by ASR."

Proceedings of the 14th International Conference on Alkali-Aggregate Reaction (ICAAR), Austin, Texas, 10 pp.

10. Thomas, M. D. A., Folliard, K. J., Fournier, B., Rivard, P., and Drimalas, T. (2013). "Methods for evaluating and treating ASR-affected structures: results of field application and demonstration projects (Report No. FHWA-HIF-14-0002)." *Federal Highway Administration*, U.S. Department of Transportation, Washington DC, 80 pp.

11. Wehrle, E. R. (2010) "The effects of coatings and sealers used to mitigate alkali-silica reaction and/or delayed ettringite formation in hardened concrete." *Doctoral dissertation*, University of Texas at Austin, TX, 166 pp.

12. Mayer, H. (1998). "The chemistry and properties of silicone resins." *Pigment & Resin Technology*, 26(6). 364-373.

13. Rust, C. (2009). "Role of RH in concrete expansion due to alkali-silica reaction and delayed ettringite formation: RH thresholds, measurement methods, and coatings to mitigate expansion." *M.S. Thesis*, The University of Texas at Austin, Austin, TX, 120 pp.

14. Fournier, B., Bérubé, M.A., Thomas, M. D. A., Smaoui, N. & Folliard, K. J. (2004). "Evaluation and management of concrete structures affected by alkali-silica reaction - A review (MTL 2004-11)." *Natural* Resources *Canada*, Ottawa (Canada), 59 pp.

15. Fournier, B., Bérubé, M-A., Folliard, K.J., & Thomas, M.D.A. (2010). "Report on the diagnosis, prognosis, and mitigation of alkali- silica reaction (ASR) in transportation structures (Report No. FHWA-HIF-09-004)." *Federal Highway Administration*, U.S. Department of Transportation, Washington DC, 154 pp.

16. Stark, D. (1990). "The moisture condition of field concrete exhibiting alkali-silica reactivity." CANMET/*ACI International Workshop on Alkali-Aggregate Reaction in Concrete*, Halifax, Nova Scotia, 19 pp.

17. Bérubé, M.A., Chounard, D., Boisvert, L., Frenetter, J., and Pigeon, M. (1996). "Influence of wetting-drying and freezing-thawing cycles, and effectiveness of sealers on ASR". *Proceedings of the 10th International Conference on Alkali-Aggregate Reaction (ICAAR)*, Melbourne, Australia, August 18-23, 1056-1063.

18. Deschenes Jr. R., Murray C.D., and Hale W. M. (2017). "Mitigation of ASR and freezing and thawing through surface treatment." *ACI Materials Journal*, 114(2), 307-314. DOI: 10.14359/51689493.

19. Sanchez, L. F. M., Fournier, B., Jolin, M., Duchesne, J. (2015). “Reliable quantification of AAR damage through assessment of the damage rating index (DRI).” Cement and Concrete Research, 67, 74-92.

20. Rivard, P., Founrier, B., Ballivy, G. (2002). “The damage rating index method for ASR affected concrete—a critical review of petrographic features of deterioration and evaluation criteria*”. Cement, Concrete, and Aggregates*, 24(2), 1-11.

21. Grattan-Bellew, P.E., Mitchell, L.D. (2006). “Quantitative petrographic analysis of concrete –the damage rating index (DRI) method, a review”. *Proc. Marc-André Bérubé symposium on AAR in concrete, CANMET/ACI Advances in concrete technology seminar*, Montréal, Canada, 321-334.

22. Dunbar, P.A.; Grattan-Bellew, P.E. (1995). “Results of damage rating evaluation of condition of concrete from a number of structures affected by ASR*”. CANMET/ACI International Workshop on Alkali-Aggregate Reactions in Concrete*, Dartmouth, Canada, October, 257-266.

23. Sanchez, L., Fournier, B., Drimalas, B., Bastien, J., Mitchell, D., and Noël, M. (2016). “Semi-quantitative condition assessment of concrete distress through the damage rating index.” *Proceedings of the 15th International Conference on Alkali-Aggregate Reaction (ICAAR),* San Paulo, Brazil, 10 pp.

24. Shrimer, F. (2000). “Application and use of damage rating index in assessment of AAR-affected concrete-selected case studies.” *Proceeding of the 11th International Conference on Alkali Aggregate Reaction (ICAAR),* Quebec, Canada, 899-907.

25. Sanchez, L. F. M., Fournier, B., Jolin, M., Bedoya, M. A. B., Bastien, J., & Duchesne, J. (2016). “Use of damage rating index to quantify alkali-silica reaction damage in concrete: fine versus coarse aggregate.” *ACI Materials Journal,* 113(04), 395-407.

26. Sanchez, L.F.M., Fournier, B., Jolin, M., Mitchell, D., Bastien, J. (2017). “Overall assessment of Alkali-Aggregate Reaction (AAR) in concretes presenting different strengths and incorporating a wide range of reactive aggregate types and natures.” *Cement and Concrete Research,* 93, 17-31.

27. Villeneuve, V.; Fournier, B.; Duchesne, J. (2012). “Determination of the damage in concrete affected by ASR – The damage rating index (DRI)”. *Proceedings of the 14th International conference on alkali-aggregate reaction (ICAAR).* Austin, Texas, 10 pp.

28. Deschenes, R. Jr., and Hale, W. M. (2016). “Alkali-Silica Reaction in Concrete with Previously Inert Aggregates,” *Journal of Performance of Constructed Facilities,* ASCE, p. 04016084. DOI: 10.1061/(ASCE) CF.1943-5509.0000946.

29. CTL Group (Construction Technology Laboratories Group). (2012). “Petrographic examination of concrete specimens from I-540 roadway and barrier wall (Project No. 157501).” *CTLGroup,* Skokie, IL. 17 pp.

30. ASTM C1260-05. (2008a). “Standard test method for potential alkali reactivity of aggregates (mortar-bar method).” *Annual Book of ASTM Standards 04.02,* American Society for Testing and Materials (ASTM), West Conshohocken, Pennsylvania, 676-680.

31. ASTM C1293-08b. (2012). “Standard test method for determination of length change of concrete due to alkali-silica reaction.” *Annual Book of ASTM Standards 04.02,* American Society for Testing and Materials (ASTM), West Conshohocken, Pennsylvania, 687-686.

32. Janssen, D., and Snyder, M. (1994). “Resistance of Concrete to Freezing and Thawing.” SHRP-C-391, *Strategic Highway Research Program,* National Research Council, Washington, DC, 217 pp.

33. Reed, R., and Deschenes Jr., R. A., and Hale W. M. (2016). “Measuring Relative Humidity in Concrete Pavements as a Method to Assess ASR Mitigation Measures.” *Proceedings of the 15th International Conference on Alkali-Aggregate Reaction (ICAAR),* San Paulo, Brazil, 9 pp.

34. Waidner, M. (2015). “Identifying Damage, Predicting Expansion, and Determining the Effectiveness of Sealers on Concrete Affected by Alkali-Silica Reaction and Freeze-Thaw.” *Master’s Thesis*, University of Arkansas, 88 pp.

35. Sanchez, L.F.M., Fournier, B., Jolin, M., Mitchell, D., Bastien, J. (2017). “Overall assessment of Alkali-Aggregate Reaction (AAR) in concretes presenting different strengths and incorporating a wide range of reactive aggregate types and natures.” Cement and Concrete Research, 93, 17-31.

5. PAPER 4: ANOTHER LOOK AT THE EFFECTS OF RELATIVE HUMIDITY, TEMPERATURE, AND FREEZING AND THAWING ON ASR

Richard A. Deschenes Jr., Eric Giannini, Thano Drimalas, Benoit Fournier, W. Micah Hale

Biography: ACI member **Richard A. Deschenes Jr.** is a Graduate Assistant at the University of Arkansas, Fayetteville, where he received his BS and MS in civil engineering in 2012 and 2014, respectively. He is currently a PhD candidate in civil engineering at the University of Arkansas. He received the 2013 ACI Schwing American Scholarship and the 2015 ACI BASF Construction Chemicals Fellowship. His research interests include durability issues of concrete structures.

ACI member **Eric R. Giannini** is an Assistant Professor at The University of Alabama. He is a member of several ACI committees including 123, Research and Current Developments; 201, Durability of Concrete; and 228, Nondestructive Testing of Concrete. He also chaired subcommittee 228-B. His research interests include alkali-silica reaction and nondestructive testing. He received his PhD in civil engineering from The University of Texas at Austin in 2012.

ACI member **Thanos Drimalas** is a Research Associate in the Department of Civil, Architectural, and Environmental Engineering at the University of Texas at Austin. He received a PhD in civil and environmental engineering from the University of Texas at Austin in 2007. He is a member of ACI Committees 201, Durability of Concrete; and 350, Environmental Engineering Concrete Structures. His research interests include durability of concrete materials and alkali-aggregate reaction.

Benoit Fournier is a professor in the Department of Geology and Geological Engineering at Université Laval. He is a member of the ACI Durability Committee 201 and chair of CSA AAR

TSC in Canada. His research interests include aggregate technology, durability of concrete, alkali-aggregate reactions, and incorporating SCMs.

ACI Fellow **W. Micah Hale** is Professor and Head of the Department of Civil Engineering at the University of Arkansas. He is Chair of ACI Committee 363, High Strength Concrete, and is a member of ACI Committees 239, Ultra-High-Performance Concrete, 233, Slag Cement, and 423 Prestressed Concrete. His research interests include concrete materials, mixture proportioning, and prestressed concrete. He holds a B.S., M.S., and Ph.D. in Civil Engineering from the University of Oklahoma.

Abstract: Alkali-silica reaction (ASR) and freezing and thawing (F/T) deterioration reduce the service life of transportation structures. Understanding the mechanisms of deterioration and the influences of moisture are imperative to developing mitigation measures. The influence of relative humidity (RH) and temperature on the development of ASR were evaluated herein. Additionally, the influence of wetting and drying (W/D) and F/T on the development of ASR were examined. These factors exacerbate concrete deterioration, and understanding the relationship between moisture and deterioration is necessary for mitigation of deterioration. The results of this study confirm a relationship between the reactivity of aggregates and temperature, and a relationship between deleterious expansion and RH. The results also confirm the deleterious effects of F/T on the development of ASR. Sufficient drying prevents the development of both ASR and F/T deterioration in non-air-entrained concrete. Silane was therefore evaluated as a possible mitigation measure for concrete exposed to a combination of ASR, F/T, and W/D.

Keyword: Alkali-silica reaction (ASR), relative humidity (RH), wetting-and-drying, freezing-and-thawing (F/T), mitigation, silane.

5.1. INTRODUCTION

Alkali-silica reaction (ASR) and freezing and thawing (F/T) deterioration in concrete are both related to the moisture state within concrete. ASR deterioration occurs when moisture within the pore solution is drawn into alkali-silica gel, resulting in expansive pressure and cracking. The F/T deterioration mechanism occurs when water within the cement or aggregate pores freezes repeatedly and exerts pressure on the cement paste causing cracking. The ambient conditions to which concrete is subjected affect the moisture state within the pore structure, which influences the development of expansive pressures and deterioration.

Alkali-silica reaction (ASR): ASR occurs when siliceous minerals within certain reactive aggregates dissolve under the action of hydroxides within the cement pore solution. The presence of alkali cations (Na^+ and K^+) within the pore solution frees hydroxyl ions (OH-), which interact with silanol groups within the siliceous minerals [1]. As the silica structure is broken down, a water-insoluble gel product forms comprised of calcium, alkalis, and dissolved silica [1]. Cations (K^+, Na^+, Ca^{++}) are absorbed at the reaction site, penetrating further into the silica structure, hydrolyzing siloxane bonds and allowing the reaction to proceed [2]. The rate of reaction is dependent on the concentration of cations in the pore solution, the silica structure, and the temperature. Formation of expansive alkali-silica gel products depends on the concentration of cations. Expansion occurs when pore solution is absorbed into the gel product. The hypothesized expansive mechanism occurs by osmosis, due to the solute concentration gradient between the alkali-silica gel product and the cement pore solution, with the water-insoluble alkali-silica gel acting as a membrane [3]. Expansion causes microcracks in the aggregates and cement paste, which extend to form a network of microcracks. As deterioration progresses visible cracking becomes apparent at the exposed surface of the concrete.

The solubility of siliceous phases within aggregates depend on the internal structure, texture, and temperature. Siliceous minerals range from ordered quartz to amorphous silica. Ordered minerals such as quartz are less soluble, and require higher alkalinity and temperature to dissolve. Chalcedony, opal, and amorphous silica are increasingly disordered and dissolve faster and at lower temperatures. The moderately-reactive aggregate used herein contains a fraction of chalcedony which dissolves slower than the siliceous phases within the highly-reactive sand.

Bérubé et al. [4] and Nishibayashi et al. [5] note cycles of wetting and drying (W/D) cause surface cracking in concrete. The cycles lead to a moisture and alkali gradient between the bulk concrete and the exposed surface, which leads to a strain gradient. The drying concrete at the surface expands less relative to the bulk concrete, causing macro-cracking at the surface [4, 6].

Freezing and thawing (F/T): F/T deterioration occurs when pressure develops within the capillary spaces of the cement paste during cooling. The exact mechanism by which F/T stress occurs is not fully understood. The development of pressures in concrete is complicated by the colloidal nature of the cement paste and the concentration of cations within the pore solution. Powers [8] postulated pressure develops when pore-water freezes and expands, forcing water into the surrounding capillary spaces. The capillary spaces are small and pressure develops due to viscous resistance to the movement of water. If this pressure is greater than the tensile strength of the concrete, microcracks develop. Powers and Helmuth [9] later found a concentration gradient draws water towards the freezing site by osmosis. Deterioration occurs when water migrates through the capillary space and diffuses into the pore space [10, 12]. A critical distance occurs, over which water can migrate before deterioration occurs [10]. In non-air-entrained concrete elements, the symptoms of distress materialize as cracks in the cement paste, which track parallel to the exposed surface of the concrete. Air-entrainment, however, can

be used to protect concrete from the development of F/T distress by providing a network of small, dispersed voids with a spacing factor of about 0.006 in ($2.4x10^{-4}$ mm) [10].

F/T related deterioration also arises due to water diffusing from aggregate particles [10]. Litvan [11] postulated that pressure develops as RH decreases in the aggregate pores, and water diffuses out of aggregate pores into cement pores. Thereby inducing stresses on the cement capillary space as water migrates from the aggregates to the cement paste [12]. Typically, aggregate particles contain pores and capillary networks larger than those of the cement paste and are not saturated after hydration of the cement [10]. However, if the aggregate particles become fully saturated before freezing, water may be expelled into the surrounding cement paste by hydraulic pressure [10]. Even in air-entrained concrete, the high porosity of certain aggregates relative to cement paste results in an abundance of water being expelled on freezing, which causes deterioration in the surrounding cement [10]. To prevent F/T deterioration in concrete, susceptible aggregates must not remain saturated after initial drying of the concrete, or become saturated on exposure to external moisture [10].

In air-entrained concrete pavements, F/T susceptible aggregates can become saturated and cause D-cracking near joints. These F/T susceptible aggregates have fine, interconnected pores, and water cannot disperse into the less permeable cement paste on freezing. Therefore, micro-cracking develops within the interfacial transition zone (ITZ). On repeated F/T, the cracks may extend until a network of macro-cracks form. This process occurs due to water intrusion at the joints leading to re-saturation of the susceptible aggregate particles. The deterioration materializes as cracks at exposed pavement surface parallel to the joint. The crack form at the pavement edges and curve along the corners forming a ‘D’ shape, named D-cracking (as shown in **Fig. 5.1-1**).

Fig. 5.1-1-D-Cracking in concrete pavement, Interstate 49 (by Richard Deschenes Jr.).

ASR and F/T: As noted by Bérubé et al. [4] and Deschenes et al. [13], a combination of ASR and F/T deterioration can occur in concrete elements. The hypothesized mechanism of deterioration occurs when cracking initiated by ASR provides an avenue for water to penetrate the concrete which causes saturation of the cement paste and aggregates [4]. Both ASR and F/T require moisture within the concrete and cause expansion and deterioration. A network of cracks forms along the exposed surface and the permeability of concrete increases, decreasing the resistance to ASR and F/T deterioration. As a result, the concrete is maintained at a higher moisture state closer to saturation, further reducing resistance to F/T.

Relative Humidity (RH): ASR and F/T deterioration in concrete are related to the internal moisture state of the concrete. Therefore, it is useful to quantify the state of moisture within concrete. The moisture state of concrete can be quantified as moisture content, measured in the laboratory by calculating the mass-loss on drying. However, this is impractical in the field where samples cannot be weighed or dried. Therefore, a relationship between moisture state and internal-RH would be useful. RH, defined as the ratio of the vapor-pressure (VP) of an air-water solution relative to the saturation-VP of the same air-water solution (at the same temperature), provides a useful index of the moisture state within concrete. The saturation-VP is calculated as

a function of temperature, whereas VP is measured using a hygrometer. RH can then be calculated as the ratio of VP to saturation-VP. VP could alternatively be used as an index of the state of moisture within concrete. RH is a function of VP and is relative to temperature, whereas VP can be reported as a single value independent of temperature.

The nature of internal-RH in concrete is complicated by the colloidal nature of cement paste. The sorption characteristics of concrete are influenced by the tortuosity and size of capillary, interlayer, and pore spaces. Concrete absorbs water as ambient-RH increases and desorbs water as ambient-RH decreases. This process continued until the concrete is in equilibrium with the ambient conditions [14, 15]. On drying, water evaporates from larger cement pores first, followed by smaller cement pores. As this occurs, the internal-VP decreases due to the pronounced curvature of water-menisci in the smaller cement pores [16].

When temperature increases and the absolute volume of moisture within the concrete is held constant, internal-RH increases due to the excitation of water and reduced surface tension [16]. Additionally, water in the colloidal cement paste is transported from the capillary and interlayer spaces into the cement pores, thereby reducing the curvature of the water-menisci and increasing VP [14]. This increase in internal-RH with temperature is opposite to what occurs for noncolloidal materials, where RH decreases with increasing temperature at a constant moisture content [14].

The relationship between internal-RH and moisture content in concrete is therefore dependent on material properties such as hydration age and pore distribution. Although sorption isotherms can be developed by measuring mass-change and internal-RH as concrete dries, it is impractical to develop such relationships for each concrete structure. Internal-RH (and VP) can however be measured in the field using capacitive-type probes, and provides a useful quantification of the

state of moisture within the concrete. The threshold internal and ambient-RH (and VP) required for ASR or F/T deterioration to occur in concrete can be determined through laboratory testing, and used to evaluate the efficacy of mitigation measures.

Measuring RH in Concrete: To better understand the relationship between internal-RH and moisture state in concrete, Gause [14] evaluated the drying characteristics of a 0.64 w/c concrete. Internal-RH and moisture content were monitored for 300 days within concrete samples (12 in. cubes (30.5 cm)). A hygrometer was embedded within the concrete and allowed to equilibrate with the concrete over time. The samples were sealed on five sides, and drying occurred only through the exposed face. Depending on the initial moisture condition of the samples, the internal-RH at 1.5 (38 mm) and 3 in. (76 mm) were within 10% of the ambient conditions within 300 days. The 300-day RH at 6 in. (152 mm) was up to 40% higher than the ambient conditions. Ambient and internal-RH of concrete should not be confused because the permeability of concrete is low and may requires years for the internal-RH to reach equilibrium with ambient-RH. However, equilibrium can occur rapidly (less than 300 days) for elements smaller than 6 in. (152 mm) and exposed to drying from multiple sides. Stark [7] evaluated the drying characteristics of concrete in the field and found that even in arid environments, the internal-RH at depths greater than 8 in. (203 mm) was unaffected by ambient conditions due to the low permeability of concrete. Although not measured, the depth to which drying occurs depends on permeability, and therefore w/c ratio. A w/c ratio of 0.30 or less would result in sufficient desiccation on hydration to cause an internal-RH less than required to sustain ASR [7].

Stark [7] and Bérubé et al. [4] determined an internal-RH of 80 to 85% (21 °C) was required for ASR to occur in certain concretes. These thresholds were determined for specific concrete mixtures containing different aggregates and alkali loadings. Stark [7] determined this value

through a combination of lab and field tests. In the lab, mortar bar samples (1 in. square (25 mm)) were subjected to a range of ambient conditions and internal-RH assumed equal to ambient-RH. In the field, concrete samples were collected at multiple depths within concrete elements, and then stored in hermetically sealed containers at 21 °C, followed by measuring the RH above the sample. Bérubé et al. [4] measured the internal-RH for samples stored in the lab by embedding capacitive-type RH probes within concrete cylinders. ASR related expansion slowed when the internal-RH decreased below 80-85% (21 C). The threshold was shown by Pedneault [17] to depend on the form of siliceous minerals present within the aggregate.

Silane Sealers: Silanes are a low-viscosity penetrating silicon sealers, comprised of alcohol and alkyl functional groups [18]. The hydrophobic and breathable nature of silane sealers make them useful for treating concrete elements and reducing the internal moisture state. Silanes have been applied to many field concrete, as a means of mitigating ASR-related deterioration [6, 13, 19, 20, 21, 22, 23, 24]. The low permeability of concrete limits the efficacy of silane because drying can only occur in the first 6 to 8 in. (152 to 203 mm) of the exposed surface [7].

Janssen [12] also noted treating concrete susceptible to F/T deterioration with a sealer improves the durability factor of the concrete relative to untreated control specimens. Specimens were treated with silane and exposed to cycles of F/T. The treatment appeared to slow deterioration of D-cracking susceptible concrete [12]. Bérubé et al. [4] evaluated silane as a possible means of mitigating combinations of ASR and F/T deterioration in concrete. Silane treatment reduced the moisture state of the concrete and improved the durability as compared to untreated samples for both non-air-entrained and air-entrained concrete. Bérubé et al. [4], Deschenes et al. [13], and others found silane reduced ASR and F/T related deterioration in concrete barriers.

Research Objectives: Deschenes [13] reported on a field investigation of concrete barriers exhibiting moderate to severe deterioration from a combination of ASR and F/T. The barrier contained the same moderately-reactive aggregate evaluated herein. This aggregate is borderline reactive, and sometimes passes the ASTM C1293 standardized test. Therefore, an investigation to determine the exacerbating effects of F/T on the development of ASR in concrete containing this moderately-reactive aggregate was warranted. The fundamental mechanisms of ASR and F/T are well documented and methods for mitigating both are well established. However, understanding the relationships between ASR, F/T and the moisture state of concrete is important for developing effective mitigation measures. The objective of this research was thus to better understand the relationship between exposure conditions and combined ASR and F/T deterioration in concrete. More specifically, this work determines the effects of storage temperature and ambient-RH on the development of ASR in concrete with moderately-reactive and highly-reactive aggregates. Additionally, the effects of F/T, moisture state, and silane treatment on the development of ASR were assessed.

5.2. RESEARCH SIGNIFICANCE

Understanding the relationship between internal-RH, temperature, exposure conditions, and ASR is important in developing durable concrete. This research investigates the threshold-RH, at various temperature, required for ASR deterioration to occur in concretes containing moderate and highly reactive aggregates. Specimens containing a moderately-reactive aggregate were also stored in various exposure conditions which accelerate ASR or F/T deterioration. The results indicate concrete with marginally-reactive aggregates sometimes pass required testing for ASR and F/T performance, while deteriorating when exposed to cycles of conditions promoting ASR and F/T. ASR deterioration reduces the F/T performance of concrete, causing premature failure.

5.3. EXPERIMENTAL INVESTIGATION

The research was conducted in two phases: the relationship between ambient-RH, temperature, and ASR was evaluated first. The relationship between ASR, W/D, and F/T was then evaluated.

5.3.1. Relative Humidity (RH)

Materials: An ASTM C150 Type I/II cement (0.89% Na_2O_{eq}) was used for RH testing. The coarse aggregate was a non-reactive crushed limestone. Two fine aggregates were compared, the first a very highly-reactive (per ASTM C1778) siliceous sand with a one-year concrete prism test (CPT) expansion of 0.500%. The second aggregate was a moderately-reactive (per ASTM C1778) river sand containing chalcedony with a one-year CPT expansion of 0.040%. The concrete mixtures were designed in accordance with ASTM C1293, and are summarized in **Table 5.3-1**. Sodium Hydroxide (NaOH) was added to the concrete mixing water to achieve a total Na_2O_{eq} content of 8.85 lb/yd^3 (5.25 kg/m^3).

Specimens: Thirty-six concrete prisms were cast for each aggregate tested. The prisms were 3 x 3 x 11.25 in (75 x 75 x 285 mm), with metal gage studs embedded at each end for measuring length change. Length-change was periodically measured using a length comparator. The highly-reactive specimens were monitored for 167 days, and the moderately-reactive specimens for 422 days.

Curing: Three prisms were cast each day, and then cured in the mold for 24 hours at 95% RH (21 °C). The prisms were then removed from the mold and stored an additional 14 days at 50% RH (21 °C). After 14 days, the prisms were wrapped in cellophane and placed in a freezer at -10 °C to slow curing and prevent drying. The prisms remained in the freezer until all subsequent prisms had cured for 14 days.

Table 5.3-1. Materials used for CPT prisms.

Material	**Highly-reactive** lb/yd^3 (kg/m^3)	**Moderately-reactive** lb/yd^3 (kg/m^3)	**Notes**
Cement	708 (420)	708 (420)	0.89% Na_2O_{eq}
Coarse Agg.	1782 (1057)	1782 (1057)	Non-reactive limestone
Fine Agg.	1152 (683)	1161 (688)	Reactive Agg. (F.M. = 3.0)
Water	331 (196)	331 (196)	w/c 0.45
NaOH	3.29 (1.95)	3.29 (1.95)	Na_2O_{eq} 1.25%

Exposure Conditions: After curing, the prisms were placed in hermetically sealed 6-gallon (23 L) containers with screw-on covers, each container holding three prisms. A salt solution was placed in the bottom of each container to control RH within the container. The containers were then stored in a temperature controlled environment. The containers were periodically moved to an environmental chamber at a set temperature of 21 °C for 24 hours and then length-change of the prisms measured.

Salt Solutions: ACS-grade crystalline salts were used to control RH. The salts held RH between 50 and 100%, at temperatures of 21, 30, and 40 °C. Sodium Bromide (NaBr) was used to control RH between 49.8 and 58.6% RH over the temperature range. Sodium Chloride (NaCl) and Potassium Chloride (KCl) were selected for RH of approximately 75 and 85% over the temperature range, and Potassium Nitrate (KNO_3) for a RH range of 88 to 93%. The highly-reactive aggregate mixture was initially tested with Sodium Nitrite ($NaNO_2$) to evaluate 60% RH. However, the salt was too difficult to work with given its toxicity, and results for the prisms are not available. Sodium Bromide was used in its place for the moderately-reactive prisms. The salt solutions, RH, VP, and temperature used for the highly-reactive prisms are summarized in **Table 5.3-2** and those used for the moderately-reactive prisms are summarized in **Table 5.3-3**. The ambient-VP for the storage conditions were calculated using psychometric equations.

Table 5.3-2. RH (%) and VP (kPa) salt solutions for highly-reactive prisms [25, 26, 27].

Salt	**NaCl**		**KCl**		**KNO_3**		**H_2O**	
Temp (°C)	RH	VP	RH	VP	RH	VP	RH	VP
21.0	75.5	1.88	85.8	2.14	93.1	2.32	100	2.50
30.0	75.6	3.22	84.2	3.56	90.6	3.86	100	4.26
40.0	74.6	5.52	82.4	6.10	88.0	6.51	100	7.40

Table 5.3-3. RH (%) and VP (kPa), salt solutions for moderately-reactive prisms [25, 26, 27].

Salt	**NaBr**		**NaCl**		**KCl**		**H2O**	
Temp (°C)	RH	VP	RH	VP	RH	VP	RH	VP
21.0	58.6	1.46	75.5	1.88	85.8	2.14	100	2.50
30.0	54.6	2.33	75.6	3.22	84.2	3.59	100	4.26
40.0	49.8	3.69	74.6	5.52	82.4	6.10	100	7.40

The salt solutions were prepared following the recommendations of Wexler and Hasegawa [25] and Menzel [15]. Saturated salt solutions were mixed by first boiling 1.0 L of de-ionized water, and then mixing crystalline salt into the water until the solution was supersaturated. After the solution cooled to 21 °C, additional salt was added to produce a slurry consistency which remained saturated. The solution was then added to each container, and the prisms suspended above the solution. When the prisms were removed for measurements, additional salt or water was added to the solution to maintain the slurry consistency. The solubility of each salt is dependent on temperature, and additional salt was required for higher temperature storage conditions.

5.3.2. ASR, W/D, and F/T

Materials: An ASTM C150 Type I/II cement (0.96% Na_2O_{eq}) was used ASR, W/D, and F/T testing. The prisms contained a non-reactive crushed limestone and a moderately-reactive river sand containing chalcedony. The concrete was non-air-entrained to promote the development of F/T distress. The moderately-reactive aggregate used in this study has been found to causes expansion near the ASTM C1293 threshold for deleterious expansion (0.04%) [28]. Concrete

containing this moderately-reactive sand performs well in the field under normal exposure, but deteriorates when exposed to combinations of ASR and F/T [13]. The aggregate was selected to determine if conditions promoting ASR and F/T in the laboratory replicate deterioration observed in the field. Sodium hydroxide (NaOH) was added to the concrete mixing water to achieve a total Na_2O_{eq} content of 8.85 lb/yd^3 (5.25 kg/m^3). The concrete was not air-entrained, and contained approximately 2% entrapped air. The concrete mixture is summarized in **Table 5.3-4**.

Specimens: Fifteen prisms were cast for the ASR, W/D, and F/T exposure. The prisms were 3 x 3 x 11.25 in (75 x 75 x 285 mm), with metal gage studs embedded at each end for measuring length-change. Length-change was periodically measured using a length comparator. The mass-change was also measured to evaluate variations in moisture imparted by the storage conditions. For the ASR, F/T and F/T + ASR specimens, mass-change was measured after the ASR, F/T, or W cycles, and again after the F/T exposure. For the ASR + F/T + W/D prisms, mass-change was measured after the ASR cycle and again after the drying (D) cycle. The prisms were monitored periodically for 300 days.

Curing: The prisms were cured following the same procedure use for the RH testing.

Table 5.3-4. Concrete mixture for prisms subjected to ASR, W/D, and F/T.

Material	**ASR, W/D, F/T** lb/yd^3 (kg/m^3)	**Notes**
Cement	708 (420)	0.96% Na_2O_{eq}
Coarse Agg.	1800 (1068)	Non-reactive limestone
Fine Agg.	1147 (680)	Moderately-reactive sand
Water	319 (189)	w/c 0.45
Air	2%	Non-air-entrained
NaOH	2.65 (1.57)	Na_2O_{eq} 1.25%

Exposure Conditions: After curing, the prisms were exposed to 21 cycles intended to promote ASR and/or F/T related deterioration. The storage conditions are summarized in **Table 5.3-5**. The prisms were stored in hermetically sealed 6-gallon (23 L) containers with screw-on covers, each holding three prisms. The prisms were suspended over water, which was used to maintain a RH greater than 95% within the container.

Table 5.3-5. Storage cycles for ASR, W/D, and F/T (prisms exposed to 21 repeated cycles).

Regimen	ASR (days)	W (days)	D (days)	F/T (days (cycles))
	38 °C, 95% RH	21 °C, 95% RH	21 °C, 50% RH	-15 °C to 10 °C
ASR	13 (LC, MC)*	--	--	--
F/T	--	9 (LC, MC1)	--	4 (12) (MC2)
F/T + ASR	9 (LC, MC1)	--	--	4 (12) (MC2)
ASR + W/D + F/T	7 (LC, MC1)	--	3 (MC2)	3 (9)

*Length-change measurement (LC), first mass-change measurement (MC1), second mass-change measurement after drying (MC2).

The ASR specimens were stored at 95% RH and 38 °C for thirteen days, and then 21 °C for one day before measurements were taken. The F/T specimens were stored at 95% RH (21 °C) for nine days, and then measured and moved to a freeze-thaw chamber for four days. The ASR, F/T, and F/T + ASR prisms absorbed water while stored at 95% RH, but not directly exposed to liquid water. Some drying occurred during F/T as the prisms were not directly exposed to liquid water. The F/T chamber was used to rapidly cycle the concrete between -15 °C and 10 °C, at a rate of 3 cycles per day. The prisms were subjected to F/T cycles at the moisture state produced by the preceding storage at 95% RH. The prisms were not saturated during freezing to better represent the deterioration which occurs in concrete in the field.

The ASR + W/D + F/T prisms were stored in containers at 95% RH (38 °C) for seven days, then dried at 50% RH (21 °C) for three days, measured, and finally subjected to three days of F/T cycles.

5.4. Experimental Results and Discussion

5.4.1. Relative Humidity (RH) and Vapor Pressure (VP)

Relative Humidity (RH): The influences of ambient-RH and temperature on the development of ASR were evaluated by storing specimens at combinations of ambient-RH and temperature, and periodically measuring strain. An expansion of 0.04% within one year for prisms stored at 100% (38 °C) RH constitutes deleterious deterioration per ASTM C1293. Strains exceeding 0.04% may cause cracking for unrestrained concrete. Therefore, a limit of 0.04% strain was selected as the threshold expansion which constituted deleterious expansion in prisms.

The strain results for prisms containing the very highly-reactive aggregate are summarized in **Fig. 5.4-1**. Noting the difference in scale between **Fig. 5.4-1 A**, **B** and **C**, storage temperature has a greater effect on the development of ASR than ambient-RH (or VP). Noting the difference between **Fig. 5.4-1 A** and **C**, humidity affects the development of ASR more at higher temperatures than at lower temperatures. The 167-day expansion for prisms stored at 75.5% RH (21 °C) was less than 0.04% for this highly-reactive aggregate and alkali loading. Based on the RH and strain results, the threshold-RH may occur between 75.5 and 85.8% (21 °C). This corresponds to a threshold-VP between 1.88 and 2.14 kPa.

The samples stored at 75.5% RH (21 °C) (**Fig. 5.4-1 A**) contracted slightly over the first 90 days, and then began to expand. This initial contraction is likely due to drying shrinkage occurring in the concrete as equilibration occurs between the concrete and ambient air. The internal-RH of the concrete had reached equilibrium with the ambient-RH within 120 days (defined as the point where drying shrinkage stops). As the concrete was not immediately in equilibrium with the ambient conditions, water remaining in the cement pore solution after hydration may have led to the formation of expansive alkali-silica gel. As the internal moisture state equilibrated with the

ambient conditions, the lower degree of saturation may have caused a delay in swelling of the alkali-silica gel.

The development of ASR followed by expansion at low ambient-RH and temperature may be explained by the loss of moisture and resulting increase in alkalinity within the pore solution. This hypothesis is based on the nature of cement paste and the physics of water in colloidal gels (C-S-H), however validation requires additional testing over a wider range of fixed internal-VPs. After hydration, the concentration of alkalis remaining in solution increases when water evaporates out of the cement pore solution, leaving cations behind. The siliceous minerals become soluble in the presence of a higher concentration of cations, resulting in the development of alkali-silica gel and absorption of water into the alkali-silica gel from the pore solution. The curvature of the meniscus within the cement pores increases because water is absorbed into alkali-silica gel and water evaporates due to drying. The VP within the cement pores decreases along with RH, and water is transported from the capillary spaces into the cement pores. Once the internal-RH (and VP) within the cement pores is in equilibrium with the ambient conditions, water is no longer transferred from the air to the concrete. If the equilibrium-RH is sufficiently low, the osmotic pressure required for water to be absorbed from the cement pore solution into the alkali-silica gel is greater than the VP in the cement pores, and expansion cannot be sustained.

From **Fig. 5.4-1 B and C**, it appears a threshold-RH does not exist at 30 or 40 °C for the range of ambient-RH's evaluated. Even at 75.6% ambient-RH, the very highly-reactive concrete continues to expand. As noted in the introduction, the internal-RH of concrete increases with temperature, and the equilibrium VP within the concrete is higher at 30 °C than would occur at 21 °C. The result is less osmotic pressure required for moisture to be absorbed into the alkali-

silica gel product, and greater expansion at the same ambient-RH. Another factor which increases the expansion observed at higher temperatures is the solubility of silica [17]. Noting the difference in expansion between **Fig. 5.4-1 B** and **Fig. 5.4-1 C**, the prisms stored at 100% RH (30 °C) expanded 0.33% less than those stored at 100% (40 °C). The very highly-reactive concrete stored at 40 °C expanded between 0.269 and 0.545% within 167-days. The variability between samples stored in the same container increased over time, and was up to 0.10% strain. Testing was stopped after 167 days, and new samples containing a moderately-reactive aggregate were cast.

The strain results for the prisms containing a moderately-reactive aggregate are summarized in **Fig. 5.4-1 D, E, F**. The CPT expansion for the moderately-reactive aggregate was previously tested, and samples stored at 100% RH (38 °C) had one-year expansions ranging from 0.025 to 0.040%, depending on the inert coarse-aggregate used in combination with the reactive sand [28]. The prisms evaluated herein appear to reach equilibrium with the ambient storage conditions within 120 days (when expansion or contraction becomes stable). The strain results for prisms stored at 21 °C are summarized in **Fig. 5.4-1 D**. The prisms stored at 85.5% RH show no dilation or contraction, indicating the prisms had an initial internal-RH close to this value. The prisms stored at 100% RH expanded 0.011% within 80 days and then remained stable until 323 days. After which, the prisms expanded for the remaining 100 days, reaching a final expansion of 0.020%. The prisms stored at 58.6 and 75.5% RH contracted and then became stable once equilibrium occurred between internal and ambient-RH. **Fig. 5.4-1 E** summarizes the strain data for prisms stored at 30 °C, which also reached equilibrium within 120 days and then remained stable until 323 days. After which 0.008% and 0.023% expansion occurred in the prisms stored at 84.2 (3.59 kPa) and 100% RH (4.26 kPa), respectively.

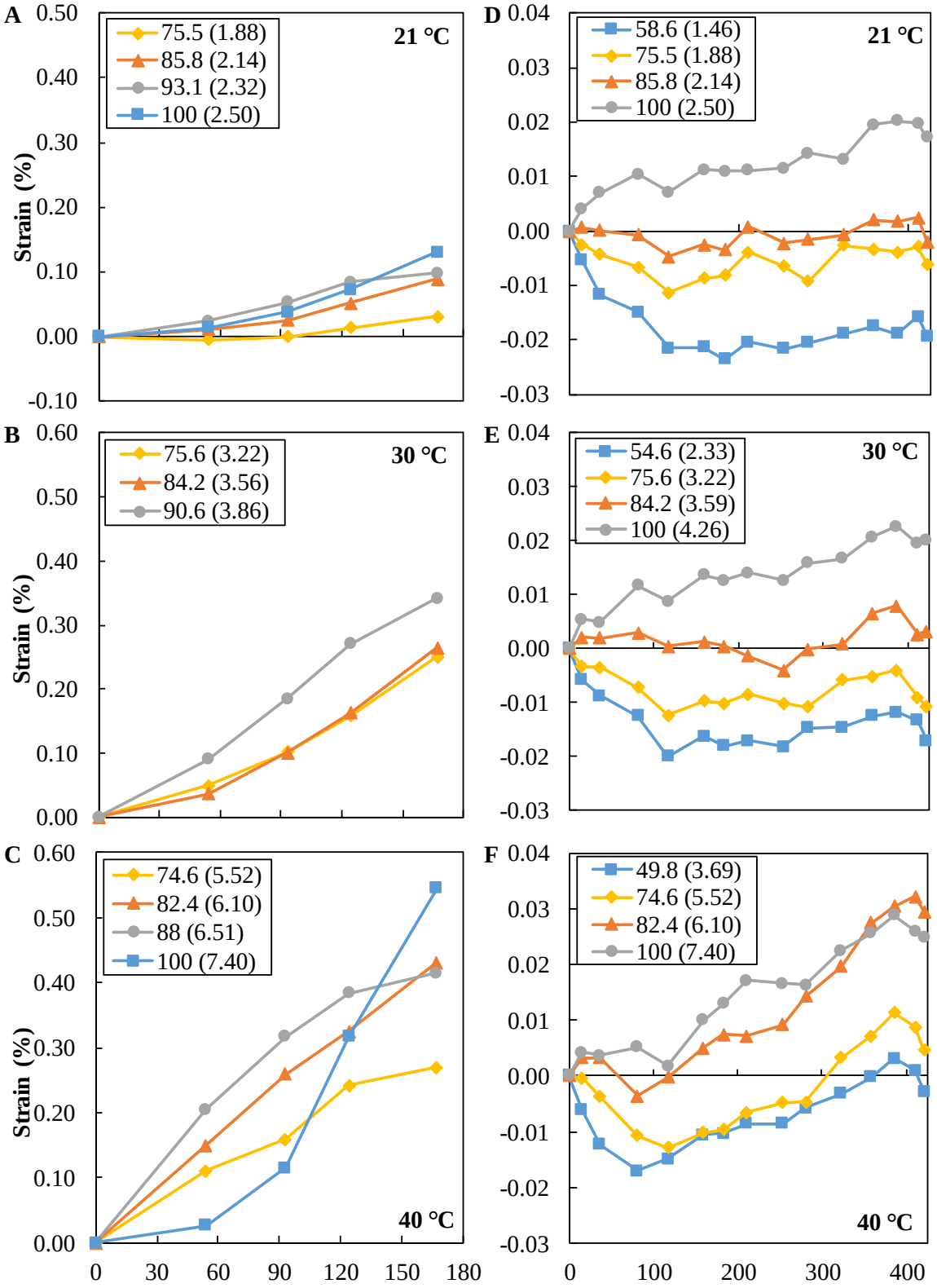

Fig. 5.4-1–Strain (%) with respect to time (days), highly-reactive fine aggregates (A, B, C) and moderately-reactive aggregates (D, E, F).

The strain data for prisms stored at 40 °C are summarized in **Fig. 5.4-1 F**. The ambient-VP was 3.69 kPa for prisms stored at 49.8% RH (40 °C) as compared 3.59 kPa for those stored at 84.2% RH (30 °C). Both sets of prisms exhibited a small net expansion (0.003% and 0.008%, respectively) within the monitoring period.

The prisms exposed to an ambient-VP of 6.10 kPa and higher (82.4 and 100% RH at 40 °C) had a net expansion of 0.032% within the monitoring period. The prisms stored at 74.6% RH (40 °C) expanded less (0.011%) than prisms stored at 100% RH (30 °C) (0.023%) despite having a higher ambient-VP. This indicates that temperature has a greater impact on expansion than the availability of moisture. This is perhaps due to a combination of increasing solubility of siliceous minerals and increasing internal-VP (due to the decreased curvature of the menisci) at higher temperatures. The prisms stored at 82.4 (6.10 kPa) and 100% RH (7.40 kPa) and 40 °C reached a final expansion of 0.032% and 0.029%, respectively within 380 days. The ambient-RH required to cause deleterious expansion, for this aggregate and alkali loading, appears to be greater than 100% RH (40 °C), corresponding to a VP greater than 7.40 kPa.

This moderately-reactive fine aggregate has caused ASR and deleterious expansion in the field and in laboratory concretes, confirmed through petrographic examination [24, 28]. The prisms containing the moderately-reactive aggregate in combination with a non-reactive limestone (at a single alkali loading) did not cause deleterious expansion for any of the storage conditions evaluated herein. This may be due to alkali-leaching as the prisms stored at 30 and 40 °C were moved to a temperature of 21 °C for 24 hours prior to measurements. On cooling the dew-point temperature within the containers was reached causing condensation of moisture on the concrete prisms. This can lead to alkali-leaching, and a decrease in expansion as measured after 380 days in the prisms stored at 40 °C. For the prisms stored at 100% RH, minor fluctuations in

temperature cause condensation on the specimens, causing significant alkali-leaching throughout the monitoring period. This potentially explains the lesser expansion measured in the prisms stored at 100% RH as compared to those stored at 82.4% (**Fig. 5.4-1 F**).

Vapor Pressure (VP): The data were also plotted as strain with respect to VP, as summarized in **Fig. 5.4-2**. The data were plotted for select measurement times over the monitoring period. The data for the prisms containing very highly-reactive sand are summarized in **Fig. 5.4-2 A**. The results indicate the coefficient of determination (R^2) increases with time, along with the slope. As observed from **Fig. 5.4-1 C**, the rate of strain slows after 124 days and the slope of the VP-strain increases less between 124 and 167 days. The best correlation for the very highly-reactive prisms occurred at 167-days, with an R^2 of 0.876. The equation of the trend-line was determined and used to calculate the point where the line intercepts a strain of 0.04%. This occurred at a VP of 1.24 kPa, which corresponds to a RH of 50.0% (21 °C). Given the very-high-reactivity of this concrete mixture, such a threshold seems reasonable.

VP results for prisms containing the moderately-reactive sand are summarized in **Fig. 5.4-2 B**. The coefficient of determination again increases with time until 386 days, after which it begins decreased. Noting the strain with respect to time for this aggregate shown in **Fig. 5.4-1 D, E, F**, the prisms begin to contract after 386 days. This was attributed to alkali leaching from the prisms. The equation relating 386-day strain to VP had an R^2 of 0.627, and was used to calculate a threshold-VP. Based on the 386-day results, this concrete would require a VP of 8.74 kPa to achieve an expansion of 0.04%. This VP corresponds to a RH of 100% (42.5 °C). A lower threshold may be expected for a concrete containing the same aggregate at a higher alkali loading and different coarse aggregate. Prisms containing the same fine aggregate and alkali

loading were tested in combination with a granite coarse aggregate and developed deleterious expansion at a VP of 6.63 kPa (100% RH at 38 °C).

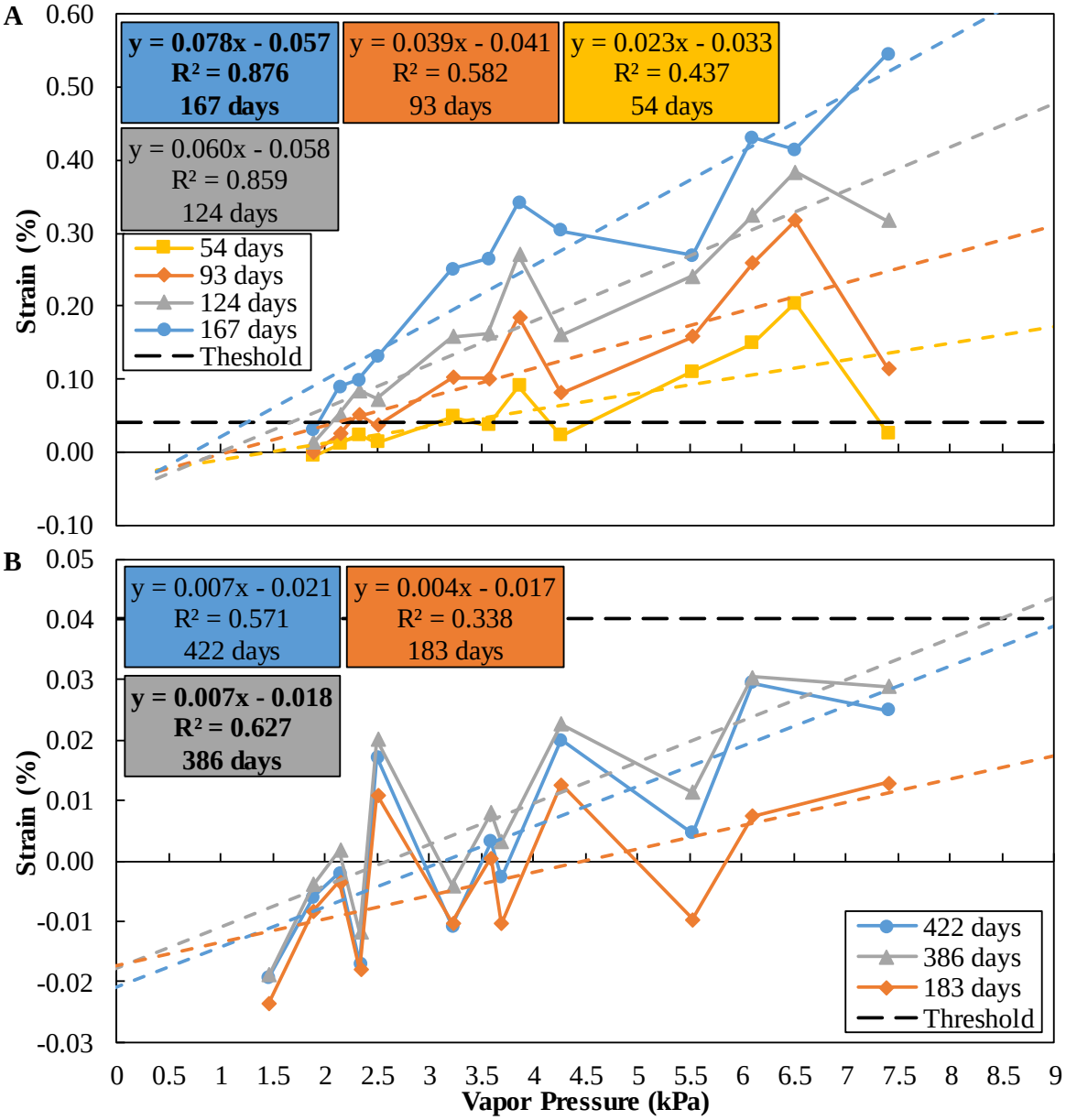

Fig. 5.4-2–Strain (%) with respect to VP (kPa), highly-reactive aggregate (A) and moderately-reactive aggregate (B).

The hypothesized mechanism of expansion (for concrete with a large surface-are-to-volume ratio) occurs due to increasing internal-RH (and VP) in the concrete at higher temperature and increasing pore solution alkalinity as water evaporates. As a result, alkali-silica gel develops in

the presence of the concentrated solution, and water is adsorbed into the alkali-silica gel. The concentration of alkalis decreases over time due to alkali-leaching, until the development of alkali-silica gel ceases. Expansion ceases when the VP of water in the cement pores is lower than the osmotic pressure exerted by the alkali-silica gel. This threshold pressure depends on the osmotic pressure exerted by the alkali-silica gel, which varies with the solubility of silica and the gradient between the concentration of ions in solution and those in the alkali-silica gel. Of note is the threshold-RH (or VP) required for deleterious expansion to occur, which according to testing is highly dependent on the solubility of the reactive siliceous minerals within the aggregate [17]. RH is a function of temperature, therefore VP may be a more intuitive means of quantifying the threshold moisture state required for deleterious expansion in concrete.

5.4.2. ASR, W/D, F/T

The results of strain and mass-change measurements are summarized in **Fig. 5.4-3** and **Fig. 5.4-4**. From **Fig. 5.4-3 A**, the prisms subjected to conditions promoting the development of ASR expanded 0.028% within 250 days, and remained stable, despite variability due to the exposure cycles. In comparison, the prisms exposed to F/T cycles expanded rapidly to 0.013% and then stayed relatively stable, fluctuating due to cyclic exposure conditions. The prisms exposed to F/T + ASR were subjected to 21 exposure cycles, corresponding to a total 175 days of conditions promoting ASR and 160 F/T cycles. The final expansion for the prisms exposed to F/T + ASR was 0.045%. Despite being exposed to less overall days of conditions promoting ASR, the prisms exposed to F/T + ASR exhibited an increasing expansion trend. Bérubé [4] also observed that combinations of ASR and F/T exacerbate deterioration as compared to ASR or F/T alone. Bérubé [4] included specimens with air-entrainment exposed to similar cycles of ASR and F/T and found deterioration to increase as compared to cylinders exposed to ASR or F/T alone. The

highly-reactive coarse aggregate used in Bérubé [4] develops deleterious expansion due to ASR when used in combination with high-alkali cements, which makes the deterioration contribution of F/T less apparent.

The mass change before and after drying are summarized in **Fig. 5.4-3 B**. The prisms exposed to ASR, F/T, and F/T + ASR absorbed ~0.75% moisture by mass within the first 45 days and then varied with cycles throughout the test duration. Some drying occurred during F/T due to the lower humidity within the F/T chamber. The mass-change after F/T is shown for comparison (hollow markers and dotted lines). The mass decreases by 0.23% during F/T and increased back to 0.75% after returning to 95% RH. The F/T prisms were exposed to nine days at 95% RH (21 °C) and four days of F/T. The F/T prisms absorbed less (~0.2%) water than the F/T + ASR prisms exposed to nine days at 95% RH (38 °C) followed by four days of F/T. This difference may be attributed to additional moisture absorbed by the concrete stored at higher temperatures. However, the mass-change of the ASR prisms did not increase appreciably compared to those exposed to F/T + ASR, and the difference in expansion measured for the ASR + F/T samples is likely due to the formation of microcracks and deterioration rather than absorption of water.

Neither the samples exposed to conditions promoting ASR or F/T developed deleterious expansion over the monitoring period. However, the samples exposed to F/T + ASR developed deleterious expansion and exhibited an expansive trend (> 0.04%) within the same period. No available standardized laboratory test method would deem this concrete unfit for use in the field. Field performance has also shown that concrete, containing this moderately-reactive fine aggregate, deteriorated in when exposed to conditions promoting ASR in the summer and F/T in the winter [13].

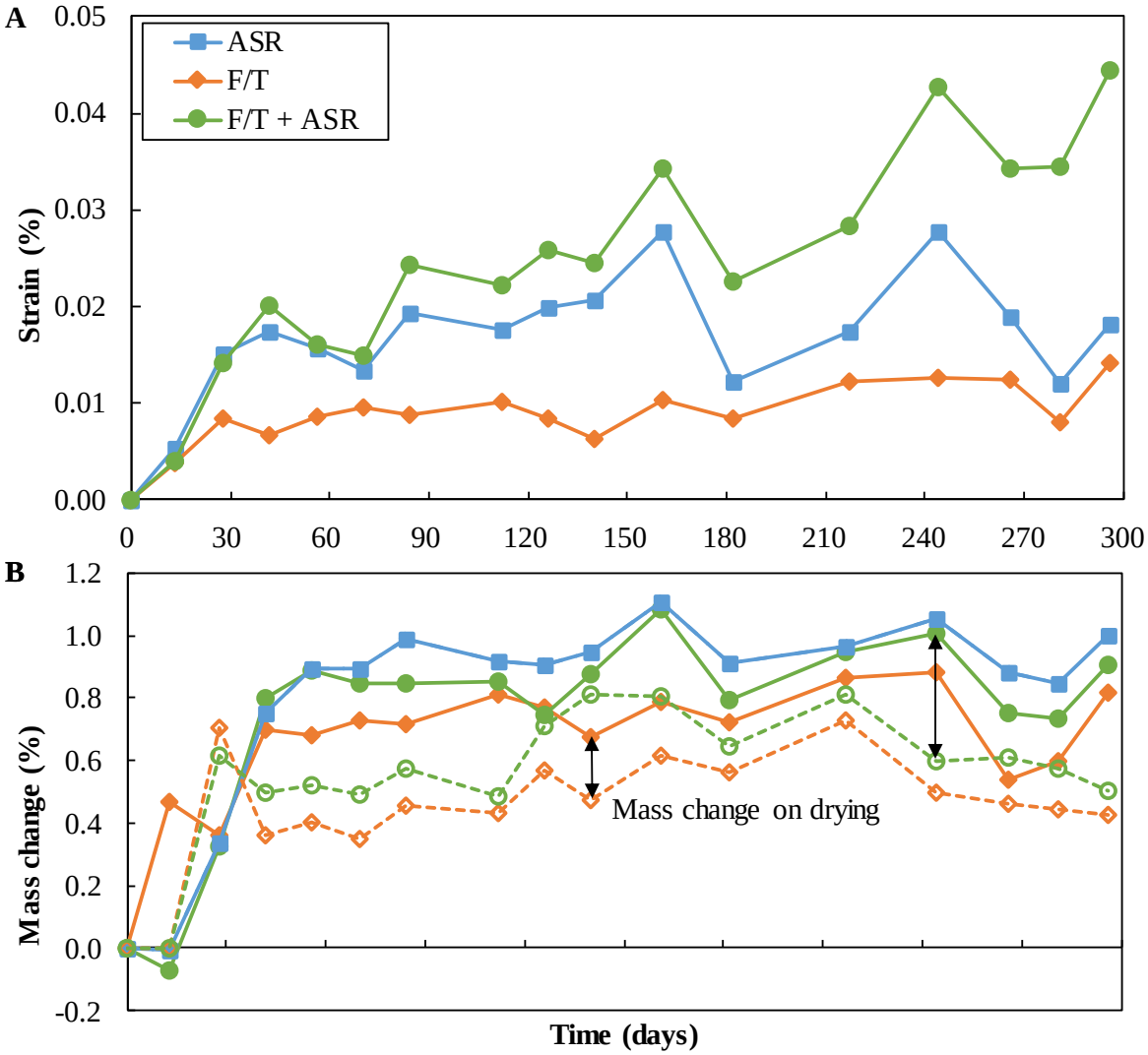

Fig. 5.4-3– Strain (%) (A) and mass change (B) with respect to time (days), concrete prisms exposed to conditions which promote ASR, F/T, or ASR and F/T.

Prisms exposed to a combination of ASR + W/D + F/T exhibited no expansion after 300 days of monitoring. Based on the mass-change results, it appears the mass-change after drying and F/T (**Fig. 5.4-4 B** dotted lines) was sufficient to prevent the development of either ASR or F/T deterioration. The prisms treated with silane (ASR + W/D + F/T (S)) exhibited similar behavior on drying as the prisms without silane treatment. However, on wetting, the untreated prisms absorbed an average 0.28% more water by mass than the silane treated prisms. The untreated prisms expanded similarly to the silane treated prisms (**Fig. 5.4-4 A)**. This expansion was likely due to moisture gain, rather than deterioration. This result shows the ability of silane to limit

absorption of water into concrete and to increase desorption, when the concrete is exposed to water-vapor. Interestingly, the only difference between the ASR + W/D + F/T and F/T + ASR samples **(Fig. 5.4-3)**, is the reduced period in conditions accelerating ASR replaced with 4 days of drying. The additional period of drying was sufficient to reduce the moisture content of the concrete to the point where neither ASR or F/T could occur.

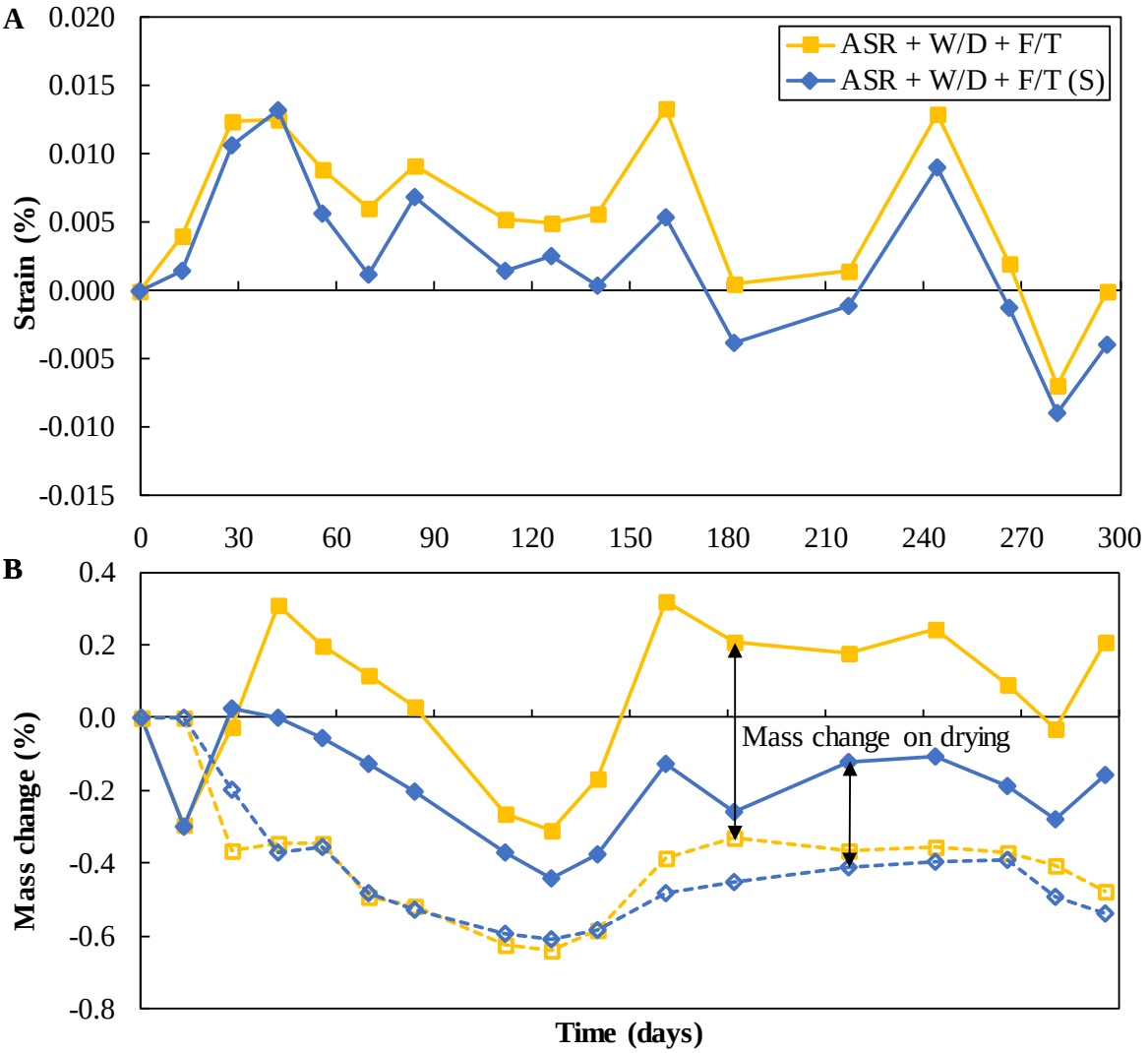

Fig. 5.4-4– Strain (%) (A) and mass change (B) with respect to time (days), concrete prisms exposed to conditions which promote a combination of ASR and F/T.

5.5. CONCLUSIONS AND RECOMMENDATIONS

5.5.1. Relative Humidity (RH) and Vapor Pressure (VP)

- The critical or threshold-RH required for deleterious ASR to occur in concrete at a given alkali loading depends on temperature and the reactive form of silica present within the aggregate. The prisms containing a highly-reactive sand in this study exhibited a threshold-RH less than 80% (21 °C). The prisms stored at combinations of RH and temperature above this value showed deleterious expansion within 167 days.
- Comparing VP may provide a more useful and intuitive tool for developing threshold values for ASR, as it is not referenced to temperature. VP is a function of RH and temperature and thus can be measured using commercial RH probes. Alternatively, it can be calculated from RH and temperature measurements. The threshold-VP will be useful for evaluating mitigation measures in the field, where controlling the internal moisture state of concrete is necessary for slowing ASR and/or F/T related deterioration. VP is a more useful index of concrete moisture state as it can be measured at a range of ambient temperatures, rather than when temperatures are between 21 and 24 °C.
- The development of ASR followed by expansion at low ambient-RH's may be explained by the loss of moisture within the pore solution (for concrete elements with sufficient surface-area-to-volume-ratios). As only water evaporates, the concentration of alkalis remaining in solution increases. When a threshold concentration is reached, siliceous minerals dissolve in the presence of alkalis, resulting in the development of alkali-silica gel and adsorption of water into the alkali-silica gel from the surrounding pore solution. This process may also affect the viscosity of the alkali-silica gel and its expansive properties. The extent of expansion would then be limited by the amount of moisture available in the system, which is

lower at reduced RH (and VP) values. Alkali leaching from the concrete causes the concentration of alkalis to decrease over time. When the concentration decreases below a threshold value, the formation of alkali-silica gel ceases. As water is adsorbed into the alkali-silica gel product, and water continues to evaporate due to drying, the curvature of the meniscus within the cement pores increases. The VP within the cement pores decreases along with RH. Water is drawn from the capillary space into the pore space by the lower VP within the cement pores. This continues until equilibrium occurs between ambient conditions, cement pores, and alkali-silica gel. After equilibration, the osmotic pressure exerted by the alkali-silica gel is lower than the internal-VP and expansion ceases.

5.5.2. ASR, W/D, F/T

- The moderately-reactive aggregates used in this research have been associated with ASR and F/T related expansion in a concrete barrier wall [13, 28]. The aggregate sometimes passes the ASTM C1293 test. However, prisms containing the moderately-reactive aggregate and exposed to conditions promoting a combination of ASR and F/T, expanded more than prisms exposed to conditions promoting ASR or F/T alone. The exposure conditions used in this study better replicate the expansion observed in the field.
- Prisms exposed to cycles of W/D expand less than prisms subjected to conditions promoting ASR and/or F/T. Drying reduces the moisture state of the concrete protecting the concrete from expansive deterioration during conditions which promote ASR or F/T. In addition, prisms treated with silane and exposed to cycles of ASR, W/D, and F/T expanded less and absorbed significantly less water than untreated prisms.
- Concrete containing reactive aggregates and exposed to seasons of warm, humid conditions which promote ASR followed by seasons of daily F/T cycles may deteriorate faster than

concrete exposed to conditions promoting ASR or F/T alone. Air-entrainment alone cannot prevent deterioration in concrete containing reactive aggregates and D-cracking susceptible coarse aggregates. Additional preventative measures may be required to limit the development of alkali-silica gel, and to reduce the moisture state of concrete during F/T.

5.6. ACKNOWLEDGEMENTS

The authors would like to thank the Mack Blackwell Rural Transportation Center (MBTC) and the Arkansas State Highway and Transportation Department (AHTD) for providing financial support for this research program. The authors greatly appreciate the help provided by M. Waidner, and R. Reed in conducting this research.

5.7. REFERENCES

1. Powers, T. C. and Steinour, H. H. (1955). "An interpretation of some published researches on the Alkali-Aggregate Reaction, Part 1-the chemical reactions and mechanism of expansion." *Journal of the American Concrete Institute*, 26(6), 497-516.

2. Chatterji, S. (1989) "Mechanisms of Alkali-Silica Reaction and Expansion." *Proceeding of the 8th International Conference on Alkali-Aggregate Reaction (ICAAR)*, Kyoto, Japan, 101-105.

3. Diamond, S. (1989). "ASR—another look at mechanisms." *Proceedings from 8th international Conference on Alkali-Aggregate Reaction (ICAAR)*, Kyoto, Japan, 83-94.

4. Bérubé, M-A., Chouinard, D., Pigeon, M., Frenette, J., Boisvert, L., and Rivest, M. (2002b). "Effectiveness of sealers in counteracting alkali–silica reaction in plain and air-entrained laboratory concretes exposed to wetting and drying, freezing and thawing, and salt water." *Canadian Journal of Civil Engineering*, 29, 289-300.

5. Nishibayashi, S., Yamura, K., and Sakata, K. (1989). "Evaluation of cracking of concrete due to alkali–aggregate reaction." *Proceedings of the 8th International Conference on Alkali–Aggregate Reaction in Concrete*, Society of Materials Science, Kyoto, Japan, 759–764.

6. Fournier, B., Bérubé, M-A., Folliard, K.J., and Thomas, M.D.A. (2010). "Report on the diagnosis, prognosis, and mitigation of alkali- silica reaction (ASR) in transportation structures (Report No. FHWA-HIF-09-004)." *Federal Highway Administration*, U.S. Department of Transportation, Washington DC, 154 pp.

7. Stark, D. (1990). “The moisture condition of field concrete exhibiting alkali-silica reactivity.” *CANMET/ACI International Workshop on Alkali-Aggregate Reaction in Concrete, Halifax,* Nova Scotia, 19 pp.

8. Powers, T. C. (1945), “A working hypothesis for further studies of frost resistance of concrete.” *Journal of the American Concrete Institute*, 16(4), 245-272.

9. Powers, T. C. and R. A. Helmuth. (1953). “Theory of volume changes in hardened portland-cement paste during freezing.” *Highway Research Board Proceedings*, 32, 285-297.

10. Powers, T. C. (1975). “Freezing effects in concrete.” *American Concrete Institute SP 47-1*, 1-11.

11. Litvan, G. G. (1972). “Phase transitions of adsorbates, IV, mechanism of frost action in hardened cement paste.” *American Ceramic Society Journal*, 55(1), 38-42.

12. Janssen, D. J., and Snyder, M. B. (1994). “Resistance of concrete to freezing and thawing (No. SHRP-C-391).” *National Research Council*. Washington, DC, 217 pp.

13. Deschenes Jr. R., Murray C.D., and Hale W. M. (2017). “Mitigation of ASR and freezing and thawing through surface treatment.” *ACI Materials Journal*, 114(2), 307-314. DOI: 10.14359/51689493.

14. Gause, R. G. and Tucker, Jr. J. (1940). “Method for determining the moisture condition in hardened concrete.” *Journal of Research of the National Bureau of Standards*, 25, October, 14 pp.

15. Menzel, C. A. (1955) “A method for determining the moisture condition of hardened concrete in terms in of relative humidity.” *Proceedings of the American Society for Testing Materials,* 55, 1-26.

16. Rust, C. (2009). “Role of relative humidity in concrete expansion due to alkali-silica reaction and delayed ettringite formation: relative humidity thresholds, measurement methods, and coatings to mitigate expansion.” *M.S. Thesis*, The University of Texas at Austin, Austin, TX, 120 pp.

17. Pedneault, A. (1996). “Development of testing and analytical procedures for the evaluation of the residual potential of reaction, expansion, and deterioration of concrete affected by ASR.” *M.Sc. Memoir,* Laval University, Québec City, Canada, 133 p.

18. Mayer, H. (1998). “The chemistry and properties of silicone resins.” *Pigment & Resin Technology*, 26(6), 364-373.

19. Kobayashi, A., Kirimura, K., Kuboyama, K., and Kojima, T. (1989). "Evaluation of surface treatment effect for preventing excessive expansion due to alkali-silica reaction." *Proceeding of the 8th International Conference on Alkali-Aggregate Reaction (ICAAR*), Kyoto, Japan, 821-826.

20. Bérubé, M.A., Chounard, D., Boisvert, L., Frenetter, J., and Pigeon, M. (1996). "Influence of wetting-drying and freezing-thawing cycles, and effectiveness of sealers on ASR". *Proceedings of the 10th International Conference on Alkali-Aggregate Reaction (ICAAR),* Melbourne, Australia, August 18-23, 1056-1063.

21. Bérubé, M.-A., Chouinard, D., Pigeon, M., Frenette, J., Rivest, M., and Vézina D. (2002a). "Effectiveness of sealers in counteracting alkali–silica reaction in highway median barriers exposed to wetting and drying, freezing and thawing, and deicing salt." *Canadian Journal of Civil Engineering*, 29, 329-337.

22. Folliard, K.J., Thomas, M.D.A., Fournier, B., Resendez, Y., Drimalas, T., and Bentivegna, A. (2012). "Evaluation of mitigation measures applied to ASR-affected concrete elements: preliminary findings from Austin, TX Exposure Site." *Proceeding of the 14th International Conference on Alkali Aggregate Reaction (ICAAR),* Austin, Texas, 10 pp.

23. Thomas, M.D.A., Folliard, K.J., Fournier, B., Drimalas, T., and Rivard, P. (2012). "Study of remedial actions on highway structures affected by ASR*." Proceedings of the 14th International Conference on Alkali-Aggregate Reaction (ICAAR),* Austin, Texas, 10 pp.

24. Thomas, M. D. A., Folliard, K. J., Fournier, B., Rivard, P., and Drimalas, T. (2013). "Methods for evaluating and treating ASR-affected structures: results of field application and demonstration projects (Report No. FHWA-HIF-14-0002)." *Federal Highway Administration*, U.S. Department of Transportation, Washington DC, 80 pp.

25. Wexler, A. and Hasegawa, S. (1954). "Relative humidity-temperature relationships of some saturated salt solutions in the temperature range 0° to 50° C." *Journal of Research of the National Bureau of Standards*, 53(1), 19-26.

26. Rockland, L. B. (1960). "Saturated salt solutions for static control of relative humidity between 5° and 40° C." *Analytical Chemistry*, 32(10), 1375-1376.

27. Greenspan, L. (1977). "Humidity fixed points of binary saturated aqueous solutions." *Journal of Research of the National Bureau of Standards–A. Physics and Chemistry*, 81(1), 89-96.

28. Deschenes, R. Jr., and Hale, W. M. (2016). "Alkali-Silica Reaction in Concrete with Previously Inert Aggregates," *Journal of Performance of Constructed Facilities*, ASCE, p. 04016084. DOI: 10.1061/(ASCE) CF.1943-5509.0000946.

6. CONCLUSIONS AND CONTRIBUTIONS

The primary objective of this research was to develop methods which slow the rate of deterioration within concrete transportation structures deteriorating due to a combination of ASR and F/T. Reducing the moisture state of concrete, measured as RH (or VP), slows deterioration in concrete deteriorating from ASR, F/T or a combination of ASR and F/T. The influence of exposure conditions and moisture on ASR and F/T deterioration in concrete were evaluated to better understand mitigation methods.

6.1. Synthesis of Results

- Premature deterioration was noted in an interstate median barrier and pavement in 2011. A petrographic investigation indicated ASR and F/T deterioration. The fine aggregate appeared to cause ASR deterioration in cases were the cement alkalinity was too high. However, laboratory testing revealed the aggregate was borderline-reactive (0.040% expansion) per the CPT (ASTM C1293) and only potentially deleteriously reactive (0.015% expansion) per the AMBT (ASTM C1260). The level of deterioration observed in the concrete barrier wall ranged from minimal to severe, with the rate of expansion exceeding 0.10%/yr. in some sections of the wall. This rate of expansion could not be explained by ASR alone. Three years of monitoring indicated F/T deterioration was progressing rapidly during winter months. The concrete was not air-entrained, but had performed well historically.
- A laboratory investigation of combined deterioration was therefore necessary to determine the cause of rapid expansion measured in the field. A modified laboratory test method was developed to expose concrete prisms to conditions promoting the development on ASR and F/T deterioration. The concrete contained the same potentially reactive fine aggregate used in the barrier wall and a non-reactive limestone coarse aggregate. The prisms were exposed

to cycles of ASR, F/T, or ASR + F/T. The modified test method results indicate the concrete did not deteriorate on exposure to ASR or F/T alone. However, the concrete prisms exposed to a combination of ASR and F/T exhibited an increasing deterioration trend throughout the exposure period, with a final expansion greater than 0.04%. The results indicate the concrete is not durable on exposure to ASR + F/T. The combined effects of ASR + F/T caused cracking in the concrete and an increased moisture state, which led to exacerbated deterioration on F/T.

- The interstate pavement exhibited minor deterioration due to ASR and F/T, which reduced the service life of the pavement. Silane was investigated as a possible treatment for combined ASR and F/T deterioration in pavement. A three-year study was conducted and strain, internal-RH, and DRI were monitored. The research program was conducted in accordance with the FHWA *Report on the Diagnosis, Prognosis, and Mitigation of Alkali-Silica Reaction (ASR) in Transportation Structures* to assess and mitigate ASR, and to provide recommendations on improvements for future field-evaluation programs.
- The results were inconsistent, but indicate silane slowed the rate of expansion and deterioration in the pavement. The 100% solvent-based silane compound slowed expansion, lowered internal-RH, and decreased DRI. However, the 40% water-based silane products did not consistently reduce the rate of deterioration within the pavement.
- A combination of strain, internal-RH, and DRI monitoring were invaluable in evaluating the efficacy of treatment. Strain provided a quantification of deterioration occurring in the travel and transverse direction. Internal-RH provided an index of the moisture state within the concrete. The DRI method provided an index of deterioration occurring within the cross section of the pavement and a semi-quantitative measure of the efficacy of treatment. The

DRI also provided insight into the mechanism of deterioration and deterioration which occurred prior to the monitoring period. The rate of deterioration within the pavement was slow and a statistically significant decrease in strain, internal-RH, and DRI was not measured in all cases. Only the strain within the 100% silane treated panels was lower by a statistically significant amount.

- Site visits, for both the barrier wall and pavement, were conducted regularly. Therefore, seasonal changes in the rate of deterioration were observed and useful for diagnosis of the mechanisms of deterioration.

6.2. CONCLUSIONS

6.2.1. Paper 1

- Arkansas River sand has a long-proven satisfactory field performance record. However, cases of ASR have been diagnosed when the aggregate is used in combination with higher-alkali cements.
- Field performance records alone may not be sufficient to determine the risk of ASR for concrete containing moderately-reactive aggregates. Limiting cement alkalis to less than 0.6% Na_2O_{eq} will reduce the occurrence of ASR. Many specifying agencies have moved to limiting total alkalis (lb./yd^3 [kg/m^3]). This limit is more appropriate as the total cementitious alkalis depends on the cementitious content of the mixture. Additional mitigation measures such as fly ash may be required as external or internal sources (deicing salts, aggregates) may introduce additional alkalis into the cement pore solution causing ASR.

- Laboratory testing of concrete mixtures should be used in combination with field performance records when determining the potential reactivity of concrete, as variations in cement compositions may lead to ASR in mixtures which performed well historically.
- Much of the concrete barrier wall studied in this research exhibited good F/T resistance despite lack of sufficient air-entrainment. However, sections of the wall with ASR-related cracking experienced rapid F/T deterioration due to increased permeability. As ASR progressed and cracks formed along the surface, moisture entered the concrete, which increased the saturation state of the concrete leading to exacerbated F/T deterioration.

6.2.2. Paper 2

- Silane-treated wall sections exhibited lower expansion as compared to untreated control sections. Silane treated sections exhibited a measurable decrease in internal-RH for sections of minimal damage. It was recommended that the barrier wall be treated with silane to prevent most of the concrete, which had minimal damage, from cracking leading to F/T deterioration.
- As observed in the sections of moderate and severe deterioration, expansion occurred primarily due to F/T. This was not observed in sections of minimal deterioration as cracking had not occurred along the exposed surface. It was hypothesized that as ASR deterioration progresses, void spaces are occupied by alkali-silica gel, which reduces space for moisture during freezing and entraps water, thereby exacerbating F/T deterioration.
- The results of treatment and monitoring indicate silane treatment reduced F/T-related deterioration for sections of moderate and severe damage. The silane treatment provided a breathable barrier which reduced internal-RH of the concrete. The moisture state decreases over time until reaching equilibrium with average ambient-conditions, which are below the

threshold state required for F/T deterioration to occur. The F/T performance for the non-air-entrained concrete improved relative to the untreated control sections. This hypothesis needs to be confirmed through laboratory evaluation, but the results suggest silane may be an effective treatment for slowing F/T-related deterioration in concrete elements.

6.2.3. Paper 3

- The 100% silane treatment resulted in a statistically significant reduction in strain and measurable reduction in internal-RH in concrete pavement panels over a three-year monitoring period. The alkyltrialkoxysilane (Silane 100) was most effective in limiting strain in the concrete pavement, while the 40% alkylalkoxysilane water-based Silane 40A and Silane 40B products proved inconsistent. As observed by Wehrle [11], solvent-based silane products are more effective when higher permeable concrete allows greater penetration of the silane.
- Three-years of strain and internal-RH monitoring was not sufficient to definitively confirm the efficacy of silane treatments in slowing the rate of ASR and F/T deterioration in concrete pavement.
- Internal-RH is difficult to measure in the field, and an improved method is required to assess the actual internal-RH of concrete in the field. Internal-RH measurements in the field are dependent on ambient conditions and the stability of the concrete temperature during measurements. The method employed in this research program proved more accurate when fresh holes were drilled at each visit, and the probes were epoxied in place. Based on laboratory testing, leaving the probes in the holes for more than four hours did not provide an increase in accuracy.

- The DRI method requires experience and judgement, and remains subject to operator bias. The method provides a small cross-sectional analysis of the concrete, which is very useful for diagnostic purposes. Strain monitoring only provides a measure of expansion occurring along the surface of the pavement. The DRI method provides a measure of deterioration occurring within the concrete, including expansion occurring out-of-plane.
- The DRI method is an effective semi-quantitative measure of concrete deterioration. The DRI numbers measured in this study were low, indicating minimal to moderate deterioration within the pavement. As a result, the difference in DRI between the control and treated specimens is relatively small and the results are not statistically significant.
- DRI results indicate silane treatments slow further F/T deterioration in the treated sections relative to the untreated control sections. The treated sections underwent a minimal increase in closed cracks in the aggregate particles (CCA) and opened cracks in the aggregate particles (OCA) as compared to the control samples from 2013. This indicates treatment slowed F/T deterioration as compared to the untreated control pavement.
- Based on the findings of this research, an 18-mile (29 km) section of the Interstate 49 pavement was diamond ground and treated with a 100% solvent-free, isobutylalkoxysilane (similar to the Silane 100 used in this research) in October 2016. The site will be periodically monitored to evaluate the efficacy of the applied silane treatment

6.2.4. Paper 4

- The critical or threshold-RH required for ASR to occur in concrete depends on temperature and the reactive aggregate type within the concrete. Prisms containing a highly-reactive sand exhibited a threshold ambient-RH lower than 80% (21 °C). The prisms stored at

combinations of RH and temperature above this value showed deleterious expansion within 167 days.

- Comparing VP may provide a more useful and intuitive tool for developing threshold values for ASR, as it is not referenced to temperature. VP is a function of RH and temperature and thus can be measured using commercial RH probes. Alternatively, it can be calculated from RH and temperature. The threshold-VP will be useful for evaluating mitigation measures in the field, where controlling the internal moisture state of concrete is necessary for slowing ASR and/or F/T related deterioration. VP is a more useful index of concrete moisture state as it can be measured at a range of ambient temperatures, rather than when temperatures are between 21 and 24 °C.
- When concrete elements with sufficient surface-area-to-volume ratios dry towards equilibrium with ambient conditions, water evaporates and the concentration of alkalis within the cement pore solution increases. When a threshold concentration is reached, siliceous minerals become soluble, resulting in the development of alkali-silica gel. The pore solution alkalinity decreases, due to alkali leaching, until the concentration falls below a threshold and the formation of alkali-silica gel ceases. As water continues to evaporate, the curvature of the meniscus within the cement pores increases. VP within the cement pores decreases along with RH and water is transported from the capillary space into the pore space by the VP gradient. This process continues until equilibrium occurs between the ambient conditions, cement pores, and alkali-silica gel. After equilibrium occurs, the osmotic pressure exerted by the alkali-silica gel is no longer sufficient to draw water into the gel, and expansion ceases.
- The moderately-reactive aggregates used in this research have been associated with ASR and F/T related expansion in a concrete barrier wall. The aggregate sometimes passes the ASTM

C1293 test. However, prisms containing the moderately-reactive aggregate and exposed to conditions promoting a combination of ASR and F/T, expanded more than prisms exposed to conditions promoting ASR or F/T alone. The exposure conditions used in this study were observed to better replicate expansion measured in the field.

- Prisms exposed to cycles of W/D expand less than prisms subjected to conditions promoting ASR and/or F/T. Drying reduces the moisture state of the concrete protecting the concrete from expansive deterioration during conditions which promote ASR or F/T. Prisms treated with silane and exposed to cycles of ASR, W/D, and F/T expanded less and absorbed significantly less water than untreated prisms.

6.3. CONTRIBUTIONS

- Mitigating ASR through surface treatment with silane reduces the moisture state of concrete over time, thereby limiting expansion due to ASR. The rate of deterioration in this study ranged from 0.01 and 0.12%/yr. for the minimally to severely deteriorated barrier wall sections evaluated. Additionally, several surface treatment methods were evaluated in addition to silane, to determine the most economical and practical treatment.
- Silane was applied to a concrete pavement and strain, internal-RH, and DRI monitored for three-years. This is the longest running field-evaluation of silane applied to concrete pavement. The results were inconsistent, but indicate silane may slow expansion and deterioration in concrete pavement relative to untreated controls.
- Previous studies of the relationship between RH and ASR have considered various RH fixing points at a single temperature. This research evaluated the effect of ambient-RH, temperature, and time on the progression of ASR in concrete containing two different reactive aggregates.

- The relationship between ASR and ambient-VP was also evaluated. VP combines RH and temperature into a single variable, which is more readily compared to strain and time. The results were used to determine threshold-VP levels for the two concrete mixtures considered in this study. The threshold-VP depends on the solubility and reactivity of the aggregate at the alkali-loading considered. Threshold-VP values can be determined for concrete mixtures through laboratory evaluation. The threshold-VP can then be used to evaluate mitigation measured applied to concrete elements in the field. The advantage of measuring VP rather than RH, is that the temperature of the concrete at the time of measurements does not have to be at a specific temperature. However, the concrete temperature must still be stable during measurements.
- Prisms exposed to combinations of ASR and F/T confirm F/T exacerbates deterioration in concrete containing reactive aggregates. Existing standardized test methods indicate concrete containing this aggregate to be potentially deleteriously reactive. However, these test methods did not indicate the severe level of deterioration observed in concrete barrier walls. The modified test method developed in this research better reproduced the combination of ASR and F/T deterioration observed in the field.
- This new test method is a starting point for developing methods for evaluating the effects of combined exposure conditions on the deteriorating of concrete structures.
- Results indicate the moisture state of concrete is critical to the development of both ASR and F/T related deterioration, and controlling the moisture state of concrete is a viable option for slowing ASR and F/T deterioration in concrete.

7. REFERENCES

ACI Committee 221, (1998). "Report on Alkali-Aggregate Reactivity (ACI 221.1R-98)," *American Concrete Institute*, Farmington Hills, MI, 31 pp.

ACI Committee 228. (2013). "Report on Nondestructive Test Methods for Evaluation of Concrete in Structures (Report No. ACI 228.2R-13)." *American Concrete Institute*, Farmington Hills, MI, 86 pp.

ASTM C1260-05. (2008a). "Standard test method for potential alkali reactivity of aggregates (mortar-bar method)." Annual Book of ASTM Standards 04.02, *American Society for Testing and Materials (ASTM)*, West Conshohocken, Pennsylvania, 676-680.

ASTM C1567-04. (2008a). "Standard test method for determining the potential alkali-silica reactivity of combinations of cementitious materials and aggregate (accelerated mortar-bar method)." Annual Book of ASTM Standards 04.02, *American Society for Testing and Materials (ASTM)*, West Conshohocken, PA, 772–775.

ASTM C1293-08b. (2012). "Standard test method for determination of length change of concrete due to alkali-silica reaction." Annual Book of ASTM Standards 04.02, *American Society for Testing and Materials (ASTM)*, West Conshohocken, Pennsylvania, 687-686.

ASTM C1778-14. (2016). "Standard Guide for Reducing the Risk of Deleterious Alkali-Aggregate Reaction in Concrete." West Conshohocken, PA: ASTM International, 11 pp. doi: https://doi.org/10.1520/C1778-16.

Bérubé, M. A., Chounard, D., Boisvert, L., Frenetter, J., and Pigeon, M. (1996). "Influence of wetting-drying and freezing-thawing cycles, and effectiveness of sealers on ASR." *Proceedings of the 10th Intonational Conference on Alkali-Aggregate Reaction (ICAAR)*, ARRB Group, Australia, 1056–1063.

Bérubé, M.-A., Chouinard, D., Pigeon, M., Frenette, J., Boisvert, L., and Rivest, M. (2002). "Effectiveness of sealers in counteracting alkali silica reaction in plain and air-entrained laboratory concretes exposed to wetting and drying, freezing and thawing, and salt water." *Canadian Journal of Civil Engineering*, 29(2), 289–300.

Bérubé, M.-A., Chouinard, D., Pigeon, M., Frenette, J., Rivest, M., and Vézina, D. (2002). "Effectiveness of sealers in counteracting alkali silica reaction in highway barrier walls exposed to wetting and drying, freezing and thawing, and deicing salt." *Canadian Journal of Civil Engineering*, 29(2), 329–337.

Bérubé, M.A., Frenette, J., Pedneault, A., Rivest, M. (2002). "Laboratory Assessment of the Potential Rate of ASR Expansion of Field Concrete." *Cement, Concrete and Aggregates*, 24(1), 13-19.

Bérubé, M.A., Frenette, J., Rivest, M. and Vézina, D. (2002). "Measurement of the Alkali Content of Concrete Using Hot Water Extraction." *Cement, Concrete, and Aggregates*, 24(1), 28-36.

Bérubé, M.A., Fournier, B. (2004). "Alkalis releasable by aggregates in concrete – significance and test methods. (invited Keynote paper)." *Proceedings of the 12th International conference on Alkali-Aggregate Reaction (AAR) in Concrete (ICAAR)*, Beijing (China), Tang and Deng Editors, International Academic Publishers, Beijing World Publishing Corp., 1, 17-30.

Bleszynski, R. F., and Thomas, M. D. A. (1998). "Microstructural Studies of alkali-silica reaction in fly ash concrete immersed in alkaline solution." *Advanced Cement Based Materials*, 7, 66-78.

Chatterji, S. (1989) "Mechanisms of Alkali-Silica Reaction and Expansion." *Proceeding of the 8th International Conference on Alkali-Aggregate Reaction (ICAAR)*, Kyoto, Japan, 101-105.

Diamond, S. (1989). "ASR—Another look at mechanisms." *Proceeding of the 8th International Conference on Alkali-Aggregate Reaction (ICAAR)*, Kyoto, Japan, 83–94.

Crisp, T. M., Waldron. P., Wood. J. G. M. (1989) "Development of a non-destructive test to quantity damage in deteriorated concrete". *Magazine of Concrete Research*, 45, 165 pp.

CTL Group (Construction Technology Laboratories Group). (2012). "Petrographic examination of concrete specimens from I-540 roadway and barrier wall." CTL Group Project No. 157501, Skokie, IL.

Deschenes, R.A. (2014). "Mitigation of Alkali-Silica Reaction (ASR) in an Interstate Median Barrier." *Master's Thesis*, University of Arkansas, Fayetteville Arkansas, 108 pp.

Deschenes, R. Jr., and Hale, W. M. (2016). "Alkali-Silica Reaction in Concrete with Previously Inert Aggregates," *Journal of Performance of Constructed Facilities*, ASCE, p. 04016084. DOI: 10.1061/(ASCE) CF.1943-5509.0000946.

Deschenes Jr. R., Murray C.D., and Hale W. M. (2017). "Mitigation of ASR and freezing and thawing through surface treatment." *ACI Materials Journal*, 114(2), 307-314. DOI: 10.14359/51689493.

Diamond, S. (1989). "ASR—Another look at mechanisms." Proc., 8th Int. Conf. on Alkali-Aggregate Reaction (ICAAR), Elsevier, Essex, England, 83–94.

Drimalas, T.; Folliard, K. J.; Thomas, M. D. A.; Fournier, B.; and Bentivegna, A., "Study of the Effectiveness of Lithium and Silane Treatments on Field Structures Affected by ASR,"

Proceedings of the 14th International Conference on Alkali-Aggregate Reaction (ICAAR), Austin, TX, 2012, 10 pp.

Duchesne, J. and Bérubé, M. A. (1994). "The effectiveness of supplementary cementing materials in suppressing expansion due to ASR: Another look at the reaction mechanisms Part 2: pore solution chemistry." *Cement and Concrete Research*, 24(2), 221-230.

Dunbar, P.A.; Grattan-Bellew, P.E. (1995). "Results of damage rating evaluation of condition of concrete from a number of structures affected by ASR". *CANMET/ACI International Workshop on Alkali-Aggregate Reactions in Concrete*, Dartmouth, Canada.

FHWA (Federal Highway Administration). (2011). "Coefficient of thermal expansion in concrete pavement design." Rep. No. FHWA-HIF-09-015, U.S. Dept. of Transportation, Washington, DC.

Folliard, K. J., Thomas, M. D. A., Fournier, B., Resendez, Y., Drimalas, T., and Bentivegna, A. (2012). "Evaluation of Mitigation Measures Applied to ASR-Affected Concrete Elements: Preliminary Findings from Austin, TX Exposure Site," *Proceeding of the 14th International Conference on Alkali Aggregate Reaction (ICAAR),* Austin, TX, 10 pp.

Fournier, B., and Bérubé, M. A. (2000). "Alkali-aggregate reaction in concrete: A review of basic concepts and engineering implications." Can. J. Civ. Eng., 27(2), 167–191.

Fournier, B., Bérubé, M.A., Thomas, M.D.A., Smaoui, N. & Folliard, K.J. (2004). Evaluation and Management of Concrete Structures Affected by Alkali-Silica Reaction - A Review (MTL 2004-11)." *Natural Resources*, Canada. Ottawa, 59 pp.

Fournier, B., Bérubé, M-A., Folliard, K.J., & Thomas, M.D.A. (2010). "Report on the Diagnosis, Prognosis, and Mitigation of Alkali- Silica Reaction (ASR) in Transportation Structures (Report No. FHWA-HIF-09-004)." *Federal Highway Administration*, U.S. Department of Transportation, Washington DC, 154 pp.

Gause, R. G. and Tucker, Jr. J. (1940). "Method for determining the moisture condition in hardened concrete." *Journal of Research of the National Bureau of Standards*, 25, October, 14 pp.

Giannini, R. (2012). "Evaluation of Concrete Structures Affected by Alkali-Silica Reaction and Delayed Ettringite Formation." *Doctoral Dissertation*, University of Texas, Austin Texas, 328 pp.

Grattan-Bellew, P.E., and Mitchell, L.D. (2006). "Quantitative petrographic analysis of concrete –The Damage Rating Index (DRI) method, a review". *Proceedings of the Marc-André Bérubé*

symposium on AAR in concrete, CANMET/ACI Advances in concrete technology seminar, Montréal, Canada, 321-334.

Greenspan, L. (1977). "Humidity fixed points of binary saturated aqueous solutions." *Journal of Research of the National Bureau of Standards–A. Physics and Chemistry*, 81(1), 89-96.

Helmuth, R., Stark, D., Diamond, S., and Moranville-Regourd, M. (1993). "Alkali-silica reactivity: and overview of research (SHRP-C-342)." *Strategic Highway Research Program*, National Research Council, Washington, DC. 108 pp.

Ideker, J. H., Bentivegna, A. F., Folliard, K. J., and Juenger, M. C. G. (2012). "Do current laboratory test methods accurately predict alkali silica reactivity?" ACI Mater. J., 109(4), 395–402.

Institution of Structural Engineers (ISE). (1992). "Structural Effects of Alkali-Silica Reaction - Technical Guidance Appraisal of Existing Structures." *Institution of Structural Engineers*, 11 Upper Belgrave Street, London, 45 pp.

Janssen, D. J., and Snyder, M. B. (1994). "Resistance of concrete to freezing and thawing (No. SHRP-C-391)." *National Research Council*. Washington, DC. 217 pp.

Jensen, V. (2008). "Measurement of cracks, relative humidity and effects of surface treatment on concrete structures damaged by Alkali Silica Reaction." *Proceedings of the 13th Intonational Conference on Alkali-Aggregate Reaction (ICAAR)*, Trondheim, Norway.

Kobayashi, A., Kirimura, K., Kuboyama, K., and Kojima, T. (1989). "Evaluation of surface treatment effect for preventing excessive expansion due to alkali-silica reaction." *Proceeding of the 8th International Conference on Alkali-Aggregate Reaction (ICAAR)*, Kyoto, Japan, 821-826.

Laboratoire Central des Ponts et Chaussées (LCPC). (1997). "Détermination de l'indice de fissuration d'un parement de béton Méthode no. 47" *Ministère de l'équipement*, des transports et du logement, Paris.

Litvan, G. G. (1972). "Phase transitions of adsorbates, IV, mechanism of frost action in hardened cement paste." *American Ceramic Society Journal*, 55(1),. 38-42.

Mayer, H. (1998). "The chemistry and properties of silicone resins." *Pigment & Resin Technology*, 26(6) 364-373.

Menzel, C. A. (1955) "A method for determining the moisture condition of hardened concrete in terms in of *relative* humidity." *Proceedings of the American Society for Testing Materials*, 55, 1-26.

Moradi-Marani, F., Kodjo, S. A., Rivard, P., and Lamarche C-P. (2014). “Nonlinear Acoustic Technique of Time Shift for Evaluation of Alkali-Silica Reaction Damage in Concrete Structures.” *ACI Materials Journal*, 111(5), 581-591.

Multon, S. Barin, F.-X., Godart, B., Toutlemonde, F. (2008). “Estimation of the Residual Expansion of Concrete Affected by Alkali Silica Reaction).” *Journal of Materials in Civil Engineering*, ASCE, 20(1), 54-62.

Nilsson, L.-O. (1980). “Hygroscopic moisture in concrete—drying, measurements & related material properties,” *Division of Building Materials*, Lund University, Lund, Sweden, 162 pp.

Powers, T.C. (1945). “A working hypothesis for further studies of frost resistance of concrete.” *ACI Journal Proceedings*, 41(1), 245-272.

Powers, T. C. and Brownyard, T. L. (1947). “Studies of the Physical Properties of Hardened Cement Paste, Part 8.” *Journal of the American Concrete Institute*, 18(8), pp. 933-969.

Powers, T. C. and R. A. Helmuth. (1953). “Theory of volume changes in hardened portland-cement paste during freezing.” *Highway Research Board Proceedings*, 32, 285-297.

Powers, T. C., and Steinour, H. H. (1955). “An interpretation of some published researches on the alkali-*aggregate* reaction. Part 1: The chemical reactions and mechanism of expansion.” J. *American Concrete Institute*, 51(2), 497–516.

Powers, T. C. (1975). “Freezing effects in concrete.” *American Concrete Institute Special Publication*, 47(1), 1-12.

Plusquellec, G., Geiker, M.R., Lindgård, J., Duchesne, J., Fournier, B., DeWeerdt, K. (2017). “Determination of the pH and the free alkali metal content in the pore solution of concrete: Review and experimental comparison.” *Cement and Concrete Research*, 96, 13-26.

Prezzi, M., Monteiro, P. J. M., and Sposito, G. (1997). “The alkali-silica reaction, part I: use of double layer theory to explain the behavior of reaction product gels.” *ACI Materials Journal*, 94(1), 10-16.

Quincot, G., Azenha, M., Barros, J., and Faria. R. (2011) “State of the art – methods to measure moisture in concrete.” *Projetos De Investigação Científica E Desenvolvimento Tecnológico*, Portugal, 40 pp.

Rajabipour, F., Giannini, E., Dunant, C., Ideker, J. H., and Thomas, M. D. A. (2015). “Alkali-silica reaction: current understanding of the reaction mechanisms and the knowledge gaps.” *Cement and Concrete Research*, 76, 130-146.

Rivard, P., Founrier, B., Ballivy, G. (2002). “The Damage Rating Index Method for ASR Affected Concrete—A Critical Review of Petrographic Features of Deterioration and Evaluation Criteria.” *Cement, Concrete, and Aggregates*, 24(2), 1-11.

Rockland, L. B. (1960). “Saturated salt solutions for static control of relative humidity between 5° and 40° C.” *Analytical Chemistry*, 32(10), 1375-1376.

Rodrigues, F.A., Monteiro, P. J., and Sposito, G. (1999). “The alkali-silica reaction: the surface charge density of silica and its effect on expansive pressure.” *Cement and Concrete Research*, 29(4), 527-530.

Rust, C. (2009). “Role of Relative Humidity in Concrete Expansion due to Alkali-Silica Reaction and Delayed Ettringite Formation: Relative Humidity Thresholds, Measurement Methods, and Coatings to Mitigate Expansion,” *Master’s Thesis*, University of Texas at Austin, Austin, TX, 120 pp.

Sanchez, L.F.M., Fournier, B., Jolin, M., and Bastien, J. (2014). “Evaluation of the Stiffness Damage Test (SDT) as a tool for assessing damage in concrete due to ASR: test loading and output responses for concretes incorporating fine or coarse reactive aggregates.” *Cement and Concrete Research*, 56, 213-229.

Sanchez, L. (2014). “Contribution to the Assessment of Damage in Aging Concrete Infrastructures Affected by Alkali-Aggregate Reaction.” *Doctoral Thesis*, Université Laval, Quebec, Canada, 401 pp.

Sanchez, L. F. M., Fournier, B., Jolin, M., and Bastien, J. (2015). “Evaluation of the Stiffness Damage Test (SDT) as a tool for assessing damage in concrete due to alkali-silica reaction (ASR): input parameters and variability of the test responses.” *Construction and Building Materials*, 77, 20-32.

Sanchez, L. F. M., Fournier, B., Jolin, M., Duchesne, J. (2015). “Reliable quantification of AAR damage through assessment of the Damage Rating Index (DRI).” *Cement and Concrete Research*, 67, 74-92.

Sanchez, L. F. M., Fournier, B., Jolin, M., Bedoya, M. A. B., Bastien, J., & Duchesne, J. (2016). “Use of damage rating index to quantify alkali-silica reaction damage in concrete: fine versus coarse aggregate.” *ACI Materials Journal*, 113(4), 395-407.

Sanchez, L.F.M., Fournier, B., Jolin, M., Bastien, J., Mitchell, D. (2016b). “Practical use of the Stiffness Damage Test (SDT) for assessing damage in concrete infrastructure affected by alkali-silica reaction.” Construction and Building Materials, 125, 1178-1188.

Sanchez, L.F.M., Fournier, B., Jolin, M., Mitchell, D., Bastien, J. (2017). “Overall assessment of Alkali-Aggregate Reaction (AAR) in concretes presenting different strengths and incorporating a wide range of reactive aggregate types and natures.” Cement and Concrete Research, 93, 17-31.

Shehata, M. H., Thomas, M. D. A., and Bleszynski, R. F. (1999). “The effect of fly ash composition on the chemistry of pore solution in hydrated cement pastes.” *Cement and Concrete Research,* 29, 1915-1920.

Shehata, M. H., and Thomas, M. D. A. (2000). “The effect of fly ash composition on the expansion of concrete due to alkali-silica reaction.” Cem. Concr. Res., 30(7), 1063–1072.

Shrimer, F. (2000). “Application and use of damage rating index in assessment of AAR-affected concrete-selected case studies.” *Proceeding of the 11th International Conference on Alkali Aggregate Reaction (ICAAR),* Quebec, Canada, 899-907.

Smaoui, N., Bérubé, M. A., Fournier, B., Bissonnette, B., & Durand, B. (2004). “Evaluation of the expansion attained to date by concrete affected by alkali-silica reaction. Part 1: Experimental study.” *Canadian Journal of Civil Engineering*, 31(5), 826-845.

Stanton, T. E. (1940). “Expansion of concrete through reaction between cement and aggregate.” *Proceedings of the American Society of Civil Engineering*, 66(10), 1781–1811.

Stark, D. (1990). “The moisture condition of field concrete exhibiting alkali-silica reactivity.” *CANMET/ACI International Workshop on Alkali-Aggregate Reaction in Concrete,* Halifax, Nova Scotia, 19 pp.

Stark, D. (1991). “Handbook for the identification of alkali-silica reactivity in highway structures (SHRP-C/FR-91-101).” *Strategic Highway Research Program*, National Research Council, Washington, DC. 50 pp.

Stark, D. C., Morgan, B., Okamoto, P., & Diamond, S. (1993). Eliminating or minimizing alkali-silica reactivity (Report No. SHRP-C-343). *Strategic Highway Research Program (SHRP),* National Research Council, Washington, DC, 266 pp.

Tanesi, J., & Meininger, R. (2006). “Freeze-thaw resistance of concrete with marginal air content.” *Federal Highway Administration* Report No. HRT-06-117, 1-96.

Thomas, M. D. A. (1995). “The role of fly ash and slag alkalis in alkali silica reactions in concrete.” *CABNET/ACI Int. Workshop on Alkali-Aggregate Reactions in Concrete*, Natural Resources Canada, Canada, 181–204.

Thomas, M. D. A., Shehata, M. H., and Shashiprakash, S. G. (1999). “The use of fly ash in concrete: Classification by composition.” *Cement, Concrete, and Aggregates,* 21(2), 105–110.

Thomas, M.D.A., Fournier, B., Folliard, K.J., Resendez, Y.A. (2011). "Alkali-Silica Reactivity Field Identification Handbook (FHWA-HIF-12-022)." *Federal Highway Administration*, U.S. Department of Transportation, Washington DC, 80 pp.

Thomas, M. D. A., Folliard, K. J., Fournier, B., Drimalas, T., and Rivard, P. (2012). "Study of Remedial Actions on Highway Structures Affected by ASR," *Proceedings of the 14th International Conference on Alkali-Aggregate Reaction (ICAAR),* Austin, TX, 10 pp.

Thomas, M.D.A., Folliard, K.J., Fournier, B., Rivard, P., Drimalas, T. (2013a). "Methods for evaluating and treating ASR-affected structures: results of field application and demonstration projects. Volume I: Summary of findings and recommendations (Report FHWA-HIF-14-002)." *Federal Highway Administration (FHWA),* U.S. Dept of Transportation, 70 pp.

Thomas, M.D.A., Folliard, K.J., Fournier, B., Rivard, P., Drimalas, T. (2013b). "Methods for evaluating and treating ASR-affected structures: results of field application and demonstration projects. Volume II: Details of field applications and analysis (Report FHWA-HIF-14-003)." *Federal Highway Administration (FHWA),* U.S. Dept of Transportation, 342 pp.

Touma, W. E., Fowler, D. W., and Carrasquillo, R. L. (2001). "Alkali-silica reaction in portland cement concrete: Testing procedures and mitigation methods (Research Rep. ICAR 301-1F)." *International Center for Aggregates Research*, Austin, TX. 556 pp.

Villeneuve, V.; Fournier, B.; Duchesne, J. (2012). "Determination of the damage in concrete affected by ASR – The damage rating index (DRI)." *Proceedings of the 14th International conference on alkali-aggregate reaction (ICAAR).* Austin, Texas 10 pp.

Vivian, H. F. (1947). "Studies in Cement-Aggregate Reaction, VII-The Effect of Storage Condition on Expansion and tensile Strength Changes of Mortar*." Journal of the Council for Scientific and Industrial Research*, 20(4), 585-594.

Vuorinen, J. (1970). "On use of the dilation factor and degree of saturation in testing concrete for frost resistance." *Nordisk Berong*, 1, 37-64.

Walker, H. N., Lane, D. S., and Stutzman, P. E. (2006). "Petrographic Methods of Examining Hardened Concrete: A Petrographic Manual (No. FHWA-HRT-04-150)." *Federal Highway Administration,* U.S. Department of Transportation, Washington DC, 353 pp.

Wang, H., and Gillott, J. E. (1991) "Mechanism of alkali-silica reaction and the significance of calcium hydroxide." *Cement and Concrete Research*, 21, 647-654.

Wehrle, E. R. (2010) "The effects of coatings and sealers used to mitigate alkali-silica reaction and/or delayed ettringite formation in hardened concrete." *Doctoral dissertation*, University of Texas at Austin, TX, 166 pp.

Wexler, A. and Hasegawa, S. (1954). “Relative humidity-temperature relationships of some saturated salt solutions in the temperature range 0° to 50° C.” *Journal of Research of the National Bureau of Standards*, 53(1), 19-26.

8. APPENDIX

8.1. APPENDIX A: INTERSTATE 49 BARRIER DATA

The strain, temperature, and RH data for the Interstate 49 barrier wall is summarized in **Table 8.1-1**, **Table 8.1-2**, **Table 8.1-3**, for the sections of minimal, moderate, and severe deterioration respectively. The data is also summarized in plots which show the individual data points for each measurement at each section from the top and bottom, or left and right, of each length-change grid. The data within the tables and figures have not been corrected for temperature. The data for sections with minimal deterioration are summarized in **Fig. 8.1-1**, **Fig. 8.1-2**, **Fig. 8.1-3**, **Fig. 8.1-4**, and **Fig. 8.1-5,** for the control, silane, linseed, elastomeric paint, and silane 2 sections, respectively. The data for sections with moderate deterioration are summarized in **Fig. 8.1-6**, **Fig. 8.1-7**, **Fig. 8.1-8**, **Fig. 8.1-9**, and **Fig. 8.1-10,** for the control, silane, linseed, elastomeric paint, and silane 2 sections, respectively. The data for sections with severe deterioration are summarized in **Fig. 8.1-11**, **Fig. 8.1-12**, **Fig. 8.1-13**, **Fig. 8.1-14**, and **Fig. 8.1-15,** for the control, silane, linseed, elastomeric paint, and silane 2 sections, respectively.

Table 8.1-1. Interstate 49 barrier wall data for sections with minimal deterioration

(C-1)	**Horizontal**				**Vertical**				**RH**	
Date	ID	Read 1	Read 2	Strain (%)	ID	Read 1	Read 2	Strain (%)	RH (%)	T (°C)
1/31/13	B	0.02695	0.02695	0.00000	L	0.01860	0.01900	0.00000	96.00	3.60
1/31/13	T	-0.05075	-0.05065	0.00000	R	0.01080	0.01120	0.00000		
1/31/13				**0.00000**				**0.00000**	**96.00**	**3.60**
3/12/13	B	0.02825	0.02795	0.00584	L	0.02065	0.02035	0.00864	92.90	3.20
3/12/13	T	-0.05010	-0.05020	0.00279	R	0.01300	0.01285	0.00978		
3/12/13				**0.00432**				**0.00921**	**92.90**	**3.20**
5/2/13	B	0.03045	0.03030	0.01740	L	0.02380	0.02355	0.02477	99.10	15.00
5/2/13	T	-0.04835	-0.04850	0.01156	R	0.01610	0.01585	0.02527		
5/2/13				**0.01448**				**0.02502**	**99.10**	**15.00**
6/6/13	B	0.03105	0.03105	0.02083	L	0.02455	0.02465	0.02946	96.10	24.50
6/6/13	T	-0.04770	-0.04770	0.01524	R	0.01730	0.01730	0.03200		
6/6/13				**0.01803**				**0.03073**	**96.10**	**24.50**
7/11/13	B	0.03215	0.03200	0.02604	L	0.02615	0.02610	0.03721	98.50	28.10
7/11/13	T	-0.04735	-0.04760	0.01638	R	0.01855	0.01855	0.03835		
7/11/13				**0.02121**				**0.03778**	**98.50**	**28.10**
8/15/13	B	0.03224	0.03160	0.02523	L	0.02460	0.02505	0.03061	98.20	18.70
8/15/13	T	-0.04860	-0.04855	0.01080	R	0.01750	0.01730	0.03251		
8/15/13				**0.01801**				**0.03156**	**98.20**	**18.70**
10/17/13	B	0.03065	0.03055	0.01854	L	0.02295	0.02280	0.02070	98.40	9.50
10/17/13	T	-0.05010	-0.05000	0.00330	R	0.01545	0.01535	0.02235		
10/17/13				**0.01092**				**0.02153**	**98.40**	**9.50**
1/14/14	B	0.03050	0.03040	0.01778	L	0.02230	0.02220	0.01753	94.50	4.50
1/14/14	T	-0.05010	-0.05020	0.00279	R	0.01490	0.01460	0.01905		
1/14/14				**0.01029**				**0.01829**	**94.50**	**4.50**
7/15/14	B	0.03175	0.03165	0.02413	L	0.02460	0.02500	0.03048	97.70	22.70
7/15/14	T	-0.04915	-0.04895	0.00838	R	0.01700	0.01685	0.03010		
7/15/14				**0.01626**				**0.03029**	**97.70**	**22.70**
6/4/15	B	0.03015	0.02990	0.01562	L	0.02440	0.02380	0.02692	98.10	24.80
6/4/15	T	-0.05065	-0.05085	-0.00025	R	0.01665	0.01625	0.02769		
6/4/15				**0.00768**				**0.02731**	**98.10**	**24.80**
10/13/15	B	0.02980	0.03010	0.01524	L	0.02180	0.02215	0.01613	71.20	16.10
10/13/15	T	-0.05130	-0.05130	-0.00305	R	0.01415	0.01445	0.01676		
10/13/15	B	0.03015	0.03010	0.01613	L	0.02220	0.02170	0.01600	71.20	21.80
10/13/15	T	-0.05085	-0.05095	-0.00102	R	0.01460	0.01425	0.01740		
10/13/15				**0.00756**				**0.01670**	**71.20**	**18.95**
3/14/16	B	0.02905	0.02880	0.01003	L	0.02140	0.02150	0.01346	91.40	15.00
3/14/16	T	-0.05180	-0.05175	-0.00546	R	0.01360	0.01395	0.01410		
3/14/16	B	0.02960	0.02935	0.01283	L	0.02290	0.02320	0.02159	91.40	20.30

Table 8.1-1. Interstate 49 barrier wall data for sections with minimal deterioration (cont.)

(C-1)	**Horizontal**				**Vertical**				**RH**	
Date	ID	Read 1	Read 2	Strain (%)	ID	Read 1	Read 2	Strain (%)	RH (%)	T (°C)
3/14/16	T	-0.05115	-0.05160	-0.00343	R	0.01510	0.01525	0.02121		
3/14/16				**0.00470**				**0.02140**	**91.40**	**17.65**
(S-1)	**Horizontal**				**Vertical**				**RH**	
Date	ID	Read 1	Read 2	Strain (%)	ID	Read 1	Read 2	Strain (%)	RH (%)	T (°C)
1/31/13	B	-0.06986	-0.07000	0.00000	L	-0.05090	-0.05045	0.00000	96.15	4.40
1/31/13	T	-0.00265	-0.00245	0.00000	R	0.01645	0.01640	0.00000		
1/31/13				**0.00000**				**0.00000**	**96.15**	**4.40**
3/12/13	B	-0.06875	-0.06885	0.00574	L	-0.04915	-0.04915	0.00775	92.80	3.20
3/12/13	T	-0.00190	-0.00185	0.00343	R	0.01845	0.01810	0.00940		
3/12/13				**0.00458**				**0.00857**	**92.80**	**3.20**
5/2/13	B	-0.06655	-0.06665	0.01692	L	-0.04550	-0.04585	0.02540	99.50	14.50
5/2/13	T	-0.00060	-0.00055	0.01003	R	0.02215	0.02230	0.02946		
5/2/13				**0.01347**				**0.02743**	**99.50**	**14.50**
6/6/13	B	-0.06670	-0.06635	0.01730	L	-0.04415	-0.04450	0.03226	93.40	24.70
6/6/13	T	-0.00020	-0.00015	0.01207	R	0.02330	0.02330	0.03493		
6/6/13				**0.01468**				**0.03359**	**93.40**	**24.70**
7/11/13	B	-0.06580	-0.06610	0.02022	L	-0.04290	-0.04240	0.04077	81.40	28.10
7/11/13	T	0.00015	0.00010	0.01359	R	0.02525	0.02555	0.04559		
7/11/13				**0.01690**				**0.04318**	**81.40**	**28.10**
8/15/13	B	-0.06640	-0.06680	0.01692	L	-0.04430	-0.04420	0.03264	82.00	18.70
8/15/13	T	-0.00070	-0.00095	0.00876	R	0.02375	0.02370	0.03708		
8/15/13				**0.01284**				**0.03486**	**82.00**	**18.70**
10/17/13	B	-0.06800	-0.06795	0.00993	L	-0.04640	-0.04665	0.02108	86.10	9.40
10/17/13	T	-0.00285	-0.00290	-0.00165	R	0.02175	0.02165	0.02680		
10/17/13				**0.00414**				**0.02394**	**86.10**	**9.40**
1/14/14	B	-0.06825	-0.06820	0.00866	L	-0.04785	-0.04680	0.01702	95.40	4.50
1/14/14	T	-0.00320	-0.00325	-0.00343	R	0.02110	0.02075	0.02286		
1/14/14				**0.00262**				**0.01994**	**95.40**	**4.50**
7/15/14	B	-0.06785	-0.06765	0.01107	L	-0.04510	-0.04545	0.02743	65.20	22.50
7/15/14	T	-0.00250	-0.00250	0.00025	R	0.02320	0.02355	0.03531		
7/15/14				**0.00566**				**0.03137**	**65.20**	**22.50**
6/4/15	B	-0.06980	-0.07005	0.00003	L	-0.04710	-0.04725	0.01778	97.50	24.40
6/4/15	T	-0.00520	-0.00510	-0.01321	R	0.02200	0.02190	0.02807		
6/4/15				**-0.00659**				**0.02292**	**97.50**	**24.40**
10/13/15	B	-0.07070	-0.07065	-0.00378	L	-0.05060	-0.05010	0.00165	73.20	16.40
10/13/15	T	-0.00585	-0.00610	-0.01740	R	0.01955	0.01960	0.01600		
10/13/15	B	-0.07055	-0.07070	-0.00353	L	-0.05010	-0.05065	0.00152	73.20	22.90
10/13/15	T	-0.00545	-0.00530	-0.01435	R	0.01945	0.01930	0.01499		

Table 8.1-1. Interstate 49 barrier wall data for sections with minimal deterioration (cont.)

(S-1)	**Horizontal**				**Vertical**				**RH**	
Date	ID	Read 1	Read 2	Strain (%)	ID	Read 1	Read 2	Strain (%)	RH (%)	T (°C)
10/13/15				**-0.00894**				**0.00826**	**73.20**	**19.65**
3/14/16	B	-0.07175	-0.07245	-0.01102	L	-0.05190	-0.05135	-0.00483	86.00	15.00
3/14/16	T	-0.00680	-0.00670	-0.02134	R	0.01785	0.01800	0.00762		
3/14/16	B	-0.07085	-0.07120	-0.00556	L	-0.05110	-0.05035	-0.00025	86.00	21.80
3/14/16	T	-0.00665	-0.00640	-0.02019	R	0.01890	0.01875	0.01219		
3/14/16				**-0.01288**				**0.00597**	**86.00**	**18.40**
(L-1)	**Horizontal**				**Vertical**				**RH**	
Date	ID	Read 1	Read 2	Strain (%)	ID	Read 1	Read 2	Strain (%)	RH (%)	T (°C)
1/31/13	B	0.01390	0.01400	0.00000	L	-0.02585	-0.02590	0.00000	96.45	1.40
1/31/13	T	0.00505	0.00490	0.00000	R	-0.07265	-0.07220	0.00000		
1/31/13				**0.00000**				**0.00000**	**96.45**	**1.40**
3/12/13	B	0.01505	0.01495	0.00533	L	-0.02435	-0.02490	0.00635	92.90	3.00
3/12/13	T	0.00565	0.00580	0.00381	R	-0.07050	-0.07110	0.00826		
3/12/13				**0.00457**				**0.00730**	**92.90**	**3.00**
5/2/13	B	0.01720	0.01710	0.01626	L	-0.02175	-0.02195	0.02045	100.00	14.70
5/2/13	T	0.00765	0.00770	0.01372	R	-0.06785	-0.06810	0.02261		
5/2/13				**0.01499**				**0.02153**	**100.00**	**14.70**
6/6/13	B	0.01760	0.01775	0.01892	L	-0.02050	-0.02080	0.02654	96.60	25.80
6/6/13	T	0.00880	0.00885	0.01956	R	-0.06710	-0.06720	0.02680		
6/6/13				**0.01924**				**0.02667**	**96.60**	**25.80**
7/11/13	B	0.01850	0.01825	0.02248	L	-0.02060	-0.02035	0.02743	95.70	28.10
7/11/13	T	0.00925	0.00940	0.02210	R	-0.06675	-0.06635	0.02985		
7/11/13				**0.02229**				**0.02864**	**95.70**	**28.10**
8/15/13	B	0.01805	0.01790	0.02045	L	-0.02225	-0.02195	0.01918	96.30	18.60
8/15/13	T	0.00845	0.00855	0.01791	R	-0.06835	-0.06820	0.02108		
8/15/13				**0.01918**				**0.02013**	**96.30**	**18.60**
10/17/13	B	0.01720	0.01730	0.01676	L	-0.02390	-0.02410	0.00953	96.00	9.30
10/17/13	T	0.00745	0.00745	0.01257	R	-0.07030	-0.07040	0.01054		
10/17/13				**0.01467**				**0.01003**	**96.00**	**9.30**
1/14/14	B	0.01625	0.01590	0.01080	L	-0.02455	-0.02420	0.00762	95.60	4.80
1/14/14	T	0.00680	0.00695	0.00965	R	-0.07165	-0.07130	0.00483		
1/14/14				**0.01022**				**0.00622**	**95.60**	**4.80**
7/15/14	B	0.01680	0.01645	0.01359	L	-0.02325	-0.02340	0.01295	99.50	22.60
7/15/14	T	0.00795	0.00790	0.01499	R	-0.07080	-0.07020	0.00978		
7/15/14				**0.01429**				**0.01137**	**99.50**	**22.60**
6/4/15	B	0.01515	0.01520	0.00622	L	-0.02365	-0.02420	0.00991	96.00	24.30
6/4/15	T	0.00615	0.00625	0.00622	R	-0.07085	-0.07030	0.00940		
6/4/15				**0.00622**				**0.00965**	**96.00**	**24.30**

Table 8.1-1. Interstate 49 barrier wall data for sections with minimal deterioration (cont.)

(L-1)	**Horizontal**				**Vertical**				**RH**	
Date	ID	Read 1	Read 2	Strain (%)	ID	Read 1	Read 2	Strain (%)	RH (%)	T (°C)
10/13/15	B	0.01520	0.01540	0.00686	L	-0.02730	-0.02730	-0.00724	71.50	16.00
10/13/15	T	0.00545	0.00560	0.00279	R	-0.07455	-0.07480	-0.01143		
10/13/15	B	0.01540	0.01520	0.00686	L	-0.02660	-0.02695	-0.00457	71.50	21.90
10/13/15	T	0.00620	0.00600	0.00572	R	-0.07415	-0.07405	-0.00851		
10/13/15				**0.00629**				**-0.00654**	**71.50**	**18.95**
3/14/16	B	0.01455	0.01420	0.00216	L	-0.02650	-0.02655	-0.00330	93.80	15.00
3/14/16	T	0.00525	0.00490	0.00051	R	-0.07360	-0.07375	-0.00635		
3/14/16	B	0.01525	0.01470	0.00521	L	-0.02600	-0.02550	0.00064	93.80	20.70
3/14/16	T	0.00570	0.00540	0.00292	R	-0.07295	-0.07305	-0.00292		
3/14/16				**0.00406**				**-0.00114**	**93.80**	**17.85**
(EP-1)	**Horizontal**				**Vertical**				**RH**	
Date	ID	Read 1	Read 2	Strain (%)	ID	Read 1	Read 2	Strain (%)	RH (%)	T (°C)
1/31/13	B	-0.00955	-0.00955	0.00000	L	0.00730	0.00770	0.00000	96.30	-0.30
1/31/13	T	-0.02880	-0.02870	0.00000	R	0.00660	0.00665	0.00000		
1/31/13				**0.00000**				**0.00000**	**96.30**	**-0.30**
3/12/13	B	-0.00905	-0.00915	0.00229	L	0.00970	0.00955	0.01080	93.10	3.20
3/12/13	T	-0.02840	-0.02860	0.00127	R	0.00845	0.00840	0.00914		
3/12/13				**0.00178**				**0.00997**	**93.10**	**3.20**
5/2/13	B	-0.00790	-0.00765	0.00902	L	0.01065	0.01045	0.01549	99.50	12.90
5/2/13	T	-0.02730	-0.02750	0.00686	R	0.01160	0.01140	0.02477		
5/2/13				**0.00794**				**0.02013**	**99.50**	**12.90**
6/6/13	B	-0.00715	-0.00715	0.01219	L	0.01325	0.01305	0.02870	92.60	22.70
6/6/13	T	-0.02695	-0.02690	0.00927	R	0.01205	0.01195	0.02731		
6/6/13				**0.01073**				**0.02800**	**92.60**	**22.70**
7/11/13	B	-0.00640	-0.00690	0.01473	L	0.01440	0.01455	0.03543	93.30	26.20
7/11/13	T	-0.02650	-0.02670	0.01092	R	0.01320	0.01325	0.03353		
7/11/13				**0.01283**				**0.03448**	**93.30**	**26.20**
8/15/13	B	-0.00715	-0.00695	0.01270	L	0.01255	0.01260	0.02578	94.10	16.80
8/15/13	T	-0.02695	-0.02740	0.00800	R	0.01150	0.01170	0.02527		
8/15/13				**0.01035**				**0.02553**	**94.10**	**16.80**
10/17/13	B	-0.00850	-0.00860	0.00508	L	0.01075	0.01045	0.01575	96.30	8.30
10/17/13	T	-0.02860	-0.02840	0.00127	R	0.00955	0.00930	0.01422		
10/17/13				**0.00318**				**0.01499**	**96.30**	**8.30**
1/14/14	B	-0.00920	-0.00915	0.00191	L	0.00995	0.00975	0.01194	95.10	3.90
1/14/14	T	-0.02840	-0.02870	0.00102	R	0.00875	0.00900	0.01143		
1/14/14				**0.00146**				**0.01168**	**95.10**	**3.90**
7/15/14	B	-0.00830	-0.00900	0.00457	L	0.01030	0.01000	0.01346	97.20	21.00
7/15/14	T	-0.02760	-0.02790	0.00508	R	0.01175	0.01220	0.02718		

Table 8.1-1. Interstate 49 barrier wall data for sections with minimal deterioration (cont.)

(EP-1)	**Horizontal**				**Vertical**				**RH**	
Date	ID	Read 1	Read 2	Strain (%)	ID	Read 1	Read 2	Strain (%)	RH (%)	T (°C)
7/15/14				**0.00483**				**0.02032**	**97.20**	**21.00**
6/4/15	B	-0.01005	-0.01000	-0.00241	L	0.01110	0.01075	0.01740	97.10	23.10
6/4/15	T	-0.02980	-0.02970	-0.00508	R	0.01000	0.00990	0.01689		
6/4/15				**-0.00375**				**0.01715**	**97.10**	**23.10**
10/13/15	B	-0.01075	-0.01070	-0.00597	L	0.00890	0.00860	0.00635	64.80	13.50
10/13/15	T	-0.03030	-0.02985	-0.00673	R	0.00675	0.00700	0.00127		
10/13/15	B	-0.01070	-0.01095	-0.00648	L	0.00880	0.00860	0.00610	64.80	18.20
10/13/15	T	-0.02990	-0.03000	-0.00610	R	0.00725	0.00715	0.00292		
10/13/15				**-0.00629**				**0.00451**	**64.80**	**15.85**
3/14/16	B	-0.01170	-0.01170	-0.01092	L	0.00840	0.00820	0.00406	95.60	15.00
3/14/16	T	-0.03115	-0.03160	-0.01334	R	0.00715	0.00670	0.00152		
3/14/16	B	-0.01090	-0.01155	-0.00851	L	0.00840	0.00915	0.00648	95.60	16.80
3/14/16	T	-0.03035	-0.03075	-0.00914	R	0.00795	0.00800	0.00686		
3/14/16				**-0.00883**				**0.00667**	**95.60**	**15.90**
(S2-1)	**Horizontal**				**Vertical**				**RH**	
Date	ID	Read 1	Read 2	Strain (%)	ID	Read 1	Read 2	Strain (%)	RH (%)	T (°C)
1/31/13	B	-0.02240	-0.02225	0.00000	L	-0.00360	-0.00380	0.00000	96.60	1.00
1/31/13	T	-0.01665	-0.01610	0.00000	R	-0.06380	-0.06370	0.00000		
1/31/13				**0.00000**				**0.00000**	**96.60**	**1.00**
3/12/13	B	-0.02125	-0.02140	0.00508	L	-0.00180	-0.00215	0.00876	93.20	3.30
3/12/13	T	-0.01545	-0.01545	0.00470	R	-0.06175	-0.06195	0.00965		
3/12/13				**0.00489**				**0.00921**	**93.20**	**3.30**
5/2/13	B	-0.01970	-0.01970	0.01334	L	0.00170	0.00140	0.02667	100.00	13.80
5/2/13	T	-0.01350	-0.01370	0.01410	R	-0.05850	-0.05845	0.02680		
5/2/13				**0.01372**				**0.02673**	**100.00**	**13.80**
6/6/13	B	-0.01960	-0.01955	0.01397	L	0.00300	0.00250	0.03277	95.10	26.30
6/6/13	T	-0.01315	-0.01325	0.01613	R	-0.05785	-0.05770	0.03035		
6/6/13				**0.01505**				**0.03156**	**95.10**	**26.30**
7/11/13	B	-0.01915	-0.01915	0.01613	L	0.00415	0.00369	0.03871	84.00	28.30
7/11/13	T	-0.01305	-0.01290	0.01727	R	-0.05645	-0.05620	0.03772		
7/11/13				**0.01670**				**0.03821**	**84.00**	**28.30**
8/15/13	B	-0.01930	-0.01945	0.01499	L	0.00260	0.00261	0.03202	82.70	18.40
8/15/13	T	-0.01385	-0.01400	0.01245	R	-0.05805	-0.05815	0.02870		
8/15/13				**0.01372**				**0.03036**	**82.70**	**18.40**
10/17/13	B	-0.02075	-0.02110	0.00711	L	0.00030	-0.00010	0.01930	91.00	9.20
10/17/13	T	-0.01285	-0.01600	0.00991	R	-0.06020	-0.06065	0.01689		
10/17/13				**0.00851**				**0.01810**	**91.00**	**9.20**
1/14/14	B	-0.02175	-0.02140	0.00381	L	-0.00120	-0.00070	0.01397	91.80	4.50

Table 8.1-1. Interstate 49 barrier wall data for sections with minimal deterioration (cont.)

(S2-1)	**Horizontal**				**Vertical**				**RH**	
Date	ID	Read 1	Read 2	Strain (%)	ID	Read 1	Read 2	Strain (%)	RH (%)	T (°C)
1/14/14	T	-0.01640	-0.01595	0.00102	R	-0.06120	-0.06100	0.01346		
1/14/14				**0.00241**				**0.01372**	**91.80**	**4.50**
7/15/14	B	-0.02105	-0.02155	0.00521	L	0.00125	0.00115	0.02489	86.30	23.30
7/15/14	T	-0.01520	-0.01510	0.00622	R	-0.06010	-0.05990	0.01905		
7/15/14				**0.00572**				**0.02197**	**86.30**	**23.30**
6/4/15	B	-0.02320	-0.02325	-0.00457	L	-0.00080	-0.00135	0.01334	98.60	25.50
6/4/15	T	-0.01760	-0.01770	-0.00648	R	-0.06090	-0.06115	0.01384		
6/4/15				**-0.00552**				**0.01359**	**98.60**	**25.50**
10/13/15	B	-0.02330	-0.02350	-0.00546	L	-0.00305	-0.00340	0.00241	72.90	16.50
10/13/15	T	-0.01810	-0.01785	-0.00813	R	-0.06415	-0.06375	-0.00102		
10/13/15	B	-0.02325	-0.02375	-0.00597	L	-0.00345	-0.00380	0.00038	72.90	22.70
10/13/15	T	-0.01750	-0.01785	-0.00660	R	-0.06375	-0.06415	-0.00102		
10/13/15				**-0.00629**				**-0.00032**	**72.90**	**19.60**
3/14/16	B	-0.02485	-0.02525	-0.01384	L	-0.00510	-0.00470	-0.00610	89.00	15.00
3/14/16	T	-0.01900	-0.01910	-0.01359	R	-0.06470	-0.06480	-0.00508		
3/14/16	B	-0.02415	-0.02480	-0.01092	L	-0.00380	-0.00345	0.00038	89.00	21.30
3/14/16	T	-0.01825	-0.01825	-0.00953	R	-0.06370	-0.06380	0.00000		
3/14/16				**-0.01022**				**0.00019**	**89.00**	**18.15**

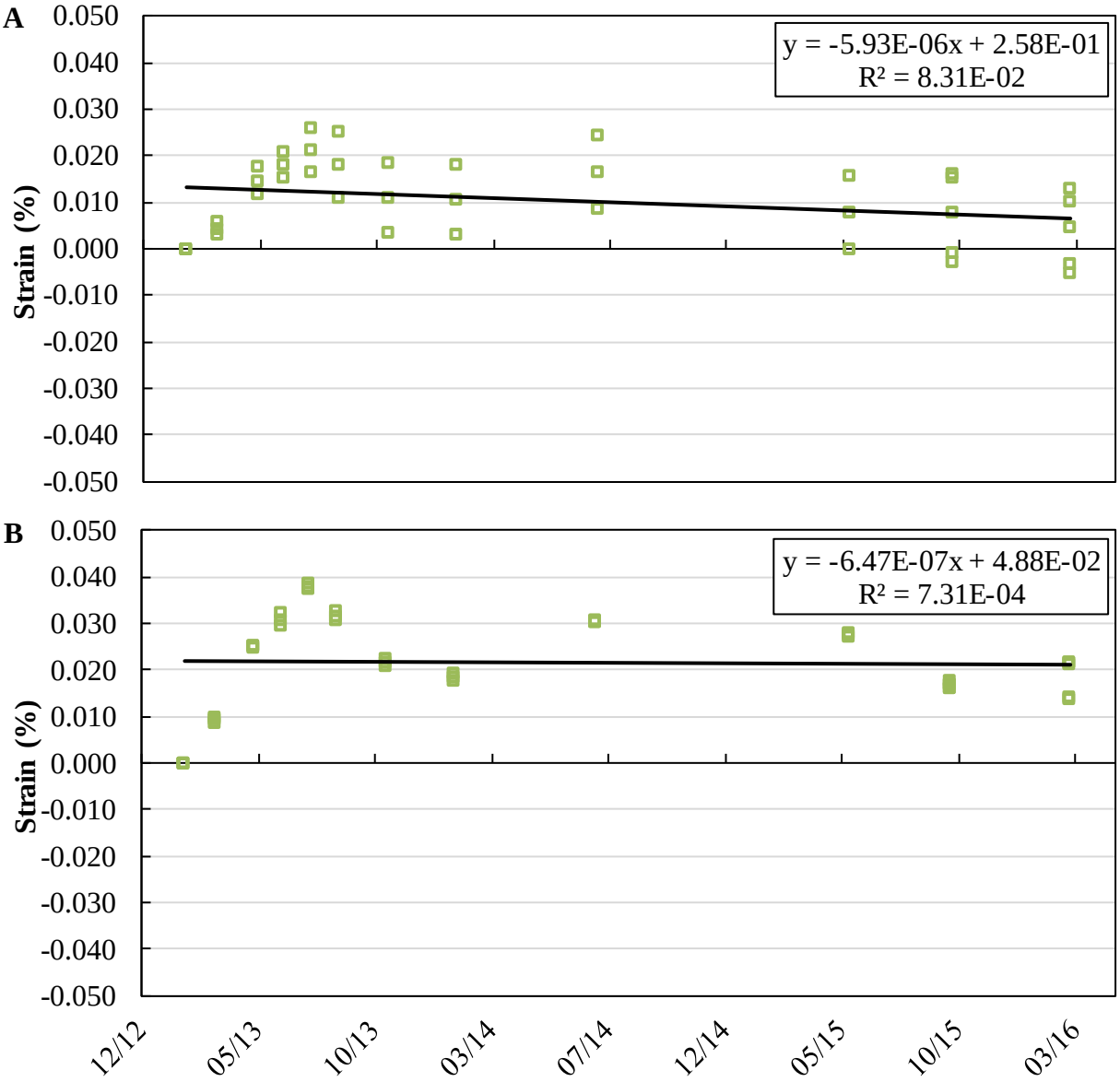

Fig. 8.1-1–Horizontal (A) and vertical (B) strain (%) with respect to date, Interstate 49 barrier wall exhibiting minimal deterioration, control section (C-1).

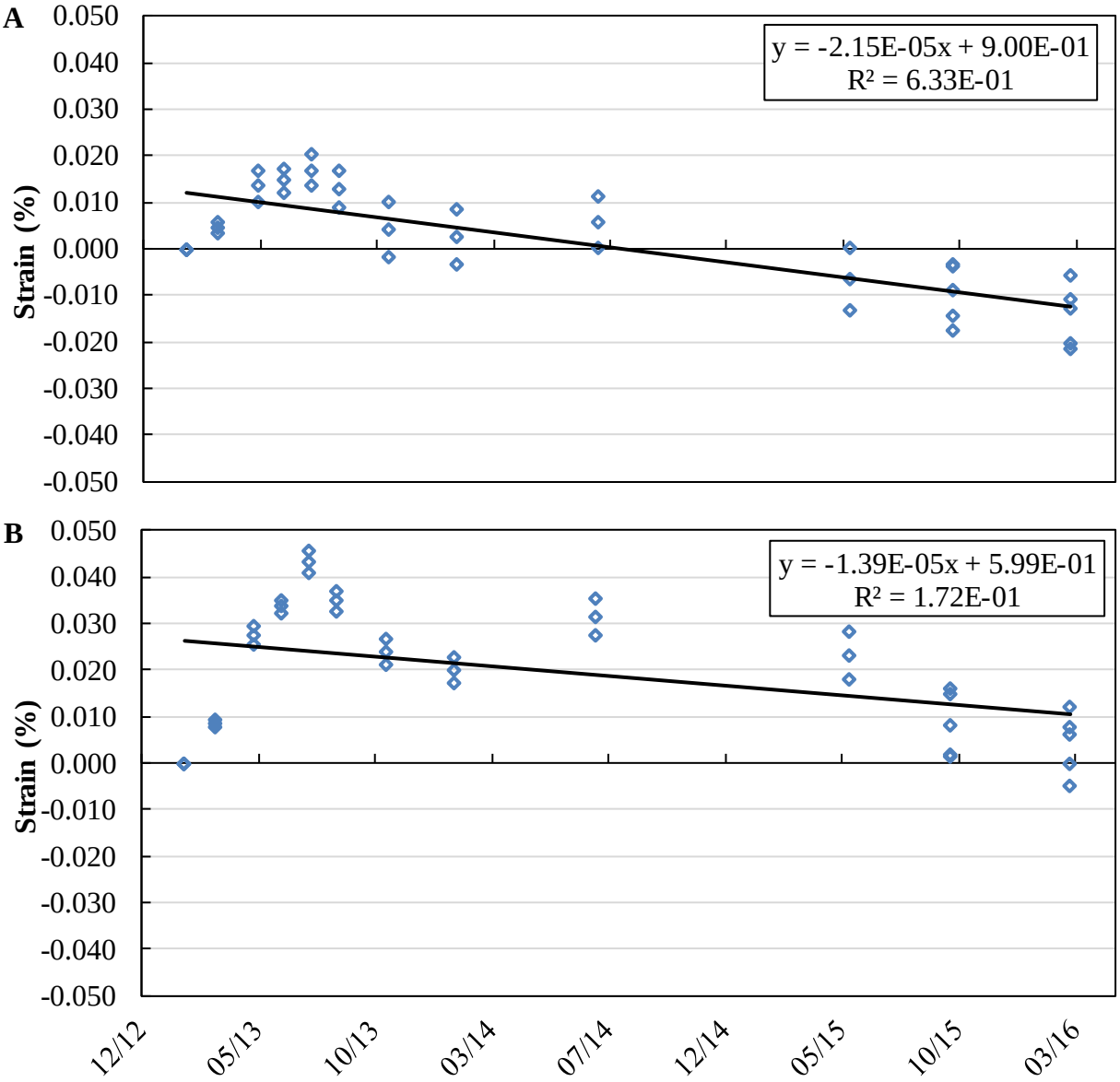

Fig. 8.1-2–Horizontal (A) and vertical (B) strain (%) with respect to date, Interstate 49 barrier wall exhibiting minimal deterioration, silane section (S-1).

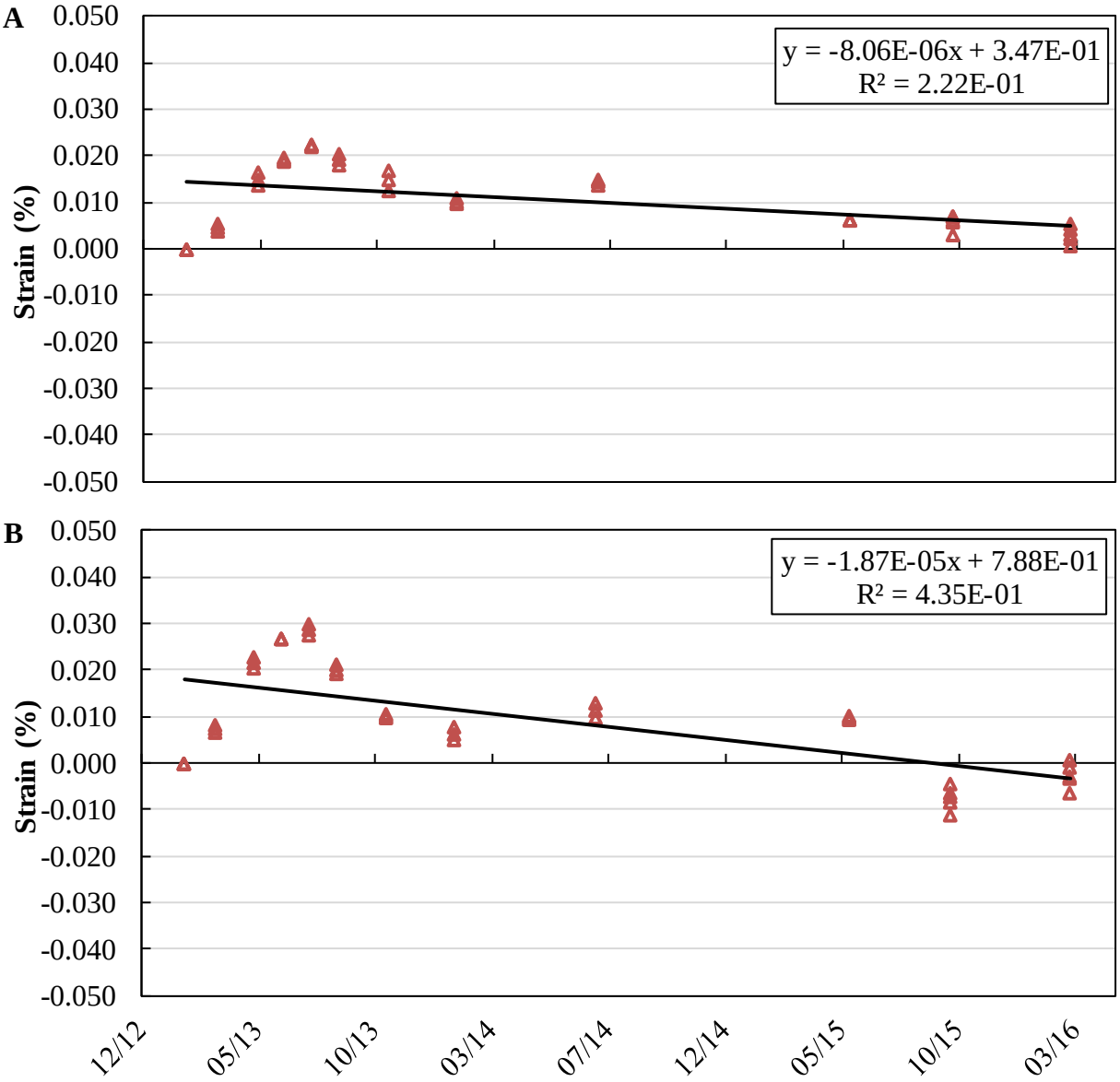

Fig. 8.1-3–Horizontal (A) and vertical (B) strain (%) with respect to date, Interstate 49 barrier wall exhibiting minimal deterioration, linseed section (L-1).

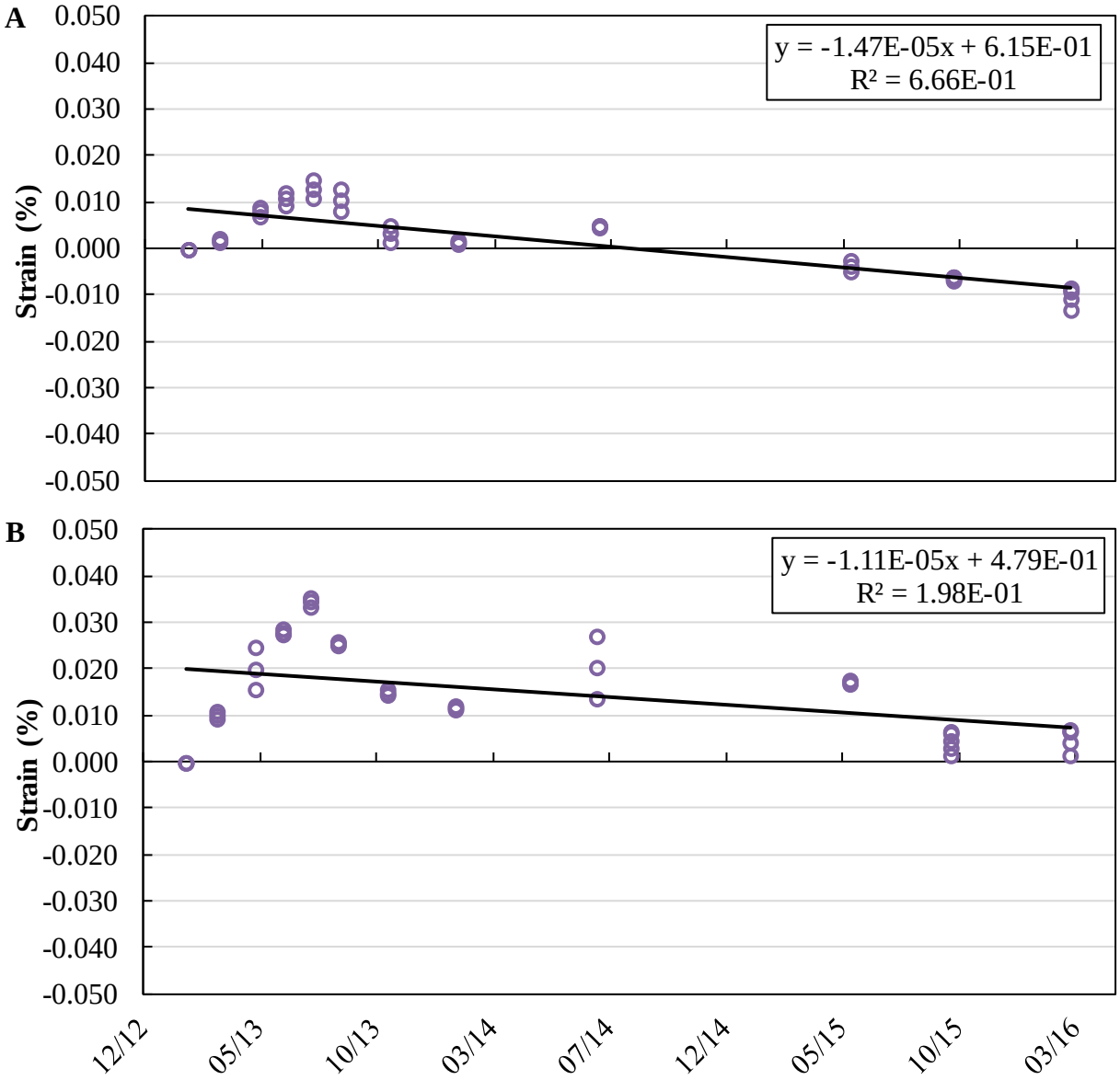

Fig. 8.1-4–Horizontal (A) and vertical (B) strain (%) with respect to date, Interstate 49 barrier wall exhibiting minimal deterioration, elastomeric paint section (EP-1).

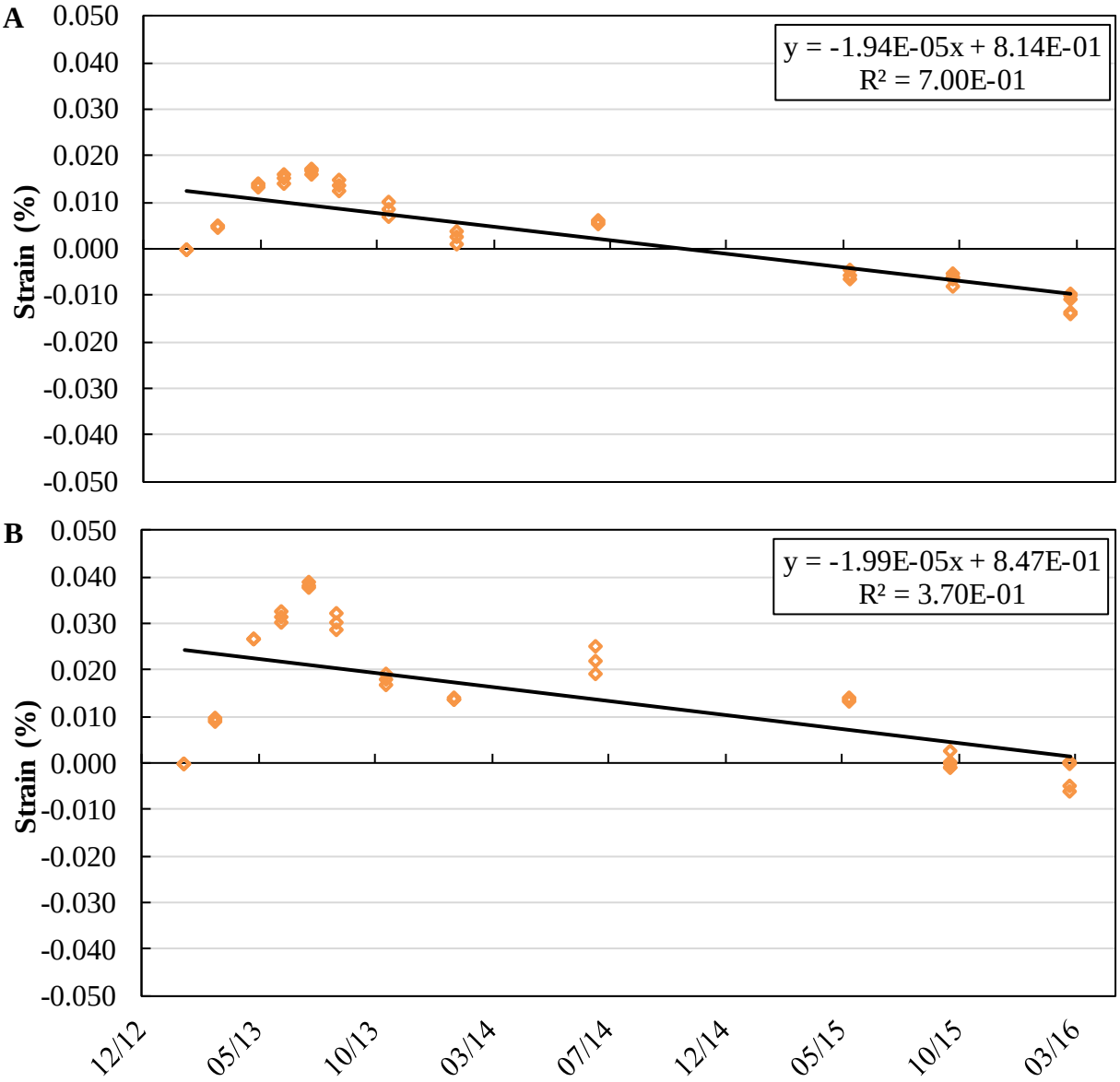

Fig. 8.1-5–Horizontal (A) and vertical (B) strain (%) with respect to date, Interstate 49 barrier wall exhibiting minimal deterioration, silane 2 section (S2-1).

Table 8.1-2. Interstate 49 barrier wall data for sections with moderate deterioration

(C-2)	**Horizontal**				**Vertical**				**RH**	
Date	ID	Read 1	Read 2	Strain (%)	ID	Read 1	Read 2	Strain (%)	RH (%)	T (°C)
1/31/13	B	0.05105	0.05120	0.00000	L	-0.01325	-0.01300	0.00000	96.70	0.50
1/31/13	T	0.01480	0.01490	0.00000	R	-0.00405	-0.00375	0.00000		
1/31/13				**0.00000**				**0.00000**	**96.70**	**0.50**
3/12/13	B	0.05145	0.05155	0.00191	L	-0.01085	-0.01100	0.01118	94.00	4.10
3/12/13	T	0.01510	0.01530	0.00178	R	-0.00155	-0.00175	0.01143		
3/12/13				**0.00184**				**0.01130**	**94.00**	**4.10**
5/2/13	B	0.05175	0.05165	0.00292	L	-0.00690	-0.00730	0.03061	99.40	14.80
5/2/13	T	0.01610	0.01605	0.00622	R	0.00300	0.00260	0.03404		
5/2/13				**0.00457**				**0.03232**	**99.40**	**14.80**
6/6/13	B	0.05195	0.05175	0.00368	L	-0.00435	-0.00450	0.04420	96.80	25.70
6/6/13	T	0.01640	0.01630	0.00762	R	0.00545	0.00545	0.04750		
6/6/13				**0.00565**				**0.04585**	**96.80**	**25.70**
7/11/13	B	0.05150	0.05160	0.00216	L	-0.00390	-0.00380	0.04712	94.50	29.00
7/11/13	T	0.01585	0.01590	0.00521	R	0.00640	0.00660	0.05283		
7/11/13				**0.00368**				**0.04997**	**94.50**	**29.00**
8/15/13	B	0.05210	0.05175	0.00406	L	-0.00455	-0.00455	0.04356	96.40	18.90
8/15/13	T	0.01595	0.01560	0.00470	R	0.00575	0.00585	0.04928		
8/15/13				**0.00438**				**0.04642**	**96.40**	**18.90**
10/17/13	B	0.05140	0.05160	0.00191	L	-0.00615	-0.00615	0.03543	96.50	9.80
10/17/13	T	0.01500	0.01505	0.00089	R	0.00450	0.00435	0.04229		
10/17/13				**0.00140**				**0.03886**	**96.50**	**9.80**
1/14/14	B	0.05225	0.05215	0.00546	L	-0.00460	-0.00400	0.04483	95.20	5.90
1/14/14	T	0.01535	0.01545	0.00279	R	0.00670	0.00740	0.05563		
1/14/14				**0.00413**				**0.05023**	**95.20**	**5.90**
7/15/14	B	0.05070	0.05060	-0.00241	L	0.00095	0.00096	0.07153	98.00	23.60
7/15/14	T	0.01475	0.01475	-0.00051	R	0.01330	0.01340	0.08763		
7/15/14				**-0.00146**				**0.07958**	**98.00**	**23.60**
6/4/15	B	0.04825	0.04850	-0.01397	L	0.00450	0.00465	0.08992	98.80	26.20
6/4/15	T	0.01280	0.01285	-0.01029	R	0.01810	0.01845	0.11265		
6/4/15				**-0.01213**				**0.10128**	**98.80**	**26.20**
10/13/15	B	0.04845	0.04855	-0.01334	L	0.00425	0.00375	0.08700	71.80	16.90
10/13/15	T	0.01230	0.01230	-0.01295	R	0.01795	0.01785	0.11074		
10/13/15	B	0.04840	0.04845	-0.01372	L	0.00415	0.00415	0.08776	71.80	22.10
10/13/15	T	0.01240	0.01245	-0.01232	R	0.01800	0.01825	0.11189		
10/13/15				**-0.01302**				**0.09982**	**71.80**	**19.5**
3/14/16	B	0.04835	0.04810	-0.01473	L	0.00575	0.00585	0.09614	89.00	15.00
3/14/16	T	0.01200	0.01200	-0.01448	R	0.02025	0.02010	0.12230		
3/14/16	B	0.04860	0.04830	-0.01359	L	0.00645	0.00710	0.10109	89.00	21.80

Table 8.1-2. Interstate 49 barrier wall data for sections with moderate deterioration (cont.)

(C-2)	**Horizontal**				**Vertical**				**RH**	
Date	ID	Read 1	Read 2	Strain (%)	ID	Read 1	Read 2	Strain (%)	RH (%)	T (°C)
3/14/16	T	0.01250	0.01245	-0.01207	R	0.02155	0.02170	0.12967		
3/14/16				**-0.01283**				**0.11538**	**89.00**	**18.40**
(S-2)	**Horizontal**				**Vertical**				**RH**	
Date	ID	Read 1	Read 2	Strain (%)	ID	Read 1	Read 2	Strain (%)	RH (%)	T (°C)
1/31/13	B	0.04955	0.04965	0.00000	L	0.02380	0.02395	0.00000	97.05	-0.10
1/31/13	T	0.00190	0.00185	0.00000	R	-0.00700	-0.00675	0.00000		
1/31/13				**0.00000**				**0.00000**	**97.05**	**-0.10**
3/12/13	B	0.04990	0.04990	0.00152	L	0.02585	0.02565	0.00953	94.60	4.30
3/12/13	T	0.00165	0.00145	-0.00165	R	-0.00475	-0.00525	0.00953		
3/12/13				**-0.00006**				**0.00953**	**94.60**	**4.30**
5/2/13	B	0.05045	0.05030	0.00394	L	0.02995	0.03010	0.03124	99.50	14.50
5/2/13	T	0.00160	0.00135	-0.00203	R	-0.00150	-0.00165	0.02692		
5/2/13				**0.00095**				**0.02908**	**99.50**	**14.50**
6/6/13	B	0.05050	0.05050	0.00457	L	0.03160	0.03140	0.03874	97.40	25.70
6/6/13	T	0.00105	0.00100	-0.00432	R	-0.00030	-0.00025	0.03353		
6/6/13				**0.00013**				**0.03613**	**97.40**	**25.70**
7/11/13	B	0.05090	0.05085	0.00648	L	0.03355	0.03320	0.04826	96.80	29.40
7/11/13	T	0.00105	0.00110	-0.00406	R	0.00110	0.00115	0.04064		
7/11/13				**0.00121**				**0.04445**	**96.80**	**29.40**
8/15/13	B	0.05140	0.05140	0.00914	L	0.03225	0.03250	0.04318	98.00	19.30
8/15/13	T	0.00175	0.00130	-0.00178	R	0.00030	0.00050	0.03696		
8/15/13				**0.00368**				**0.04007**	**98.00**	**19.30**
10/17/13	B	0.05130	0.05140	0.00889	L	0.03080	0.03060	0.03467	95.30	10.10
10/17/13	T	0.00170	0.00190	-0.00038	R	-0.00105	-0.00105	0.02959		
10/17/13				**0.00425**				**0.03213**	**95.30**	**10.10**
1/14/14	B	0.05090	0.05115	0.00724	L	0.03325	0.03325	0.04763	94.10	6.20
1/14/14	T	0.00110	0.00140	-0.00318	R	0.00190	0.00140	0.04331		
1/14/14				**0.00203**				**0.04547**	**94.10**	**6.20**
7/15/14	B	0.05030	0.05010	0.00305	L	0.03920	0.03905	0.07747	99.60	24.30
7/15/14	T	0.00010	-0.00090	-0.01156	R	0.00635	0.00670	0.06807		
7/15/14				**-0.00425**				**0.07277**	**99.60**	**24.30**
6/4/15	B	0.04820	0.04835	-0.00673	L	0.04330	0.04380	0.09995	97.40	26.00
6/4/15	T	-0.00240	-0.00235	-0.02159	R	0.01045	0.01083	0.08898		
6/4/15				**-0.01416**				**0.09446**	**97.40**	**26.00**
10/13/15	B	0.04920	0.04925	-0.00191	L	0.04360	0.04320	0.09919	70.30	16.60
10/13/15	T	-0.00145	-0.00125	-0.01638	R	0.01010	0.01005	0.08611		
10/13/15	B	0.04900	0.04880	-0.00356	L	0.04315	0.04325	0.09817	70.30	21.30
10/13/15	T	-0.00155	-0.00175	-0.01791	R	0.00990	0.01000	0.08547		

Table 8.1-2. Interstate 49 barrier wall data for sections with moderate deterioration (cont.)

(S-2)	**Horizontal**				**Vertical**				**RH**	
Date	ID	Read 1	Read 2	Strain (%)	ID	Read 1	Read 2	Strain (%)	RH (%)	T (°C)
10/13/15				**-0.01073**				**0.09182**	**70.30**	**18.95**
3/14/16	B	0.04835	0.04825	-0.00660	L	0.04420	0.04490	0.10503	93.80	15.00
3/14/16	T	-0.00250	-0.00270	-0.02273	R	0.01090	0.01135	0.09144		
3/14/16	B	0.04860	0.04870	-0.00483	L	0.04525	0.04575	0.10986	93.80	19.80
3/14/16	T	-0.00220	-0.00250	-0.02146	R	0.01180	0.01195	0.09525		
3/14/16				**-0.01314**				**0.10255**	**93.80**	**17.40**
(L-2)	**Horizontal**				**Vertical**				**RH**	
Date	ID	Read 1	Read 2	Strain (%)	ID	Read 1	Read 2	Strain (%)	RH (%)	T (°C)
1/31/13	B	-0.00175	-0.00140	0.00000	L	-0.01035	-0.01010	0.00000	97.45	0.00
1/31/13	T	-0.02915	-0.02890	0.00000	R	0.01685	0.01690	0.00000		
1/31/13				**0.00000**				**0.00000**	**97.45**	**0.00**
3/12/13	B	-0.00125	-0.00120	0.00178	L	-0.00750	-0.00770	0.01334	94.90	4.30
3/12/13	T	-0.02915	-0.02915	-0.00064	R	0.01910	0.01905	0.01118		
3/12/13				**0.00057**				**0.01226**	**94.90**	**4.30**
5/2/13	B	-0.00085	-0.00100	0.00330	L	-0.00270	-0.00310	0.03721	100.00	15.70
5/2/13	T	-0.02920	-0.02935	-0.00127	R	0.02340	0.02340	0.03315		
5/2/13				**0.00102**				**0.03518**	**100.00**	**15.70**
6/6/13	B	-0.00075	-0.00100	0.00356	L	-0.00200	-0.00175	0.04242	96.50	26.20
6/6/13	T	-0.02940	-0.02945	-0.00203	R	0.02440	0.02450	0.03848		
6/6/13				**0.00076**				**0.04045**	**96.50**	**26.20**
7/11/13	B	-0.00085	-0.00105	0.00318	L	0.00020	-0.00010	0.05220	97.00	30.00
7/11/13	T	-0.02980	-0.02970	-0.00368	R	0.02630	0.02625	0.04775		
7/11/13				**-0.00025**				**0.04997**	**97.00**	**30.00**
8/15/13	B	-0.00045	-0.00100	0.00432	L	-0.00100	-0.00080	0.04737	97.80	20.00
8/15/13	T	-0.02920	-0.02955	-0.00178	R	0.02515	0.02505	0.04178		
8/15/13				**0.00127**				**0.04458**	**97.80**	**20.00**
10/17/13	B	-0.00120	-0.00115	0.00203	L	-0.00280	-0.00240	0.03874	96.10	10.10
10/17/13	T	-0.02915	-0.02925	-0.00089	R	0.02340	0.02365	0.03378		
10/17/13				**0.00057**				**0.03626**	**96.10**	**10.10**
1/14/14	B	-0.00080	-0.00105	0.00330	L	0.00310	0.00295	0.06731	94.80	6.30
1/14/14	T	-0.02805	-0.02805	0.00495	R	0.02935	0.02930	0.06325		
1/14/14				**0.00413**				**0.06528**	**94.80**	**6.30**
7/15/14	B	-0.00150	-0.00135	0.00076	L	0.01265	0.01260	0.11608	99.30	24.30
7/15/14	T	-0.02965	-0.02935	-0.00241	R	0.03770	0.03790	0.10630		
7/15/14				**-0.00083**				**0.11119**	**99.30**	**24.30**
6/4/15	B	-0.00345	-0.00290	-0.00813	L	0.02420	0.02465	0.17602	98.50	26.30
6/4/15	T	-0.03085	-0.03090	-0.00940	R	0.04965	0.04995	0.16726		
6/4/15				**-0.00876**				**0.17164**	**98.50**	**26.30**

Table 8.1-2. Interstate 49 barrier wall data for sections with moderate deterioration (cont.)

(L-2)	**Horizontal**				**Vertical**				**RH**	
Date	ID	Read 1	Read 2	Strain (%)	ID	Read 1	Read 2	Strain (%)	RH (%)	T (°C)
10/13/15	B	-0.00275	-0.00295	-0.00648	L	0.02415	0.02385	0.17386	69.30	16.80
10/13/15	T	-0.03045	-0.03070	-0.00787	R	0.04915	0.04900	0.16358		
10/13/15	B	-0.00305	-0.00310	-0.00762	L	0.02405	0.02395	0.17386	69.30	20.70
10/13/15	T	-0.03065	-0.03075	-0.00851	R	0.04910	0.04890	0.16320		
10/13/15				**-0.00806**				**0.16853**	**69.30**	**18.75**
3/14/16	B	-0.00360	-0.00380	-0.01080	L	0.02765	0.02760	0.19228	97.10	15.00
3/14/16	T	-0.03100	-0.03065	-0.00914	R	0.05280	0.05285	0.18263		
3/14/16	B	-0.00315	-0.00340	-0.00864	L	0.02085	0.02845	0.17717	97.10	19.90
3/14/16	T	-0.03060	-0.03060	-0.00800	R	0.05345	0.05365	0.18631		
3/14/16				**-0.00832**				**0.18174**	**97.10**	**17.45**
(EP-2)	**Horizontal**				**Vertical**				**RH**	
Date	ID	Read 1	Read 2	Strain (%)	ID	Read 1	Read 2	Strain (%)	RH (%)	T (°C)
1/31/13	B	-0.01435	-0.01400	0.00000	L	-0.00165	-0.00170	0.00000	97.35	0.20
1/31/13	T	0.00345	0.00395	0.00000	R	-0.01150	-0.01100	0.00000		
1/31/13				**0.00000**				**0.00000**	**97.35**	**0.20**
3/12/13	B	-0.01415	-0.01410	0.00025	L	0.00030	0.00020	0.00978	95.40	4.20
3/12/13	T	0.00355	0.00345	-0.00102	R	-0.00950	-0.01035	0.00673		
3/12/13				**-0.00038**				**0.00826**	**95.40**	**4.20**
5/2/13	B	-0.01430	-0.01450	-0.00114	L	0.00340	0.00370	0.02654	99.30	13.70
5/2/13	T	0.00210	0.00180	-0.00889	R	-0.00665	-0.00755	0.02108		
5/2/13				**-0.00502**				**0.02381**	**99.30**	**13.70**
6/6/13	B	-0.01545	-0.01525	-0.00597	L	0.00455	0.00440	0.03124	95.20	23.00
6/6/13	T	0.00075	0.00035	-0.01600	R	-0.00735	-0.00685	0.02108		
6/6/13				**-0.01099**				**0.02616**	**95.20**	**23.00**
7/11/13	B	-0.01560	-0.01525	-0.00635	L	0.00545	0.00490	0.03480	95.60	28.10
7/11/13	T	0.00010	-0.00015	-0.01892	R	-0.00580	-0.00545	0.02858		
7/11/13				**-0.01264**				**0.03169**	**95.60**	**28.10**
8/15/13	B	-0.01455	-0.01495	-0.00292	L	0.00440	0.00420	0.03035	96.30	18.30
8/15/13	T	0.00175	0.00140	-0.01080	R	-0.00710	-0.00695	0.02146		
8/15/13				**-0.00686**				**0.02591**	**96.30**	**18.30**
10/17/13	B	-0.01435	-0.01475	-0.00191	L	0.00310	0.00260	0.02299	96.20	9.20
10/17/13	T	0.00280	0.00325	-0.00343	R	-0.00805	-0.00890	0.01410		
10/17/13				**-0.00267**				**0.01854**	**96.20**	**9.20**
1/14/14	B	-0.01470	-0.01455	-0.00229	L	0.00975	0.00990	0.05842	96.90	5.00
1/14/14	T	0.00345	0.00315	-0.00203	R	-0.00270	-0.00270	0.04343		
1/14/14				**-0.00216**				**0.05093**	**96.90**	**5.00**
7/15/14	B	-0.01645	-0.01730	-0.01372	L	0.01810	0.01815	0.10058	98.80	22.10
7/15/14	T	-0.00090	-0.00125	-0.02426	R	0.00455	0.00380	0.07836		

Table 8.1-2. Interstate 49 barrier wall data for sections with moderate deterioration (cont.)

(EP-2)	**Horizontal**				**Vertical**				**RH**	
Date	ID	Read 1	Read 2	Strain (%)	ID	Read 1	Read 2	Strain (%)	RH (%)	T (°C)
7/15/14				**-0.01899**				**0.08947**	**98.80**	**22.10**
6/4/15	B	-0.01935	-0.01905	-0.02553	L	0.02695	0.02750	0.14681	96.90	24.40
6/4/15	T	-0.00415	-0.00415	-0.03988	R	0.01065	0.01130	0.11290		
6/4/15				**-0.03270**				**0.12986**	**96.90**	**24.40**
10/13/15	B	-0.01860	-0.01880	-0.02299	L	0.02620	0.02585	0.14072	64.30	14.70
10/13/15	T	-0.00255	-0.00250	-0.03162	R	0.00900	0.00950	0.10414		
10/13/15	B	-0.01900	-0.01900	-0.02451	L	0.02575	0.02590	0.13970	64.30	17.60
10/13/15	T	-0.00330	-0.00325	-0.03543	R	0.00945	0.00960	0.10554		
10/13/15				**-0.02997**				**0.12262**	**64.30**	**16.15**
3/14/16	B	-0.01925	-0.01965	-0.02680	L	0.02885	0.02935	0.15634		15.00
3/14/16	T	-0.00390	-0.00380	-0.03835	R	0.01210	0.01185	0.11798		
3/14/16	B	-0.01930	-0.01910	-0.02553	L	0.03000	0.03015	0.16129		19.60
3/14/16	T	-0.00405	-0.00390	-0.03899	R	0.01315	0.01255	0.12243		
3/14/16				**-0.03226**				**0.14186**	**N/A**	**17.30**
(S2-2)	**Horizontal**				**Vertical**				**RH**	
Date	ID	Read 1	Read 2	Strain (%)	ID	Read 1	Read 2	Strain (%)	RH (%)	T (°C)
1/31/13	B	0.01545	0.01560	0.00000	L	0.01340	0.01365	0.00000	97.55	0.40
1/31/13	T	-0.00690	-0.00695	0.00000	R	0.00390	0.00380	0.00000		
1/31/13				**0.00000**				**0.00000**	**97.55**	**0.40**
3/12/13	B	0.01565	0.01565	0.00064	L	0.01610	0.01590	0.01257	95.30	4.20
3/12/13	T	-0.00715	-0.00715	-0.00114	R	0.00695	0.00675	0.01524		
3/12/13				**-0.00025**				**0.01391**	**95.30**	**4.20**
5/2/13	B	0.01620	0.01590	0.00267	L	0.02105	0.02090	0.03785	99.80	15.00
5/2/13	T	-0.00755	-0.00770	-0.00356	R	0.01230	0.01205	0.04229		
5/2/13				**-0.00044**				**0.04007**	**99.80**	**15.00**
6/6/13	B	0.01585	0.01560	0.00102	L	0.02215	0.02195	0.04331	96.60	26.00
6/6/13	T	-0.00785	-0.00790	-0.00483	R	0.01360	0.01345	0.04915		
6/6/13				**-0.00191**				**0.04623**	**96.60**	**26.00**
7/11/13	B	0.01590	0.01590	0.00191	L	0.02380	0.02330	0.05093	96.10	30.00
7/11/13	T	-0.00810	-0.00810	-0.00597	R	0.01540	0.01565	0.05931		
7/11/13				**-0.00203**				**0.05512**	**96.10**	**30.00**
8/15/13	B	0.01625	0.01585	0.00267	L	0.02210	0.02220	0.04382	95.90	20.10
8/15/13	T	-0.00805	-0.00825	-0.00622	R	0.01370	0.01385	0.05042		
8/15/13				**-0.00178**				**0.04712**	**95.90**	**20.10**
10/17/13	B	0.01575	0.01550	0.00051	L	0.02065	0.02035	0.03543	95.10	10.00
10/17/13	T	-0.00910	-0.00905	-0.01092	R	0.01260	0.01225	0.04356		
10/17/13				**-0.00521**				**0.03950**	**95.10**	**10.00**
1/14/14	B	0.01515	0.01500	-0.00229	L	0.02270	0.02270	0.04661	94.00	6.20

Table 8.1-2. Interstate 49 barrier wall data for sections with moderate deterioration (cont.)

(S2-2)	**Horizontal**				**Vertical**				**RH**	
Date	ID	Read 1	Read 2	Strain (%)	ID	Read 1	Read 2	Strain (%)	RH (%)	T (°C)
1/14/14	T	-0.00955	-0.00950	-0.01321	R	0.01475	0.01455	0.05486		
1/14/14				**-0.00775**				**0.05074**	**94.00**	**6.20**
7/15/14	B	0.01425	0.01430	-0.00635	L	0.02685	0.02695	0.06795	95.80	24.30
7/15/14	T	-0.01040	-0.01040	-0.01765	R	0.01885	0.01875	0.07595		
7/15/14				**-0.01200**				**0.07195**	**95.80**	**24.30**
6/4/15	B	0.01175	0.01175	-0.01918	L	0.02810	0.02865	0.07544	95.20	26.60
6/4/15	T	-0.01365	-0.01345	-0.03366	R	0.01930	0.01980	0.07976		
6/4/15				**-0.02642**				**0.07760**	**95.20**	**26.60**
10/13/15	B	0.01195	0.01155	-0.01918	L	0.02685	0.02635	0.06642	68.30	16.00
10/13/15	T	-0.01405	-0.01400	-0.03607	R	0.01760	0.01785	0.07049		
10/13/15	B	0.01150	0.01145	-0.02057	L	0.02685	0.02630	0.06629	68.30	20.10
10/13/15	T	-0.01415	-0.01415	-0.03670	R	0.01715	0.01715	0.06756		
10/13/15				**-0.02864**				**0.06693**	**68.30**	**18.05**
3/14/16	B	0.01090	0.01060	-0.02426	L	0.02580	0.02605	0.06299	96.30	15.00
3/14/16	T	-0.01560	-0.01545	-0.04369	R	0.01745	0.01750	0.06922		
3/14/16	B	0.01100	0.01100	-0.02299	L	0.02680	0.02700	0.06795	96.30	19.60
3/14/16	T	-0.01525	-0.01510	-0.04191	R	0.01840	0.01835	0.07379		
3/14/16				**-0.03245**				**0.07087**	**96.30**	**17.30**

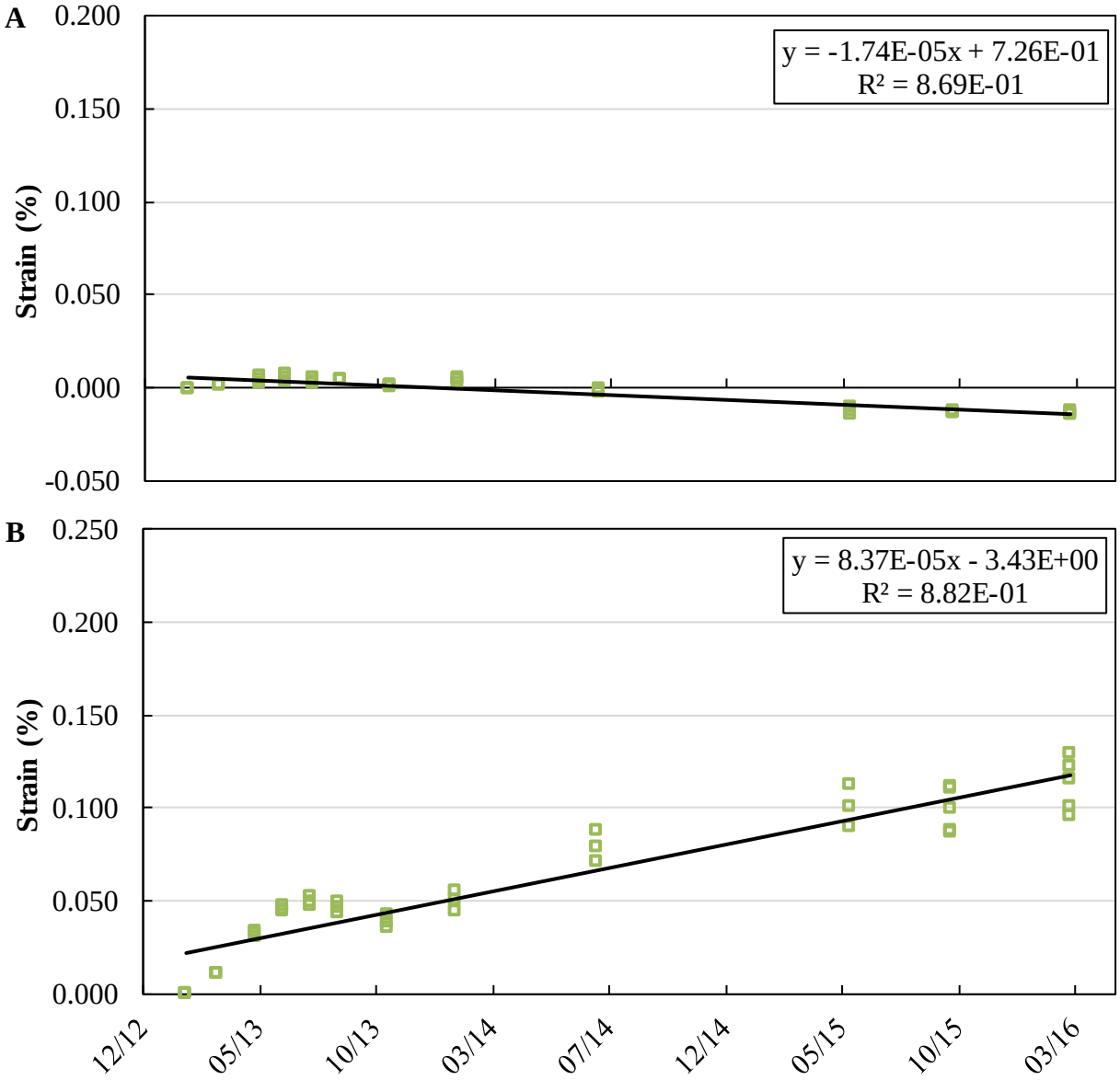

Fig. 8.1-6–Horizontal (A) and vertical (B) strain (%) with respect to date, Interstate 49 barrier wall exhibiting moderate deterioration, control section (C-2).

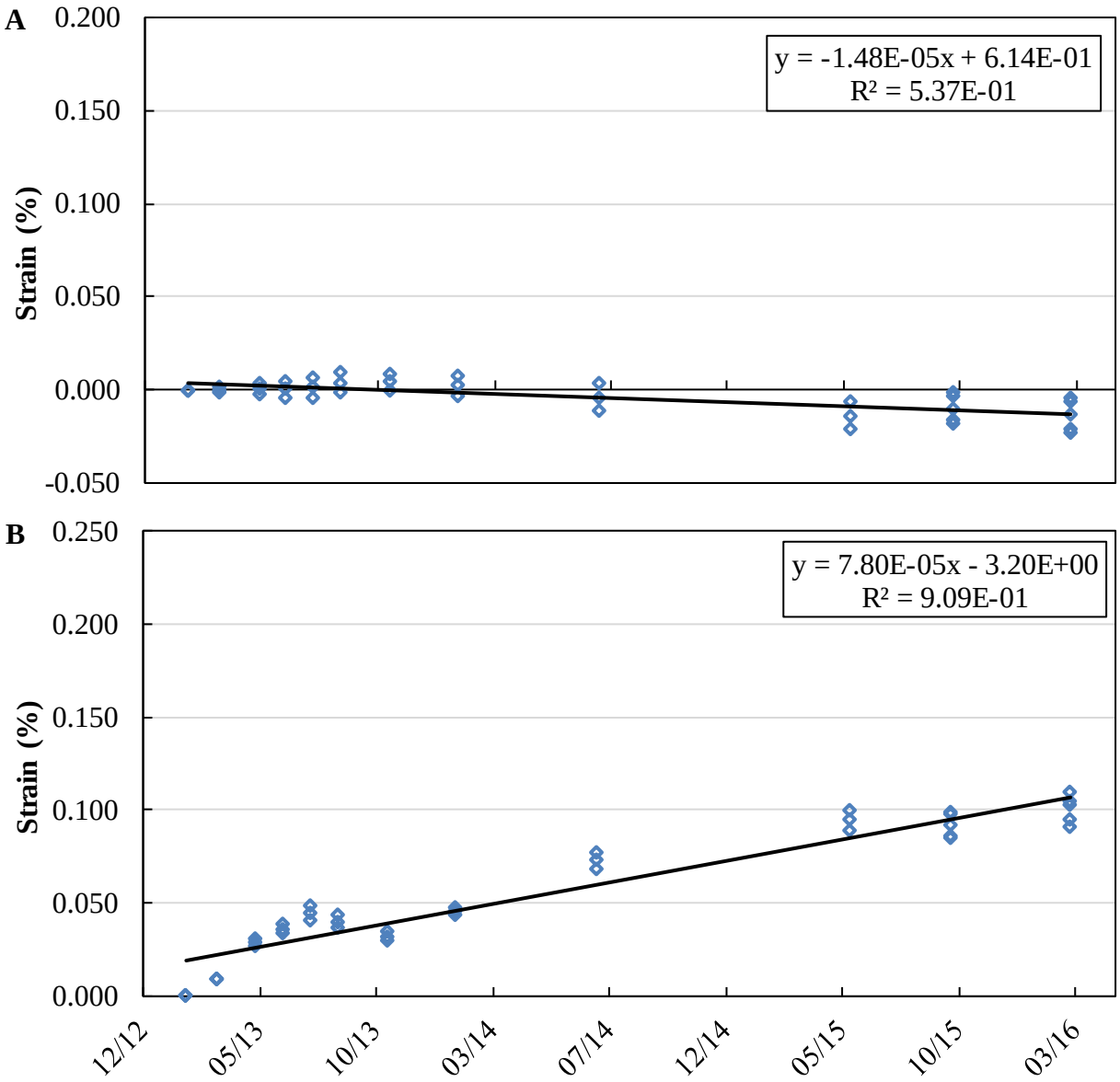

Fig. 8.1-7–Horizontal (A) and vertical (B) strain (%) with respect to date, Interstate 49 barrier wall exhibiting moderate deterioration, silane section (S-2).

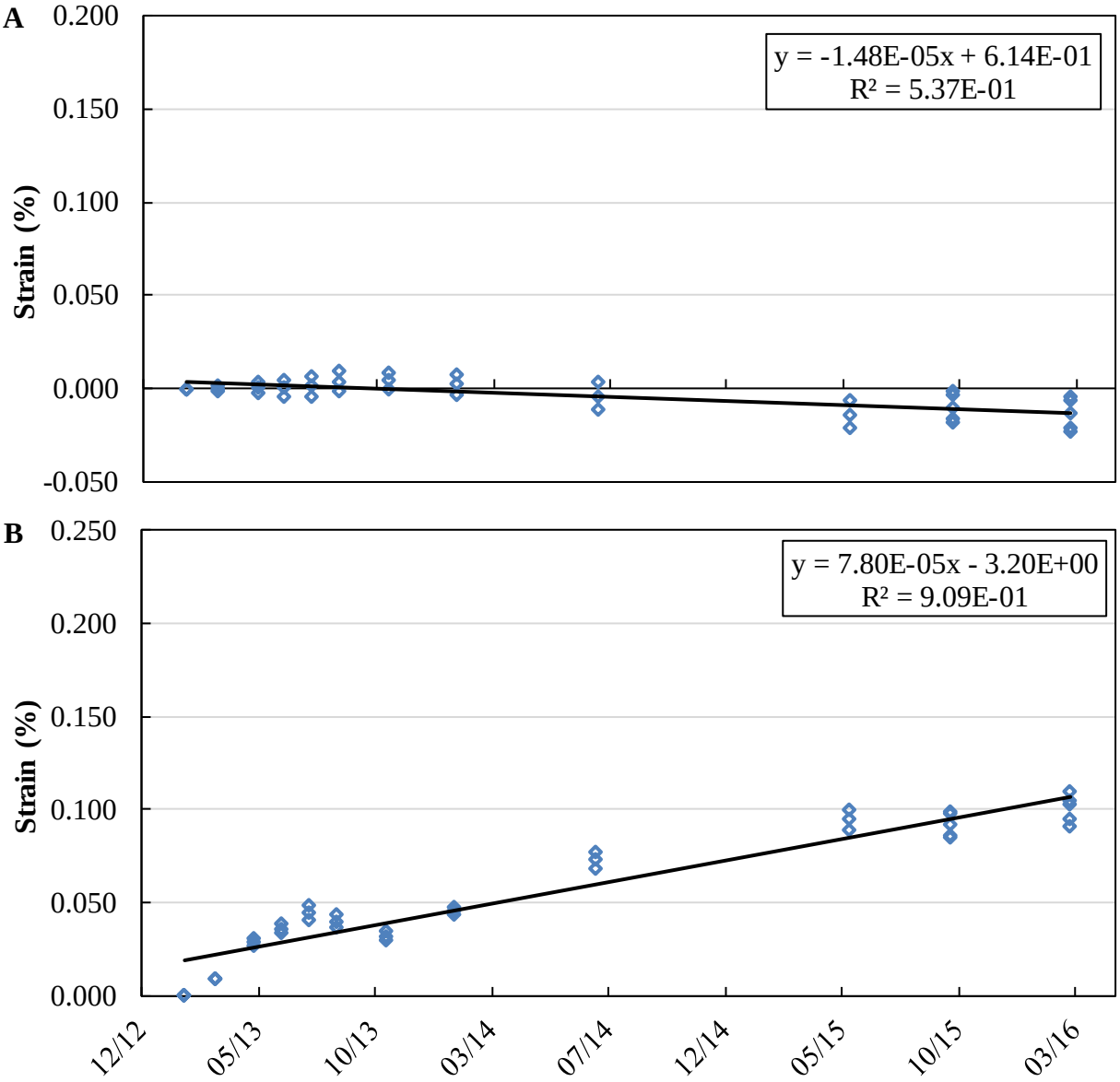

Fig. 8.1-8–Horizontal (A) and vertical (B) strain (%) with respect to date, Interstate 49 barrier wall exhibiting moderate deterioration, linseed section (L-2).

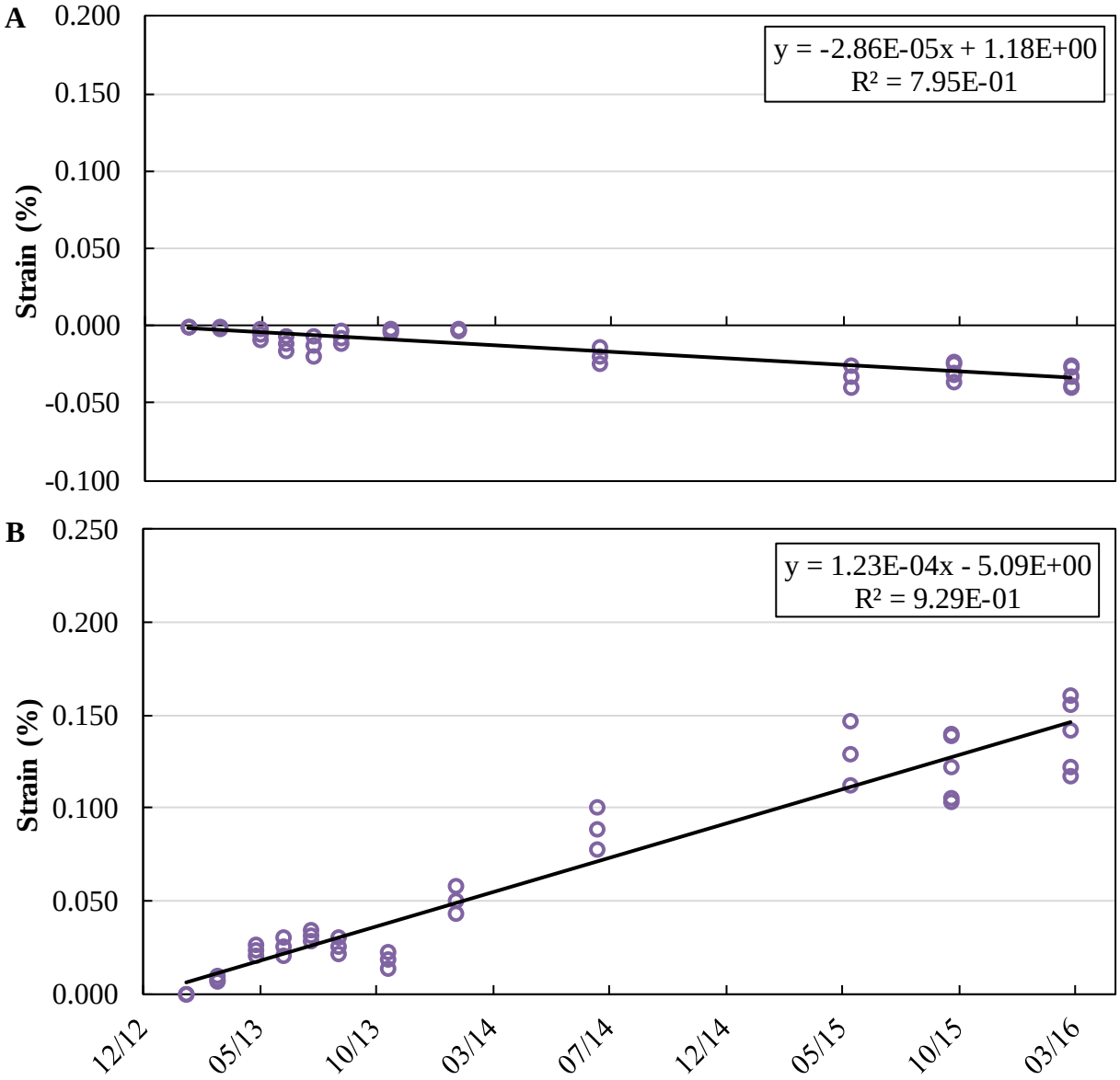

Fig. 8.1-9–Horizontal (A) and vertical (B) strain (%) with respect to date, Interstate 49 barrier wall exhibiting moderate deterioration, elastomeric paint section (EP-2).

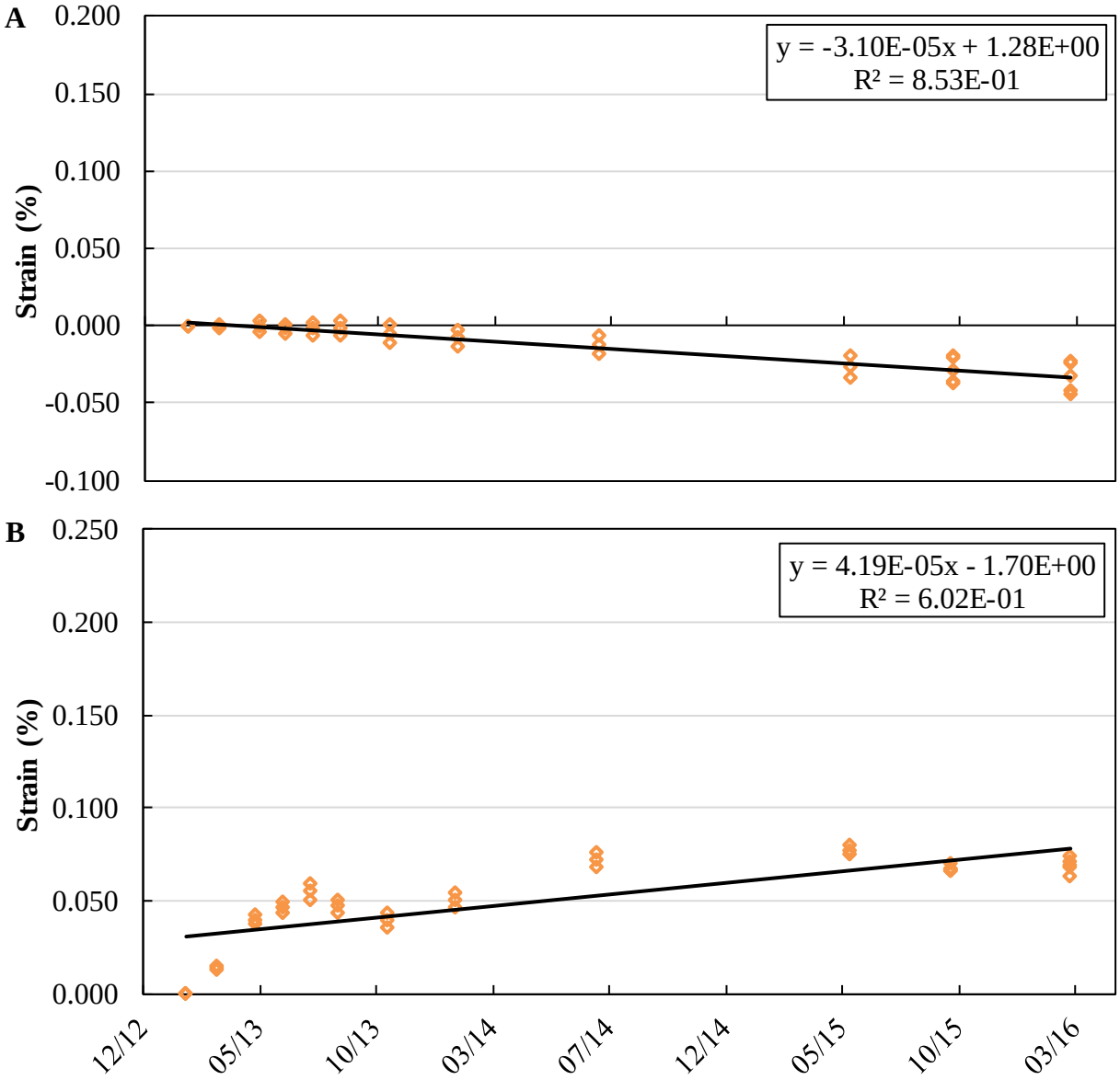

Fig. 8.1-10–Horizontal (A) and vertical (B) strain (%) with respect to date, Interstate 49 barrier wall exhibiting moderate deterioration, silane 2 section (S2-2).

Table 8.1-3 Interstate 49 barrier wall data for sections with severe deterioration

(C-3)	**Horizontal**				**Vertical**				**RH**	
Date	ID	Read 1	Read 2	Strain (%)	ID	Read 1	Read 2	Strain (%)	RH (%)	T (°C)
1/31/13	B	-0.02525	-0.02525	0.00000	L	0.02655	0.02640	0.00000	95.85	2.40
1/31/13	T	-0.09795	-0.09805	0.00000	R	-0.04415	-0.04445	0.00000		
1/31/13				**0.00000**				**0.00000**	**95.85**	**2.40**
3/12/13	B	-0.02495	-0.02520	0.00089	L	0.02940	0.02930	0.01461	92.00	8.90
3/12/13	T	-0.09795	-0.09785	0.00051	R	-0.04040	-0.04070	0.01905		
3/12/13				**0.00070**				**0.01683**	**92.00**	**8.90**
5/2/13	B	-0.02465	-0.02475	0.00279	L	0.03620	0.03605	0.04902	99.70	14.70
5/2/13	T	-0.09790	-0.09780	0.00076	R	-0.03330	-0.03320	0.05613		
5/2/13				**0.00178**				**0.05258**	**99.70**	**14.70**
6/6/13	B	-0.02465	-0.02470	0.00292	L	0.03770	0.03745	0.05639	96.70	27.60
6/6/13	T	-0.09790	-0.09760	0.00127	R	-0.03155	-0.03185	0.06401		
6/6/13				**0.00210**				**0.06020**	**96.70**	**27.60**
7/11/13	B	-0.02435	-0.02465	0.00381	L	0.03900	0.03860	0.06261	97.10	30.70
7/11/13	T	-0.09770	-0.09940	-0.00279	R	-0.03030	-0.03020	0.07137		
7/11/13				**0.00051**				**0.06699**	**97.10**	**30.70**
8/15/13	B	-0.02405	-0.02425	0.00559	L	0.03825	0.03840	0.06020	97.90	20.10
8/15/13	T	-0.09710	-0.09735	0.00394	R	-0.03085	-0.03115	0.06756		
8/15/13				**0.00476**				**0.06388**	**97.90**	**20.10**
10/17/13	B	-0.02435	-0.02435	0.00457	L	0.03680	0.03660	0.05194	96.50	10.90
10/17/13	T	-0.09755	-0.09760	0.00216	R	-0.03285	-0.03325	0.05715		
10/17/13				**0.00337**				**0.05455**	**96.50**	**10.90**
1/14/14	B	-0.02470	-0.02455	0.00318	L	0.04925	0.04935	0.11595	95.80	6.90
1/14/14	T	-0.09785	-0.09755	0.00152	R	-0.01825	-0.01790	0.13322		
1/14/14				**0.00235**				**0.12459**	**95.80**	**6.90**
7/15/14	B	-0.02540	-0.02585	-0.00191	L	0.06255	0.06265	0.18352	99.80	25.30
7/15/14	T	-0.09760	-0.09760	0.00203	R	-0.00115	-0.00110	0.21933		
7/15/14				**0.00006**				**0.20142**	**99.80**	**25.30**
6/4/15	B	-0.02820	-0.02815	-0.01486	L	0.08030	0.08060	0.27419	97.20	27.50
6/4/15	T	-0.09805	-0.09770	0.00064	R	0.02125	0.02190	0.33465		
6/4/15				**-0.00711**				**0.30442**	**97.20**	**27.50**
10/13/15	B	-0.02725	-0.02720	-0.01003	L	0.08065	0.08055	0.27496	70.70	17.90
10/13/15	T	-0.09840	-0.09855	-0.00241	R	0.02190	0.02180	0.33604		
10/13/15	B	-0.02730	-0.02750	-0.01092	L	0.08085	0.08060	0.27559	70.70	21.50
10/13/15	T	-0.09850	-0.09865	-0.00292	R	0.02205	0.02200	0.33693		
10/13/15				**-0.00692**				**0.30626**	**70.70**	**19.70**
3/14/16	B	-0.02770	-0.02770	-0.01245	L	0.08510	0.08575	0.29947	93.90	15.00
3/14/16	T	-0.09705	-0.09710	0.00470	R	0.02950	0.02955	0.37503		
3/14/16	B	-0.02825	-0.02860	-0.01613	L	0.08600	0.08630	0.30315	93.90	20.30

Table 8.1-3. Interstate 49 barrier wall data for sections with severe deterioration (cont.)

(C-3)	**Horizontal**				**Vertical**				**RH**	
Date	ID	Read 1	Read 2	Strain (%)	ID	Read 1	Read 2	Strain (%)	RH (%)	T (°C)
3/14/16	T	-0.09845	-0.09870	-0.00292	R	0.02990	0.03010	0.37744		
3/14/16				**-0.00953**				**0.34030**	**93.90**	**17.65**
(S-3)	**Horizontal**				**Vertical**				**RH**	
Date	ID	Read 1	Read 2	Strain (%)	ID	Read 1	Read 2	Strain (%)	RH (%)	T (°C)
1/31/13	B	0.00025	0.00040	0.00000	L	-0.00055	-0.00060	0.00000	97.50	3.10
1/31/13	T	0.05380	0.05390	0.00000	R	-0.01070	-0.01095	0.00000		
1/31/13				**0.00000**				**0.00000**	**97.50**	**3.10**
3/12/13	B	-0.00005	-0.00010	-0.00203	L	0.00380	0.00360	0.02172	95.20	8.60
3/12/13	T	0.05380	0.05375	-0.00038	R	-0.00635	-0.00625	0.02299		
3/12/13				**-0.00121**				**0.02235**	**95.20**	**8.60**
5/2/13	B	-0.00060	-0.00060	-0.00470	L	0.01095	0.01105	0.05880	99.80	15.00
5/2/13	T	0.05375	0.05360	-0.00089	R	0.00090	0.00060	0.05880		
5/2/13				**-0.00279**				**0.05880**	**99.80**	**15.00**
6/6/13	B	-0.00125	-0.00125	-0.00800	L	0.01250	0.01359	0.06919	97.20	27.80
6/6/13	T	0.05355	0.05350	-0.00165	R	0.00175	0.00175	0.06388		
6/6/13				**-0.00483**				**0.06654**	**97.20**	**27.80**
7/11/13	B	-0.00155	-0.00160	-0.00965	L	0.01290	0.01250	0.06744	97.30	31.10
7/11/13	T	0.05350	0.05345	-0.00191	R	0.00175	0.00200	0.06452		
7/11/13				**-0.00578**				**0.06598**	**97.30**	**31.10**
8/15/13	B	-0.00070	-0.00095	-0.00584	L	0.01160	0.01175	0.06223	97.90	21.10
8/15/13	T	0.05415	0.05380	0.00064	R	0.00015	0.00010	0.05563		
8/15/13				**-0.00260**				**0.05893**	**97.90**	**21.10**
10/17/13	B	-0.00055	-0.00040	-0.00406	L	0.00910	0.00920	0.04940	97.20	11.10
10/17/13	T	0.05395	0.05385	0.00025	R	-0.00250	-0.00330	0.04026		
10/17/13				**-0.00191**				**0.04483**	**97.20**	**11.10**
1/14/14	B	0.00030	0.00030	-0.00013	L	0.01730	0.01730	0.09081	96.40	6.60
1/14/14	T	0.05410	0.05400	0.00102	R	0.00395	0.00400	0.07518		
1/14/14				**0.00044**				**0.08299**	**96.40**	**6.60**
7/15/14	B	-0.00175	-0.00250	-0.01245	L	0.02550	0.02545	0.13233	99.80	25.30
7/15/14	T	0.05215	0.05205	-0.00889	R	0.01010	0.01015	0.10643		
7/15/14				**-0.01067**				**0.11938**	**99.80**	**25.30**
6/4/15	B	-0.00415	-0.00400	-0.02235	L	0.03990	0.03995	0.20574	98.20	27.20
6/4/15	T	0.04935	0.04955	-0.02235	R	0.01990	0.02000	0.15634		
6/4/15				**-0.02235**				**0.18104**	**98.20**	**27.20**
10/13/15	B	-0.00320	-0.00335	-0.01829	L	0.03890	0.03870	0.20003	72.00	18.20
10/13/15	T	0.05020	0.05020	-0.01854	R	0.01840	0.01805	0.14757		
10/13/15	B	-0.00345	-0.00370	-0.01981	L	0.03895	0.03880	0.20041	72.00	22.20
10/13/15	T	0.04990	0.04975	-0.02045	R	0.01825	0.01840	0.14808		

Table 8.1-3. Interstate 49 barrier wall data for sections with severe deterioration (cont.)

(S-3)	**Horizontal**				**Vertical**				**RH**	
Date	ID	Read 1	Read 2	Strain (%)	ID	Read 1	Read 2	Strain (%)	RH (%)	T (°C)
10/13/15				**-0.02013**				**0.17424**	**72.00**	**20.20**
3/14/16	B	-0.00315	-0.00350	-0.01854	L	0.04440	0.04415	0.22784	95.10	15.00
3/14/16	T	0.04950	0.05000	-0.02083	R	0.02270	0.02270	0.17031		
3/14/16	B	-0.00365	-0.00400	-0.02108	L	0.04460	0.04485	0.23012	95.10	22.10
3/14/16	T	0.04935	0.04900	-0.02375	R	0.02290	0.02315	0.17196		
3/14/16				**-0.02242**				**0.20104**	**95.10**	**18.55**
(L-3)	**Horizontal**				**Vertical**				**RH**	
Date	ID	Read 1	Read 2	Strain (%)	ID	Read 1	Read 2	Strain (%)	RH (%)	T (°C)
1/31/13	B	0.00280	0.00270	0.00000	L	-0.02065	-0.02045	0.00000	97.90	3.10
1/31/13	T	-0.04415	-0.04425	0.00000	R	-0.00035	-0.00010	0.00000		
1/31/13				**0.00000**				**0.00000**	**97.90**	**3.10**
3/12/13	B	0.00285	0.00285	0.00051	L	-0.01750	-0.01760	0.01524	95.80	9.20
3/12/13	T	-0.04430	-0.04420	-0.00025	R	0.00205	0.00210	0.01168		
3/12/13				**0.00013**				**0.01346**	**95.80**	**9.20**
5/2/13	B	0.00325	0.00325	0.00254	L	-0.01025	-0.01045	0.05182	100.00	15.50
5/2/13	T	-0.04415	-0.04420	0.00013	R	0.00865	0.00860	0.04496		
5/2/13				**0.00133**				**0.04839**	**100.00**	**15.50**
6/6/13	B	0.00305	0.00320	0.00191	L	-0.00935	-0.00970	0.05601	98.20	28.50
6/6/13	T	-0.04440	-0.04435	-0.00089	R	0.00975	0.00925	0.04940		
6/6/13				**0.00051**				**0.05271**	**98.20**	**28.50**
7/11/13	B	0.00320	0.00320	0.00229	L	-0.00875	-0.00905	0.05918	97.70	31.40
7/11/13	T	-0.04455	-0.04455	-0.00178	R	0.01080	0.01095	0.05639		
7/11/13				**0.00025**				**0.05779**	**97.70**	**31.40**
8/15/13	B	0.00360	0.00340	0.00381	L	-0.01025	-0.01000	0.05296	97.70	21.20
8/15/13	T	-0.04425	-0.04455	-0.00102	R	0.00950	0.00950	0.04940		
8/15/13				**0.00140**				**0.05118**	**97.70**	**21.20**
10/17/13	B	0.00263	0.00290	0.00008	L	-0.01280	-0.01245	0.04026	96.00	11.20
10/17/13	T	-0.04480	-0.04485	-0.00318	R	0.00685	0.00725	0.03696		
10/17/13				**-0.00155**				**0.03861**	**96.00**	**11.20**
1/14/14	B	0.00261	0.00260	-0.00074	L	-0.00705	-0.00730	0.06795	97.70	6.30
1/14/14	T	-0.04490	-0.04510	-0.00406	R	0.01265	0.01260	0.06528		
1/14/14				**-0.00240**				**0.06661**	**97.70**	**6.30**
7/15/14	B	0.00225	0.00195	-0.00330	L	0.00045	0.00075	0.10744	98.60	26.20
7/15/14	T	-0.04605	-0.04605	-0.00940	R	0.02160	0.02145	0.11049		
7/15/14				**-0.00635**				**0.10897**	**98.60**	**26.20**
6/4/15	B	-0.00025	-0.00010	-0.01486	L	0.01155	0.01120	0.16218	97.90	28.20
6/4/15	T	-0.04855	-0.04845	-0.02184	R	0.03325	0.03345	0.17056		
6/4/15				**-0.01835**				**0.16637**	**97.90**	**28.20**

Table 8.1-3. Interstate 49 barrier wall data for sections with severe deterioration (cont.)

(L-3)	**Horizontal**				**Vertical**				**RH**	
Date	ID	Read 1	Read 2	Strain (%)	ID	Read 1	Read 2	Strain (%)	RH (%)	T (°C)
10/13/15	B	0.00035	0.00020	-0.01257	L	0.01065	0.01050	0.15812	71.60	18.30
10/13/15	T	-0.04780	-0.04790	-0.01854	R	0.03245	0.03250	0.16612		
10/13/15	B	0.00020	-0.00010	-0.01372	L	0.01075	0.01045	0.15824	71.60	22.00
10/13/15	T	-0.04800	-0.04795	-0.01918	R	0.03205	0.03230	0.16459		
10/13/15				**-0.01645**				**0.16142**	**71.60**	**20.15**
3/14/16	B	-0.00010	-0.00020	-0.01473	L	0.01275	0.01320	0.17031	96.50	15.00
3/14/16	T	-0.04880	-0.04895	-0.02375	R	0.03570	0.03590	0.18301		
3/14/16	B	-0.00040	-0.00065	-0.01664	L	0.01350	0.01380	0.17374	96.50	21.50
3/14/16	T	-0.04900	-0.04910	-0.02464	R	0.03610	0.03635	0.18517		
3/14/16				**-0.02064**				**0.17945**	**96.50**	**18.25**
(EP-3)	**Horizontal**				**Vertical**				**RH**	
Date	ID	Read 1	Read 2	Strain (%)	ID	Read 1	Read 2	Strain (%)	RH (%)	T (°C)
1/31/13	B	0.01075	0.01060	0.00000	L	0.01260	0.01265	0.00000	97.75	3.20
1/31/13	T	-0.00500	-0.00490	0.00000	R	0.02475	0.02485	0.00000		
1/31/13				**0.00000**				**0.00000**	**97.75**	**3.20**
3/12/13	B	0.01045	0.01060	-0.00076	L	0.01650	0.01620	0.01892	95.80	8.90
3/12/13	T	-0.00510	-0.00495	-0.00038	R	0.02915	0.02880	0.02121		
3/12/13				**-0.00057**				**0.02007**	**95.80**	**8.90**
5/2/13	B	0.01075	0.01055	-0.00013	L	0.02355	0.02370	0.05588	99.70	13.70
5/2/13	T	-0.00490	-0.00515	-0.00038	R	0.03535	0.03510	0.05296		
5/2/13				**-0.00025**				**0.05442**	**99.70**	**13.70**
6/6/13	B	0.01000	0.01020	-0.00292	L	0.02380	0.02460	0.05880	95.90	24.30
6/6/13	T	-0.00525	-0.00540	-0.00191	R	0.03610	0.03565	0.05626		
6/6/13				**-0.00241**				**0.05753**	**95.90**	**24.30**
7/11/13	B	0.01020	0.01015	-0.00254	L	0.02510	0.02465	0.06223	95.00	29.80
7/11/13	T	-0.00510	-0.00520	-0.00102	R	0.03715	0.03735	0.06325		
7/11/13				**-0.00178**				**0.06274**	**95.00**	**29.80**
8/15/13	B	0.01085	0.01045	-0.00013	L	0.02400	0.02415	0.05817	95.30	19.80
8/15/13	T	-0.00460	-0.00475	0.00140	R	0.03605	0.03625	0.05766		
8/15/13				**0.00064**				**0.05791**	**95.30**	**19.80**
10/17/13	B	0.01085	0.01090	0.00102	L	0.02210	0.02261	0.04943	96.50	9.90
10/17/13	T	-0.00440	-0.00425	0.00318	R	0.03445	0.03490	0.05017		
10/17/13				**0.00210**				**0.04980**	**96.50**	**9.90**
1/14/14	B	0.01175	0.01170	0.00533	L	0.03905	0.03900	0.13411	97.60	5.20
1/14/14	T	-0.00320	-0.00320	0.00889	R	0.05045	0.05055	0.13056		
1/14/14				**0.00711**				**0.13233**	**97.60**	**5.20**
7/15/14	B	0.01005	0.00985	-0.00368	L	0.05535	0.05530	0.21692	95.80	22.90
7/15/14	T	-0.00485	-0.00460	0.00114	R	0.06610	0.06485	0.20663		

Table 8.1-3. Interstate 49 barrier wall data for sections with severe deterioration (cont.)

(EP-3)	**Horizontal**				**Vertical**				**RH**	
Date	ID	Read 1	Read 2	Strain (%)	ID	Read 1	Read 2	Strain (%)	RH (%)	T (°C)
7/15/14				**-0.00127**				**0.21177**	**95.80**	**22.90**
6/4/15	B	0.00770	0.00805	-0.01422	L	0.07960	0.07955	0.34011	96.40	25.30
6/4/15	T	-0.00595	-0.00625	-0.00584	R	0.08770	0.08820	0.32080		
6/4/15				**-0.01003**				**0.33045**	**96.40**	**25.30**
10/13/15	B	0.00890	0.00880	-0.00927	L	0.07895	0.07855	0.33592	66.20	16.10
10/13/15	T	-0.00500	-0.00490	0.00000	R	0.08740	0.08775	0.31890		
10/13/15	B	0.00860	0.00855	-0.01067	L	0.07915	0.07880	0.33706	66.20	19.00
10/13/15	T	-0.00525	-0.00530	-0.00165	R	0.08730	0.08780	0.31877		
10/13/15				**-0.00616**				**0.32791**	**66.20**	**17.55**
3/14/16	B	0.00880	0.00850	-0.01029	L	0.08960	0.09010	0.39230		15.00
3/14/16	T	-0.00485	-0.00455	0.00127	R	0.09805	0.09840	0.37300		
3/14/16	B	0.00830	0.00790	-0.01308	L	0.08970	0.09000	0.39230		20.70
3/14/16	T	-0.00505	-0.00500	-0.00038	R	0.09855	0.09895	0.37567		
3/14/16				**-0.00673**				**0.38399**	**N/A**	**17.85**
(S2-3)	**Horizontal**				**Vertical**				**RH**	
Date	ID	Read 1	Read 2	Strain (%)	ID	Read 1	Read 2	Strain (%)	RH (%)	T (°C)
1/31/13	B	0.07800	0.07805	0.00000	L	0.01310	0.01325	0.00000	97.60	3.30
1/31/13	T	0.00120	0.00115	0.00000	R	0.07315	0.07325	0.00000		
1/31/13				**0.00000**				**0.00000**	**97.60**	**3.30**
3/12/13	B	0.07800	0.07810	0.00013	L	0.01510	0.01490	0.00927	95.20	8.90
3/12/13	T	0.00120	0.00135	0.00051	R	0.07520	0.07505	0.00978		
3/12/13				**0.00032**				**0.00953**	**95.20**	**8.90**
5/2/13	B	0.07800	0.07780	-0.00064	L	0.01975	0.01970	0.03327	100.00	15.80
5/2/13	T	0.00140	0.00115	0.00051	R	0.07990	0.07980	0.03378		
5/2/13				**-0.00006**				**0.03353**	**100.00**	**15.80**
6/6/13	B	0.07710	0.07725	-0.00432	L	0.02140	0.02090	0.04051	97.70	27.60
6/6/13	T	0.00100	0.00120	-0.00038	R	0.08175	0.08125	0.04216		
6/6/13				**-0.00235**				**0.04134**	**97.70**	**27.60**
7/11/13	B	0.07700	0.07690	-0.00546	L	0.02275	0.02250	0.04801	97.30	31.70
7/11/13	T	0.00095	0.00100	-0.00102	R	0.08310	0.08305	0.05017		
7/11/13				**-0.00324**				**0.04909**	**97.30**	**31.70**
8/15/13	B	0.07750	0.07705	-0.00381	L	0.02140	0.02155	0.04216	97.60	21.30
8/15/13	T	0.00140	0.00135	0.00102	R	0.08160	0.08205	0.04382		
8/15/13				**-0.00140**				**0.04299**	**97.60**	**21.30**
10/17/13	B	0.07715	0.07745	-0.00368	L	0.01875	0.01925	0.02959	97.00	11.10
10/17/13	T	0.00105	0.00120	-0.00025	R	0.07945	0.07970	0.03239		
10/17/13				**-0.00197**				**0.03099**	**97.00**	**11.10**
1/14/14	B	0.07745	0.07730	-0.00330	L	0.02300	0.02295	0.04978	97.60	6.50

Table 8.1-3. Interstate 49 barrier wall data for sections with severe deterioration (cont.)

(S2-3)	**Horizontal**				**Vertical**				**RH**	
Date	ID	Read 1	Read 2	Strain (%)	ID	Read 1	Read 2	Strain (%)	RH (%)	T (°C)
1/14/14	T	0.00080	0.00080	-0.00191	R	0.08365	0.08275	0.05080		
1/14/14				**-0.00260**				**0.05029**	**97.60**	**6.50**
7/15/14	B	0.07655	0.07655	-0.00749	L	0.03090	0.03095	0.09017	97.30	25.50
7/15/14	T	-0.00020	-0.00025	-0.00711	R	0.09045	0.09055	0.08788		
7/15/14				**-0.00730**				**0.08903**	**97.30**	**25.50**
6/4/15	B	0.07425	0.07435	-0.01892	L	0.04000	0.04010	0.13653	97.40	27.90
6/4/15	T	-0.00260	-0.00265	-0.01930	R	0.09715	0.09755	0.12268		
6/4/15				**-0.01911**				**0.12960**	**97.40**	**27.90**
10/13/15	B	0.07490	0.07505	-0.01549	L	0.03915	0.03885	0.13119	70.00	17.90
10/13/15	T	-0.00215	-0.00205	-0.01664	R	0.09600	0.09585	0.11544		
10/13/15	B	0.07485	0.07460	-0.01676	L	0.03935	0.03920	0.13259	70.00	21.10
10/13/15	T	-0.00210	-0.00220	-0.01689	R	0.09600	0.09600	0.11582		
10/13/15				**-0.01683**				**0.12421**	**70.00**	**19.50**
3/14/16	B	0.07435	0.07480	-0.01753	L	0.04235	0.04260	0.14884	92.20	15.00
3/14/16	T	-0.00240	-0.00285	-0.01930	R	0.09850	0.09870	0.12903		
3/14/16	B	0.07460	0.07420	-0.01842	L	0.04205	0.04245	0.14770	92.20	19.90
3/14/16	T	-0.00295	-0.00275	-0.02045	R	0.09870	0.09915	0.13068		
3/14/16				**-0.01943**				**0.13919**	**92.20**	**17.45**

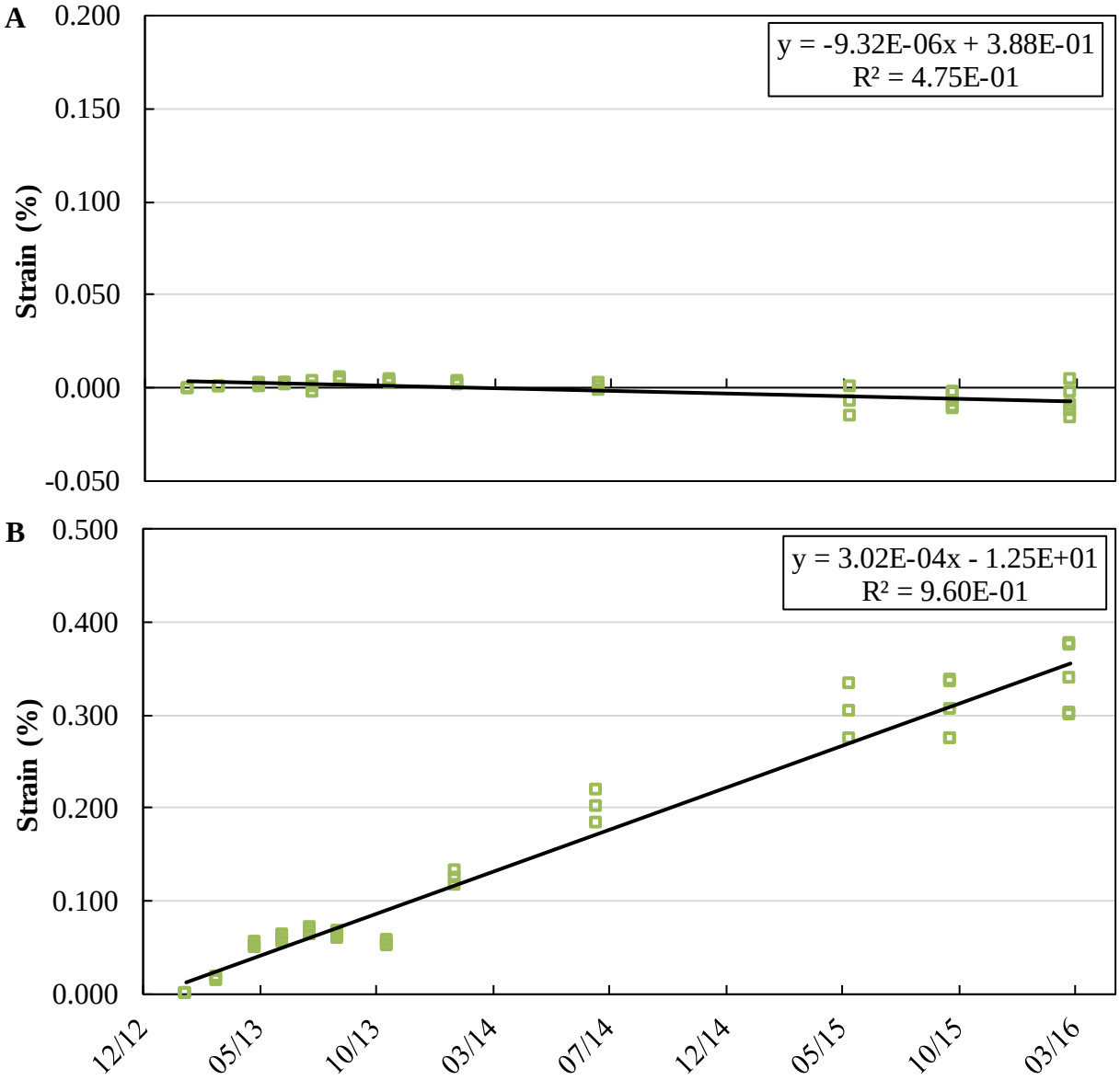

Fig. 8.1-11–Horizontal (A) and vertical (B) strain (%) with respect to date, Interstate 49 barrier wall exhibiting severe deterioration, control section (C-3).

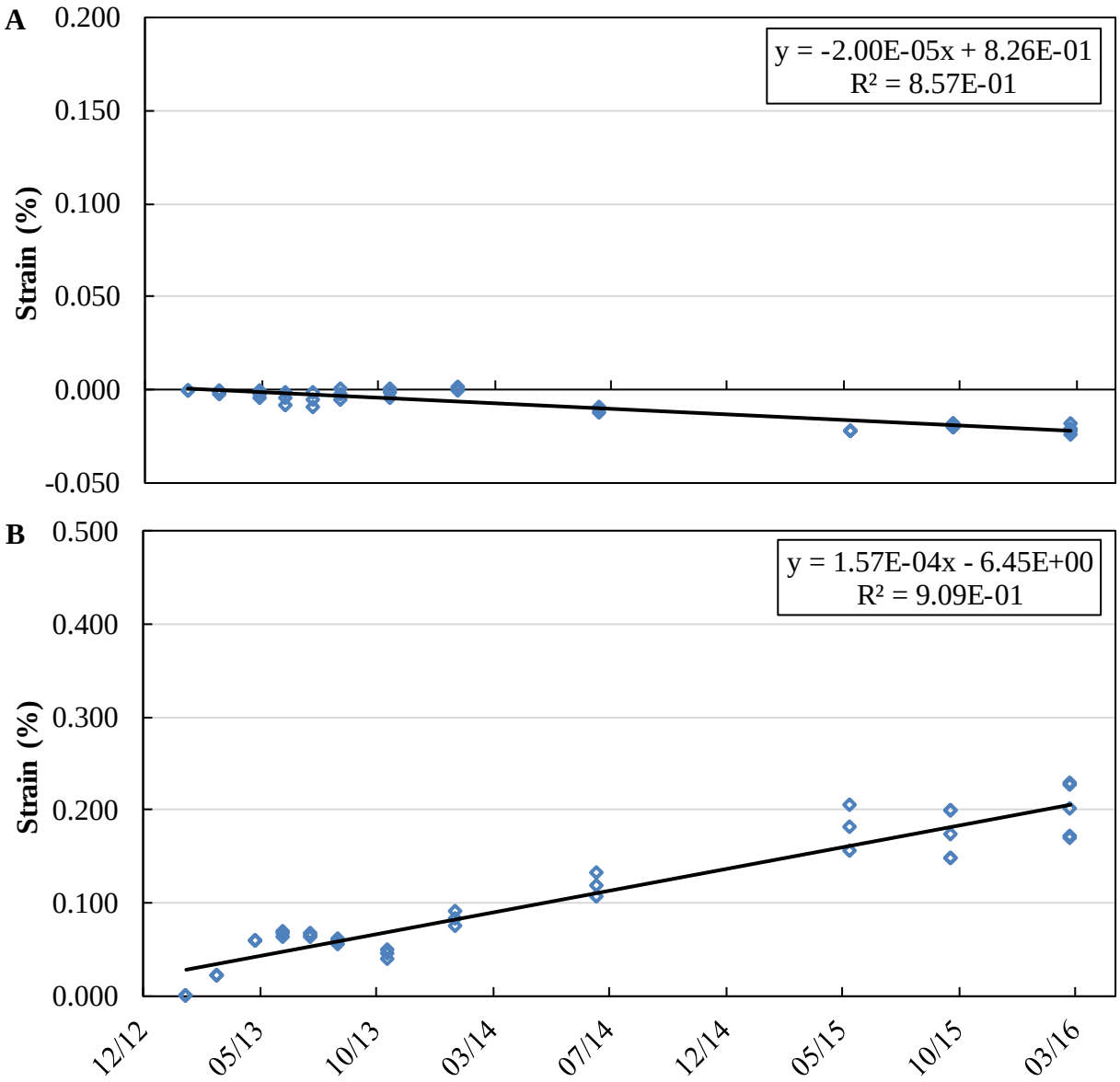

Fig. 8.1-12–Horizontal (A) and vertical (B) strain (%) with respect to date, Interstate 49 barrier wall exhibiting severe deterioration, silane section (S-3).

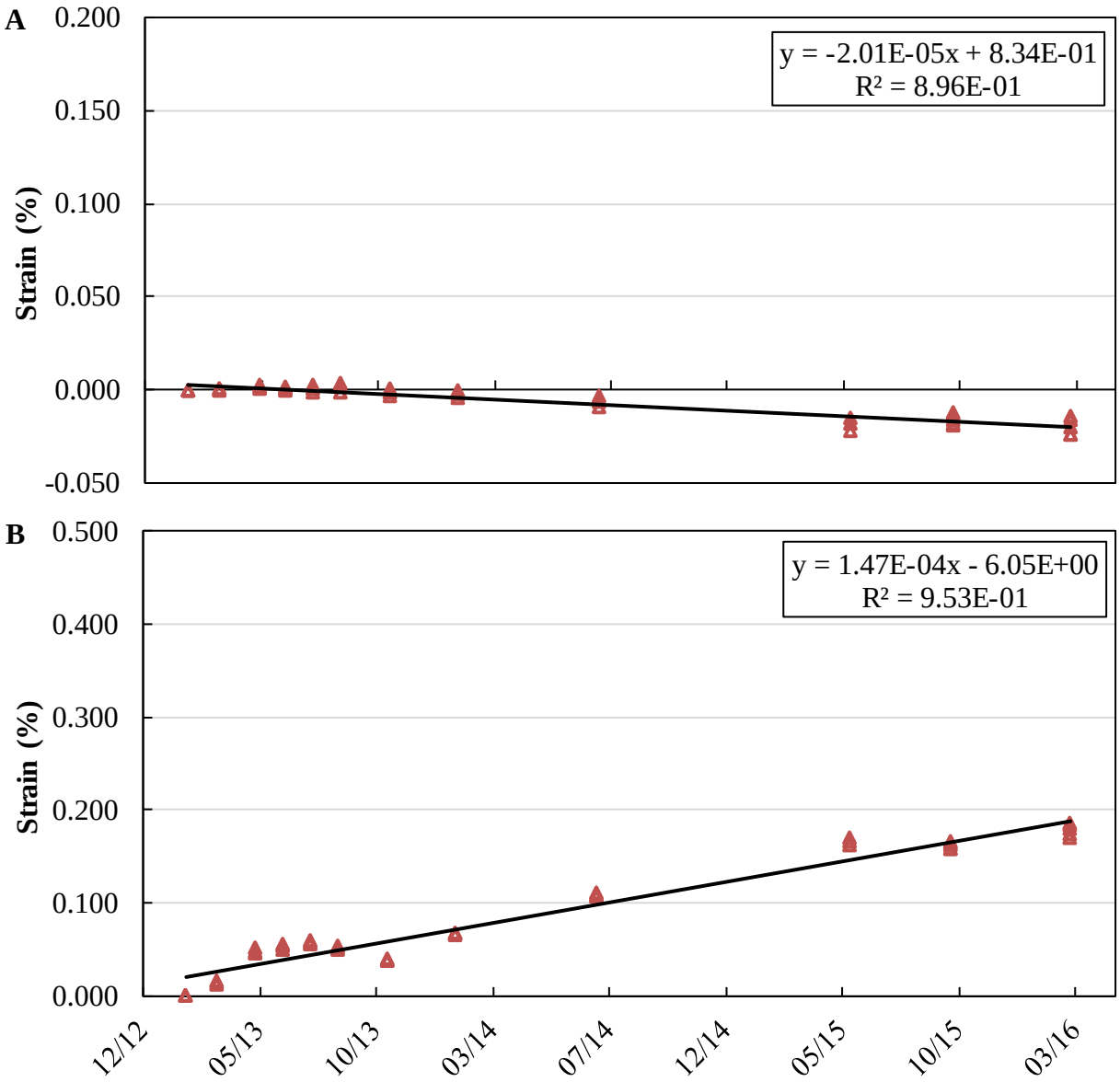

Fig. 8.1-13–Horizontal (A) and vertical (B) strain (%) with respect to date, Interstate 49 barrier wall exhibiting severe deterioration, linseed section (L-3).

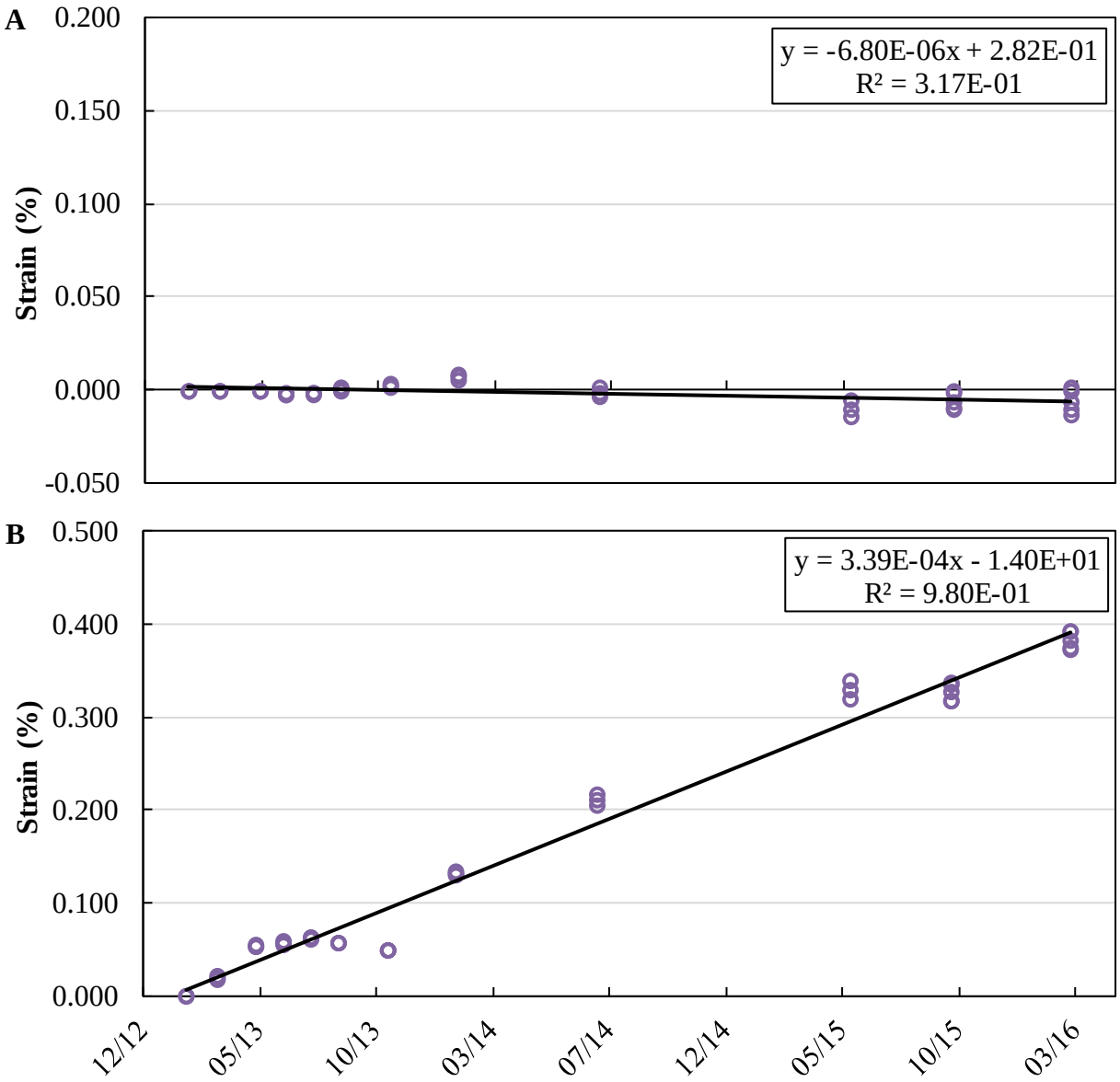

Fig. 8.1-14–Horizontal (A) and vertical (B) strain (%) with respect to date, Interstate 49 barrier wall exhibiting severe deterioration, elastomeric paint (EP-3).

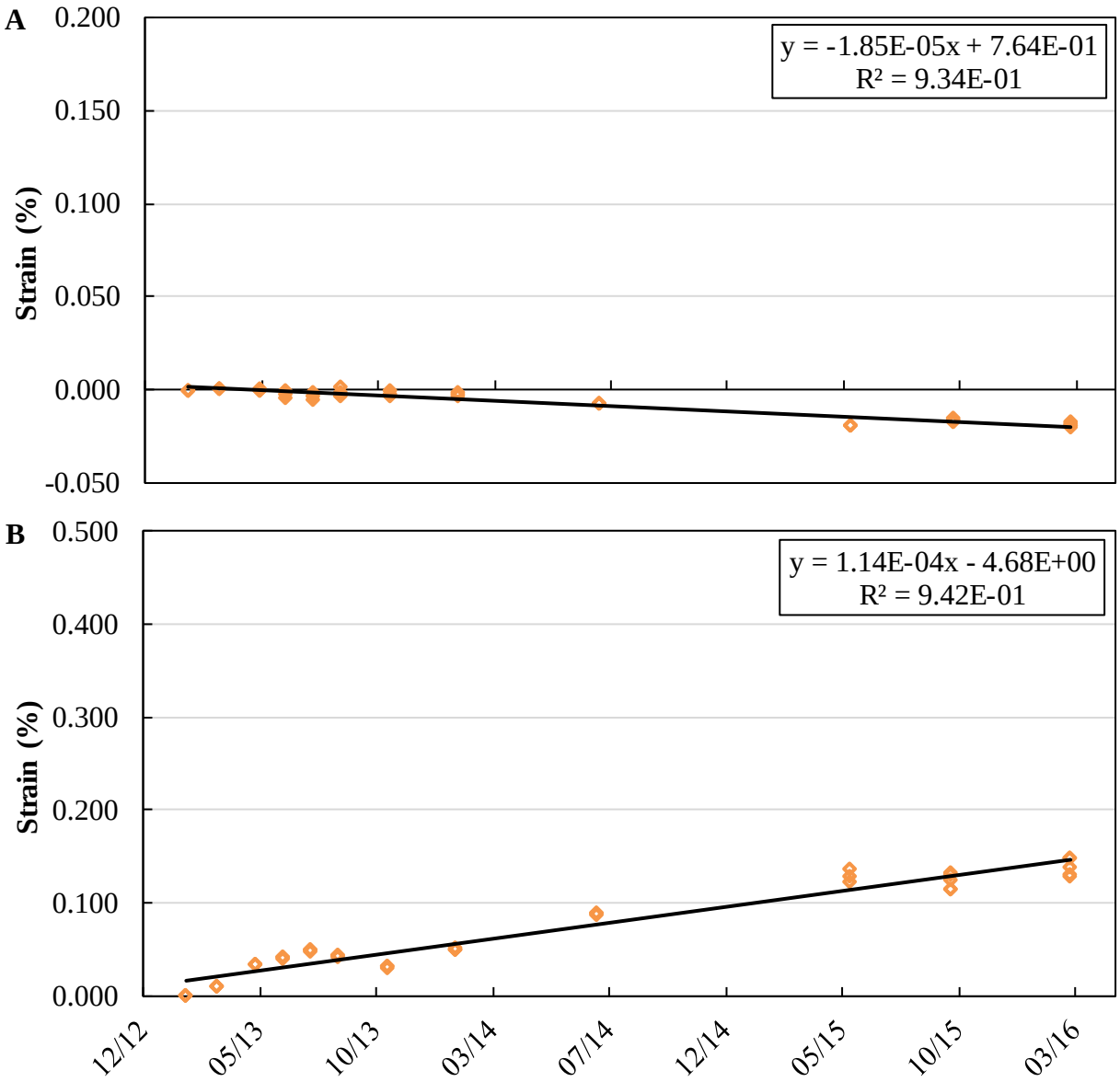

Fig. 8.1-15–Horizontal (A) and vertical (B) strain (%) with respect to date, Interstate 49 barrier wall exhibiting severe deterioration, silane 2 section (S2-3).

8.2. APPENDIX B: INTERSTATE 49 PAVEMENT DATA

Summary of data from Interstate 49 pavement. Data for the control sections is summarized in **Table 8.2-1**. The Silane 40A, Silane 100, and Silane 40B data are summarized in **Table 8.2-2**, **Table 8.2-3**, and **Table 8.2-4**, respectively. The strain data is also summarized in **Fig. 8.2-1**, **Fig. 8.2-2**, **Fig. 8.2-3**, and **Fig. 8.2-4** for the Control, Silane 40A, Silane 100, and Silane 40B, respectively. Note the initial data points from January 2014 are included in the tables, but were not used in calculating strain. The points were installed and initial readings taken a few hours later; however, it appears the epoxy had not sufficiently set and the readings varied significantly. Therefore, the May 2014 readings were used as initial readings for calculating strain. Temperature and RH readings were taken starting in January 2014. Gaps in the temperature and RH record indicate a sensor malfunction, while gaps in the stain record indicate the strain could not be read due to the distance between length-change pins being either too long or short for the DEMEC gauge to align.

Table 8.2-1. Interstate 49 control panels raw data

Control		**Travel**			**Transverse**			**RH**	
Date	ID	Read 1	Read 2	Strain	Read 1	Read 2	Strain	T	RH
1/14/14	1	-0.00875	-0.00895	0.00000	0.03915	0.03910	0.00000	20.00	89.50
1/14/14	1	-0.00595	-0.00580	0.00000	-0.02950	-0.02985	0.00000		
1/14/14	6	-0.00100	-0.00115	0.00000	0.08840	0.08860	0.00000	20.40	
1/14/14	6	-0.08480	-0.08480	0.00000	0.00570	0.00585	0.00000		
1/14/14	7	-0.04005	-0.04030	0.00000	0.07115	0.07125	0.00000	20.20	
1/14/14	7	--	--	--	-0.01995	-0.01995	0.00000		
1/14/14				**0.00000**			**0.00000**	**20.20**	**89.50**
5/15/14	1	-0.00915	-0.00915	0.00000	0.03930	0.03930	0.00000	13.50	97.10
5/15/14	1	-0.00460	-0.00460	0.00000	-0.03030	-0.03030	0.00000		
5/15/14	6	-0.00370	-0.00370	0.00000	0.08630	0.08630	0.00000	22.90	92.50
5/15/14	6	-0.08355	-0.08355	0.00000	0.00375	0.00375	0.00000		
5/15/14	7	-0.04010	-0.04010	0.00000	0.07170	0.07170	0.00000	20.40	92.40
5/15/14	7	--	--	--	-0.02120	-0.02120	0.00000		
5/15/14				**0.00000**			**0.00000**	**18.93**	**94.00**
9/9/14	1	-0.00795	-0.00815	0.00325	0.04085	0.04085	0.00701	25.00	97.60
9/9/14	1	-0.00305	-0.00315	0.01128	-0.02925	-0.02900	0.00224		
9/9/14	6	-0.00370	-0.00375	-0.01077	0.08810	0.08835	-0.00112	27.40	95.00
9/9/14	6	-0.08250	-0.08235	0.00965	0.00520	0.00515	-0.00244		
9/9/14	7	-0.03945	-0.03935	0.00315	0.07325	0.07350	0.00884	30.40	92.70
9/9/14	7	--	--	--	-0.02030	-0.02005	-0.00091		
9/9/14				**0.00331**			**0.00227**	**27.60**	**95.10**
3/24/15	1	-0.00835	-0.00860	0.00152	0.04025	0.04005	0.00417	14.90	97.70
3/24/15	1	-0.00330	-0.00325	0.01057	-0.03055	-0.03065	-0.00376		
3/24/15	6	-0.00305	-0.00355	-0.00904	0.08730	0.08750	-0.00447	16.60	93.50
3/24/15	6	-0.08245	-0.08280	0.00884	0.00485	0.00440	-0.00467		
3/24/15	7	-0.03995	-0.04000	0.00081	0.07230	0.07200	0.00386	18.10	91.80
3/24/15	7	--	--	--	-0.02160	-0.02155	-0.00660		
3/24/15	1	-0.00785	-0.00785	0.00406	0.04125	0.04135	0.00884	19.80	
3/24/15	1	-0.00255	-0.00270	0.01321	-0.02950	-0.02970	0.00030		
3/24/15	6	-0.00300	-0.00275	-0.00732	0.08795	0.08810	-0.00193	21.40	
3/24/15	6	-0.08235	-0.08220	0.01026	0.00505	0.00510	-0.00284		
3/24/15	7	-0.03865	-0.03885	0.00579	0.07380	0.07380	0.01057	21.10	
3/24/15	7	--	--	--	-0.01985	-0.01990	0.00030		
3/24/15				**0.00387**			**0.00031**	**18.65**	**94.33**
4/22/15	1	-0.00805	-0.00800	0.00335	0.04085	0.04080	0.00691	15.00	99.40
4/22/15	1	-0.00270	-0.00275	0.01280	-0.03010	-0.03010	-0.00173		
4/22/15	6	-0.00315	-0.00325	-0.00864	0.08700	0.08725	-0.00559	16.90	97.90
4/22/15	6	-0.08225	-0.08215	0.01057	0.00455	0.00445	-0.00518		

Table 8.2-1. Interstate 49 control panels raw data (cont.)

Control		**Travel**			**Transverse**			**RH**	
Date	ID	Read 1	Read 2	Strain	Read 1	Read 2	Strain	T	RH
4/22/15	7	-0.03945	-0.03946	0.00294	0.07255	0.07260	0.00559	18.00	97.10
4/22/15	7	--	--	--	-0.02120	-0.02140	-0.00549		
4/22/15	1	-0.00805	-0.00810	0.00315	0.04095	0.04095	0.00742	15.00	99.40
4/22/15	1	-0.00290	-0.00275	0.01240	-0.03000	-0.02995	-0.00122		
4/22/15	6	-0.00285	-0.00290	-0.00732	0.08750	0.08755	-0.00396	16.90	
4/22/15	6	-0.08210	-0.08195	0.01128	0.00500	0.00510	-0.00295		
4/22/15	7	-0.03860	-0.03860	0.00640	0.07375	0.07375	0.01036	18.00	
4/22/15	7	--	--	--	-0.01990	-0.01990	0.00020		
4/22/15				**0.00469**			**0.00036**	**16.63**	**98.45**
9/15/15	1	-0.00770	-0.00760	0.00488	0.04260	0.04260	0.01412	21.28	81.32
9/15/15	1	-0.00240	-0.00210	0.01473	-0.02920	-0.02920	0.00193		
9/15/15	6	-0.00365	-0.00375	-0.01067	0.08830	0.08830	-0.00081	21.97	85.64
9/15/15	6	-0.08230	-0.08225	0.01026	0.00560	0.00560	-0.00071		
9/15/15	7	-0.03870	-0.03860	0.00620	0.07435	0.07435	0.01280	21.86	76.17
9/15/15	7	--	--	--	-0.01960	-0.01960	0.00142		
9/15/15	1	-0.00725	-0.00760	0.00579	0.04345	0.04345	0.01758	30.40	
9/15/15	1	-0.00165	-0.00160	0.01727	-0.02840	-0.02840	0.00518		
9/15/15	6	-0.00350	-0.00370	-0.01026	0.08915	0.08915	0.00264	30.98	
9/15/15	6	-0.08230	-0.08200	0.01077	0.00650	0.00650	0.00295		
9/15/15	7	-0.03830	-0.03840	0.00742	0.07530	0.07530	0.01666	30.82	
9/15/15	7	--	--	--	-0.01860	-0.01860	0.00549		
9/15/15				**0.00564**			**0.00660**	**26.22**	**81.04**
2/29/16	1	-0.00700	-0.00720	0.00711	0.04045	0.04060	0.00569	19.40	82.83
2/29/16	1	-0.00345	-0.00340	0.00996	-0.03130	-0.03120	-0.00640		
2/29/16	6	-0.00435	-0.00440	-0.01341	0.08655	0.08655	-0.00792	19.40	87.46
2/29/16	6	-0.08290	-0.08285	0.00782	0.00415	0.00415	-0.00660		
2/29/16	7	-0.03915	-0.03920	0.00406	0.07295	0.07285	0.00691	19.40	88.70
2/29/16	7	--	--	--	-0.02135	-0.02125	-0.00549		
2/29/16	1	-0.00775	-0.00780	0.00437	0.04165	0.04195	0.01087	20.54	
2/29/16	1	-0.00180	-0.00175	0.01666	-0.03010	-0.03010	-0.00173		
2/29/16	6	-0.00425	-0.00415	-0.01270	0.08740	0.08740	-0.00447	21.40	
2/29/16	6	-0.08275	-0.08260	0.00864	0.00515	0.00515	-0.00254		
2/29/16	7	-0.03885	-0.03880	0.00549	0.07365	0.07365	0.00996	21.24	
2/29/16	7	--	--	--	-0.02030	-0.02025	-0.00132		
2/29/16				**0.00380**			**-0.00025**	**20.23**	**86.33**
5/26/16	1	-0.00760	-0.00775	0.00478	0.04350	0.04345	0.01768	25.90	
5/26/16	1	-0.00195	-0.00195	0.01595	-0.02865	-0.02855	0.00437		
5/26/16	6	-0.00405	-0.00400	-0.01199	0.08915	0.08925	0.00284	25.90	87.50
5/26/16	6	-0.08265	-0.08265	0.00874	0.00650	0.00600	0.00193		

Table 8.2-1. Interstate 49 control panels raw data (cont.)

Control		**Travel**			**Transverse**			**RH**	
Date	ID	Read 1	Read 2	Strain	Read 1	Read 2	Strain	T	RH
5/26/16	7	-0.03845	-0.03875	0.00640	0.07510	0.07510	0.01585	25.90	86.70
5/26/16	7	--	--	--	-0.01900	-0.01925	0.00335		
5/26/16	1	-0.00745	-0.00750	0.00559	0.04400	0.04415	0.02012	28.80	
5/26/16	1	-0.00175	-0.00185	0.01656	-0.02785	-0.02780	0.00752		
5/26/16	6	-0.00400	-0.00385	-0.01158	0.08860	0.08850	0.00020	30.90	
5/26/16	6	-0.08275	-0.08250	0.00884	0.00620	0.00625	0.00183		
5/26/16	7	-0.03860	-0.03860	0.00640	0.07545	0.07530	0.01697	31.30	
5/26/16	7	--	--	--	-0.01825	-0.01815	0.00711		
5/26/16				**0.00497**			**0.00831**	**28.12**	**87.10**
9/27/16	1	-0.00665	-0.00665	0.00894	0.04345	0.04345	0.01758	25.80	
9/27/16	1	-0.00080	-0.00080	0.02062	-0.02885	-0.02885	0.00335		
9/27/16	6	-0.00340	-0.00340	-0.00945	0.08800	0.08800	-0.00203	28.30	90.50
9/27/16	6	-0.08185	-0.08185	0.01199	0.00500	0.00500	-0.00315		
9/27/16	7	-0.03845	-0.03845	0.00701	0.07400	0.07400	0.01138	29.60	89.70
9/27/16	7	--	--	--	-0.01995	-0.01995	0.00000		
9/27/16	1	-0.00545	-0.00545	0.01382	0.04470	0.04470	0.02266		
9/27/16	1	0.00035	0.00035	0.02530	-0.02750	-0.02750	0.00884		
9/27/16	6	-0.00270	-0.00270	-0.00660	0.08955	0.08955	0.00427	29.20	
9/27/16	6	-0.08125	-0.08125	0.01443	0.00655	0.00655	0.00315		
9/27/16	7	-0.03765	-0.03765	0.01026	0.07530	0.07530	0.01666		
9/27/16	7	--	--	--	-0.01845	-0.01845	0.00610		
9/27/16				**0.00963**			**0.00740**	**28.23**	**90.10**

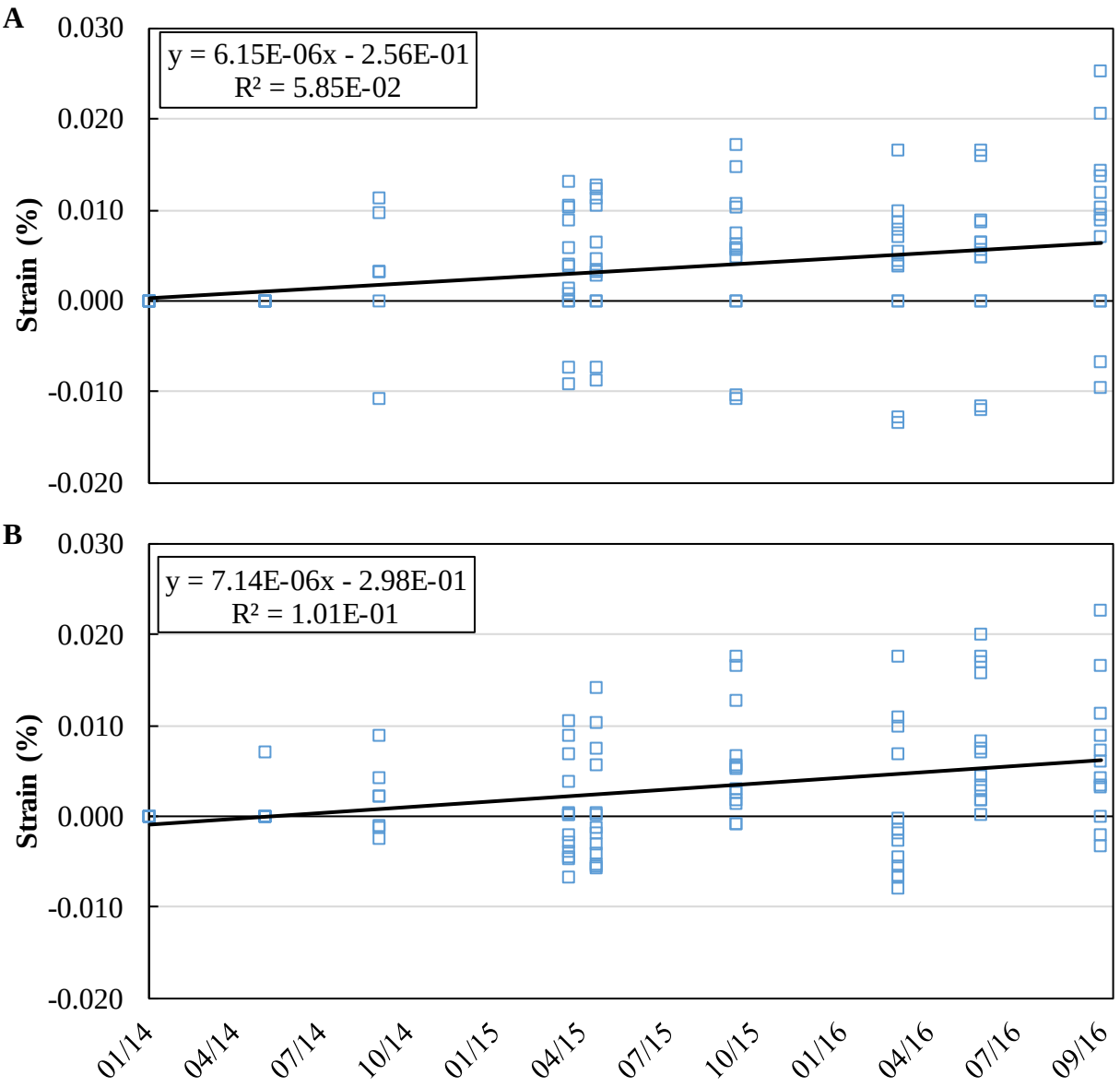

Fig. 8.2-1–Strain (%) with respect to time for Interstate 49 control panels, travel (A) and transverse (B).

Table 8.2-2. Interstate 49 Silane 40A panels raw data

Silane 40A		**Travel**			**Transverse**			**RH**	
Date	ID	1	2	Strain	1	2	Strain	T	RH
1/14/14	2	0.12005	0.12030	0.00000	0.07015	0.07030	0.00000	20.40	90.60
1/14/14	2	-0.08225	-0.08225	0.00000	0.08070	0.08055	0.00000		
1/14/14	3	-0.03840	-0.03855	0.00000	0.02315	0.02310	0.00000	20.20	84.50
1/14/14	3	--	--	--	-0.01795	-0.01805	0.00000		
1/14/14	10	0.13820	0.13830	0.00000	0.06290	0.06325	0.00000	20.00	95.90
1/14/14	10	--	--	--	0.09755	0.09750	0.00000		
1/14/14				**0.00000**			**0.00000**	**20.20**	**90.33**
5/15/14	2	0.11805	0.11820	0.00000	0.06975	0.06975	0.00000	13.50	90.30
5/15/14	2	-0.08230	-0.08230	0.00000	0.07935	0.07930	0.00000		
5/15/14	3	-0.03700	-0.03685	0.00000	0.02150	0.02150	0.00000	22.90	
5/15/14	3	--	--	--	-0.01825	-0.01825	0.00000		
5/15/14	10	0.13410	0.13405	0.00000	0.06220	0.06220	0.00000	20.40	92.80
5/15/14	10	--	--	--	0.09590	0.09590	0.00000		
5/15/14				**0.00000**			**0.00000**	**18.93**	**91.55**
9/9/14	2	0.11860	0.11855	-0.00650	0.07165	0.07175	0.00599	25.90	98.40
9/9/14	2	-0.08175	-0.08165	0.00224	0.08160	0.08165	0.00406		
9/9/14	3	-0.03640	-0.03640	0.00843	0.02295	0.02310	-0.00041	25.60	98.90
9/9/14	3	--	--	--	-0.01690	-0.01675	0.00478		
9/9/14	10	0.13435	0.13425	-0.01605	0.06400	0.06395	0.00366	32.10	94.30
9/9/14	10	--	--	--	0.09810	0.09805	0.00224		
9/9/14				**-0.00297**			**0.00339**	**27.87**	**97.20**
3/24/15	2	0.11770	0.11750	-0.01046	0.07020	0.07015	-0.00020	15.10	96.30
3/24/15	2	-0.08250	-0.08230	-0.00061	0.08010	0.07990	-0.00254		
3/24/15	3	-0.03735	-0.03735	0.00457	0.02135	0.02140	-0.00711	14.80	94.00
3/24/15	3	--	--	--	-0.01845	-0.01845	-0.00183		
3/24/15	10	0.13360	0.13355	-0.01900	0.06260	0.06270	-0.00173	19.80	92.50
3/24/15	10	--	--	--	0.09655	0.09645	-0.00417		
3/24/15	2	0.11805	0.11805	-0.00864	0.07135	0.07155	0.00498	19.80	
3/24/15	2	-0.08190	-0.08165	0.00193	0.08085	0.08085	0.00091		
3/24/15	3	-0.03675	-0.03655	0.00742	0.02245	0.02245	-0.00274	21.40	
3/24/15	3	--	--	--	-0.01720	-0.01730	0.00305		
3/24/15	10	0.13455	0.13470	-0.01473	0.06395	0.06385	0.00335	21.10	
3/24/15	10	--	--	--	0.09795	0.09780	0.00142		
3/24/15				**-0.00494**			**-0.00055**	**18.67**	**94.27**
4/22/15	2	0.11825	0.11825	-0.00782	0.07085	0.07060	0.00203	15.30	100.00
4/22/15	2	-0.08180	-0.08175	0.00193	0.08060	0.08065	0.00000		
4/22/15	3	-0.03645	-0.03660	0.00792	0.02230	0.02215	-0.00366	15.40	97.30
4/22/15	3	--	--	--	-0.01785	-0.01785	0.00061		

Table 8.2-2. Interstate 49 Silane 40A panels raw data (cont.)

Silane 40A		**Travel**			**Transverse**			**RH**	
Date	ID	1	2	Strain	1	2	Strain	T	RH
4/22/15	10	0.13360	0.13400	-0.01808	0.06285	0.06305	-0.00051	18.70	94.10
4/22/15	10	--	--	--	0.09675	0.09655	-0.00356		
4/22/15	2	0.11815	0.11825	-0.00803	0.07100	0.07100	0.00315		
4/22/15	2	-0.08205	-0.08190	0.00112	0.08085	0.08100	0.00122		
4/22/15	3	-0.03685	-0.03680	0.00671	0.02215	0.02240	-0.00345		
4/22/15	3	--	--	--	-0.01775	-0.01765	0.00122		
4/22/15	10	0.13400	0.13405	-0.01717	0.06325	0.06340	0.00102		
4/22/15	10	--	--	--	0.09720	0.09675	-0.00224		
4/22/15				**-0.00418**			**-0.00035**	**16.47**	**97.13**
9/15/15	2	0.11825	0.11840	-0.00752	0.07260	0.07260	0.00965	22.52	85.33
9/15/15	2	-0.08140	-0.08140	0.00345	0.08240	0.08240	0.00721		
9/15/15	3	-0.03670	-0.03655	0.00752	0.02330	0.02330	0.00071	22.26	85.53
9/15/15	3	--	--	--	-0.01685	-0.01685	0.00467		
9/15/15	10	0.13465	0.13460	-0.01473	0.06445	0.06445	0.00559	22.26	87.49
9/15/15	10	--	--	--	0.09850	0.09850	0.00396		
9/15/15	2	0.11840	0.11870	-0.00660	0.07360	0.07360	0.01372	29.62	
9/15/15	2	-0.08130	-0.08135	0.00376	0.08340	0.08340	0.01128		
9/15/15	3	-0.03605	-0.03625	0.00945	0.02415	0.02415	0.00417	29.73	
9/15/15	3	--	--	--	-0.01570	-0.01570	0.00935		
9/15/15	10	0.13495	0.13490	-0.01351	0.06535	0.06535	0.00925	30.82	
9/15/15	10	--	--	--	0.09915	0.09915	0.00660		
9/15/15				**-0.00227**			**0.00718**	**26.20**	**86.12**
2/29/16	2	0.11730	0.11730	-0.01168	0.07085	0.07095	0.00274	19.40	89.23
2/29/16	2	-0.08255	-0.08255	-0.00122	0.08055	0.08050	-0.00041		
2/29/16	3	-0.03765	-0.03765	0.00335	0.02140	0.02145	-0.00691	19.40	88.65
2/29/16	3	--	--	--	-0.01900	-0.01860	-0.00325		
2/29/16	10	0.13340	0.13340	-0.01971	0.06215	0.06210	-0.00386	19.40	81.90
2/29/16	10	--	--	--	0.09615	0.09610	-0.00569		
2/29/16	2	0.11785	0.11785	-0.00945	0.07200	0.07205	0.00732	24.60	
2/29/16	2	-0.08200	-0.08200	0.00102	0.08175	0.08175	0.00457		
2/29/16	3	-0.03710	-0.03710	0.00559	0.02245	0.02265	-0.00234	21.34	
2/29/16	3	--	--	--	-0.01785	-0.01745	0.00142		
2/29/16	10	0.13405	0.13405	-0.01707	0.06325	0.06340	0.00102	21.94	
2/29/16	10	--	--	--	0.09725	0.09725	-0.00112		
2/29/16				**-0.00615**			**-0.00054**	**21.01**	**86.59**
5/26/16	2	0.11805	0.11805	-0.00864	0.07310	0.07340	0.01229	25.90	
5/26/16	2	-0.08175	-0.08195	0.00163	0.08270	0.08315	0.00935		
5/26/16	3	-0.03695	-0.03700	0.00610	0.02435	0.02445	0.00518	25.90	96.20
5/26/16	3	--	--	--	-0.01565	-0.01565	0.00955		

Table 8.2-2. Interstate 49 Silane 40A panels raw data (cont.)

Silane 40A		**Travel**			**Transverse**			**RH**	
Date	ID	1	2	Strain	1	2	Strain	T	RH
5/26/16	10	0.13415	0.13415	-0.01666	0.06470	0.06470	0.00660	25.90	89.40
5/26/16	10	--	--	--	0.09880	0.09880	0.00518		
5/26/16	2	0.11820	0.11825	-0.00792	0.07400	0.07410	0.01554	31.00	
5/26/16	2	-0.08175	-0.08165	0.00224	0.08380	0.08360	0.01250		
5/26/16	3	-0.03665	-0.03660	0.00752	0.02370	0.02380	0.00254	31.40	
5/26/16	3	--	--	--	-0.01675	-0.01650	0.00559		
5/26/16	10	0.13470	0.13460	-0.01463	0.06535	0.06540	0.00935	31.30	
5/26/16	10	--	--	--	0.09945	0.09925	0.00742		
5/26/16				**-0.00380**			**0.00842**	**28.57**	**92.80**
9/27/16	2	0.11900	0.11900	-0.00478	0.07335	0.07335	0.01270	28.10	87.70
9/27/16	2	-0.08095	-0.08095	0.00528	0.08235	0.08235	0.00701		
9/27/16	3	-0.03585	-0.03590	0.01057	0.02315	0.02315	0.00010	28.20	87.60
9/27/16	3	--	--	--	-0.01725	-0.01710	0.00335		
9/27/16	10	0.13450	0.13440	-0.01544	0.06375	0.06375	0.00274	31.10	
9/27/16	10	--	--	--	0.09785	0.09805	0.00173		
9/27/16	2	0.12005	0.12005	-0.00051	0.07465	0.07465	0.01798	28.10	
9/27/16	2	-0.07985	-0.07995	0.00955	0.08400	0.08400	0.01372		
9/27/16	3	-0.03485	-0.03490	0.01463	0.02315	0.02315	0.00010	28.20	
9/27/16	3	--	--	--	-0.01625	-0.01625	0.00711		
9/27/16	10	0.13500	0.13530	-0.01260	0.06530	0.06530	0.00904	31.10	
9/27/16	10	--	--	--	0.09910	0.09910	0.00640		
9/27/16				**0.00084**			**0.00683**	**29.13**	**87.65**

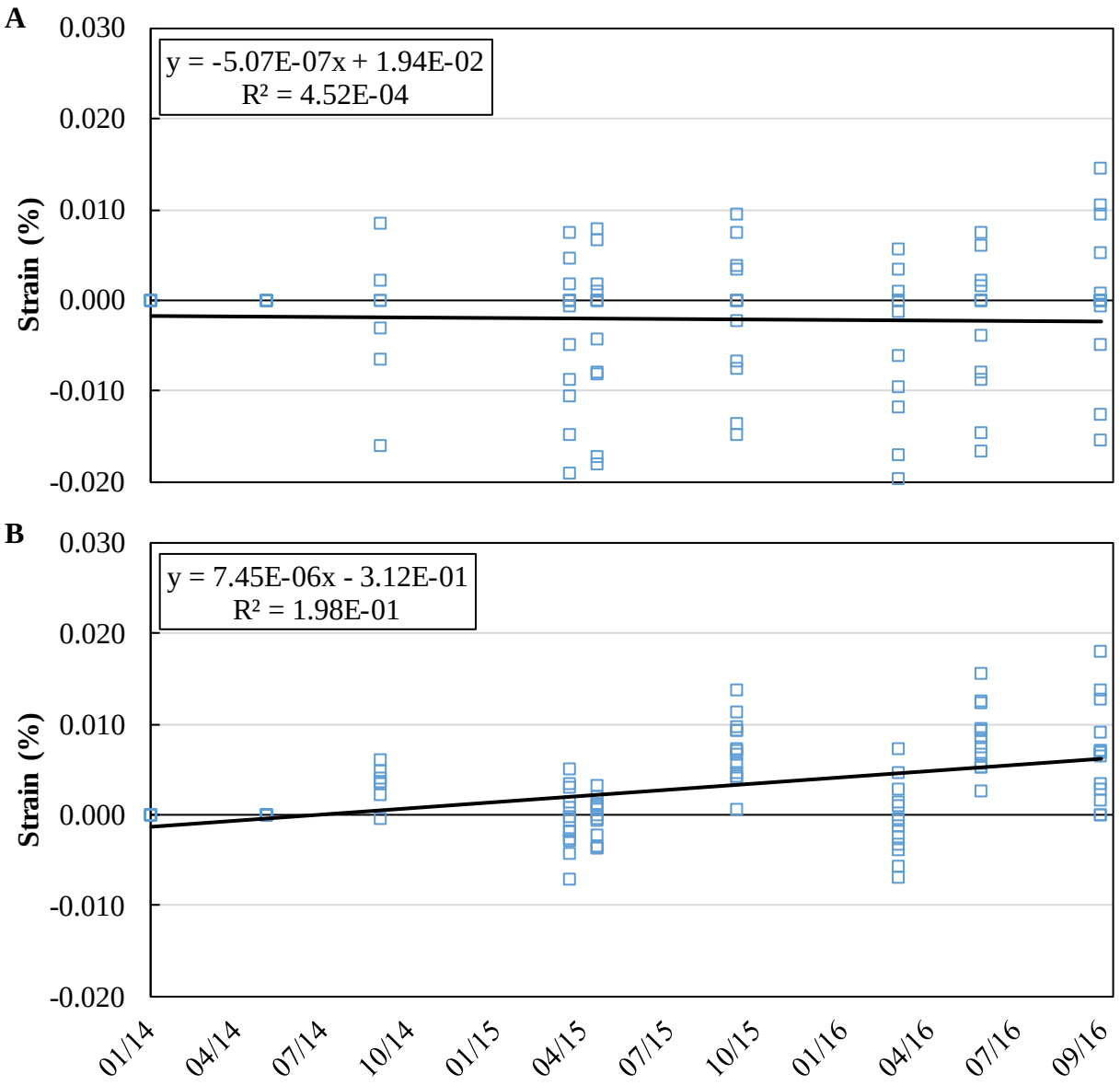

Fig. 8.2-2–Strain (%) with respect to time for Interstate 49 Silane 40A panels, travel (A) and transverse (B).

Table 8.2-3. Interstate 49 Silane 100 panels raw data

Silane 100		**Travel**			**Transverse**			**RH**	
Date	ID	1	2	Strain	1	2	Strain	T	RH
1/14/14	4	0.07965	0.07940	0.00000	0.02205	0.02205	0.00000	20.40	
1/14/14	4	-0.09505	-0.09520	0.00000	0.11845	0.11845	0.00000		
1/14/14	5	-0.01660	-0.01625	0.00000	0.00750	0.00745	0.00000	20.20	94.30
1/14/14	5	0.06120	0.06125	0.00000	0.03695	0.03690	0.00000		
1/14/14	11	0.06420	0.06440	0.00000	-0.03985	-0.03985	0.00000	20.00	98.20
1/14/14	11	-0.01040	-0.01045	0.00000	--	--	--		
1/14/14				**0.00000**			**0.00000**	**20.20**	**96.25**
5/15/14	4	0.07990	0.07995	0.00000	0.02035	0.02055	0.00000	15.50	
5/15/14	4	-0.09595	-0.09585	0.00000	0.11560	0.11580	0.00000		
5/15/14	5	-0.01470	-0.01465	0.00000	0.00770	0.00760	0.00000	22.90	
5/15/14	5	0.06180	0.06180	0.00000	0.03530	0.03510	0.00000		
5/15/14	11	0.06675	0.06715	0.00000	-0.04215	-0.04215	0.00000		
5/15/14	11	-0.01110	-0.01100	0.00000	--	--	--		
5/15/14				**0.00000**			**0.00000**	**19.20**	**N/A**
9/9/14	4	0.08055	0.08065	0.00437	0.02130	0.02135	-0.00295	26.70	97.40
9/9/14	4	-0.09540	-0.09350	0.00274	0.11775	0.11790	-0.00254		
9/9/14	5	-0.01415	-0.01410	0.00935	0.00885	0.00880	0.00549	27.20	98.00
9/9/14	5	0.06250	0.06250	0.00518	0.03695	0.03695	0.00010		
9/9/14	11	0.06780	0.06780	0.01422	-0.04065	-0.04075	-0.00345	31.90	96.80
9/9/14	11	-0.01025	-0.01040	0.00041	--	--	--		
9/9/14				**0.00605**			**-0.00067**	**28.60**	**97.40**
3/24/15	4	0.07970	0.07955	0.00041	0.01955	0.01959	-0.01008	15.70	96.80
3/24/15	4	-0.09645	-0.09640	-0.00528	0.11600	0.11590	-0.01016		
3/24/15	5	-0.01430	-0.01405	0.00914	0.00485	0.00530	-0.00975	15.20	97.50
3/24/15	5	0.06215	0.06215	0.00376	0.03610	0.03635	-0.00284		
3/24/15	11	0.06695	0.06700	0.01087	-0.04215	-0.04215	-0.00935	21.40	91.90
3/24/15	11	-0.01100	-0.01100	-0.00234	--	--	--		
3/24/15	4	0.08040	0.08050	0.00376	0.02105	0.02100	-0.00417	19.80	
3/24/15	4	-0.09545	-0.09510	-0.00061	0.11715	0.11665	-0.00630		
3/24/15	5	-0.01270	-0.01295	0.01463	0.00970	0.00950	0.00864	21.40	
3/24/15	5	0.06210	0.06255	0.00447	0.03680	0.03640	-0.00132		
3/24/15	11	0.06780	0.06780	0.01422	-0.04090	-0.04085	-0.00417	21.10	
3/24/15	11	-0.01050	-0.01045	-0.00020	--	--	--		
3/24/15				**0.00440**			**-0.00495**	**19.10**	**95.40**
4/22/15	4	0.08010	0.08010	0.00234	0.02030	0.02030	-0.00711	15.80	99.70
4/22/15	4	-0.09565	-0.09565	-0.00213	0.11590	0.11585	-0.01046		
4/22/15	5	-0.01410	-0.01425	0.00914	0.00855	0.00870	0.00467	16.90	100.00
4/22/15	5	0.06230	0.06235	0.00447	0.03535	0.03535	-0.00640		

Table 8.2-3. Interstate 49 Silane 100 panels raw data (cont.)

Silane 100		**Travel**			**Transverse**			**RH**	
Date	ID	1	2	Strain	1	2	Strain	T	RH
4/22/15	11	0.06710	0.06720	0.01158	-0.04195	-0.04215	-0.00894	21.40	96.40
4/22/15	11	-0.01140	-0.01120	-0.00356	--	--	--		
4/22/15	4	0.08030	0.08065	0.00386	0.02060	0.02065	-0.00579		
4/22/15	4	-0.09555	-0.09565	-0.00193	0.11640	0.11655	-0.00803		
4/22/15	5	-0.01380	-0.01410	0.01006	0.00935	0.00930	0.00752		
4/22/15	5	0.06230	0.06230	0.00437	0.03670	0.03675	-0.00081		
4/22/15	11	0.06720	0.06730	0.01199	-0.04155	-0.04155	-0.00691		
4/22/15	11	-0.01110	-0.01100	-0.00254	--	--	--		
4/22/15				**0.00397**			**-0.00423**	**18.03**	**98.70**
9/15/15	4	0.07970	0.08010	0.00152	0.02165	0.02165	-0.00163	22.47	85.57
9/15/15	4	-0.09560	-0.09545	-0.00163	0.11725	0.11725	-0.00488		
9/15/15	5	-0.01375	-0.01415	0.01006	0.00955	0.00955	0.00843	21.96	85.57
9/15/15	5	0.06250	0.06250	0.00518	0.03785	0.03785	0.00376		
9/15/15	11	0.06805	0.06815	0.01544	-0.04070	-0.04070	-0.00345	22.14	87.78
9/15/15	11	-0.01085	-0.01095	-0.00193	--	--	--		
9/15/15	4	0.08040	0.08035	0.00345	0.02255	0.02255	0.00203	29.77	
9/15/15	4	-0.09530	-0.09535	-0.00081	0.11805	0.11805	-0.00163		
9/15/15	5	-0.01360	-0.01365	0.01138	0.01045	0.01045	0.01209	29.76	
9/15/15	5	0.06265	0.06280	0.00610	0.03785	0.03785	0.00376		
9/15/15	11	0.06845	0.06845	0.01687	-0.03980	-0.03980	0.00020	30.98	
9/15/15	11	-0.01060	-0.01075	-0.00102	--	--	--		
9/15/15				**0.00538**			**0.00187**	**26.18**	**86.31**
2/29/16	4	0.07920	0.07915	-0.00142	0.01940	0.01895	-0.01168	19.40	93.33
2/29/16	4	-0.09675	-0.09640	-0.00589	0.11510	0.11495	-0.01392		
2/29/16	5	-0.01470	-0.01470	0.00701	0.00750	0.00770	0.00051	19.40	87.66
2/29/16	5	0.06165	0.06160	0.00163	0.03530	0.03530	-0.00660		
2/29/16	11	0.06695	0.06700	0.01087	-0.04285	-0.04290	-0.01229	19.40	84.52
2/29/16	11	-0.01200	-0.01210	-0.00660	--	--	--		
2/29/16	4	0.07925	0.07960	-0.00041	0.02030	0.02040	-0.00691	21.78	
2/29/16	4	-0.09590	-0.09600	-0.00335	0.11620	0.11625	-0.00904		
2/29/16	5	-0.01455	-0.01470	0.00732	0.00845	0.00845	0.00396	22.30	
2/29/16	5	0.06180	0.06195	0.00264	0.03600	0.03605	-0.00366		
2/29/16	11	0.06765	0.06755	0.01341	-0.04175	-0.04180	-0.00782	21.62	
2/29/16	11	-0.01150	-0.01145	-0.00427	--	--	--		
2/29/16				**0.00174**			**-0.00675**	**20.65**	**88.50**
5/26/16	4	0.08000	0.08000	0.00193	0.02180	0.02185	-0.00091	25.90	
5/26/16	4	-0.09585	-0.09585	-0.00295	0.11760	0.11765	-0.00335		
5/26/16	5	-0.01440	-0.01440	0.00823	0.01030	0.01030	0.01148	25.90	77.50
5/26/16	5	0.06205	0.06205	0.00335	0.03785	0.03785	0.00376		

Table 8.2-3. Interstate 49 Silane 100 panels raw data (cont.)

Silane 100		**Travel**			**Transverse**			**RH**	
Date	ID	1	2	Strain	1	2	Strain	T	RH
5/26/16	11	0.06770	0.06770	0.01382	-0.04060	-0.04055	-0.00295	25.90	79.60
5/26/16	11	-0.01135	-0.01135	-0.00376	--	--	--		
5/26/16	4	0.08005	0.08005	0.00213	0.02230	0.02230	0.00102	31.00	
5/26/16	4	-0.09585	-0.09585	-0.00295	0.11805	0.11785	-0.00203		
5/26/16	5	-0.01435	-0.01435	0.00843	0.00970	0.00975	0.00914	33.30	
5/26/16	5	0.06205	0.06205	0.00335	0.03745	0.03755	0.00234		
5/26/16	11	0.06785	0.06785	0.01443	-0.03990	-0.03990	-0.00020	32.30	
5/26/16	11	-0.01120	-0.01120	-0.00315	--	--	--		
5/26/16				**0.00357**			**0.00183**	**29.05**	**78.55**
9/27/16	4	0.08070	0.08045	0.00427	0.02125	0.02130	-0.00315	28.20	91.30
9/27/16	4	-0.09500	-0.09515	0.00020	0.11675	0.11665	-0.00711		
9/27/16	5	-0.01335	-0.01360	0.01199	0.00900	0.00880	0.00579	28.70	82.60
9/27/16	5	0.06315	0.06310	0.00772	0.03670	0.03670	-0.00091		
9/27/16	11	0.06730	0.06750	0.01260	-0.04175	-0.04160	-0.00742	28.10	91.70
9/27/16	11	-0.01150	-0.01140	-0.00417	--	--	--		
9/27/16	4	0.08155	0.08150	0.00813	0.02275	0.02275	0.00284	28.20	
9/27/16	4	-0.09420	-0.09420	0.00376	0.11855	0.11865	0.00061		
9/27/16	5	-0.01260	-0.01285	0.01504	0.01030	0.01010	0.01107	28.70	
9/27/16	5	0.06390	0.06385	0.01077	0.03805	0.03820	0.00488		
9/27/16	11	0.06805	0.06845	0.01605	-0.04020	-0.04030	-0.00163	28.10	
9/27/16	11	-0.01085	-0.01070	-0.00142	--	--	--		
9/27/16				**0.00708**			**0.00050**	**28.33**	**88.53**

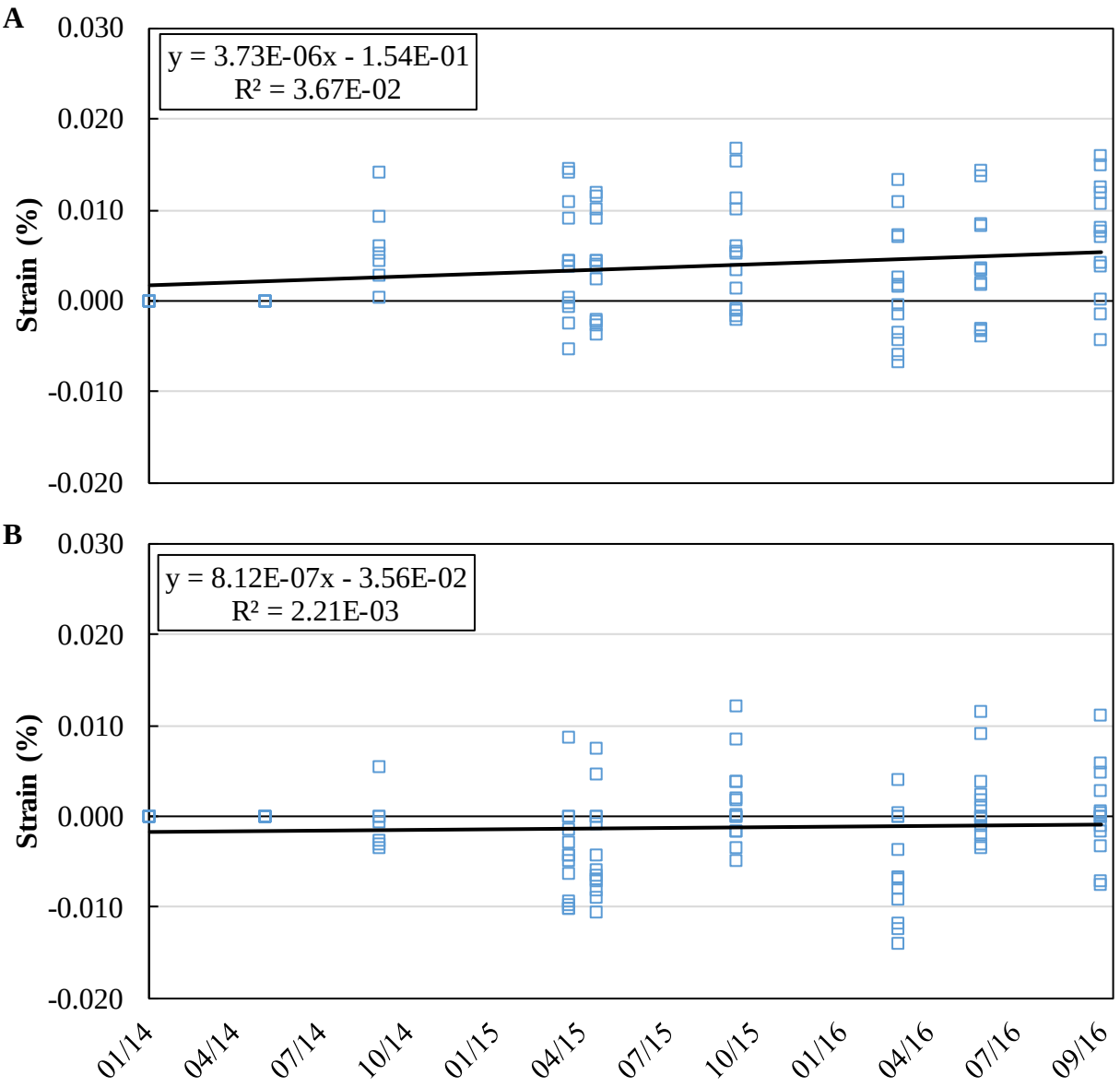

Fig. 8.2-3– Strain (%) with respect to time for Interstate 49 Silane 100 panels, travel (A) and transverse (B).

Table 8.2-4. Interstate 49 Silane 40B panels raw data

Silane 40B		**Travel**			**Transverse**			**RH**	
Date	ID	1	2	Strain	1	2	Strain	T	RH
1/14/14	8	-0.01170	-0.01180	0.00000	-0.01105	-0.01115	0.00000	20.40	97.10
1/14/14	8	-0.06025	-0.06035	0.00000	--	--	--		
1/14/14	9	--	--	--	0.04925	0.04925	0.00000	20.20	85.70
1/14/14	9	0.01085	0.01075	0.00000	-0.05090	-0.05085	0.00000		
1/14/14	12	0.05450	0.05440	0.00000	0.10315	0.10325	0.00000	20.00	
1/14/14	12	--	--	--	0.11645	0.11645	0.00000		
1/14/14				**0.00000**			**0.00000**	**20.20**	**91.40**
5/15/14	8	-0.01210	-0.01200	0.00000	-0.01165	-0.01165	0.00000	13.50	91.30
5/15/14	8	-0.05965	-0.05970	0.00000	--	--	--		
5/15/14	9	--	--	--	0.04870	0.04870	0.00000	22.90	95.20
5/15/14	9	0.01190	0.01175	0.00000	-0.05100	-0.05100	0.00000		
5/15/14	12	0.05475	0.05470	0.00000	0.10610	0.10610	0.00000	20.40	92.30
5/15/14	12	--	--	--	0.11630	0.11630	0.00000		
5/15/14				**0.00000**			**0.00000**	**18.93**	**92.93**
9/9/14	8	-0.01200	-0.01215	-0.00132	-0.00935	-0.00950	0.00681	30.90	91.90
9/9/14	8	-0.05950	-0.05960	0.00305	--	--	--		
9/9/14	9	--	--	--	0.05005	0.05005	0.00325	28.40	97.20
9/9/14	9	0.01255	0.01290	0.00782	-0.04910	-0.04910	0.00721		
9/9/14	12	0.05605	0.05620	0.00681	0.10805	0.10830	0.02022	31.10	94.50
9/9/14	12	--	--	--	0.11825	0.11820	0.00721		
9/9/14				**0.00409**			**0.00894**	**30.13**	**94.53**
3/24/15	8	-0.01270	-0.01265	-0.00376	-0.01100	-0.01085	0.00071	20.30	91.40
3/24/15	8	-0.06005	-0.05995	0.00122	--	--	--		
3/24/15	9	--	--	--	0.04955	0.04955	0.00122	15.60	96.30
3/24/15	9	0.01285	0.01305	0.00874	-0.04970	-0.04990	0.00437		
3/24/15	12	0.05505	0.05510	0.00254	0.10700	0.10685	0.01514	21.10	96.40
3/24/15	12	--	--	--	0.11640	0.11640	-0.00020		
3/24/15	8	-0.01140	-0.01155	0.00112	-0.00955	-0.00950	0.00640	19.80	
3/24/15	8	-0.05860	-0.05865	0.00681	--	--	--		
3/24/15	9	--	--	--	0.05010	0.05000	0.00325	21.40	
3/24/15	9	0.01315	0.01310	0.00945	-0.04935	-0.04905	0.00681		
3/24/15	12	0.05605	0.05615	0.00671	0.10815	0.10795	0.01971	21.10	
3/24/15	12	--	--	--	0.11790	0.11790	0.00589		
3/24/15				**0.00410**			**0.00633**	**19.88**	**94.70**
4/22/15	8	-0.01230	-0.01225	-0.00213	-0.01110	-0.01080	0.00061	18.70	100.00
4/22/15	8	-0.05935	-0.05935	0.00386	--	--	--		
4/22/15	9	--	--	--	0.04865	0.04895	-0.00183	18.00	98.90
4/22/15	9	0.01200	0.01240	0.00569	-0.05055	-0.05045	0.00152		

Table 8.2-4. Interstate 49 Silane 40B panels raw data (cont.)

Silane 40B		**Travel**			**Transverse**			**RH**	
Date	ID	1	2	Strain	1	2	Strain	T	RH
4/22/15	12	0.05530	0.05535	0.00356	0.10715	0.10720	0.01615	21.80	98.00
4/22/15	12	--	--	--	0.11655	0.11635	0.00000		
4/22/15	8	-0.01130	-0.01130	0.00183	-0.00965	-0.00960	0.00599		
4/22/15	8	-0.05850	-0.05850	0.00732	--	--	--		
4/22/15	9	--	--	--	0.05010	0.05010	0.00345		
4/22/15	9	0.01335	0.01320	0.01006	-0.04935	-0.04925	0.00640		
4/22/15	12	0.05545	0.05545	0.00406	0.10750	0.10780	0.01808		
4/22/15	12	--	--	--	0.11715	0.11720	0.00295		
4/22/15				**0.00428**			**0.00533**	**19.50**	**98.97**
9/15/15	8	-0.01165	-0.01180	0.00010	-0.00880	-0.00880	0.00935	22.08	86.63
9/15/15	8	-0.05890	-0.05890	0.00569	--	--	--		
9/15/15	9	--	--	--	0.05025	0.05025	0.00406	22.06	86.72
9/15/15	9	0.01325	0.01325	0.00996	-0.04890	-0.04890	0.00803		
9/15/15	12	0.05615	0.05600	0.00660	0.10955	0.10955	0.02581	22.12	86.88
9/15/15	12	--	--	--	0.11810	0.11810	0.00671		
9/15/15	8	-0.01155	-0.01140	0.00112	-0.00770	-0.00770	0.01382	30.35	
9/15/15	8	-0.05855	-0.05870	0.00681	--	--	--		
9/15/15	9	--	--	--	0.05025	0.05025	0.00406	30.40	
9/15/15	9	0.01350	0.01345	0.01087	-0.04810	-0.04810	0.01128		
9/15/15	12	0.05640	0.05650	0.00813	0.11055	0.11055	0.02987	30.50	
9/15/15	12	--	--	--	0.11935	0.11935	0.01179		
9/15/15				**0.00616**			**0.01248**	**26.25**	**86.74**
2/29/16	8	-0.01240	-0.01260	-0.00305	-0.01065	-0.01060	0.00193	19.40	86.73
2/29/16	8	-0.05955	-0.05975	0.00264	--	--	--		
2/29/16	9	--	--	--	0.04825	0.04835	-0.00386	19.40	88.80
2/29/16	9	0.01210	0.01190	0.00488	-0.05120	-0.05105	-0.00102		
2/29/16	12	0.05470	0.05455	0.00071	0.10740	0.10735	0.01697	19.40	87.69
2/29/16	12	--	--	--	0.11620	0.11610	-0.00122		
2/29/16	8	-0.01210	-0.01215	-0.00152	-0.00990	-0.00985	0.00498	21.77	
2/29/16	8	-0.05915	-0.05925	0.00447	--	--	--		
2/29/16	9	--	--	--	0.04935	0.04920	0.00010	21.15	
2/29/16	9	0.01270	0.01275	0.00782	-0.05010	-0.05005	0.00325		
2/29/16	12	0.05565	0.05550	0.00457	0.10870	0.10885	0.02266	21.97	
2/29/16	12	--	--	--	0.11770	0.11770	0.00508		
2/29/16				**0.00257**			**0.00489**	**20.52**	**87.74**
5/26/16	8	-0.01180	-0.01195	-0.00051	-0.00825	-0.00840	0.01128	25.90	88.90
5/26/16	8	-0.05900	-0.05910	0.00508	--	--	--		
5/26/16	9	--	--	--	0.05155	0.05155	0.00935	25.90	87.90

Table 8.2-4. Interstate 49 Silane 40B panels raw data (cont.)

Silane 40B		**Travel**			**Transverse**			**RH**	
Date	ID	1	2	Strain	1	2	Strain	T	RH
5/26/16	9	0.01270	0.01270	0.00772	-0.04805	-0.04785	0.01189		
5/26/16	12	0.05565	0.05550	0.00457	0.10980	0.10990	0.02703	25.90	93.10
5/26/16	12	--	--	--	0.11830	0.11840	0.00772		
5/26/16	8	-0.01190	-0.01205	-0.00091	-0.00795	-0.00790	0.01290	31.50	
5/26/16	8	-0.05910	-0.05920	0.00467	--	--	--		
5/26/16	9	--	--	--	0.05095	0.05100	0.00701	31.00	
5/26/16	9	0.01270	0.01270	0.00772	-0.04890	-0.04850	0.00884		
5/26/16	12	0.05600	0.05610	0.00650	0.11085	0.11085	0.03109	30.90	
5/26/16	12	--	--	--	0.11900	0.11900	0.01036		
5/26/16				**0.00436**			**0.01375**	**28.52**	**89.97**
9/27/16	8	-0.01165	-0.01170	0.00030	-0.00970	-0.00970	0.00569	28.80	87.30
9/27/16	8	-0.05885	-0.05890	0.00579	--	--	--		
9/27/16	9	--	--	--	0.04925	0.04925	0.00000	29.20	85.90
9/27/16	9	0.01240	0.01250	0.00671	-0.04530	-0.04530	0.02266		
9/27/16	12	0.05545	0.05560	0.00437	0.10940	0.10940	0.02520		
9/27/16	12	--	--	--	0.11695	0.11695	0.00203		
9/27/16	8	-0.01100	-0.01100	0.00305	-0.00845	-0.00845	0.01077	28.80	
9/27/16	8	-0.05840	-0.05825	0.00803	--	--	--		
9/27/16	9	--	--	--	0.05120	0.05120	0.00792	29.20	
9/27/16	9	0.01360	0.01340	0.01097	-0.04825	-0.04825	0.01067		
9/27/16	12	0.05620	0.05645	0.00762	0.11090	0.11090	0.03129		
9/27/16	12	--	--	--	0.11895	0.11895	0.01016		
9/27/16				**0.00585**			**0.01264**	**29.00**	**86.60**

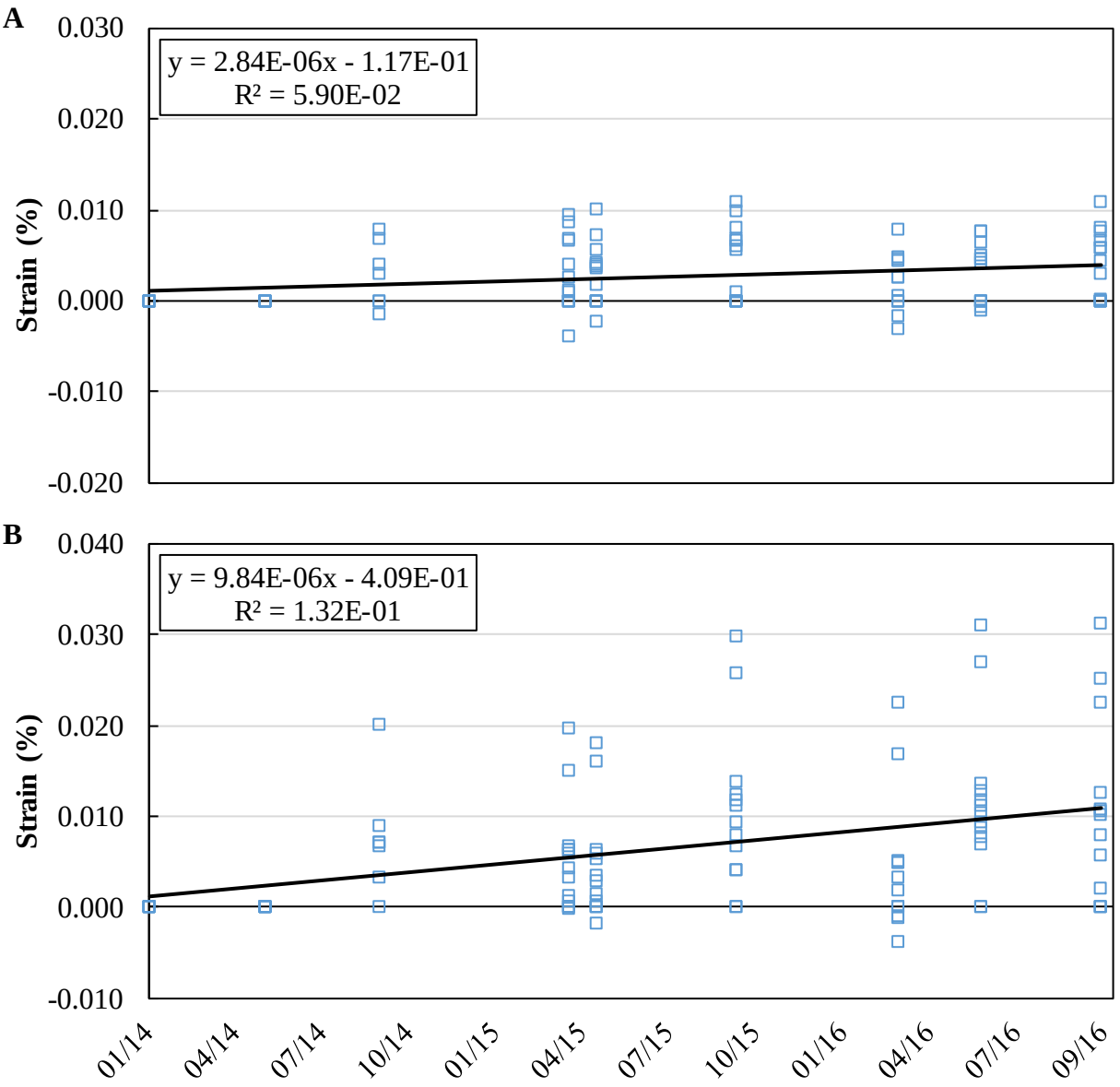

Fig. 8.2-4–Strain (%) with respect to time for Interstate 49 Silane 40B panels, travel (A) and transverse (B).